An integrative approach to understanding effects of valproate in *C. elegans*

by

Dona Helani Hemamala Munasinghe

A thesis submitted to
University of Birmingham
for the degree of
DOCTOR OF PHILOSOPHY

School of Biosciences
College of Life and Environmental Sciences
University of Birmingham
November 2013

ABSTRACT

Obesity is one of the biggest public health problemstoday, leading to type II diabetes, coronary heart disease, hypertension, sterility and cancer (Hashmi et al., 2013). *C.elegans*has been used extensively in obesity research to dissect the underlying principles. The overarching goal of my thesis has been to identify molecular signatures linking phenotypic and molecular responses of the nematode *C.elegans* to a number of experimental conditions that induce alteration in lipid metabolism. More specifically, I developed experimental procedures in *C.elegans* to studythe effects of exercise, diet and a *C.elegans* antiageing drug valproate. Using a modified lipid assay, I found for the first time that valproate induce lipid accumulation in *C.elegans* in a dose dependent manner. In this study obesity is induced in *C.elegans* by treating with either cholesterol or sodium valproate. Using microarray technology, expression profiles associated with the induction of obesity are studied. In addition, *C.elegans*were treated with monosodium glutamate which is found to decrease lipid mass. Exercise is a recommendation for obese people and hence a *C.elegans* model system is developed to study effect of exercise. Effects of valproate on *C.elegans* with respect to lipid quantity are studied in detail, with emphasis on insulin signalling pathway. Expression changes associated with insulin mutants are compared with the valproate exposure expression profile to understand how much of the valproate exposure could be explained by insulin signalling. I also found for the first time that valproate cause a global down regulation of nuclear components. A hypothesis on lipid accumulation on valproate exposure is presented. TGF-β pathway is also found to be involved in fat metabolism. Finally I report an interesting phenotype for the first time in which the TGF-β pathway receptor mutant *sma-6*shows paralysis in response to valproate.

For my parents and Duleen

ACKNOWLEDGMENTS

I was very fortunate to have some people in my life without whom this work would not have been a reality. First I must thank my teachers, primary school to postgraduate, who helped me throughout my life to come to this level in education. I should specially thank my grade 3 science teacher and Mr.Gauthamadasa who inspired me to learn science. My special thanks goes to Dr.Anil Jayasekera, Prof. Hewage, Dr. Nalin Goonesekera, Dr.Thirimanna, Dr.Ramani, Dr. Nalin de Silva and Dr.Rohini who helped me during my undergraduate studies and inspired me to continue studies in science. I am also grateful to my MSc supervisor Prof.Jehee Lee who taught me Molecular Biology Techniques and taught me to be independent.

My unending thanks must go to Prof.Robin May and Dr.Scott Hayward who supervised me throughout my research at Birmingham. I was very fortunate to have two of them as collaborators in my research. I am also indebted to Prof.Robin for giving me an opportunity to be with his research group where I learnt the qualities of the best supervision. He also helped me to relax when I was worried for being away from my kids during this study. I also thank Prof. Robin May and Prof. N. Salim for proof reading the thesis. Without their help I wouldn't have been able to complete the thesis. My sincere thanks go to Dr.Mark Viant and Prof. Anton Wagenmakers, the other two collaborators, who gave me advice during my research.

I should also thank Elizabeth and Amrith who taught me all the worm techniques. I also enjoyed being with the other members of Robin’s group and thank them for making my life easy.

Next, many thanks to people in Mark's group who helped me with NMR spectroscopy, especially Jonathan Byrne, Stefano and Allessia.

I must also thank Elsa for helping me with Western blot analysis and Simon and Wilber for teaching me microscopy.

It is Anna and Phil in my lab group who taught me microarray from scratch and Jaanika was always there when I got into trouble. Anna and Phil, thank you so much for helping me. Nil became a very good friend of mine with time. Thank you Nil for all the Bioinformatics you taught me. Rita worked with me late evenings and Rita, thank you for waiting for daily accompanying home daily (though we had to go in opposite directions!). Also thanks to Kim and Waseer for the friendship.

I am privileged to have a supervisor like Francesco Falciani and Francesco, thank you for helping me throughout this study. You were very considerate and helpful especially when I had to be away from my kids. Thank you for understanding me and helping me to be with my family.

I could do all these experiments because my mother-in-law looked after my kids during that time. Thank you for giving them love and care in my absence. Duleen, you suffered with me to make this a reality and sacrificed your studies for mine. I am fortunate to have a husband like you. Finally it's my parents who helped me throughout my life. I thank my parents too.

Finally I thank the funding agencies for financing this project.

This work has been funded by Cutting Edge and BBSRC grants. I was sponserd by Commonwealth Scholarship Commission.

TABLE OF CONTENTS

LIST OF FIGURES

Some of the figures are the output of the respective web-tool.

LIST OF TABLES

Some tables are the outputof therespective web-tool.

1.0 INTRODUCTION

1.1C.elegans as a model system

C.elegans is a free living nematode found in many countries of the world. It has been first adopted as a laboratory strain by Sydney Brenner in 1974(Brenner, 1974)leading to the Nobel Prize for Physiology or Medicine in 2002. During the last forty years *C.elegans* has been extensively used in research and some important findings were on *C.elegans.*

C.elegans can be grown in laboratory conditions with *Escherichia coli* OP50 strain, a uracil auxotroph, as the food source. The population is dominated by hermaphrodites (XX) and seldom get males (X0) characterized by the presence of male tail and lack of eggs and vulva which are found in the self-fertilizing hermaphrodite. There are four larval stages in its life cycle, L1 larva, L2 larva, L3 larva and L4 larva. Eggs hatch into LI larva which goes through L1, L2, L3 and L4 larval stages to adult in four days which is 1mm long. During food deprivation, presence of dauer hormone, high temperature or overcrowding allows this nematode to enter into a third larval arrest stage called dauer larva. This larval stage is long lived compared to the normal lifespan of three weeks at 20^{o}C and is resistant to stress. When conditions become good they complete the life cycle (Ren et al., 1996).

C.elegans is genetically tractable and a lot of phenotypic and genotypic data is available for these organisms(Hodgkin, 2005). Its genome is known and it is estimated to contain ~ 19000 genes in five pairs of autosomes and a single pair of X chromosomes in the

hermaphrodite (Fraser et al., 2000). The ease of making mutants by chemical (ethyl methane sulfonate), physical (ionizing radiation) or RNAi methods and the ability to store these mutants as frozen stock for years makes it a good model system to study gene functions and genetic interactions(Liu et al., 1999). It is also ethically more acceptable to use a lower level animal like *C.elegans* for the initial stages of research rather than using higher-level animals such as monkeys or mouse models. *C.elegans* provides a simple system to study complex gene functions in a multi-cellular organism level, which can be extended to understand the homologous mechanisms in human system.

1.2 Exercise and diet are well known factors affecting ageing and metabolism in living organisms across the tree of life

Food restriction is known to prolong life in yeast, *C.elegans,* mice and monkey (Young, 1979). Different dietary restriction methods in *C.elegans* involve different genetic mechanisms and result in varying degrees of life span extensions. These mechanisms include genes such as *sir-2*, TOR, *skn-1*, *hsf-1*, *eat-2*, *clk-1*, *aak-2* and *daf-16* (Greer and Brunet, 2009). Clinical and epidemiological studies suggest an antiageing and age related disease preventive effect of dietary restriction on humans(Kagawa, 1978). Several dietary factors are known to reduce age related decline of health. Folic acid and antioxidants are known to have a neuroprotective effect(Yu et al., 2009). For example, vitamin E reduces lipid peroxidation and protects cells from oxidative damage(Suleiman et al., 1996). Creatine increases energetics in muscles and nervous system(Andres et al., 2008).Ginkgo biloba extracts improved memory and learning in aged mice(Wesnes et al., 2000). Carotenoids such as lycopene and β-carotenes improve

memory and reduce risk of heart diseases, cancer and stroke which are implicated in ageing (Tapiero et al., 2004). Methionine restricted diets are found to cause decreased insulin and fasting blood glucose levels and increase lifespan of rats (Miller et al., 2005). Cholesterol synthesis increases with obesity (MIETTINEN, 1971) and weight reduction on a 1000cal diet resulted in lower levels of cholesterol synthesis and excretion in human (Bennion and Grundy, 1975). Increase in dietary leucine, which activates mTOR (mammalian target of rapamycin) decrease diet induced obesity, hyperglycemia and hypercholesterolemia in mice fed with a high fat diet. This is due to increased insulin sensitivity, decreased plasma glucogon and glucogenic amino acids and down regulation of hepatic glucose-6-phosphatase (Zhang et al., 2007). Several dietary factors are associated with age related decline of health. Cholesterol and saturated fat impair cognitive function in middle aged people ((Kalmijn et al., 2004). Dietary monosodium glutamate increases palatability and neonatal administration causes obesity in mice due to diminished energy expenditure (Poon and Cameron, 1978). Exercise is also known to improve age related decline of cognitive function (Mattson et al., 2002). But exercising of rats did not increase lifespan despite of caloric deficit even though dietary restriction of sedentary rats to get the same caloric deficit extends lifespan (Holloszy, 1998). Both caloric restriction and exercise have an anti-inflammatory effect measured by C-reactive protein levels (Kalani et al., 2006). Therefore both diet and exercise are determinants of lifespan.

1.3*C. elegans* is a well established model in ageing research

Ageing is an endogenous, progressive, irreversible and deleterious process. Availability of assay methods and genetic amenability to produce *C.elegans* with extended or shortened lifespans has made this nematode a good model system to elucidate mechanisms underlying ageing. Long lived dauer larval stage provides a simple system to study life extending factors (Fielenbach and Antebi, 2008).

Much research has been carried out in attempting to understand ageing using *C.elegans* as a model system. Involvement of the insulin signalling pathway on lifespan was first demonstrated in *C.elegans*(Kenyon et al., 1993). Insulin signalling pathway mutants *daf-2* and *age-1* are known to have extended lifespans and insulin like signalling in neurones alone would restore wild type life span in these mutants (Wolkow et al., 2000). These mutants require HSF-1((Hsu et al., 2003), DAF-16 activity(Lin et al., 1997) and autophagy (Hansen et al., 2008)for the extension of life span. Over expression of *sir-2* also increases lifespan in a DAF-16 dependent manner(Kenyon, 2005). Accumulation of protein similar to the proteins involved in human neurodegeneration is found in ageing *C.elegans*. The occurrence of insoluble proteins and their aggregation is decreased on suppression of insulin signalling (David et al., 2010). Valproate, which I studied in the present study is a fatty acid which is known to extend lifespan via the insulin signalling pathway(Evason et al., 2008). Supporting this hypothesis, length of fatty acids in *C.elegans* and their susceptibility to oxidation are found to be negatively correlated with lifespan in insulin pathway mutants (Reis et al., 2011). In addition to acting on lifespan, the insulin pathway is implicated in lipid metabolism but how valproate affects lipid metabolism is not known. The present study aims to fill this gap.

Transcriptional response to ageing is studied using *C.elegans* as a model system (Lund et al., 2002). Loss of VHL-1 and HIF-1 activity in *C.elegans* prolong lifespan in a mechanism different from dietary restriction and insulin signalling (Mehta et al., 2009). In addition a reduction of ATPsynthase activity and electron transport chain also results in longer lifespan (Dillin et al., 2002).

Insulin resistance is known to play a role in human ageing(Dechenes et al., 1998). Reduction in TOR decrease senescence in cultured human cells (Kapahi et al., 2010). These findings suggest *C.elegans* to be a good model system to study human metabolism.

1.4 Obesity

Obesity is a leading cause for several diseases including cancer, type II diabetes, hypertension and coronary heart disease(Chan et al., 1994). In human, there is a 40-70% genetic contribution to obesity(Comuzzie and Allison, 1998). Obesity results in when the energy expenditure is exceeded by food consumption. Unspent energy is stored as glycogen and fat, mainly triglycerides. In humans fat is stored in adipocytes in white adipose tissue which also has an endocrine function. White adipose tissue secretes leptin and pancreas secrets insulin. Both insulin and leptin secretion increases with increasing fat mass and acts on hypothalamus to decrease food consumption and increase energy expenditure(Ashrafi, 2007). *C.elegans* does not have any leptin homologue(Mullaney and Ashrafi, 2009a). Central nervous system also sense carbohydrate and lipid levels directly and is also stimulated by presence of food in the gut. A lipid sensing pathway in the brain has emerged that limits endogenous output of glucose into circulation by the liver(Yue and Lam, 2012).The brain also has glucose responsive and glucose sensitive

neurones which fire or get inactivated depending on glucose concentration(Levin et al., 1999).

Though *C.elegans* does not have adipocytes, they do share a lot of information on energy uptake and expenditure at the pathway level with human(Mullaney and Ashrafi, 2009b). Therefore *C.elegans* provides a valuable system to study lipid metabolism at a whole organism level. Unlike mammals, *C.elegans* are cholesterol auxotrophs(Mullaney and Ashrafi, 2009a). Linolenic acid and Linoleic acid are not essential fatty acids for *C.elegans* as they have all desaturases and PUFAelongases found in both animals and plants. Figure 1(page 8) and Figure 2 (page 9) show lipid synthesis and breakdown pathways found in both *C.elegans* and mammals.

There are several metabolic pathways that are interconnected which regulate energy balance in an organism. Glycolysis is the central to all which converts glucose into pyruvate to produce NADH and ATP during the process(Dukes et al., 1994). This pyruvate is converted to acetyl CoA by pyruvate dehydrogenase complex(Reed, 1969). Acetyl CoA enters the citric acid cycle where it combines with oxaloacetate to form several metabolites(Williamson and Corkey, 1969). During this process NADH, FADH2 and high energy GTP is produced. These NADH and FADH2 produced undergo oxidative phosphorylation where ATP is produced by ATPsynthase. Glucose-6-phosphate produced in glycolysis can either undergo glycolysis to produce ATP due to the action of phosphoglucose isomerise or it can be converted to 6-phospho-gluconolactone by Glucose-6-phosphate dehydrogenase where it will enter the pentose phosphate pathway to produce metabolites and reducing power in the form of NADPH. Pentose phosphate pathway makes NADPH required for biosynthesis (fatty acid biosynthesis, cholesterol biosynthesis, neurotransmitter biosynthesis and nucleotide

biosynthesis) and detoxification (reduction of oxidized glutathione and Cytochrome P450 monooxygenases). It also produces three, four, five, six and seven carbon sugars(Huck et al., 2003). During starvation glycolysis ceases and gluconeogenesis predominates (Moon and Johnston, 1980). In gluconeogenesis, noncarbohydrate precursors such as pyruvate, glycerol, lactate and amino acids are converted to glucose using up NADH, GTP and ATP in the process. Excess energy in animal tissue is stored either as glycogen or fat. Glycogen is synthesized from glucose by glycogen synthase. When cells need glucose, glycogen is converted to glucose-1-phosphate by glycogen phosphorylase. This is converted to glucose-6-phosphate by phosphoglucomutase, which can be used directly for glycolysis or pentose phosphate pathway to produce either energy or biosynthetic precursors. It can also be converted to glucose in liver where it is transported and used as an energy source by other tissues. For long term storage energy is stored as fat. Acetyl CoA is converted to malonylCoA by AcetylCoA carboxylase. Fatty acid synthase converts them into saturated fatty acids of different lengths. Fatty acid desaturases converts them into unsaturated fatty acids. Phospholipids and triglycerides are produced by combining fatty acylCoA with glycerol. When cell needs energy, triglycerides release fatty acids due to action of lipases. These fatty acids are converted to acetylCoA units via β-oxidation which can enter citric acid cycle to produce energy in the form of ATP. For more details on metabolic pathways refer Biochemistry by L. Stryer (Stryer, 1995). α-oxidation is used to degrade some fatty acids to remove one carbon unit at a time by dioxygenases (Wanders et al., 2001).

Insulin signalling pathway, TGF-β pathway, TOR pathway, AMP kinase and serotonine are implicated in *C.elegans* lipid metabolism. These pathways are interconnected via insulin signalling pathway.

This conservation of lipid metabolism pathways in *C.elegans* and human is exploited in the current study to develop a model system which is more ethically accepted than using higher organisms for such studies. How valproate increases lipid level is not known. Current study aims to fill this gap by looking at changes in gene expression profiles induced by valproate exposure. Depending on the tissue requirement lipid metabolism and other pathways which are interconnected to it are regulated to obtain a balance in energy level. Therefore it is important to look at the whole system as an entity rather than on its isolated features to get a clear understanding of the whole system and this is achieved by expression profiling.

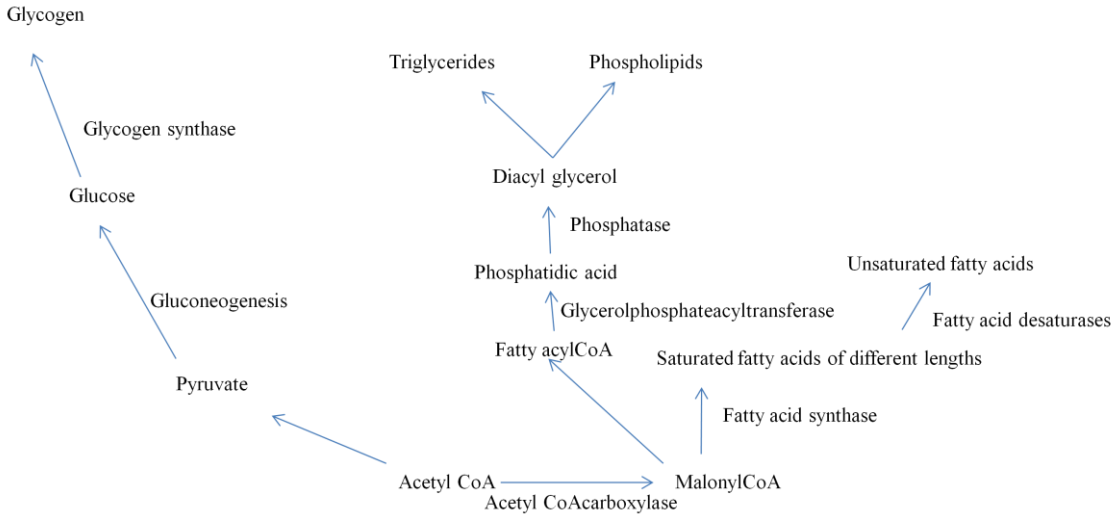

Figure 1 Lipids and glycogen synthesis pathways

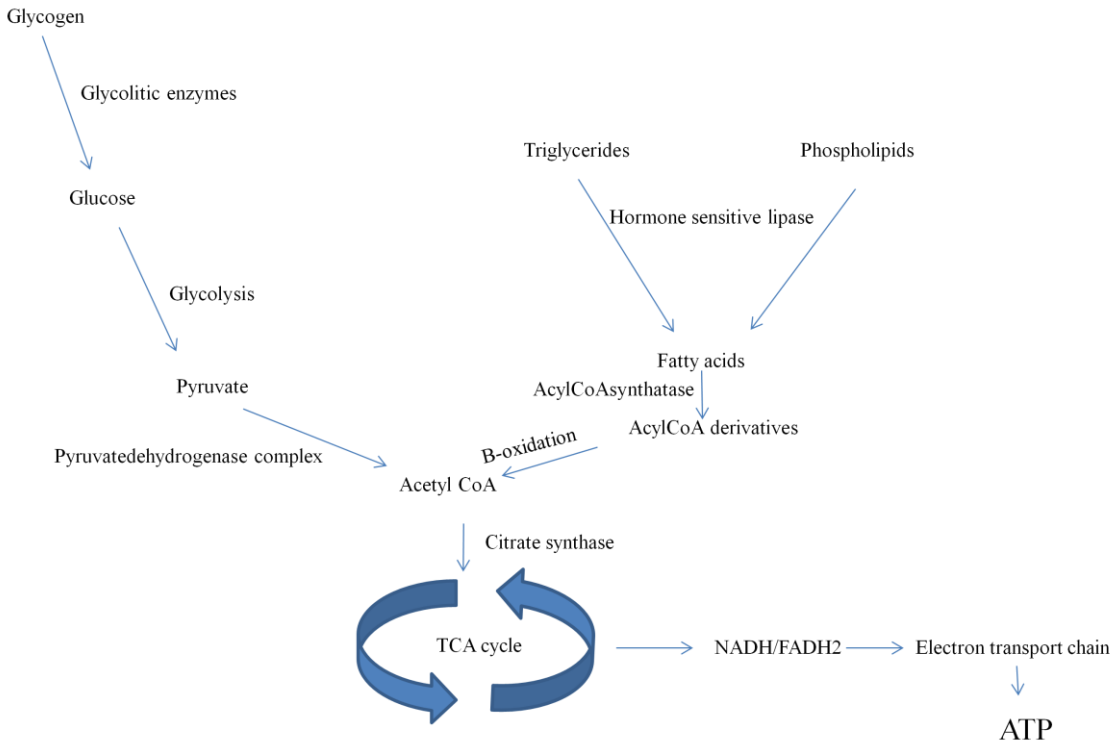

Figure 2 Lipid and glycogen breakdown pathways

1.5 Egg laying

Egg laying is another phenotype that is related to lipid metabolism and ageing. Aged *C.elegans* lay fewer eggs and high lipid content negatively correlates with egg laying(Sze et al., 2000). It is also known that high lipid content and ageing decrease fertility in human as well(Balen and Anderson, 2007). *C.elegans* hermaphrodites are self-fertile and produce sperm, which are stored in spermatheca and then produce oocytes. Fertilized eggs are stored in the uterus and are layed through the vulva when sex specific muscles contract. An adult animal would lay around 300 eggs during its lifetime. Egg laying is controlled by sensory cues. Vibration of culture medium, hypertonic salt solutions and food scarcity inhibit egg laying. Mutation of *egl-4* make nematodes insensitive to food induced egg laying and this phenotype is suppressed by

mutations in TGF-β pathway antagonistic transcription factor genes *daf-3* and *daf-5*(Daniels et al., 2000).Other TGF-β dauer pathway receptor mutants*daf-1* and *daf-4*, *daf-7* ligand mutants, *daf-8* and *daf-14*smads, which transduce the signal are all egg laying defective(Schafer, 2006). Serotonin is thought to act as a neuromodulator of egg laying and serotonin deficient mutant *tph-1* show egg laying defects, extended reproductive lifespan, arrest at dauer stage and lipid accumulation. These phenotypes are partly due to down regulation of the TGF-β and insulin signalling pathways(Sze et al., 2000). In the present study valproate is shown to down regulate *tph-1* activity, which could partly explain these three phenotypes observed on valproate exposure.

1.6 Sodium valproate

Valproate is a first line drug with antiepileptic, antipsychotic and anticancer activity. It was recently identified as a treatment for migraine(Sze et al., 2000). It is a histone deacetylase inhibitor(Göttlicher et al., 2001).Sodium valproate extends lifespan and decrease egg laying in *C.elegans* and cause obesity in human(Tokuoka et al., 2008, Isojärvi et al., 1996). It extends the lifespan of *C.elegans* in a dose dependent manner upto18mM, but reduce lifespan on higher concentrations(Evason et al., 2008). Valproate may exert this effect on life span by modulating the insulin signalling pathway because valproate causes dauer larva formation and cause nuclear localization of DAF-16 (Evason et al., 2008). Valproate inhibits egg laying by inhibiting diacylglycerol (DAG) production (Tokuoka et al., 2008). Even though valproate is reported to cause obesity in patients, the mechanism is not known. But high serum insulin levels are found in valproate treated patients compared to the control and insulin

resistance is thought to cause obesity on valproate treatment (Pylvänen et al., 2002). Some of the research done so far on valproate exposure is shown in Table 1.

Table 1 Research done on valproate up to 2012. The results of the respective reference article given is quoted or paraphrased to give an understanding of the work that has been done on Valproate by others before and during the present study period.

Function	Genes involved	Organism	Reference
Prescribing controlled release valproate or multiple daily administrations in pregnancy did not reduce the risk for malformations. Higher malformation rates observed with in utero exposure to valproate are more likely related to total daily dose, rather than peak serum levels.		Human pregnant women on VPA monotherapy	(Mawhinney et al., 2012)
VPA reduced the expression of *Homer1b/c* in cortical regions critical to motor control (medial agranular and motor cortices) and to cognitive and behavioural aspects of emotion (cingulate and insular cortices). The cortical premotor and motor areas project specifically to the dorsolateral regions of the striatum, which specifically control somatomotor inputs; cingulate and	*Homer1b/c* *Shank* *IP3R* (all down regulated and have been implicated in long-term synaptic	Rat brain	(de Bartolomeis et al., 2012)

insular cortices project to the ventral striatum, which is mostly implicated in behavioural control. *Shank* expression was mildly impacted by chronic lithium in the cortex, while VPA significantly down-regulated gene expression in motor and insular cortices. both mood stabilizers promoted *IP3R* cortical down-regulation, only lithium treatment significantly decreased *IP3R*expression in almost all cortical sub regions. In contrast, in the dorsolateral caudate-putamen, *IP3R* was down-regulated by VPA, while lithium slightly—and non-significantly—decreased gene expression.	changes)		
Serum ammonia levels were elevated without clinical or laboratory evidence of hepatotoxicity. This lead to Valproate induced hyperammonemic encephalopathy.		7 patients treated with VPA	(Gomceli et al., 2007)
Valproate (VPA)-induced hyperammonemic encephalopathy (VHE) is a serious drug-related adverse effect characterized by	Ammonia increase Glutamine inside cell	VPA treated patients	(Chopra et al., 2012)

lethargy, vomiting, cognitive slowing, focal neurological deficits and decreased levels of consciousness ranging from drowsiness to coma.	decrease Glutamate outside cells increase Glutamate transport to cells decrease		
Embryos developmentally exposed to valproate show concentration dependent alterations in locomoter activity. These data demonstrate that exposure to valproate during development affected locomoter activity at a concentration that did not cause malformations. The malformations include lordosis, stunted skeletal growth in the spinal region, stunted fins, distended abdominal and thoracic regions, microencephaly and microophthalmia. Also it caused decreases in the retino-tectal projection area.		Zebrafish embryos	(Cowden et al., 2012)

Short-term social recognition ability of adult rats was improved with VPA. No effect on VPA on olfactory discrimination, short and long term memory, locomoter activity. In forced swimming test, climbing time increased and immobility time decreased indicating antidepressant like effect of VPA. VPA increased dopamine levels in striatum but not in the olfactory bulb. Pre-treatment with VPA can reduce the effects of MPTP on olfactory discrimination and short-term memory impairments and prevent dopamine depletion in the olfactory bulb of MPTP-treated rats.	rat	(Castro et al., 2012)
VPA induced a lower fertility rate (this effect is reduced by coadministration of folinic acid (FA) or S-adenosylmethionine (SAM). Foetal weight and length were unaffected by VPA treatment. Hepatic injury was observed in foetuses treated with VPA. FA and	Wistar rats	(Ubeda et al., 2013)

SAM were able to reverse the decrease in VPA-induced foetal liver T-lymphocyte cells VPA treatment resulted in skeletal modifications in the skull, appendicular bones, vertebrae and ribs. Only FA was able to reverse the decrease in VPA-induced foetal liver T-lymphocyte cells.		
VPA decrease DAG (diacylglycerol) production and inhibit egg laying. VPA disrupt ovulation and defecation by decreasing production of inositol-1,4,5-triphosphate (IP_3). VPA may inhibit phospholipase-C mediated hydrolysis of Phosphatidylinositol-4,5-bisphosphate (PIP_2) to form DAG and IP_3.	*C.elegans*	(Tokuoka et al., 2008)
VPA increase lifespan of *C.elegans*	*C.elegans*	(Evason et al., 2008)
VPA Decrease apoptosis due to histone deacetylase inhibitor activity of VPA	Rat Cerebral cortical neurones	(Jeong et al., 2003)
Increase of G0-G1 and a decreased G2/M and S-phase following VPA treatment, indicating in vivo effects of VPA on cell cycle regulation. VPA inhibited cell proliferation in a	Multiple myeloma cells	(Neri et al., 2008)

time and dose dependent manner and induced apoptosis.		
VPA inhibit tumour growth.	Severe combined immunodeficiency mice bearing human MM xenografts.	(Neri et al., 2008)

1.7 Insulin signalling pathway

DAF-2 acts as the *C.elegans'* sole homologue of insulin receptor. There are 40 insulin homologs in *C.elegans* compared to the 10 insulin/insulin homolog genes in human which may have redundant functions (Ritter et al., 2013). Activated DAF-2 causes phosphorylation of the DAF-16 *C.elegans* FOXO transcription factor and prevents it from being transported to the nucleus and prevents transcription of downstream target genes. FKHR and AFX are the human orthologues of DAF-16(Lee et al., 2001). When ligand is bound, DAF-2 activates theAAP-1; AGE-1(PI3K) complex(Paradis and Ruvkun, 1998).This complex when activated activates PDK-1, which in turn activates both AKT-1 and AKT-2. Activated AKT-1 and AKT-2 prevent nuclear localization of DAF-16. DAF-18(PTEN) inhibits AGE-1. Genes of insulin like signalling pathway and associated pathways, which cause phenotypic changes associated with valproate exposure in *C. elegans* are given in Table2.

Table2 *C. elegans* genes of the insulin signalling or associated pathways and their nul-phenotypes. These phenotypes are also observed on valproate exposure.

Phenotype	Gene mutated	Acts via	Reference
dauer	*daf-2*	DAF-16	(Ogg et al., 1997)
	daf-1		(Ogg et al., 1997)
	daf-4		(Ogg et al., 1997)
	age-1	DAF-16	(Ogg et al., 1997)
	daf-7	Not via DAF-16	(Ogg et al., 1997)
	daf-8	DAF-3	(Ogg et al., 1997)
	daf-14	DAF-3	(Ogg et al., 1997)
Longer lifespan	*daf-2*	DAF-16	(Ogg et al., 1997)
	sir-2.1		(Tissenbaum and Guarente, 2001)
	age-1	DAF-16	(Ogg et al., 1997)
	AAK-2	In parallel to DAF-16	(Apfeld et al., 2004)
Lipid accumulation	*daf-2*	DAF-16	(Ogg et al., 1997)
	daf-7	DAF-3 (Not via DAF-16)	(Ogg et al., 1997)
	daf-14	DAF-3	(Ogg et al., 1997)
	daf-8	DAF-3	(Ogg et al., 1997)
	daf-1	DAF-3	(Greer et al., 2008)
	daf-4		(Greer et al., 2008)

Egg laying defective	*daf-7*	DAF-3	
	daf-1	DAF-3	

1.8 Non insulin pathways that could be involved in lipid metabolism

Transforming growth factor –β (TGF-β) pathway is another pathway that works in parallel to insulin signalling pathway, which is thought to bring metabolic changes in *C.elegans*(Figure3 page20). There are two TGF-β pathways. One pathway (Figure 3B) is where a ligand DAF-7 binds to the receptor DAF-1 and DAF-4 inactivates the DAF-3 smad (Georgi et al., 1990). Mutants of *daf-7,daf-1*and *daf-4* are dauer constitutive (Schackwitz et al., 1996, Georgi et al., 1990, Estevez et al., 1993). This pathway is also implicated in lipid metabolism as*daf-1, daf-4* and *daf-7* mutants all show lipid accumulation(Hellerer et al., 2007). This lipid accumulation occurs via DAF-3. Excess fat in*daf-7* mutants is due to activation of specific glutamergic receptors (*mgl-1* and *mgl-3*), and this lipid accumulation is found to be due to increased fat synthesis by the activation of the fatty acid synthase gene, *fasn-1*(Greer et al., 2008). This lipid accumulation via DAF-3 does not depend on DAF-12, which is found downstream of DAF-3 in dauer formation.

In the other TGF-β pathway(Figure 3C) DBL-1 binds to a receptor composed of SMA-6 which phosphorylates the type II receptor DAF-4 and this signal is transduced to SMA-9 in the nucleus via SMA-2, SMA-3 and SMA-4 through phosphorylation events

(Savage et al., 1996), (Savage-Dunn, 2005). SMA-6 is not associated with fat accumulation (Greer et al., 2008).

SIR-2 is a histone deacetylase that is reported to activate DAF-16 (Tissenbaum and Guarente, 2001). Its over expression is reported to cause lifespan extension in *C.elegans* and drosophila(Tissenbaum and Guarente, 2001, Rogina and Helfand, 2004,Viswanathan and Guarente, 2011). But this is doubtful as Buerrnet *et al* have found no effect of over expression of SIR-2 on lifespan of these two organisms (Burnett et al., 2011). Rizki *et al* have shown that HCF-1 probably represses DAF-16 by forming a complex with SIR-2.1 and antagonizing their abilities to stimulate DAF-16 (Rizki et al., 2011).

AMP activated protein kinase (AMPK) also activates DAF-16 by direct phosphorylation (Greer et al., 2007). *aak-1* and *aak-2* codes for the catalytic α-subunits of AMPK. *aakb-1* and *aakb-2* code for the two regulatory subunits of AMPK (Narbonne and Roy, 2008). Narbonne and Roy have shown that AMPK signalling helps the slow release of fat deposits during dauer stage and lack of this pathway causes fast release of fats from their triglyceride stores and reduce lifespan of these dauer.

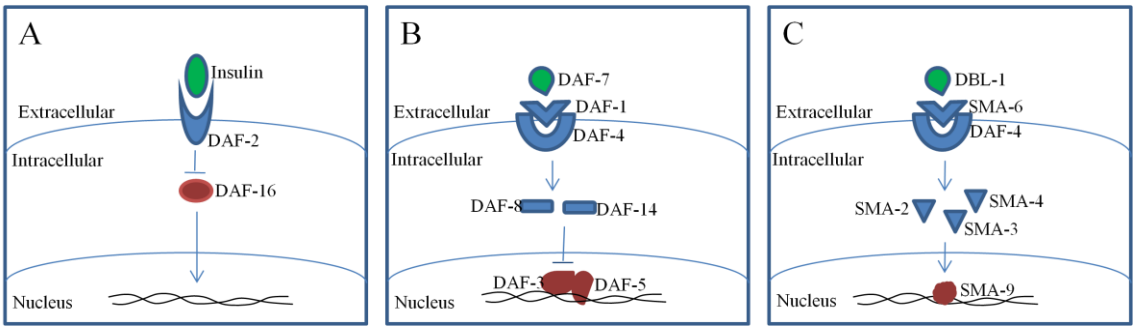

Figure3Insulin and TGF-β pathways in *C.elegans*. (A) *C.elegans* insulin signalling pathway. Insulin homologues in *C.elegans* bind to its sole insulin receptor DAF-2. Ligand bound DAF-2 inactivates the FOXO transcription factor, DFA-16 and prevents activation of downstream target genes. (B) C elegans TGF-β deaur pathway. Ligand DAF-7 binds to receptor made up of DAF-1 and DAF-4 and activates DAF-8 and DAF-14 which would inhibit the downstream transcription factors DAF-3 and DAF-5. (C) C.elegans TGF-β sma/mad pathway. The ligand DBL-1 binds to the receptors SMA-6 and DAF-4 , which activates SMA-9 transcription factor via the activation of other smads.

1.9 The general challenge of using non vertebrate species to understand drug mode of action

The activity of a drug depends on its successful uptake by the organism, interaction of the drug with its primary targets, metabolism of the drug and its resulting metabolites. These metabolites can act on specific or general targets bringing out secondary responses and finally the elimination of the drug and its metabolites from thebody, which determines the duration of the activity of drug, which cause transcriptomic or metabolomic changes. *C.elegans,* being a nematode, cannot be used to model the more complicated human disease processes or whole pathology to understand the mode of drug action. *C.elegans* also lacks certain pathways found in humans. For example

C.elegans does not have *de-novo* cholesterol synthesis pathways (Crowder et al., 2001) making it impossible to use as a study model to look into this pathway or to understand the drug mode of action which acts via this pathway. There are no orthologs for certain human genes in *C.elegans*. Understanding the drug activity on complex human organs, such as the pituitary is also not possible in *C.elegans*, as it does not have these complex organs. This also makes it difficult to understand the adverse effects of drugs and limits its use in testing drug suitability for clinical trials.

Though there are drawbacks in the use of *C.elegans* to model human systems, several studies reveal this nematode to be a good model system to understand drug mode of action in several ways. For example, *C.elegans* has been used successfully to study the mode of drug action of the antidepressant fluoxetine. Even though depression is a complex phenotype, which cannot be directly observed in *C.elegans*, fluoxetine changes feeding behaviour of *C.elegans*. Mutants of serotonin reuptake transporter MOD-5 are resistant to fluoxetine for this behaviour. This leads to the recognition of fluoxetine action where inhibition of MOD-5 is found to be the main mechanism by which this drug brings its antidepressant activity. MOD-5 homologue SERT is found to be the main target of fluoxetine in mammalian system (Ranganathan et al., 2001). Also *C.elegans* homologues have been identified for 60-80% of human genes. According to Kaletta and Hengartner (Kaletta and Hengartner, 2006) , out of the animal models, *C. elegans* is the fastest and most amenable to cost effective medium/ high-throughput technologies. Thus, *C.elegans* has been used in this study to model the effect of valproate exposure.

1.10*C.elegans* in neuronal studies

C.elegans is a model organism widely used in neuronal studies. It has two almost independent nervous systems, the pharyngeal nervous system and the extra-pharyngeal nervous system. In hermaphrodite, the pharyngeal nervous system is composed of 20 neurones with the extra-pharyngeal nervous system having 282 neurones (Dent et al., 2000). But pharyngeal pumping is independent of the pharyngeal nervous system (Avery and Horvitzt, 1989).

C.elegans hasexcitatory neurotransmission via acetylcholine.Its acetylcholine receptors a homo or heteropentamers made up of α and nonα subunits. *unc-38* codes for the α subunit (Almedom et al., 2009) and levamisole is an agonist of this receptor. Aldicarb is an acetylcholine esterase inhibitor which prevents hydrolysis of acetylcholine in the synaptic cleft(Hu et al., 2009).

C.elegans also has an inhibitory neurotransmission via γ-amino beutric acid (GABA). *unc-25* codes for glutamic acid decarboxylase, the enzyme which syntheses GABA from glutamic acid and is involved in this inhibitory neurotransmission (Jorgensen, 2005).

1.11Why an “omics” approach

The central dogma of Molecular Biology explains the flow of information in biological systems to be unidirectional, which is from genes to RNA to protein. But the identification of several complex interactions between proteins, RNA and DNA with their further complicated regulatory mechanisms has lead to the realization that the flow

of information is not in one direction. This made it important to get a holistic view of the system rather than looking at its individual components in isolation. To obtain ahigh-throughput, data driven holistic view of valproate exposure, gene expression profiling was performed on *C.elegans* treated with different concentrations of valproate.

Analysis of valproate exposure revealed the down regulation of nuclear components to be a key feature of valproate exposure. It also revealed that the lipid accumulation observed on valproate exposure could be the net effect of the concomitant activation of both lipid synthesis and lipid degradative pathways by valproate.

2.0 MATERIALS AND METHODS

2.1*C.elegans* strains used

All the experiments were based on *C.elegans* strains provided by Caenorhabditis Genetics Centre (CGC) which is funded by NIH Office of Research Infrastructure Programs (P40 OD010440). *N2*(*C. elegans* wild type; Bristol isolate),*CF1038 daf-16(mu86)I*(a null mutant where most of the coding region including the whole forkhead domain is deleated), *LT186sma-6(wk7)II*(a null mutant), *DR40daf-1(m40)IV* (a substitution mutant), *CB1370daf-2*(a substitution mutant), *daf-4(ok827)III*(provided by the *C. elegans* Reverse Genetics Core Facility at UBC, which is part of the International *C. elegans* Gene Knockout Consortium), *unc-38(e264)I*(recessive), *unc-25(n2569)III* were used in the experiments.

2.2 Culture conditions

C.elegans were grown as described previously ((Brenner, 1974). Briefly, animals were maintained on 90mm petri dishes with nematode growth medium (NGM; 1.7% agar, 0.25% peptone, 0.3% NaCl, 5µg/ml Cholesterol, with the addition of 1mM $CaCl_2$, 1mM $MgSO_4$ and 25mM KPO_4, pH6, after autoclaving). These plates were seeded with a lawn of *Escherichia coli* OP50, a natural uracil mutant strain and the standard food source of the *Caenorhabditis* nematodes. Nematodes were maintained at 20°C.

2.3 *C. elegans* bleaching protocol

This protocol was used to generate staged animal cultures and to remove any contamination from *C. elegans* stock plates. Animals were washed off from newly starved stock plates (9cm) in 3ml M9 buffer (22mM KH_2PO_4, 42mM Na_2HPO_4, 80mM NaCl, 1mM $MgSO_4$) and the suspension was transferred into 1.5ml centrifuge tubes and centrifuged at 6,500g for 30s. The supernatant was removed to leave 0.5ml in the tube. 80µl 5M NaOH and 160µl Sodium hypochlorite was added and the tubes were shaken vigorously for 2 min. The tubes were then filled with M9, centrifuged as above and the supernatant removed; this washing step was repeated twice and on the 2nd time 200-400µl M9 buffer was added to the tube. The tubes were rolled overnight to keep the animals oxygenated and transferred onto OP50 plates the following day, where the cultures developed synchronously.

2.4 Lipid assay

Lipid assay was performed on 1 day adult nematodes with modifications of the method described previously (O'Rourke et al., 2009). Assay was performed by collecting *C.elegans* into 1.5ml tubes with 1mL M9 buffer and removing supernatant by centrifuging at 4000rpm. Added 1mL dis.H_2O and 50µL of freshly prepared 10% formaldehyde into the tube and freeze thawed in liquid nitrogen twice without thawing completely. The worms were allowed to settle and formaldehyde solution was removed. Then 1ml of 1µg/mL Nile red solution prepared in M9 buffer was added and incubate at room temperature rolling for 20min in a rotator. Worms were allowed to settle, the supernatant was removed and the nematodes were washed with 1mL disH_2O. Once

again the nematodes were allowed to settle and the supernatant was removed leaving 100µl from which15µlwas added per well to 96 well plates. Fluorescent images were taken at λ_{ex} 553nm, λ_{em} 637 using Q Capture Pro programme with Q Imaging Digital Camera with 2(s) exposure time. Images were analysed using Image J software (Abràmoff et al., 2004). Around 120 nematode images were analysed per sample and t test is performed to identify significant changes.

2.5 Exercise assay

C.elegans were forced to exercise by culturing them on agar plates with different agar concentrations. Synchronized cultures of L4 larva were transferred to 90mm NGM agar OP50 bacterial plates containing drug or solvent and total lipid was measured after 24hr at one day adult stage. Sodium valproate and monosodium glutamate were dissolved in water to get stock concentrations of 1000mM and added to melted NGM agar cooled to 50^{o}C at a final concentration of 15mM and 24mM respectively. A 12mM stock solution of cholesterol was prepared in ethanol and added to NGM agar cooled to 50^{o}C to get a working concentration of 24µM. Agar plates were prepared as described previously with the drug and the desired concentration of agar to get an agar gradient.

2.6 Egg laying assay

One day adult *C.elegans* were transferred to valproate plates and removed after two hours. Number of L2 larva on each plate is counted. Sodium valproate concentrations tested were 0, 6, 12, 15, 18 and 24mM. Measurements were taken for 3 nematodes per plate with 5 replicates for each drug concentration.

2.7 Development of a paralysis assay

Previous studies have performed this assay by transferring nematodes to relevant drug plates or control plates with a hook. This method has several drawbacks. Picking *C.elegans* with a hook can damage their skin affecting drug absorption and sometimes cause death. It is also time consuming limiting the number of animals that can be assayed and the number of treatments that can be tested. The method developed during this study replaces this step by transferring *C.elegans* directly on to drug or control plates with a pipette, which saves time and does not cause any physical damage to nematode body. It makes the test much simple and easy to perform and allows the analysis of a number of treatments simultaneously. It also allows the analysis of a large number of nematodes per sample increasing statistical significance of the results. There is also less variation between samples. Also it does not require the expertise of nematode picking and can be performed by an armature. The only drawback of this method is the small volume of M9 buffer, which is transferred with the nematodes to the drug plates decreasing the drug concentration. But any liquid transferred get absorbed in to the agar and the volume transferred is negligible compared to the size of the plate.

In the method developed during this study, *C.elegans* at L4 stage were collected into 1.5mL tubes with M9 buffer, spun at 6000rpm for 30s , the supernatant was removed and *C.elegans* collected at the bottom of the tube were transferred to the relevant drug plates or control plates with a pipette. These drug or control plates had OP50 seeded and dried under laminar flow 2hrs before the experiment. Then nematodes were observed under a light microscope with x 10 magnification and the number of nematodes in a given visual field was counted. At each time point, the number of paralysed nematodes was calculated, which were not moving and was shorter as a result of muscle contraction, as a percentage of the number of total *C.elegans* in that visual field. Due to lack of time, this method could not used to compare with the existing methods.

2.8 Preparation of samples for microarray

Staged *C. elegans N2* Bristol strain was grown at 20^{o}C as explained in chapter 2. They were transferred to drug plates containing sodium valproate dissolved in MilliQ H_2O at L4 stage for 24hrs. Drug concentrations 3, 6, 9, 15, 18, and 24mM in nematode agar were prepared from a 1000mM stock solution in MilliQ H_2O. After 24hrs on drug plates, nematodes were collected with MilliQ H_2O by washing each plate twice with 1ml MilliQ H_2O. After nematodes collect to the bottom of the tube, supernatant wasremoved and transferred ~ 30mg of nematode pellet into 2ml VK05 Precellys tubes containing 600µl RLT buffer. They were homogenized twice at 6400rpm for 10s in Precellys24 homogenizer. These tubes were dipped in liqN_2 for 5min and transferred to -80oC freezer till RNA isolation. All the steps in the collection of nematodes from drug

plates to homogenization were performed quickly to avoid any changes in the transcriptome.

2.9 Microarray

Total RNA was isolated from each frozensample prepared in chapter 2.8 using RNAeasy Mini Kit from QIAGEN according to the procedure of total RNA isolation from animal tissue with DNAase digestion. The procedure followed is as given below. Thawed homogenized samples stored in RLT buffer and centrifuged lysate at full speed in a microcentrifuge for 3min. Carefully transferred the supernatant into a new microcentrifuge tube with a pipette. One volume of freshly prepared 70% ethanol was added into this and mixed by pipetting. Transferred 700µL of this including any precipitate formed to an RNeasy spin column kept in a 2mL collection tube. The lid was closed gently and centrifuged at 10000rpm for 15s. If there was more than 700 µL, repeated the step using the same column. A volume of 350 µL of buffer RW1 was added to the spin column, closed the lid gently and centrifuged at 10000rpm for 15s. The flowthrough was discarded. Ten µL DNAase 1 stock solution was added into 70 µL buffer RDD to prepare the DNAase working solution, mixed this DNAase working solution gently by inverting the tube and spun to collect any residual solution left on the sides of the tube. Forty µL of this DNAase working solution was added to the membrane of the spin column and left at room temperature for 15min. Added 350 µL of buffer RW1into the spin column and centrifuged at 10000rpm for 15s. The flowthrough was discarded. The column was washed by adding 500 µL buffer RPE into the spin column and centrifuged at 10000rpm for 2min. Then the spin column was placed ina new collection tube and centrifuged at 14000rpm for 1min to remove any

residual liquid remaining in the column. The spin column was placed in a new 1.5mL microcentrifuge tube, 40 µLof RNAase free water was added and centrifuged at 10000rpm for 1min to elute the RNA. This elution step was repeated to obtain a higher concentration of total RNA. RNA quality was assessed using 2100 Bioanalyzer from Agilent Technologies. RNA quantification was performed with NanoDrop from Thermo Scientific, UK. Amplified and labelled target RNA using Agilent Low Input Quick Amp kit, One Colour according to manufacturer's instructions. The following procedure was followed to produce labelled cRNA. Spike mix was prepared by vortexing and heating spike mix solution to 37^{o}C for 5min. Mixed again by vortexing, spun down and diluted four times (first dilution 1:20, second dilution 1:25, third dilution 1:20, fourth dilution 1:2) in the dilution buffer. Added 2µL of this diluted spike mix in to 50ng of total RNA in a volume of 1.5 µL to get a total volume of 3.5 µL. The T7 primer mix was prepared by adding 1 µL of nuclease free water into 0.8 µL of T7 primer. Added 1.7 µL of this into the tube containing total RNA and spike mix. The primer and the template were denatured by heating it to 65^{o}C for 10min in a circulating waterbath and then placed this labelling reaction tube on ice for 5min. The cDNA master mix was prepared by adding 2 µL of 5x first strand buffer, 1 µL of 0.1M DTT, 0.5 µL of 10mM dNTP mix and1.2 µL of RNase Affinity Script Block mix and then 4.7 µL of this cDNA master mix was added into the labelling reaction. The samples were first incubated at 40^{o}C for 2hrs, and then at 70^{o}C for 15min followed by incubation on ice for 5min. The samples were stored at -80^{o}C until the next step. Thetranscription master mix was prepared by adding 0.75 µL nuclease free water, 3.2 µL 5x transcription buffer, 0.6 µL 0.1M DTT, 1 µL NTP mix, 0.21 µL T7 RNA polymerase blend and 0.24 µL Cyanine 3-CTP. Six µL of this transcription mater mix was added into the labelling reaction tube

and incubated at 40^{o}C for 2hrs. Then to purify the labelled cRNA, add 84 µL nuclease free water and 350 µL buffer RLT into the reaction tube. An aliquot of 250 µL of 100% ethanol was added, mixed by pipetting and transferred into RNeasy mini spin column in a collection tube. The tube was then spun at 13000rpm 30s at 4^{o}C. A volume of 500 µL buffer RPE was added and spun at 13000rpm for 60s at 4^{o}C. Transferred the column to a new collection tube and spun at 13000rpm for 30s to remove any remaining residual buffer. Purified cRNA was eluted into a new 1.5mL collection tube by adding 30 µL RNase free water, incubating at room temperature for 1min and centrifuging at 13000rpm for 30s. cRNA was quantified with NanoDrop. Cyanine 3 dye concentration, RNA absorbance ratio at 260nm/ 280nm and cRNA concentration were recorded. The yield and the specific activity of each reaction were calculated. After purification of cRNA, the hybridization was done as follows. The blocking agent is prepared by adding 500 µL of nuclease free water into 10x Gene Expression Blocking Agent (GEBA) and warmed it at 37^{o}C for 5 min. Then 11 µL of GEBA was added to 1.65 µg labelled cRNA and made the total volume up to 52.8 µL with nuclease free water. After adding 2.2 µL 25x Fragmentation Buffer into this mixture it was incubated at 60^{o}C for 30minfor fragmentation. The fragmentation was stopped by keeping on ice for 1min and adding 55 µL of 2x Hi RPM Hybridization Buffer to 55 µL of cRNA fragmentation mix. Then carefully mixed by pipetting to avoid bubble formation. Then spun at 13000rpm for 1min at room temperature, placed the samples on ice and 100 µL loaded into *C.elegans* (V2) Gene Expression Microarray, 4x44K slides from Agilent Technologies, UK. Slides were hybridized at 65^{o}C for 17hrs. After hybridization, arrays were washed as follows. Two mL of Triton X 102 was added to wash buffer 1and 2 each in cubitainers to get a final concentration of 0.005%. One thousand mL of wash

buffer 2 was warmed to 37^{o}C overnight prior to use. Axon 4000 scanner equipped with GenePix 3.0 analysis software was used for initial analysis of microarray data.

2.10 Microarray data analysis

Raw image files are automatically loaded and processed by Agilent Feature Extraction software to generate Feature Level Extraction Output (FLEO), GenePix Results (GPR files). Expression values generated are log2 transformed to increase signal : noise ratio and Quantile normalized to remove any systematic bias such as bias due to different starting RNA quantities, strengths in dye concentration etc. Significant expression profiles are identified by Significance Analysis of Microarray (SAM). Correlation is used as a measure linking the two variables lipid level and valproate concentration. Expression profile with a threshold value of 1% BH(Bengamini Hochberg correction) corrected p value are identified and compared with the significant expression profile identified by SAM with a false discovery rate (FDR) less than 1%. Probe IDs of the union of the two expression profiles are chosen and after converting to Official Gene Symbols, SOTA and CAST clustering were performed for class discovery in TMev (Herrero et al., 2001, Dopazo and Carazo, 1997, Ben-Dor et al., 1999). Functional annotation was carried out with Database for Annotation, Visualization and Integrated Discovery (DAVID) (Da Wei Huang and Lempicki, 2008, Sherman and Lempicki, 2009)and Network analysis by Ingenuity System Pathways as shown in Figure 4.

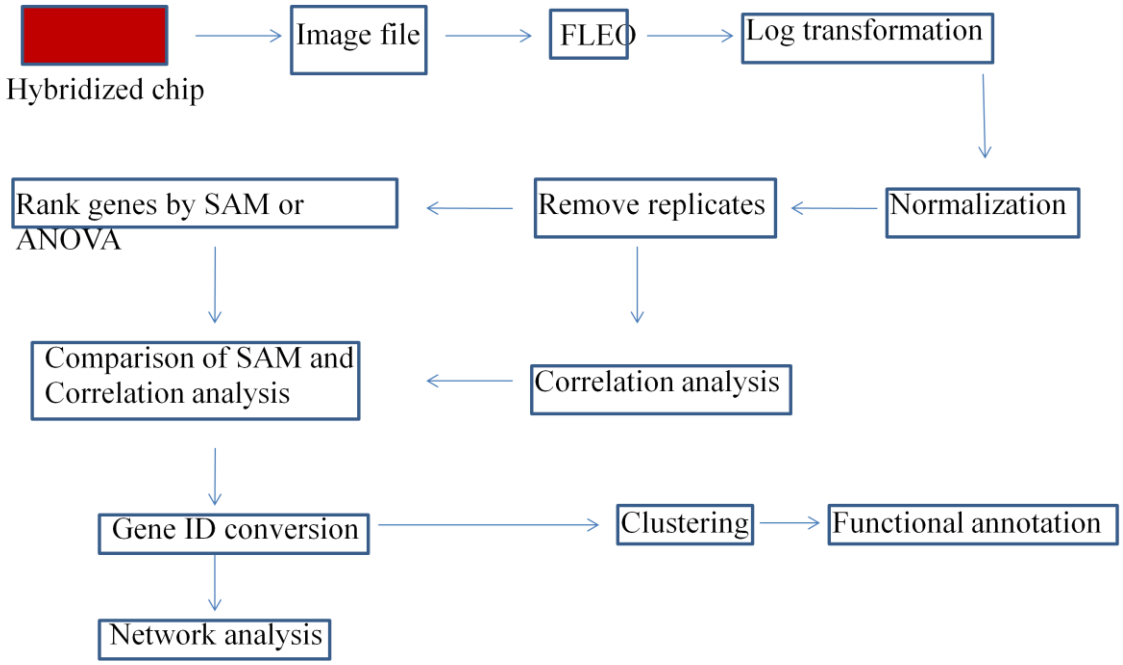

Figure 4The rational used in generating biological information from microarray. FLEO = Feature level extraction output, SAM = Significance analysis of Microarray, ANOVA= Analysis of variance

2.11 Ingenuity Systems Pathway Analysis

The Ingenuity platform is comprised of three main components, content acquisition, knowledgebase and applications. In content acquisition, information is gathered from original research articles, databases *etc.* and after quality control is integrated into Ingenuity ontology. These ontologies provide the scaffolding for the Ingenuity Knowledge Base. Research data can be overlaid onto this Knowledge Base and Applications layer provides a web based applications for data analysis and interpretation. For example, overlaying microarray data on to Knowledge Base will help to define pathways activated or inactivated under a treatment. This will lead to the

identification of transcription factors associated including ones which were not present in the data set submitted and help in identification of upstream master regulators.
In this study IPA Core Analysis (Ingenuity Systems) was performed on the significant expression profile of valproate exposure identified by SAM with less than a 1% false discovery rate pooled together with the genes from the correlation analysis with a threshold of BH corrected p value < 1%. Significant expression profile of valproate exposure is overlaid on Ingenuity Knowledge Base and networks were generated with each having 35 focus molecules. This included both focus molecules from dataset provided and focus molecules identified by Ingenuity Systems as associated with the networks generated. Predictions were made on phenotypes that could be observed as a result of the given gene expression profiles. Upstream regulators in the data set provided and predicted to be associated with which could bring the observed expression changes were predicted.

2.12 Identification of insulin dependent and insulin independent expression profilesfollowing valproate exposure

Inactivation of the receptor DAF-2 causes dephosphorylation of cytoplasmic DAF-16, which results in the nuclear translocation of DAF-16 and affects transcription of downstream targets. In literature, cytoplasmic DAF-16 is presumed to be inactive, but there is no evidence for this. Therefore there are two possibilities when compare gene expressions of *daf-2* and *daf-16* mutantsFigure5.

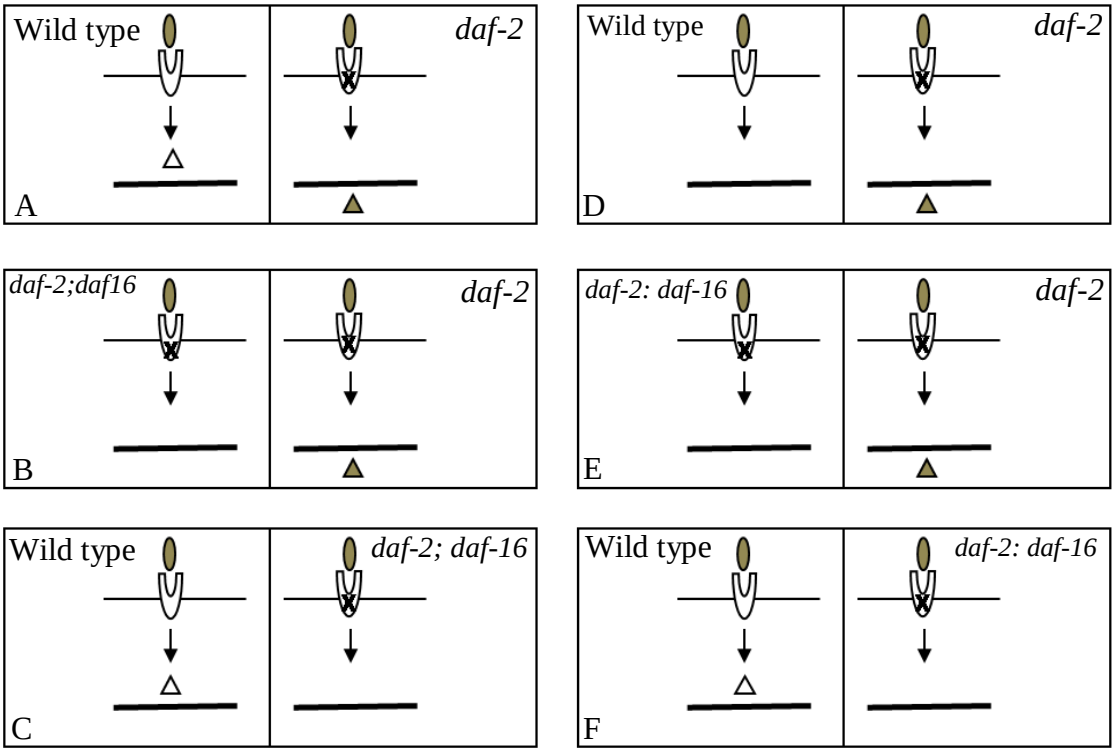

Figure5 Two different models that is used in this study to explain the gene expression profiles of *daf-2* and *daf-16* mutants. Panels A, B and C explains the gene expressions assuming cytoplasmic DAF-16 is active. Panels D, E and F shows the possibilities assuming cytoplasmic DAF-16 is inactive. Panel A and D : Pathways affected by *daf-2*. Panel B and E: Pathways affected by nuclear DAF-16. Panel C: Pathways affected by both DAF-2 and cytoplasmic DAF-16. Panel F: Pathways affected by DAF-2 independent of DAF-16.

Comparison of the microarray data of *C.elegans* exposed to sodium valproate with microarray Data of time course study done on RNAinterference inactivation of *daf-2* and *daf-2;daf-16* double mutants compared to a wild type mixed population as reference (Murphy et al., 2003)was used to identify pathways affected by sodium valproate dependent on insulin and independent of insulin (Figure 6 page 36). Only 13% of the expression profiles associated with valproate exposure was dependent on insulin.

DAF-16 and DAF-2 dependent expression profiles of valproate exposure were identified by comparing DAF-16 dependent and DAF-2 dependent expression profiles

with the expression profile of valproate exposure (Figure 7 page 37). From these the DAF-16 dependent positively and negatively correlated expression profile of valproate exposure were identified by comparing nuclear DAF-16 dependent expression profile with the positively correlated expression profile of valproate exposure (Figure 8 page 38). In a similar manner identified the DAF-2 dependent negative, DAF-2 dependent positive, DAF-16 independent of DAF-2 dependent positive and DAF-16 independent DAF-2 dependent negative expression profiles.

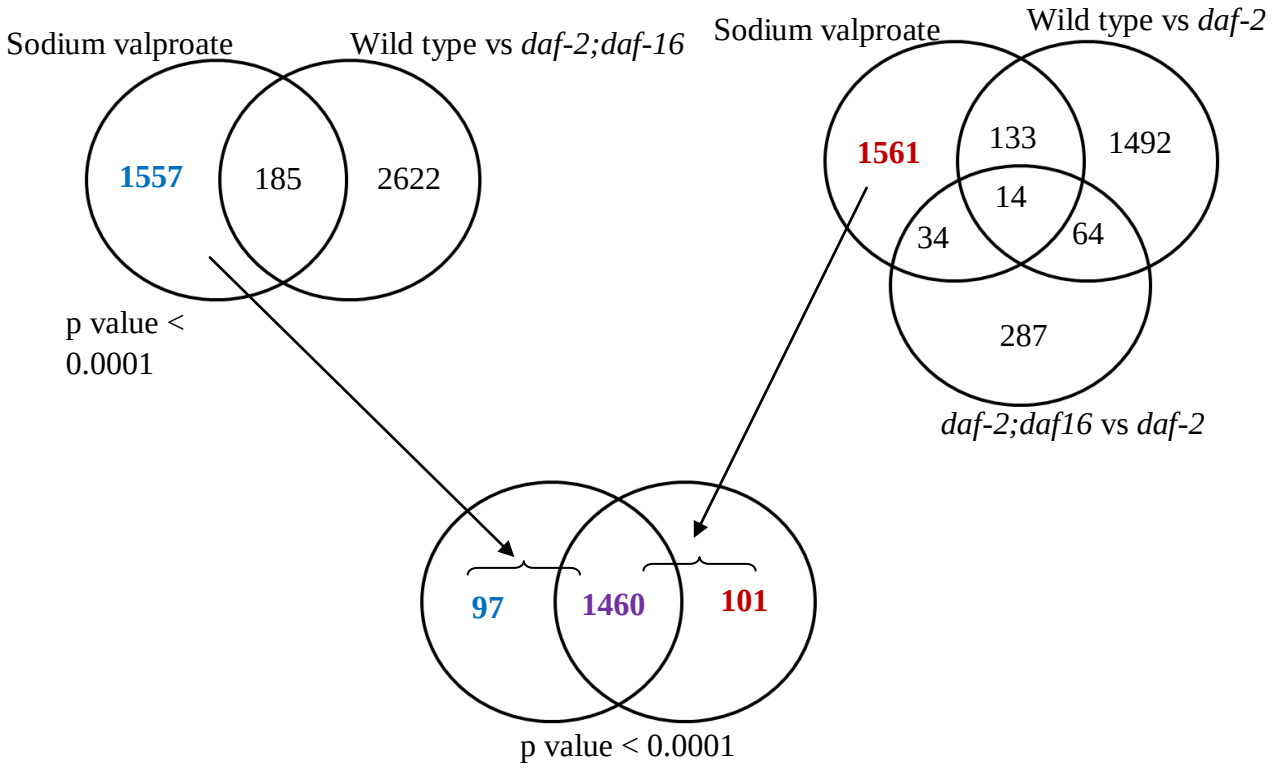

Figure 6 Insulin independent component of valproate exposure associated gene expression profile. Expression profiles of RNAinterference inactivated *daf-2* and *daf-2;daf16* double mutant (Murphy et al., 2003)were compared in Venn diagrams to identify the expression profile affected by valproate exposure independent of DAF-2 and DAF-16. There were 1460 expression profiles associated with the insulin independent component marked in purple.Sodium valproate indicates the expression profile of wild type *C.elegans* exposed to valproate for 24hrs at L4 stage. Expression profile with a threshold value of 1% BH (Bengamini Hochberg

correction) corrected p value are identified and compared with the significant expression profile identified by SAM with a false discovery rate (FDR) less than 1%. Probe IDs of the union of the two expression profiles are taken as the expresion profile associated with sodium valproate.

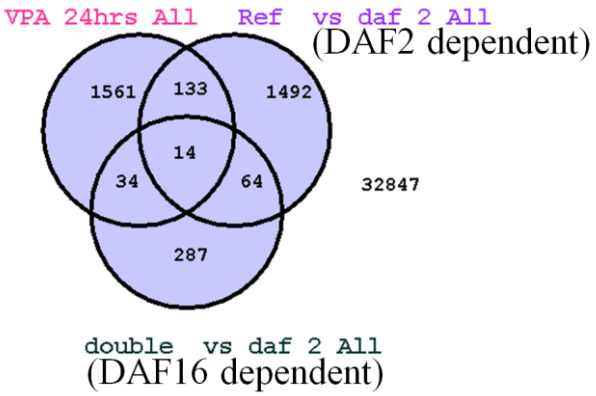

Figure 7 DAF-2 and DAF-16 dependent expression profiles were compared in a Venn diagram with the expression profile associated with valproate exposure to identify the DAF-16 dependent and DAF-2 dependent expression profiles of valproate exposure.Expression profiles of RNAinterference inactivated *daf-2* and *daf-2;daf16* double mutant (Murphy et al., 2003)were compared in Venn diagrams with the expression profile of wild type *C.elegans*exposed to sodium valproate. Sodium valproate indicates the expression profile of wild type *C.elegans* exposed to valproate for 24hrs at L4 stage. Expression profile with a threshold value of 1% BH (Bengamini Hochberg correction) corrected p value are identified and compared with the significant expression profile identified by SAM with a false discovery rate (FDR) less than 1%. Probe IDs of the union of the two expression profiles taken as the expression profile associated with sodium valproate.

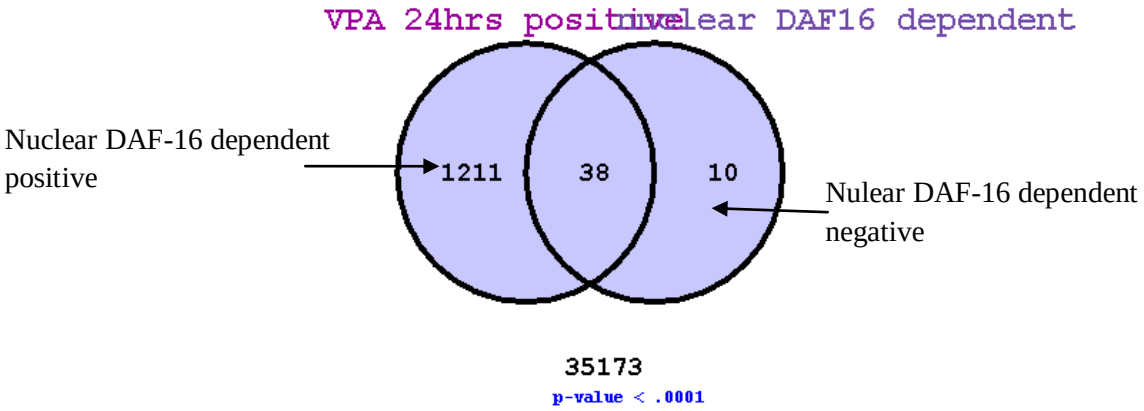

Figure 8 Nuclear DAF-16 dependent expression profile of valproate exposure is compared in a Venn diagram with the expression profile positively correlated with valproate exposure to identify the positively and negatively correlated expression profiles of valproate exposure dependent on nuclear DAF-16."VPA 24hrs positive" indicates the expression profile of wild type *C.elegans* exposed to valproate for 24hrs at L4 stage. Expression profile with a threshold value of 1% BH (Bengamini Hochberg correction) corrected p value are identified and compared with the significant expression profile identified by SAM with a false discovery rate (FDR) less than 1%. Probe IDs of the union of the two expression profiles are taken as the expression profile associated with sodium valproate. Positively correlated expression profiles are compared with nuclear DAF-16 dependent expression profile identified from RNA interference inactivated mutants of the study done by Murphy et al., 2003.

2.13 Identification of the TGF-β dependent and TGF-β independent expression profiles on valproate exposur

Expression profile associated with valproate exposure that depends on TGF-β pathway was identified by comparing the data set on valproate exposure with a microarray data set available in GEO database (accession number GSE15527) on TGF - β pathway mutant sma-6(wk7) and DBL over expressing strain. The raw data downloaded were

RMA normalized together and Affimetrix gene IDs were converted to Agilent IDs by the gene ID conversion tool available in DAVID. Genes with less than 20% NAs were chosen and the significant expression profile was selected by two class (unpaired) SAM for one colour. A threshold value of 1% FDR with 1fold change was used to select the significant expression profile.

GPR files of data (S1) and R codes used for analysis (S2) are provided as supplementary material.

3.0 PHENOTYPIC EFFECTS OF DIET, PHYSICAL EXERCISE AND VALPROATE EXPOSURE IN *C.ELEGANS*

3.1 Summary

Here the phenotypic effects of different feeding regimes, different levels of physical activity and different concentrations of sodium valproate in wild type and mutant strains in the insulin pathway is tested. To perform these studies we first had to devise an effective methodology for lipid quantification. Then a method to manipulate activity levels of *C.elegans* (level of exercise) was designed. After that the effect of diet, specifically cholesterol and monosodium glutamate, on the lipid levels in the nematode was tested and the relationship between exercise and diet was analysed. Finally the effect of valproate on lipid content and egg laying was measured and effects of valproate on components of insulin signalling pathway was investigated.

This initial study reveals cholesterol to increase lipid level in *C.elegans* while exercise and decreased lipid accumulation. In addition, the antiageing drug valproate was found to increase lipid accumulation in *C.elegans* in a dose dependent manner (Figure 9 page 41). This increase of lipid mass by valproate was found to be dependent on DAF-2 but independent of DAF-16. Comparison of insulin and TGFβ pathway mutants show an inhibitory effect of DAF-16 and DAF-1 on valproate induced lipid accumulation. This study shows the feasibility of using *C.elegans* as a model for lipid and exercise studies.

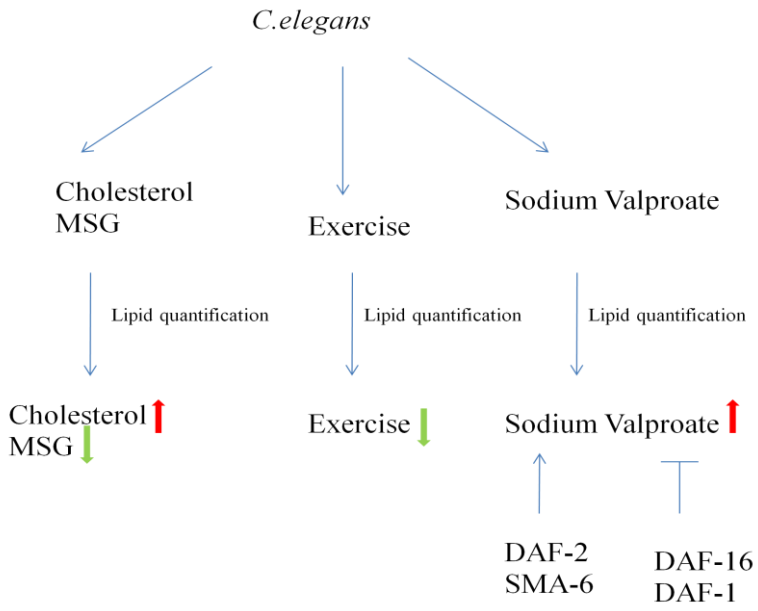

Figure 9 Summary of the methodology and conclusions. Lipid level was quantified in *C.elegans* treated with cholesterol, MSG, exercise or sodium valproate. Red arrows indicate an increase in lipid level and green arrows indicate a decrease in lipid level on each treatment. Increase in lipid due to valproate is further tested and it was found to depend on DAF-2 and SMA-6. DAF-1 and DAF-16 has an inhibitory effect on valproate induced lipid accumulation.

3.2 Results

3.2.1 Nilered staining of formalin fixed *C.elegans* can be used for lipid quantification

Since the overall objective of my work was the identification of molecular mechanisms underlying obesity in *C.elegans*, I first needed to develop a reliable assay to quantify lipid content in *C.elegans.* At the time I started this work, the gold standard methodology was Nile red staining of live *C.elegans.* This method has been used for several decades but recently its ability to provide reliable measurement in live worms has been questioned. As Nile red fails to stain major fat stores in live *C.elegans* and is rapidly degraded. Therefore, Nile red staining of fixed worms has been suggested to be

a more reliable method*(O'Rourke et al., 2009)*.The possibility of using this novel technique for lipid quantification was tested in *C.elegans* with some modifications(Chapter 2.4). To validate this technique we used mutants and dietary compounds that are known to increase lipid levels.

As expected*daf-2;* the *C.elegans* insulin receptor mutant and a mutant of NHR-80;(which is required for the expression of the *C.elegans* Δ9 desaturases FAT-5, FAT-6 and FAT-7)had higher amounts of total lipid, compared to wild type (Figure 10). *unc-22* is a twitching mutant, which resembled exercising worms and had similar lipid levels as wild type worms. Though twitching, *unc-22* moved slowly compared to wild type where net level of exercising may be similar to the wild type (data not shown).

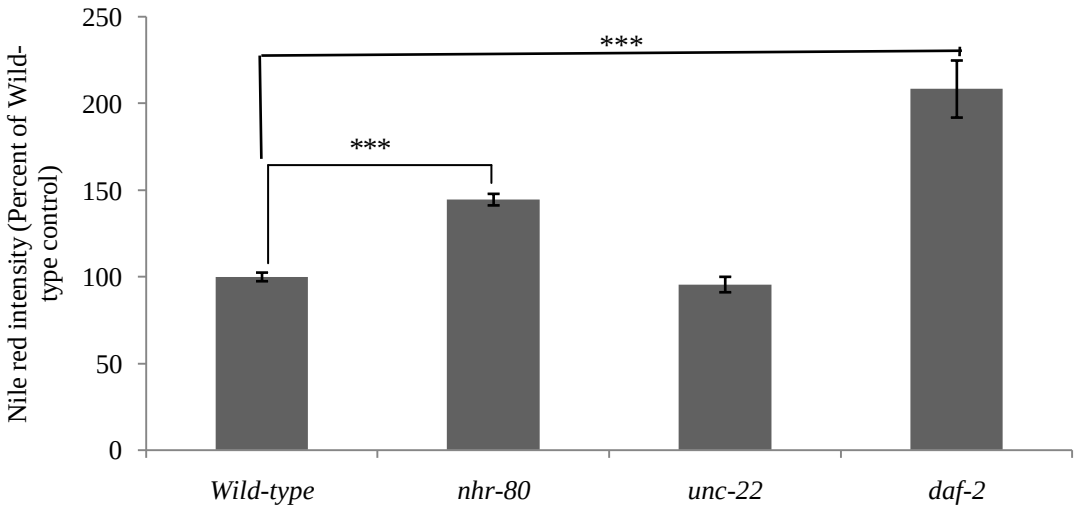

Figure 10Comparison of total lipid mass in mutants stained for lipid by Nile red staining of fixed *C.elegans*. C.elegans mutants and wild type were fixed with formalin and stained with Nile Red for total lipids at one day adult stage. *nhr-80* is defective in lipid metabolism and *unc-22* is a twitching mutant which mimics exercising and *daf-2* is an insulin receptor mutant. Error bars = ± SEM. *** = p value< 0.001.

Eggs are rich in lipids. To validate our lipid quantification method, lipid levels were quantified in both the nematode body where there are eggs and the area of the body without eggs (Figure11) using Nile red staining of fixed nematodes. Validating our methodology, it showed higher lipid content on eggs compared to the rest of the body when tested with t test at a p value < 0.001.

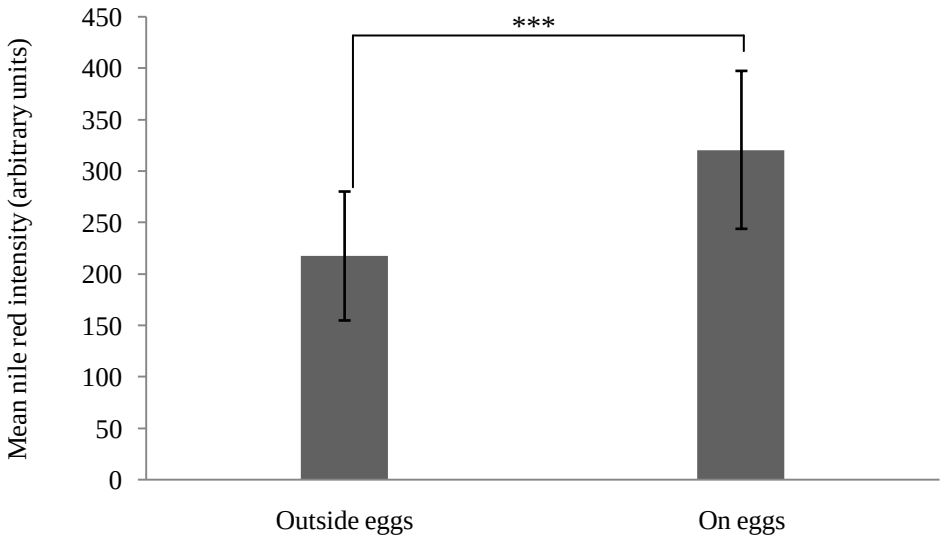

Figure11. Lipid mass detected by Nile red staining of fixed *C.elegans* at one day adult stage on areas with eggs and the rest of the body. Error bars = ± SEM. *** = p value< 0.001

3.2.2 Exercise drastically affect lipid levels in wt *C elegans*

Having shown the efficacy of the lipid quantification methodology, we then set to assess whether different levels of exercise can affect lipid content in *C.elegans*. In order to achieve this, increasing concentrations of agar were used to force the worms to use more energy when moving (Berri et al., 2009). We discovered that lipid content

decreased when nematodes were grown in concentrations of agar ranging between 5g/l to 10g/l (Figure 12, page 43). However, lipid content increased when agar concentration was raised to17g/l. At agar concentrations≥17g/l movement can be assessed by analysis of groves left on the surface of the agar when worms crawl. With increasing agar concentration above 17g/l, worms have a lower amount of total lipid.

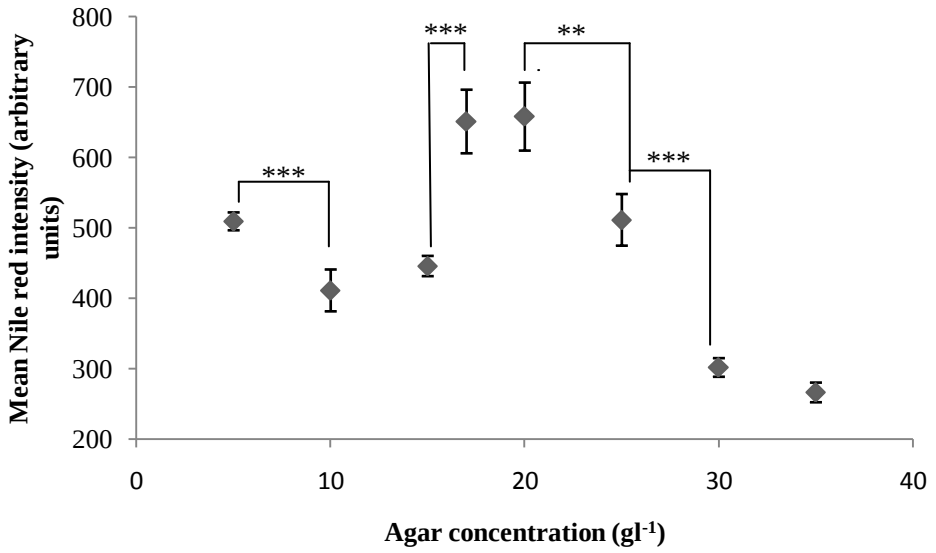

Figure 12Effect of agar concentration on the lipid mass of *C.elegans*. Wild type *C.elegans* was grown from L4 to one day adult stage on petridishes with different agar concentrations to mimic exercising. Lipid mass is measured with Nile red staining of fixed *C.elegans* at one day adult stage. Error bars = ±SEM, *** = p value < 0.001, ** = p value<0.005

3.2.3 Effects of cholesterol and MSG on lipid accumulation in wt*C.elegans*

Having demonstrated that exercise influences the amount of lipids, I then assessed the effects of diet on lipid accumulation. *C.elegans* treated with cholesterol shawed a dose dependent increase in lipid content when tested with Nile red staining of fixed nematodes (Figure 13). However, the food additive Monosodium Glutamate (MSG) had

the opposite effect, reducing lipid levels in a dose dependent manner (Figure 14). Any toxic effect was not observed at the MSG concentrations tested.

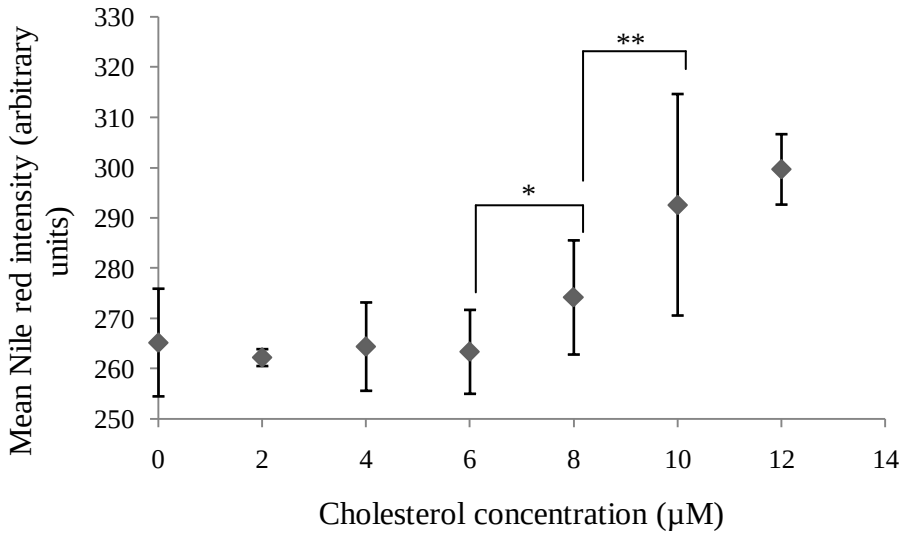

Figure 13Effect of cholesterol on *C.elegans* lipid levels. *C.elegans* were grown on OP50 agar plates with different concentrations of cholesterol from L4 stage for 24hrs and lipid level was measured using Nile red staining of fixed nematodes at one day adult stage. Error bars = ± SEM. ** = p value< 0.005. * = p value< 0.05.

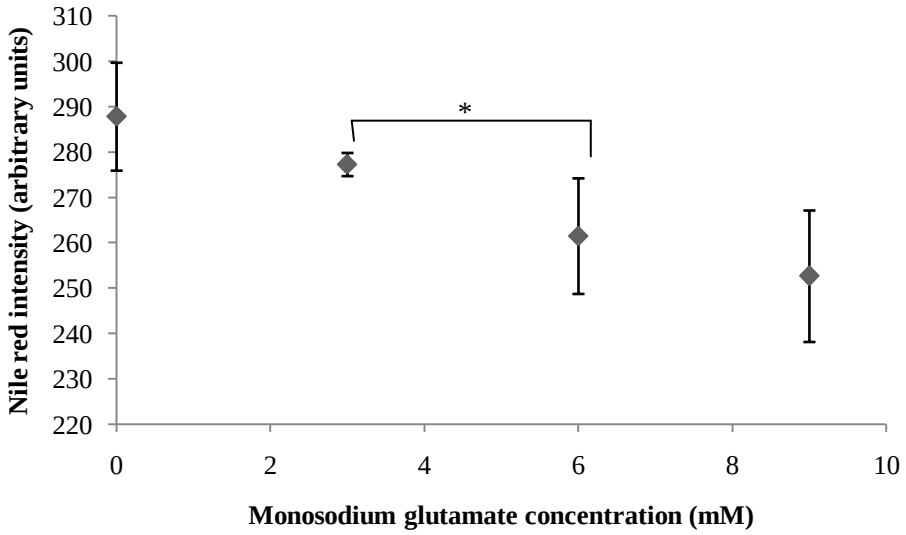

Figure 14Effect of Monosodium Glutamate on *C.elegans* lipid levels. *C.elegans* were grown on OP50 agar plates with different concentrations of monosodium glutamate from L4 stage for 24hrs and lipid level was measured using Nile red staining of fixed nematodes at one day adult stage. Error bars = ± SEM. * = p value< 0.05.

3.2.4 Interaction between exercise and diet

Since we demonstrated that exercise affects lipid content in worms, we then examined another important factor, which is the interaction between energy input and expenditure. More specifically, we focused on the interaction between diet and exercise. *C.elegans* were treated with cholesterol or food additive, monosodium glutamate and tested for lipid accumulation on exercise(Figure 15). Both exercise and monosodium glutamate decreased lipid accumulation significantly. Decrease of lipid accumulation due to exercise in cholesterol treated samples was not significant.

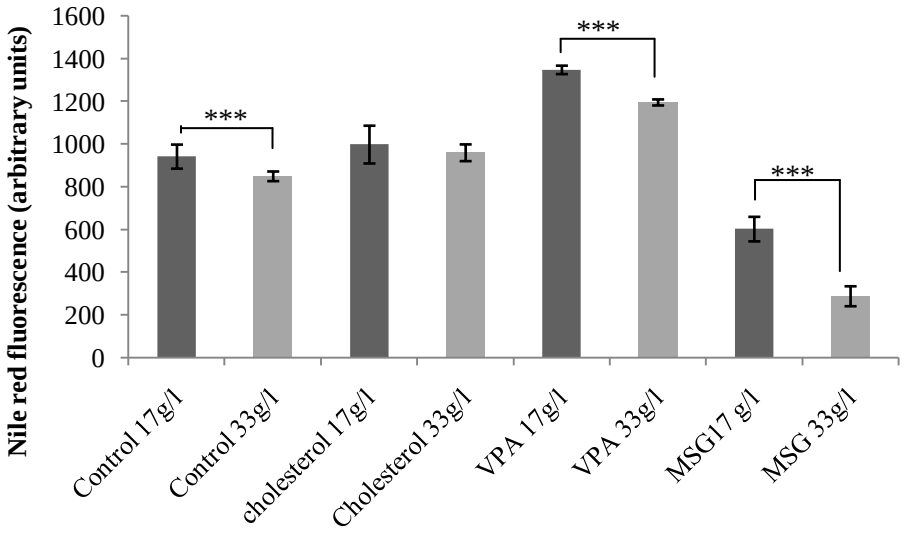

Figure 15 Exercise and monosodium glutamate reduce lipid accumulation. *C.elegans* were grown from L4 stage to one day adult stage on control, cholesterol(24µM), sodium valproate(VPA, 15mM) or monosodium glutamate(MSG, 24mM) plates with either 17g/l agar or 33g/l agar. Agar strength is changed to mimic exercising. Error bars = ± SEM. *** = p value< 0.005.

3.2.5 Effects of Valproate on lipid metabolism

After testing the effects of diet and exercise on lipid accumulation, we then tested the effect of the *C.elegans* lifespan extending drug, sodium valproate on lipid metabolism. Change in total lipid levels in response to valproate exposure is shown in Figure 16. We discovered a significant increase in lipid content between 1mM, 3mM and 9mM valproate and these three concentrations alone could explain the correlation of lipid mass to sodium valproate dose.

Having shown that valproate affects lipid metabolism, we also tested another lipid associated phenotype, defect in egg laying, observed in *C.elegans* on exposure to

valproate (Tokuoka et al., 2008). Egg laying had a perfect negative correlation with valproate dose (Figure 17).

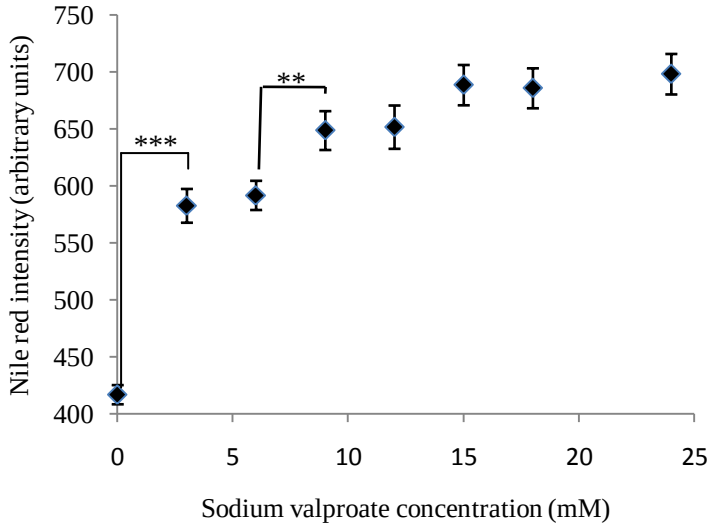

Figure 16Dose response of lipid mass. Figure shows dose response of lipid mass to valproate. Lipid mass measured by Nile Red staining of formalin fixed wild type *C.elegans* after exposure to drug for 24hrs at late L4 stage. Error bars ± SEM. ** p value < 0.01, *** p value < 0.001

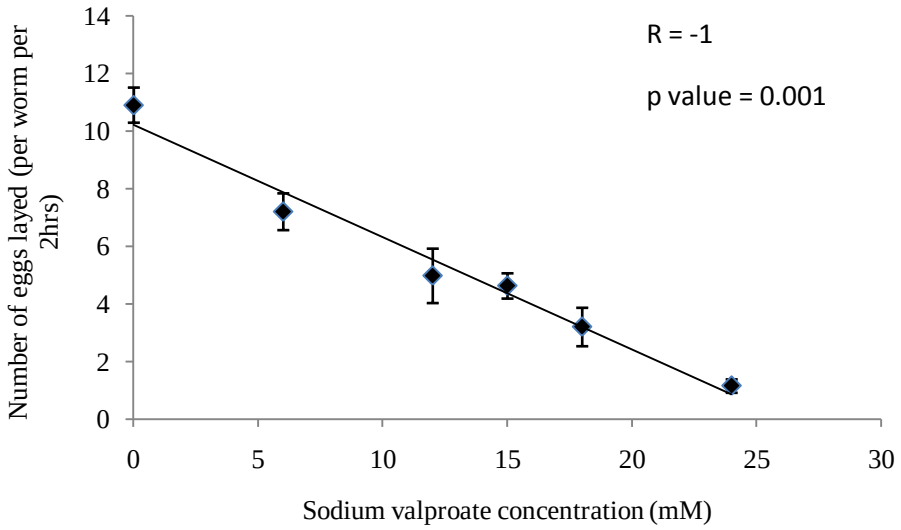

Figure 17. Correlation analysis of egg laying. Egg laying shows a perfect linear correlation with valproate dose. Egg laying assay was performed on one day adult worms on agar plates containing sodium valproate. Error bars ± SEM.

3.2.6 Effects of insulin pathway on valproate induced lipid accumulation

Having demonstrated that valproate increases lipid levels, we then tested the possible molecular mechanism of valproate induced lipid accumulation. Because the insulin signalling pathway is known to modulate fat metabolism, I tested the effect of perturbation of this pathways on valproate induced lipid accumulation. Specifically I tested the effect of down regulation of the genes coding for insulin receptor, *daf-2* and the FOXO transcription factor, *daf-16* on valproate induced lipid accumulation. Phenotypic analysis of the*daf-16* null mutant showed a significant increase of lipid mass on exposure to valproate compared to wild type control worms treated with same dose

of valproate. But*daf-2* the substitution mutant shows a decrease in lipid mass compared to control on exposure to valproate (Figure 18).

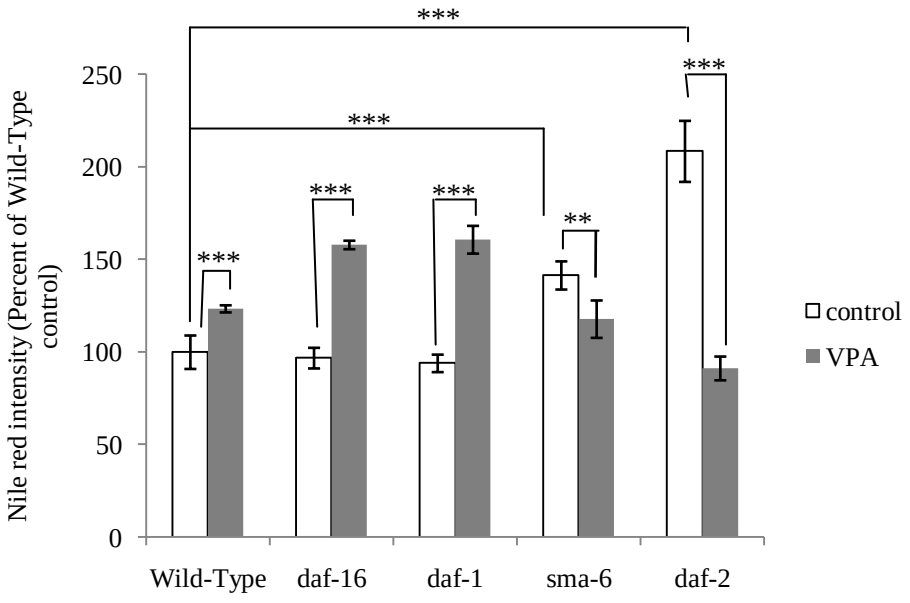

Figure 18Comparison of valproate effect on lipid mass of insulin and TGFβ pathway mutants. *daf-2* is the insulin receptor mutant and *daf-16* codes for the sole FOXO transcription factor, which acts down stream of *daf-2* and is negatively regulated by *daf-2*.*daf-1* codes for the part of receptor of TGF-β dauer pathway and *sma-6* codes for the part of the receptor of TGF-β sma/mad pathway.*C. elegans* exposed to 15mM sodium valproate at L4 stage for 24hrs. *sma-6* mutants show paralysis causing death on exposure to sodium valproate. *sma-6* mutants who survived are assayed for lipid content.

3.2.7 Comparison of insulin and TGFβ pathway mutants show a similar inhibitory effect of DAF-16 and DAF-1 on valproate induced lipid accumulation

After assessing the effect of insulin pathway on valproate induced lipid accumulation, we also tested the effects of the TGF-β pathway, which is also known to be involved in lipid metabolism, on the lipid accumulation induced by valproate. Specifically, we tested the effect of substitution mutation on *daf-1*, the type I receptor of the TGF-β dauer pathway and *sma-6*, the type I receptor of the TGF-β Sma/mad pathway. DAF-1, the type I receptor of TGF-β dauer pathway (Figure3 B, page 20) has an inhibitory effect

of valproate induced lipid accumulation, which is similar to the effect of DAF-16 (Figure3 A). Mutation of the type I receptor of Sma/Mab pathway (Figure3 C) causes a decrease in lipid when treated with valproate. *sma-6* mutants like *daf-2* insulin receptor mutants have high lipid mass compared to the wild type worms and valproate had an inhibitory effect on the lipid accumulation of these mutants. Unlike other mutants tested, *sma-6* mutants showed paralysis on exposure to valproate.

3.3 Discussion

C.elegans has been used extensively in lipid studies but this is the first time it has been used to study the link between the effects of exercise and obesity caused by valproate. The findings suggest *C.elegans* is a good model system to study obesity in a much simpler model, with different diets, variable exercise programs and ease of genetic manipulation. The availability of mutant lines for most genes also helps to dissect the underlying genetic mechanisms in obesity and exercise in *C.elegans*.

3.3.1*C.elegans* is a good obesity model

Obesity can be induced in *C.elegans* by genetic mechanisms, by varying diet or modifying exercising. For example in the present study it is found that mutants of fat metabolism such as *daf-2* and *nhr-80* accumulate fat. *daf-2*encodes the sole *C.elegans'* insulin receptor like protein. NHR-80 regulates expression of Δ9 desaturases fat-5,6 and 7 genes, which regulates fatty acid metabolism and accumulates more saturated fats(Brock and Watts, 2006).Cholesterol is a well-known dietary component that cause

obesity. The current study found that supplementation of cholesterol causes fat accumulation in wild type *C.elegans*. *C.elegans* are auxotrophs for sterol biosynthesis as they lack enzymes required for *denovo* biosynthesis of sterols (Matyash et al., 2001). Therefore, their sole source of cholesterol is from the diet and can be used to study the effects of differing concentrations of dietary cholesterol, without interference from *denovo* synthesized cholesterol. High fat diets are known to cause obesity in human and mice.

1.125% dietary monosodium glutamate (MSG) is known to cause weight gain, adiposity and reduce insulin sensitivity in feline models and it is known to cause obesity in human (Collison et al., 2009). Therefore, it is interesting to investigate how MSG may affect lipid levels and its underlying molecular mechanisms, as it is a food additive increasingly used in the fast food industry. A decrease in lipid levels was observed on exposure to MSG at the concentration range tested and may indicate a dose dependent difference in effects. These findings again suggest *C.elegans* is a good model system to study obesity.

3.3.2 Developing an effective methodology for lipid quantification in *C.elegans*

Several methods have been developed to study lipid content in nematodes. Sudan Black dye is found to be error prone in *C. elegans* due to washing steps with ethanol. Nile red staining of live *C.elegans* was a popular method as it provides a way to study lipid accumulation in the live nematode. However, the suitability of this method was questioned recently as it was found that Nile red is identified by the *C.elegans* as a foreign body and is directed to lysosoms for degradation. It is also suggested that this

has led to the misconception that *C.elegans* store fat in lysosomal bodies in the gut. Therefore lipid staining of formalin fixed *C.elegans* has been suggested. This method involves fixation of *C.elegans* with formalin followed by quick freeze thawing to crack the cuticle for Nile red staining. The stained *C.elegans* are mounted on agarose pads and Nile red fluorescence intensity is measured. This method has several drawbacks. Nile red gives fluorescence in hydrophobic environment and its fluorescence is quenched by water(Greenspan et al., 1985). When mounted on agarose pads, agarose gives high background fluorescence. Also mounting on agarose pads is time consuming and only a few samples can be done as Nile red loses its fluorescence with time. Therefore, the original method was modified to make it simple, quick and to reduce background staining. This is achieved by replacing the step of mounting on agarose pads with adding fixed stained *C.elegans* directly on to 96 well plates with 10µl water where they get attached to the plate bottom due to hydrophobic interactions. Nile red gives fluorescence in hydrophobic environments. Use of an aqueous environment for mounting reduces background fluorescence. Nile red tends to lose fluorescence intensity over time. This modified step reduces time taken and thus reduces the effect of loss of Nile red intensity during measurement between samples. This modified method shows *daf-2* mutants and cholesterol supplemented wild type *C.elegans* to have high fat levels in a dose dependent manner. Due to the high fat content of egg yolk, eggs are expected to have higher lipid levels than the rest of the body. Limitations of this novel method include the possible disruption of lipid stores on fixation with formalin and possible quenching of the signal by water in addition to background. It also does not provide any details of the types of lipids in the sample. Extraction of lipids into organic solvents followed by quantification using spectroscopy would be another possibility. However,

that will require the time consuming picking of individual worms and extraction may not be 100% efficient. Another option would be to quantify lipids using several of these methods and get the mode of the values. That will be time consuming and difficult to perform. Label free stimulated Raman scattering microscopy proposed as a better option but that requires special instrumentation(Wang et al., 2011). This modified Nile red staining of fixed worms provides an easy assay system to quantify lipid accumulation but requires fluorescence imaging facilities. Lipid quantification of *C.elegans* requires further improvements to make a reliable, simple assay system to quantify different types of lipids.

3.3.3 Exercising decreaseslipidmass in *C.elegans*

In this study, we have tested the effects of exercising on nematodes. The possibility of forcing *C.elegans* to do physical exercise is tested by growing them on agar plates with different agar concentrations ranging from 5g/l to 35g/l. Crawling on different concentrations of agar requires different amounts of energy (KIM et al., 1999) and it is therefore comparable to different amounts of physical exercise. *C.elegans* grown on 35g/l agar had the lowest amount of lipid. The total lipid level increased when agar concentration is decreased up to 20g/l. *C.elegans* makes a grove when crawling on agar surface and it needs more energy to crawl on high gel strength medium than soft agar as it may need to spend more energy to make a grove on high gel strength medium than in soft agar medium. This needs more caloric expenditure, which explains the observed results. Agar concentrations below 17g/l were soft and *C.elegans* showed burrowing and at 5g/l they changed to a swimming mode of movement. Burrowing may give more

exercise than swimming resulting in a lower level of lipid mass from 10g/l to 15g/l agar concentrations. Exercising *C.elegans* in liquid medium with varying densities may have been better because it will eliminate the possibility of changing mode of movement. But solid agar was preferred due to the difficulty of identifying contamination in liquid medium and difficulty of comparing data with other experiments.

Exercise also significantly reduced lipid level in *C.elegans* with accumulated fat due to sodium valproate (Figure 15, page 47). Exercising also reduced fat in wild type *C.elegans*and *C.elegans* treated with MSG but it failed to decrease lipid accumulated due to cholesterol. This may indicate an important medical phenomenon where lipid accumulation due to cholesterol may be resistant to exercise while lipid accumulation due to other factors may decrease by exercise. High density lipoprotein cholesterol is found to increase with increasing aerobic exercise training in men(Leon and Sanchez, 2001).Exercise reduce total serum cholesterol and triglycerides in women(Lokey and Tran, 1989).The observed differences in the Nile red intensity of Figure 13(page 45) and Figure 15(page 47)could possibly be due to a saturation effect. Other factors such as humidity, slight variations in temperature also affect growth of *C.elegans* and can cause variations in lipid level. With short life span, *C.elegans* also provides a good model system to study the effect of exercise on life span. This data suggest *C.elegans* to be a good model system to study the effects of exercise on lipid levels. The ideal method would be to monitor the energy expenditure on exercising and relate that with lipid level. This may be performed by measuring the amount of oxygen consumed or the carbon dioxide produced.

3.3.4 Increase of lipid mass by valproate is dependent on *daf-2* but independent of *daf-16*

Mutant analysis shows that valproate induced lipid accumulation requires both *daf-2* and *sma-6* activity but is independent of *daf-1* and *daf-16.* Activation of *daf-2* prevents nuclear localization of *daf-16* and its effects on transcription of downstream targets ((Tatar et al., 2003). Mutation of *daf-2* relieves this inhibitory effect on DAF-16, which may act probably via its downstream target genes to inhibit increase of lipid mass by sodium valproate. Valproate cause more lipid accumulation in *daf-1* and *daf-16* mutants than in wild type worms suggesting an inhibitory effect of DAF-16 and DAF-1 on valproate induced lipid accumulation. It has been suggested that DAF-16 may be acting as a repressor of metabolic genes that inhibit energy storage (Ogg et al., 1997) and the present study supports that.

To understand the molecular mechanisms of how insulin signalling pathway affect valproate induced lipid accumulation expression profiling was done on *C.elegans* following valproate exposure.

4.0 IDENTIFICATION OF TRANSCRIPTIONAL SIGNATURES LINKED TO VALPROATE EXPOSURE

4.1 Summary

In the previous chapter I describe a high fat phenotype observed in *C.elegans* following exposure to Sodium Valproate. I found that this lipid accumulation of valproate exposure is affected by the insulin signalling and TGF-β pathways. I also observed paralysis of the TGF-β Sma/Mad pathway type I receptor mutant in response to valproate indicating a novel neuronal phenotype. But what could be the possible molecular changes associated with these observed phenotypes?

In order to understand the underlying molecular changes associated with valproate exposure, I performed expression profiling on *C.elegans* exposed to different concentrations of Sodium Valproate. I saw a marked down regulation of nuclear components on exposure to valproate (Figure 19). By analysing these expression profiles, a possible hypothesis is generated to explain the increase of lipid accumulation in valproate exposure. In the last chapter I discuss the molecular changes of valproate exposure associated with neuronal function.

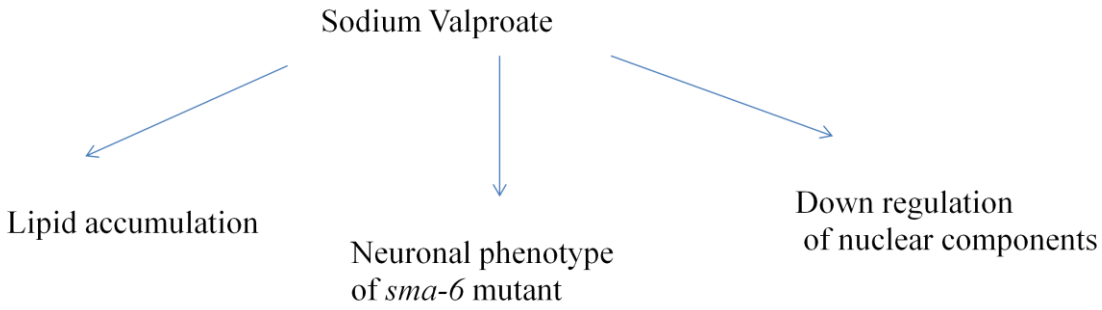

Figure 19 Diagram depicting the observations found during the present study on *C.elegans* exposed to valproate. The molecular changes associated with these observations are further tested by expression profiling of *C.elegans* treated with valproate.

4.2 Results

4.2.1 Correlation analysis

After showing that valproate has both metabolic and neuronal functions phenotypically, I assessed the molecular features associated with these phenotypes by microarray expression profiling. To do this, I first identified genes who's expression significantly varied on exposure to valproate, before investigating the correlation between valproate and lipid accumulation. Significantly changed gene expressions identified by correlation analysis with 1% BH corrected p value on valproate exposure identified an overall positively correlated gene expressions with a marked down-regulation in genes coding for components located in the nucleus. A positive correlation of cellular functions such as dephosphorylation, cellular detoxification, structural components and lipid metabolism (Table 3, page 61) are accompanied by a negative correlation of cell division, reproductive development process and neuron differentiation (Table 5, page 70). Lists of genes in each cluster are given in

Table 4 (page 63) and Table 6 (page 72). After identifying the significantly changed microarray expression profile associated with Valproate, I then put the positively correlated and negatively correlated expression profiles with valproate into functional groups using DAVID to identify any GO functional terms that were significantly enriched in each cluster.

4.2.1.1DAVID fucntional clustering of the positively correlated expression profile

The positively correlated expression profile of valproate exposure was enriched in the functional terms such as structural constituent of cuticle, phosphate metabolic process, lipid metabolism, carbohydrate binding, iron ion binding, limonene and pinene degradation and glutathione transferase.

A number of collagen genes are identified under the functional term 'structural constituent of cuticle'. Several uncharacterised phosphatases, serine/threonine kinases,

are among the genes under the functional term phosphate metabolic process. It also contains several hydroxysteroid dehydrogenases, which are involved in steroid synthesis(Stelzer et al., 2008), glycerol-3-phosphate dehydrogenase which links carbohydrate metabolism with lipid metabolism(Turyn et al., 2003) by converting dihydroxyacetone phosphate to glycerol-3-phosphate. This enzyme is involved in lipid biosynthesis by providing glycerol-3-phosphate for the formation of glycerol by dephosphorylation. Glycogen synthase kinase is also among that group. Glycogen synthase kinase phosphorylates its subject and inhibit glycogen synthesis(Jarvill-Taylor et al., 2001). Guanylate cyclase is also positively correlated with valproate under this category. Guanylate cyclase is involved in the synthesis of cGMP which signal for insulin secretion(Lucas et al., 2000). In addition to the above mentioned genes, several ABC transporters and multidrug resistance genes are also found under the functional term 'ATP binding'. Choline kinase B which catalyses the committed step of the formation of phosphocholine for phosphatidyl choline synthesis(Warden and Friedkin, 1985), the main phospholipid found in eukaryotic membranes is also positively correlated under this category. Glutamine synthase, which catalyses the formation of glutamine from glutamate terminating neurotransmission (Safran et al., 2010) is also found under this functional group. MAP kinase, which affects several biological functions is also among these positively correlated ATP binding category. Several UDP-glucuronosyl transferases and lectins are found under the functional terms 'lipid glycosylation' and 'carbohydrate binding'. Several cytochrome 450 genes were identified under the functional term 'iron ion binding. Tryptophan-2,3-dioxigenase, the enzyme that catalyzes the rate limiting step in tryptophan degradation via kynurenine pathway(Moroni, 1999) and phytanoyl-CoA dioxygenase which is involved in alpha-

oxidation of fatty acids (Wanders et al., 2003) are also included in this cluster with abnormal dauer formation genes *daf-9* and *daf-36*. emb-8 found in this cluster is known to code for NADPH cytochrome p450 reductase (Rappleye et al., 2003) that is predicted to function in fatty acid modification by reduction of P450 monooxygenase enzymes.

In addition to cytochrome p450 genes, enoyl-CoA hydrates which catalyse the second step in β-oxidation of fatty acids (Mittendorf et al., 1998) are identified under the functional term limonene and pinene degradation.

Acyl-CoA dhydrogenase and 3-hydroxyacyl-CoA dehydrogenase which catalyse the first and third steps in β-oxidation of fatty acids (Kantor et al., 2000) are found in the cluster 'oxidation reduction'. It also contains glucose-6-phosphate dehydrogenase which catalyses the rate limiting step in pentose phosphate pathway and makes NADPH required for lipid synthesis (Pandolfi et al., 1995).

In addition to these lipid metabolising genes, a number of major sperm proteins are also identified. These proteins are the most abundant proteins found in *C.elegans* sperm and they help the sperm to propel and once released they act as hormones that contracts oviduct and oocyte maturation. In addition to major sperm protein, spe-41 is a gene required for proper sperm oocyte interaction.

Several glutathione transferases involved in cellular detoxification are also enriched in the functional term 'glutathione transferase'.

Table 3 DAVID functional clustering of expression profiles positively correlated with valproate exposure. A threshold of 1% BH corrected p value is used to identify the significant expressions.

Cluster	Enrichment score	Term	Count	Benjamini
1	20.604504	SMART:PTPc	48	2.01E-25
		GOMF:phosphatase activity	79	5.66E-23
		SP_PIR:hydrolase	81	4.71E-04
2	15.848884	INTERPRO:Nematode cuticle collagen, N-terminal	56	6.12E-19
		INTERPRO:Collagen triple helix repeat	61	7.15E-18
		GOMF:structural molecule activity	99	3.80E-12
3	9.3937479	GOBP:phosphate metabolic process	151	3.70E-36
		GOBP:phosphorylation	96	1.11E-15
		SMART:SH2	26	6.30E-10
		GOMF:ATP binding	127	0.003548
		GOMF:adenyl nucleotide binding	134	0.003644
		GOMF:purine nucleotide binding	144	0.06807
4	9.3438724	INTERPRO:Metallophosphoesterase	28	1.28E-10
5	5.380872	SP_PIR:collagen	34	1.46E-09
		SP_PIR:cuticle	13	7.91E-04
6	5.2624126	INTERPRO:Glutathione S-transferase, N-terminal	20	1.83E-06
		INTERPRO:Thioredoxin fold	24	0.01276
7	5.0544358	GOBP:lipid glycosylation	16	3.09E-05
		INTERPRO:UDP-glucuronosyl/UDP-glucosyltransferase	23	5.97E-05
		GOMF:carbohydrate binding	31	0.041588
8	3.8045691	GOMF:iron ion binding	49	5.27E-04
		Cytochrome P450, conserved site	20	6.66E-04

		KEGG:Limonene and pinene degradation	8	0.006625
		GOMF:electron carrier activity	37	0.009878
		SP_PIR:Monooxygenase	19	0.013434
9	3.4384841	INTERPRO:Major sperm protein	27	5.39E-08
		INTERPRO:PapD-like	25	1.55E-07
		SP_PIR:cytoskeleton	21	0.109352
10	2.9954186	SMART:BRCT	11	0.00155
		INTERPRO:Ankyrin	17	0.100955
11	2.2248019	INTERPRO:Protein of unknown function DUF856, Caenorhabditis species	5	0.03768
12	2.0831552	SMART:CHK	8	0.054519
13	1.750404	PIR_SUPERFAMILY:glutathione transferase	8	0.15639
		KEGG:Metabolism of xenobiotics by cytochrome P450	6	0.090779
14	1.6786155	SMART:CLECT	32	0.121572
15	1.6736906	INTERPRO:NADH:flavin oxidoreductase/NADH oxidase, N-terminal	5	0.063405
16	1.4671233	PIR_SUPERFAMILY:gliadin	5	0.12707
17	1.431552	SMART:NRF	6	0.142466
18	1.3562886	INTERPRO:Protein of unknown function DUF38, Caenorhabditis species	35	0.038335
23	1.1386328	INTERPRO:2Fe-2S ferredoxin, iron-sulphur binding site	6	0.098803
26	0.9791065	INTERPRO:Heat shock protein Hsp20	6	0.166244
28	0.9443988	SMART:ZnMc	10	0.129871
29	0.8904833	KEGG:Fatty acid metabolism	8	0.164282
43	0.3840152	INTERPRO:ABC transporter-like	13	0.048339
		COG:Defense mechanisms	8	0.077149

Table 4 Lists of genes in each DAVID functional cluster of positively correlated with valproate expression profile identified by regression analysis with a BH corrected p value of 1% are shown in the table. Functional clusters with an enrichment score >2 with a p value < 0.01 are given.

Cluster	Term	Genes
1	GO:0016791~ phosphatase activity	R06B10.1, R06B10.2, ZK484.7, W03F11.4, PHOPHATASE, F23B12.1, T22C1.8, F52H3.6, F47B3.1, W01B6.6, Y57G11C.6, Y54G2A.24, Y62F5A.10, ZK783.5, F36H1.3, T20B6.1, F52E1.8, F42C5.5, Y113G7C.1, F55H12.5, C02B10.6, W03D8.2, C55B7.3, F20H11.4, C34D4.2, C17H12.5, Y105C5B.3, Y105C5B.15, C27A2.4, M05B5.1, C15H7.3, T16G12.7, Y22D7AR.12, C48B6.4, Y39B6A.18, Y22D7AR.7, M04G7.2, R09E10.9, GSP-3, C33H5.16, GSP-4, CDC-25.4, Y69E1A.4, T28F4.3, C46A5.1, Y41D4A.5, F22D6.9, F35C11.2, VHP-1, Y54F10BM.3, F13D11.1, C43E11.5, F40G12.10, B0207.1, C23G10.1, Y71H2AM.16, TYROSINE-PHOSPHATASE, F58G1.3, ZK354.8, ZK354.9, T13B5.3, F54F12.1, Y48G1C.5, ZK616.7, C24D10.1, R155.2, ZK938.1, H06I04.5, R155.3, C33F10.8, F47B3.6, C47A4.3, H25K10.1, F25B3.4, K07F5.6, T27A3.5, K07F5.8, F25H5.7, PPH-2, R13A5.11
2	GO:0042302~ structural constituent of cuticle	DPY-8, COL-58, DPY-4, DPY-20, COL-3, DPY-13, COL-156, COL-155, COL-94, COL-117, COL-152, COL-98, COL-113, COL-111, COL-112, COL-91, COL-90, COL-48, COL-13, COL-49, BLI-2, COL-150, BLI-1, SQT-2, SQT-1, LON-3, COL-85, COL-141, COL-88, COL-89, COL-107, COL-41, COL-103, COL-149, COL-182, COL-176, COL-71, COL-175, COL-137, COL-174, COL-173, COL-138, COL-79, COL-130, COL-77, COL-133, COL-73, COL-170, COL-126, COL-162, COL-127, COL-60, COL-167, ROL-1, COL-38, COL-39, ROL-6, ROL-8, COL-63
3	GO:0006796~ phosphate metabolic process	R06B10.1, K06H7.8, R06B10.2, C18H7.4, ZK666.8, F26A1.3, TAG-191, R10D12.10, ZK484.7, F48G7.10, F01D4.3, W09C3.1, C03C10.2, C14A4.13, W06F12.3, C27D8.1, F54H5.2, T22C1.8, F26E4.5, W03A5.1, F47B3.1, ZC449.3, ZC581.7, F42C5.5, F57B9.8, F55H12.5, C02B10.6, R13H9.5, M7.7, C55B7.3, F20H11.4, F26A1.4, T19D12.5, B0207.7, C56C10.6, ZC373.3, Y47G6A.13, R09E10.9, C33H5.16, CDC-25.4, DLK-1, H05L14.1, C46A5.1, F35C11.2, VHP-1, Y54F10BM.3, C43E11.5, F21F3.2, B0207.1, KIN-5, TYROSINE-PHOSPHATASE, T06C10.3, GCY-2, Y48G1C.5, ZK616.7, R155.2, ZK593.9, R155.3, C33F10.8, T25B9.4, C50F4.10, SPE-6, T05A7.6, PPH-2, D2024.1, C35E7.10, C05C12.1, Y69F12A.1, R03D7.5, T05C12.1, Y73B6A.1, W03F11.4, C25A8.5, W02B12.12, Y50E8A.6, B0218.5, TAG-344, Y116A8C.38, B0222.9, GPDH-1, Y57G11C.6, W01B6.6, FRK-1, F38E1.3, GSKA-3, Y62F5A.10, ZK783.5, F35C11.3, F36H1.3, Y39G8C.2, T20B6.1, W01B6.5, F25F2.1, ZK507.1, Y113G7C.1, M05D6.1, ZK945.6, B0252.1, VHA-19, C34F11.5, GCY-12, F59A3.8, F53C3.1, C17H12.5,

		ZK507.3, Y116A8C.24, Y43C5B.2, F59A6.4, C15H7.3, M05B5.1, KIN-26, Y22D7AR.12, C48B6.4, Y22D7AR.7, Y39B6A.18, M04G7.2, C28A5.6, T14E8.1, C08F8.6, D2045.5, F23C8.7, T28F4.3, Y41D4A.5, T15B12.2, C55C3.4, F41G3.5, F40G12.10, F36H12.8, K09C6.1, KIN-31, F36H12.9, MPK-2, Y18H1A.10, ZK354.6, C39H7.1, T11F8.4, ZK354.8, Y71F9AL.2, C49C8.1, F54F12.1, F09A5.2, C24D10.1, ZK354.2, H06I04.5, F47B3.6, ZK622.1, K07F5.6, K11C4.1, T27A3.5, HSD-3, K07F5.8, F25H5.7, R12G8.1
	GO:0005524~ ATP binding	K06H7.8, B0286.3, W02H5.8, C18H7.4, ZK666.8, F26A1.3, TAG-191, R10D12.10, F48G7.10, F01D4.3, HUM-8, W09C3.1, MRP-2, C03C10.2, C14A4.13, MRP-3, W06F12.3, HUM-5, C27D8.1, ABT-5, ABT-4, F54H5.2, ABT-2, ABT-1, F26E4.5, W03A5.1, ZC449.3, F57B9.3, ZC581.7, F57B9.8, R13H9.5, M7.7, M04C3.1, F26A1.4, T19D12.5, GARS∨AIRS∨GART, B0207.7, C56C10.6, ZC373.3, Y47G6A.13, DLK-1, H05L14.1, F21F3.2, KIN-5, T06C10.3, GCY-2, ZK593.9, WHT-4, WHT-5, HAF-7, T25B9.4, C50F4.10, WHT-8, WHT-6, SPE-6, T05A7.6, WHT-1, C35E7.10, D2024.1, C05C12.1, Y69F12A.1, R03D7.5, HSP-3, T05C12.1, Y73B6A.1, C25A8.5, CKB-2, SPE-15, W02B12.12, B0218.5, TAG-344, Y113G7B.14, B0222.9, Y116A8C.38, FRK-1, F38E1.3, GSKA-3, GLN-2, F35C11.3, Y39G8C.2, W01B6.5, F25F2.1, ZK507.1, M05D6.1, B0252.1, 6-PHOSPHOFRUCTOKINASE, C34F11.5, GCY-12, F59A3.8, F53C3.1, ZK507.3, Y116A8C.24, Y43C5B.2, F59A6.4, KIN-26, C28A5.6, T14E8.1, Y11D7A.14, C08F8.6, F23C8.7, D2045.5, TAT-2, T15B12.2, C55C3.4, F41G3.5, C01G12.8, C29F7.3, F36H12.8, K09C6.1, KIN-31, F36H12.9, MPK-2, ACT-5, Y18H1A.10, ZK354.6, C39H7.1, T11F8.4, Y71F9AL.2, C49C8.1, F09A5.2, PGP-1, ZK354.2, PGP-2, PGP-3, ZK622.1, K11C4.1, HSD-3, R12G8.1
4	IPR004843:Metallophosphoesterase	T16G12.7, R08C7.8, ZC477.2, GSP-3, GSP-4, Y69E1A.4, PHOPHATASE, F23B12.1, F22D6.9, F40B5.2, F52H3.6, Y40H4A.2, C23G10.1, F58G1.3, Y54G2A.24, ZK354.9, ZK938.1, C30A5.4, F44B9.9, W03D8.2, C47A4.3, H25K10.1, C34D4.2, F25B3.4, Y105C5B.3, Y105C5B.15, ZK856.5, R13A5.11
5	collagen	COL-58, COL-70, COL-175, COL-71, COL-3, COL-174, DPY-13, COL-155, COL-173, COL-117, COL-115, COL-113, COL-79, COL-111, COL-112, COL-110, COL-91, COL-90, COL-73, COL-48, COL-13, COL-49, COL-170, BLI-1, SQT-1, LON-3, COL-104, COL-167, COL-88, COL-141, COL-107, COL-103, COL-39, ROL-6, ROL-8
6	IPR004045:Glutathione S-transferase, N-terminal	GST-15, Y45G12C.3, F56A4.4, GST-42, GST-14, GST-29, GST-16, GST-39, GST-38, GST-33, GST-24, GST-7, GST-8, GST-22, GST-5, GST-6, GST-20, GST-31, GST-13, GST-12, GST-30
7	GO:0030259~lipid glycosylation	UGT-16, UGT-28, UGT-39, UGT-33, UGT-41, UGT-20, UGT-44, UGT-13, UGT-1, UGT-54, UGT-25, UGT-36, UGT-47, UGT-8, UGT-40, UGT-7
	IPR002213:UDP-glucuronosyl/	UGT-29, UGT-16, UGT-39, UGT-19, UGT-28, UGT-33, UGT-22, UGT-32, UGT-41, UGT-44, UGT-20, UGT-13, UGT-54, UGT-1, UGT-25, UGT-36, UGT-47, UGT-5, UDP-GLUCOSYLTRANSFERASE, UGT-62, UGT-40, UGT-8, UGT-7

	UDP-glucosyltransferase	
	GO:0030246~carbohydrate binding	T10E10.4, LEC-7, UGT-28, CLEC-85, UGT-41, CLEC-67, UGT-44, UGT-20, UGT-25, UGT-47, CLEC-168, CLEC-44, CLEC-167, UGT-40, CLEC-68, CLEC-169, LEC-11, LEC-10, UGT-16, W04B5.3, CLEC-117, UGT-39, UGT-33, UGT-13, UGT-1, UGT-54, PQN-74, UGT-36, CLEC-79, UGT-8, UGT-7
8	GO:0005506~iron ion binding	CYP-13A2, CYP-13A6, CYP-13A7, CYP-13A4, CYP-13A5, CYP-13A8, MLT-7, PHOPHATASE, F23B12.1, GLB-32, CYP-43A1, F52H3.6, CYP-33C8, CYP-14A3, B0222.9, Y54G2A.24, VEM-1, W03D8.2, C28H8.11, Y105C5B.9, C34D4.2, CYC-2.2, CYP-33D3, CYP-35C1, DAF-9, T16G12.7, GSP-3, GSP-4, Y69E1A.4, CYP-33B1, CYP-33E2, CYP-33E3, F22D6.9, F55B11.1, DAF-36, C23G10.1, F58G1.3, ZK354.9, F15E6.6, CYP-34A8, EMB-8, CYP-34A6, ZK938.1, CYP-13A12, C47A4.3, CYP-35A3, F25B3.4, CYP-36A1, R13A5.11
	IPR001128:Cytochrome P450	DAF-9, CYP-13A2, CYP-34A8, CYP-13A6, CYP-13A7, CYP-34A6, CYP-13A4, CYP-13A5, CYP-13A8, CYP-13A12, CYP-33B1, CYP-33E2, CYP-33E3, CYP-35A3, CYP-33D3, CYP-43A1, CYP-35C1, CYP-36A1, CYP-33C8, CYP-14A3
	cel00903:Limonene and pinene degradation	ECH-6, CYP-13A2, CYP-13A6, CYP-13A7, CYP-13A4, CYP-13A5, CYP-36A1, CYP-13A8
	GO:0055114~oxidation reduction	DAF-9, W01C9.4, CYP-13A2, CYP-13A6, ACDH-4, CYP-13A7, CYP-13A4, CYP-13A5, F54C8.1, CYP-13A8, ACDH-2, CYP-33B1, CYP-33E2, T05C12.3, ACDH-8, DHS-25, F39B2.3, F55B11.1, Y50E8A.6, Y9C9A.16, SOD-5, CYP-33C8, CYP-14A3, DAF-36, GPDH-1, R05D8.7, FMO-3, F36A2.3, ZC449.3, CYP-34A8, CYP-34A6, Y39G8B.1, C28H8.11, CYP-13A12, Y105C5B.9, CYP-35A3, CYC-2.2, CYP-33D3, F02C12.2, CYP-35C1, GLUCOSE-6-PHOSPHATE-1-DEHYDROGENASE, DHS-14, HSD-3, Y54E5A.1, CYP-36A1
9	IPR000535:Major sperm protein	F38H4.6, MSP-31, MSP-32, Y48B6A.5, MSP-36, ZC262.1, Y38F2AR.10, MSP-113, Y59E9AR.7, ZK1248.4, C10H11.7, C35E7.9, SSP-11, F13A7.1, MSP-40, MSP-152, Y59E9AR.1, SSP-16, Y53F4B.19, R05D3.5, Y23H5A.4, MSP-142, F42A9.7, C14A4.8, MSP-56, MSP-57, ZK1307.4, MSP-59, MSP-53, MSP-19, MSP-55, T13F2.12, DCT-9, F58A6.9, MSP-10, F36H12.3, MSP-64, MSP-63, MSP-65, SSP-9, K06A5.3, F52F12.8, C35D10.11, SSP-32, MSP-45, ZK354.7, F58E6.5, C35A5.4, MSP-81, C36H8.1, MSP-49, C25D7.1, F44D12.3, MSP-76, F44D12.5, MSP-74, F44D12.7, MSP-51, MSP-50
	GO:0043228~non-membrane-bounded organelle	F38H4.6, MSP-31, Y48B6A.5, MSP-32, MSP-36, Y38F2AR.10, MSP-113, Y73B6A.1, HUM-8, Y59E9AR.7, HUM-5, SPE-15, TBA-8, ZK1248.4, TBA-7, C10H11.7, C35E7.9, TBB-6, F13A7.1, MSP-40, MSP-152, Y59E9AR.1, W02A2.5, Y53F4B.19, Y113G7C.1, Y19D2B.1, DLC-6, Y23H5A.4, MSP-142, F42A9.7, F55D12.6, MSP-56, MSP-57, ZC155.2, MSP-59, MSP-53, MSP-19, MSP-55, Y11D7A.14, F58A6.9, MSP-10, F36H12.3, MSP-64, MSP-63, MSP-65, HIS-70, K06A5.3, F52F12.8, ACT-5, ZK354.7,

		MSP-45, F58E6.5, Y48G1C.5, C35A5.4, T06E4.5, MSP-81, H06I04.5, C36H8.1, MSP-49, C25D7.1, MSP-76, MSP-74, MSP-51, SPE-41, MSP-50, ZK1251.1
10	IPR002110:Ankyrin	F26D2.10, C49G7.1, Y47D3A.22, F36D3.5, C01G10.1, H32C10.3, C18H2.3, C18H2.5, T08G3.7, K02F6.4, SPE-41, Y75B7B.2, M60.7, K02F6.2, F37A4.4, Y67A10A.3, F40E12.2
11	IPR008574:Protein of unknown function DUF856, Caenorhabditis species	F58A6.5, Y37D8A.5, K06A5.2, Y69E1A.1, W03D8.10
12	SM00587:CHK	Y45G12C.4, F56A4.5, F59B1.8, F59B1.10, C29F7.2, C29F7.1, T16G1.5, E02C12.8, T16G1.6
13	PIRSF000503: glutathione transferase	GST-42, GST-38, GST-7, GST-8, GST-5, GST-22, GST-6, GST-30

4.2.1.2 DAVID fucntional analysis of the negatively correlated expression cluster

Genes showing negative correlated expression profiles following valproate exposure were enriched in functional terms such as cell division, DNA replication, regulation of transcription, mediator complex and RNAII transcription factor activity. The genes negatively correlated under the functional term cell division include*mes-1* involved in the positioning of early mitotic spindle and associated P granules(Berkowitz and Strome, 2000), *ptc-1* required for the isolation of meiotic nuclei from one another(Bürglin and Kuwabara, 2006), *pig-1* gene product required for normal polarity in asymmetric cell division yielding apoptotic cells vs neurones(Chien et al., 2013), *cdk-5* that affects pronuclear migration (Park et al., 2012, Goodwin et al., 2012), *sqv-5* which encodes a chondroitin synthase that is required for cytokinesis; gonad migration

and vulval morphogenesis (Herman et al., 1999, Yamada et al., 1999, Toyoda et al., 2000), *let-99* required for mitotic spindle orientation(Tsou et al., 2002),*evl-20* required for micron cytokinesis (Antoshechkin and Han, 2002, Radcliffe et al., 2000, Bhamidipati et al., 2000), *cks-1,* which encodes the cyclin dependent protein kinase regulatory subunit that inactivates M-phase promoting factor (Polinko and Strome, 2000), *mei-1* and *mei-2* required for oocyte meiotic spindle formation(Mains et al., 1990, Clark-Maguire and Mains, 1994), *mau-2* required for mitotic chromosome segregation; egg laying and axonal migration (Hekimi et al., 1995, Takagi et al., 1997, Bénard et al., 2004, Seitan et al., 2006), *knl-1* and *knl-3*; the components of kinetochore required for spindle elongation and chromosome separation (Gönczy et al., 2000, Desai et al., 2003, Cheeseman et al., 2004), ligase, *puf-3* required for spindle positioning (Piano et al., 2000, Wickens et al., 2002), *cpg-1* which codes for chondroitin proteoglycan required for chromosomal segregation during meiosis (Lee and Schedl, 2001, Kamath et al., 2003) and*cdc-26,* which codes for anaphase promoting complex (Li et al., 2004, Dong et al., 2007).

DNA polymerase, DNA helicase, *cel-1*; an mRNA capping enzyme, ligase, *rnr-2* ; a ribonucleotide reductase, which synthesises deoxyribonucleotides from ribonucleotides, *rfc-2* and *rfc-3* ; DNA replication factors, *pcn-1,*which codes for proliferating cell nuclear antigen ; an essential component of DNA replication and repair machinery are enriched in the functional term ‘DNA replication’.

nhr-66 a transcription factor whose expression is known to up-regulate on exposure to cholesterol(Novillo et al., 2005, Miyabayashi et al., 1999), histone deacetylase 6 which repress transcription, *isw-1* which codes for a chromatin remodelling protein(Andersen et al., 2006), *lin-40* which forms part of the nucleosome remodelling and histone

deacetylation (NURD) complex(Solari and Ahringer, 2000, Chen and Han, 2001), transcription initiation factor IIA small chain homolog, *met-2* a histone methyltransferase, *spr-2*, which codes for a member of the SET protein complex that functions in chromatin remodelling; DNA repair and transcriptional regulation (Wen et al., 2000, Fan et al., 2003),*atf-2* which activates transcription factor 2(Wang et al., 2006),*lsd-1* a lysine specific histone demethylase that repress transcription comes under the functional term regulation of transcription.

In addition to these chromatin remodelling and general transcription factors several transcription factors involved in neurone growth and differentiation are also found in this cluster. They include *ceh-30* which is involved in neuronal cell fate; determination(Peden et al., 2007), *ast-1* which codes an ETS-box transcription factor that is required for proper initiation and maintenance of dopamine neuron fate which itself is regulated by LIN 11(Hutter et al., 2005, Schmid et al., 2006, Flames and Hobert, 2009),*egl-43* which is egg laying defective and affects HSN cell migration and the development of the phasmid neurones(Desai et al., 1988),*unc-120* required for locomotion and muscle development,*ceh-36* which codes for a transcription factor required for specification of the AWC olfactory neuron and for establishing left-right asymmetry of the ASEL and ASER gustatory neurons(Lanjuin et al., 2003), *pcaf-1* which codes *C.elegans'* sole histone acetyl transferase, *lim-4* which is required for differentiation of AWB chemosensory neurones; some RID motor neurone differentiation; expression of *ser-2* and SAA neutrite outgrowth(Sagasti et al., 1999, Tsalik et al., 2003); *lin-32* required for the development of neurones(Mitani et al., 1993), *cfi-1* which acts downstream of LIN-32 and affects differentiation of URA sensory neurone; AVD and PVC inter-neurones(Shaham and Bargmann, 2002), *unc-130*

that affects the generation of AWA and ASG chemosensory neurones and is required for the expression of *unc-129* TGFβ guidance factor(Sarafi-Reinach and Sengupta, 2000), *unc-42* which are egg laying defective and is required to specify the fate of ASH sensory neurones, AVA; AVD and AVE interneurones and some motor neurones(Wightman et al., 1997, Baran et al., 1999, Brockie et al., 2001).

Several other genes coding for transcription factors including *egl-18* which is egg laying defective, *nhr-40* a nuclear hormone receptor where the mutants are slow moving and uncoordinated with reversing direction and going in circles and several components of the transcription mediator complex *rgr-1; mdt-8; mdt-11* and *mdt-15* are enriched in the functional term 'regulation of transcription'. It is observed that *C.elegans* goes in circles and change direction more frequently on exposure to valproate. Several components of the mediator complex and the RNAII transcription factor activity are also negatively correlated with valproate.

A striking feature of this negatively correlated expression profile of valproate exposure is that most of them code for nuclear components. The above analysis identified the molecular pathways linked to this down regulation of nuclear components. Ninety-two of them made a single network indicating a common mechanism for gene expression, which is affected by valproate. Most of them are interconnected with *rfc-3* having the highest connectivity score (Figure 20, page74). *rfc-3*is connected to 27 components out of the 92 interconnected components (Table 7, page 75). The top ten genes found in this search are mapped in WormNet to identify their connectivity among themselves and is given in Table 8. Therefore*rfc-3* could be a key gene through which down-regulation of nuclear components occur following valproate exposure. To identify the regulators of these pathways, I looked at the transcription factors connected to these components.

vab-3 is the transcription regulator that had the highest connectivity score. It was connected to 7 components implying it to be a key regulator of the negative correlation of nuclear components with valproate dose. Since *vab-3* is also down-regulated on exposure to valproate, it may be having an inhibitory effect on a key component that cause down regulation of genes coding for nuclear components. TheWnt signalling pathway, which has been described previously to be involved in valproate exposure(Gurvich and Klein, 2002) regulates *vab-3* expression (Johnson and Chamberlin, 2008). I also mapped the transcription factors identified in this analysis on WormNet to find the transcription factor with highest connectivity to other transcription factors which are negatively correlated and that was also found to be *vab-3* (Figure 21, page80). vab-3 is also positively regulated by RNA polymerase II promoter supporting the hypothesis that valproate may be acting on this promoter to bring its effects. *sma-6*, *daf-2* and *daf-16* which are found to be involved in valproate induced lipid accumulation in the phenotypic analysis are connected to this cluster of transcription factors via *unc-3*, an immunoglobulin domain containing transcription factor.

Table 5 DAVID functional clustering of gene expression profiles negatively correlated with valproate. A threshold of 1% BH corrected p value is used to identify the significant expressions.

Cluster	Enrichment score	Term	Count	Benjamini
1	5.418025	GOBP:tissue morphogenesis	50	8.70E-05
		GOBP:morphogenesis of an epithelium	48	1.06E-04
		GOBP:reproductive developmental process	86	0.003037
		GOBP:hermaphrodite genitalia development	74	0.003626
		GOBP:sex differentiation	80	0.003775

2	4.5862188	SP_PIR:cell cycle	18	6.34E-05
		GOBP:cell division	29	0.004132
3	2.7895358	GOBP**:**DNA replication	14	0.006634
		GOBP:DNA metabolic process	21	0.086511
		KEGG:Mismatch repair	6	0.099903
		KEGG:Base excision repair	5	0.198048
4	2.333731	INTERPRO:Immunoglobulin-like fold	13	0.067869
5	2.1367808	SP_PIR:nucleus	80	3.93E-04
		SP_PIR:Homeobox	18	4.73E-04
		GOMF:DNA binding	79	0.087607
		SMART:HOX	18	0.14043
		SP_PIR:dna-binding	47	0.075483
6	2.0183949	GOCC:nucleoplasm	11	0.019123
		GOCC:nuclear lumen	12	0.064516
		GOCC:Srb-mediator complex	5	0.123916
		GOCC:intracellular organelle lumen	14	0.157436
8	1.9788232	GOCC:chromatin	12	0.003851
9	1.9677001	SP_PIR:sh3 domain	8	0.072719
10	1.9072694	GOBP:cellular component morphogenesis	20	0.036085
		GOBP:neuron differentiation	13	0.062106
		GOBP:cell projection organization	14	0.079005
		GOBP:cell motion	15	0.145949
11	1.8748935	GOBP:chromosome organization	24	0.003969
		GOBP:kinetochore assembly	4	0.088987
		GOBP:centromere complex assembly	4	0.088987
13	1.7863499	SP_PIR:tpr repeat	7	0.079355
16	1.7044824	GOBP:cell cycle	42	0.004196

17	1.6861614	SP_PIR:wnt signaling pathway	6	0.076356
19	1.5877662	GOBP:glycosaminoglycan metabolic process	4	0.052188
25	1.345056	SP_PIR:glycoprotein	39	0.037395
		SP_PIR:signal	34	0.150913
27	1.2345633	GOBP:protein-DNA complex assembly	9	0.088448
41	0.9299484	SP_PIR:mitosis	7	0.177892
63	0.5220007	SP_PIR:myristate	6	0.103074

Table 6 Lists of genes in each DAVID functional cluster of down-regulated valproate correlated expression profile identified by regression analysis with a BH corrected p value of 1% are shown in the table. Functional clusters with an enrichment score >2 with a p value < 0.01 are given.

Cluster	Term	Genes
1	GO:0003006 ~reproductive development al process	LIN-17, C31H1.8, EGL-43, SDZ-30, EVL-14, MIG-14, GFI-2, SQV-5, SOX-2, DPY-17, Y65B4A.6, HCP-3, SEM-5, MOM-1, M01B12.5, ARL-5, CEH-30, HTZ-1, CE7X_3.2, CYK-1, TAG-246, KNL-1, UNC-61, KNL-3, F39B2.1, Y65B4BR.8, MCM-7, F33H2.5, CLEC-1, CPG-1, KBP-4, CSN-1, EGL-18, Y110A7A.8, NPP-4, F42G2.6, ABI-1, R08C7.4, VAB-1, CHTL-1, SCC-1, MET-2, KBP-1, TCL-2, UFD-2, ANI-1, UBA-2, ISW-1, LIN-40, WEE-1.3, DSH-2, F25B5.2, CPAR-1, RFC-3, EIF-3.E, C06A5.3, EVL-20, ZK858.1, RSP-6, RSP-5, TEN-1, ZK616.4, C07A9.2, GEI-17, ZK686.1, UNC-6, C15C6.4, UNC-5, T20B12.1, F48C1.4, COGC-3, RNP-6, SYS-1, SAN-1, F09F9.4, DPY-22, NCBP-1, F25H5.5, Y71G12B.11, UTX-1, LIN-54, LIN-53, RNR-2, MES-4, LSY-12, DMD-5
	GO:0048806 ~genitalia development	LIN-17, EGL-43, SDZ-30, EVL-14, MIG-14, GFI-2, SOX-2, DPY-17, Y65B4A.6, HCP-3, MOM-1, SEM-5, M01B12.5, CE7X_3.2, HTZ-1, CYK-1, TAG-246, KNL-1, UNC-61, KNL-3, F39B2.1, Y65B4BR.8, MCM-7, F33H2.5, CLEC-1, KBP-4, CSN-1, EGL-18, Y110A7A.8, NPP-4, F42G2.6, ABI-1, R08C7.4, CHTL-1,

		SCC-1, MET-2, KBP-1, TCL-2, ANI-1, UBA-2, ISW-1, LIN-40, F25B5.2, DSH-2, RFC-3, CPAR-1, EIF-3.E, C06A5.3, EVL-20, ZK858.1, RSP-6, RSP-5, ZK616.4, C07A9.2, GEI-17, ZK686.1, C15C6.4, T20B12.1, F48C1.4, COGC-3, RNP-6, SYS-1, SAN-1, F09F9.4, DPY-22, NCBP-1, F25H5.5, Y71G12B.11, UTX-1, LIN-54, LIN-53, RNR-2, LSY-12, DMD-5
	GO:0007548 ~sex differentiation	LIN-17, EGL-43, SDZ-30, EVL-14, MIG-14, GFI-2, SQV-5, SOX-2, DPY-17, Y65B4A.6, HCP-3, SEM-5, MOM-1, M01B12.5, ARL-5, CEH-30, HTZ-1, CE7X_3.2, CYK-1, TAG-246, KNL-1, UNC-61, KNL-3, F39B2.1, Y65B4BR.8, MCM-7, F33H2.5, CLEC-1, KBP-4, CSN-1, EGL-18, Y110A7A.8, NPP-4, F42G2.6, ABI-1, R08C7.4, CHTL-1, SCC-1, MET-2, KBP-1, TCL-2, ANI-1, UBA-2, ISW-1, LIN-40, F25B5.2, DSH-2, CPAR-1, RFC-3, EIF-3.E, C06A5.3, EVL-20, ZK858.1, RSP-6, RSP-5, TEN-1, ZK616.4, C07A9.2, GEI-17, ZK686.1, UNC-6, C15C6.4, UNC-5, T20B12.1, F48C1.4, COGC-3, RNP-6, SYS-1, SAN-1, F09F9.4, DPY-22, NCBP-1, F25H5.5, Y71G12B.11, UTX-1, LIN-54, LIN-53, RNR-2, LSY-12, DMD-5
2	GO:0051301 ~cell division	F22B3.4, MES-1, PTC-1, CDK-5, PIG-1, CDC-25.2, MCM-5, F23C8.9, ANI-1, SQV-5, LET-99, C28C12.2, CYK-1, EVL-20, CKS-1, MEI-1, MEI-2, MAU-2, KNL-1, KNL-3, ZK353.1, LIG-1, MCM-7, PUF-3, CPG-1, CDC-26, CSN-1, PCN-1, INSC-1
3	GO:0006260 ~DNA replication	DNA-2, Y57A10A.15, DIV-1, CEL-1, MCM-5, LIG-1, F23C8.9, MTSS-1, MCM-7, F33H2.5, RNR-2, PCN-1, RFC-2, RFC-3
	GO:0006259 ~DNA metabolic process	DNA-2, Y57A10A.15, DIV-1, CEL-1, GEI-17, LIG-1, MCM-5, F23C8.9, MTSS-1, Y75B8A.6, NUC-1, MCM-7, T09A5.8, F33H2.5, POLH-1, PMS-2, RNR-2, UNG-1, PCN-1, RFC-2, RFC-3
4	IPR007110:Immunoglobulin-like	VER-1, IGCM-2, ZIG-8, UNC-89, TTN-1, Y102A11A.8, Y37E3.13, OIG-3, NCAM-1, UNC-5, SYG-2, RIG-5
5	GO:0003677 ~DNA binding	C48E7.2, Y38A10A.6, AST-1, CEH-27, MCM-5, SOX-2, SOX-3, T09A5.8, TBX-33, RAD-54, HCP-3, C07E3.6, MLS-2, Y62E10A.17, CEH-30, HTZ-1, CEH-32, HLH-1, CEH-34, NHR-66, UNC-120, Y75B8A.6, CEH-36, F44E2.7, MCM-7, CEY-1, F33H2.5, CEY-2, CEY-3, HMG-1.1, PMS-2, ZTF-1, LIM-4, EGL-18, HIL-5, PCN-1, HIL-7, LIN-32, F42G2.6, DNA-2, CEH-45, VAB-3, NHR-58, GAK-1, Y57A10A.15, CFI-1, C05D10.1, DIV-1, CEC-1, MET-2, ATF-2, NHR-15, FKH-5, UNC-130, UNC-42, ISW-1, LIN-40, RFC-2, Y116A8C.13, CPAR-1, RFC-3, CEH-2, CEH-5, CEH-13, LIG-1, CEH-16, MTSS-1, UNC-3, NHR-40, Y53G8AM.8, HMG-5, POLH-1, DCT-1, ZK673.4, CEH-8, TAF-11.2, UNC-30, PAX-1, DMD-5
	GO:0045449 ~regulation of transcription	SET-1, AST-1, EGL-43, CEH-27, MCM-5, LSD-1, TBX-33, F41H10.6, C07E3.6, MLS-2, Y62E10A.17, CEH-30, CEH-32, HLH-1, CEH-34, CEH-36, UNC-120, NHR-66, CEY-1, CEY-2, PCAF-1, CEY-3, LIM-4, EGL-18, LIN-32, F42G2.6, CEH-45, VAB-3, NHR-58, CFI-1, MET-2, ATF-2, NHR-15, UNC-130, FKH-5, SPR-2, UNC-42, ISW-1, LIN-40, CEH-2, B0336.13, CEH-5, CEH-13, CEH-16, UNC-3, NHR-40, RGR-1,

		MDT-8, Y53G8AM.8, DPY-22, MDT-11, CEH-8, LIN-54, LIN-53, UNC-30, PAX-1, MDT-15, DMD-5
	GO:0051252 ~regulation of RNA metabolic process	CEH-45, VAB-3, AST-1, NHR-58, MET-2, CEH-27, NHR-15, ATF-2, FKH-5, UNC-130, TBX-33, UNC-42, C07E3.6, LIN-40, MLS-2, Y62E10A.17, CEH-30, CEH-2, CEH-32, CEH-5, CEH-13, HLH-1, CEH-34, CEH-16, UNC-3, NHR-66, CEH-36, UNC-120, NHR-40, RGR-1, CEY-1, MDT-8, CEY-2, CEY-3, PCAF-1, DPY-22, MDT-11, LIM-4, CEH-8, EGL-18, UNC-30, PAX-1, MDT-15, DMD-5, F42G2.6
6	GO:0016592 ~Srb-mediator complex	RGR-1, MDT-8, DPY-22, MDT-11, MDT-15
	GO:0003702 ~RNA polymerase II transcription factor activity	Y39B6A.36, B0336.13, RGR-1, MDT-8, DPY-22, MDT-11, TAF-11.2, MDT-15

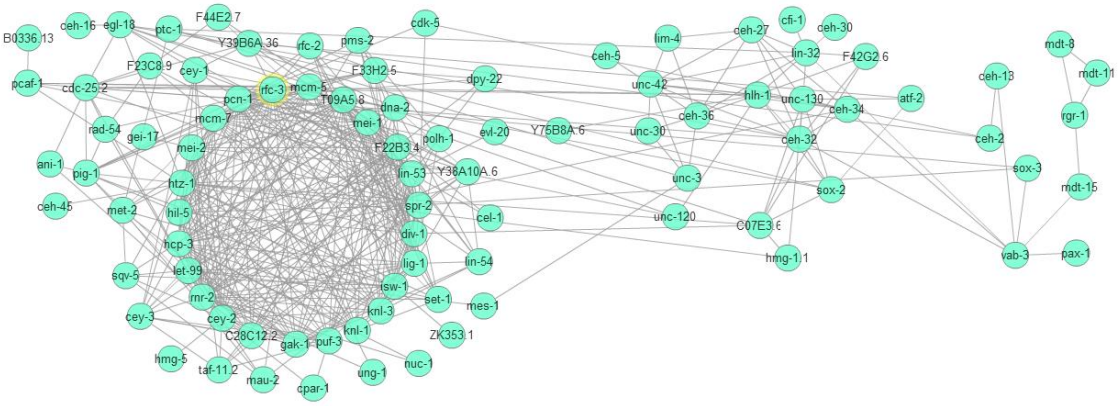

Figure 20Network of interconnected nuclear component genes in the down-regulated expression profile of sodium valproate exposure. Connections between the nuclear components of the down-regulated expression profile of valproate exposure identified in regression analysis at BH corrected p valur of 1% are mapped in WormNet. rfc-3 connected with 27 genes with the highest score of 4.76.

Table 7 WormNet analysis of the genes ranked by highest connectivity. Nuclear component genes down-regulated on valproate exposure identified in regression analysis with a BH corrected p value of 1% are ranked according to the highest connectivity. 92 Seed genes were mapped with a p value of $9.8461e^{-70}$.

Rank	Locus_ID	Symbol	Score	#_linked_seed / #_valid_seed	GO_P
1	C39E9.13	rfc-3	4.76	27/92	DNA replication; DNA repair; gametogenesis; locomotory behavior; embryonic development (sensu Metazoa); positive regulation of growth rate; hermaphrodite genitalia development;
2	W03D2.4	pcn-1	4.72	35/92	reproduction; cytokinesis; regulation of DNA replication; embryonic development (sensu Metazoa); embryonic cleavage;
3	F32D1.10	mcm-7	4.67	24/92	reproduction; cytokinesis; DNA replication initiation; embryonic development (sensu Metazoa); embryonic cleavage; hermaphrodite genitalia development;
4	F58F6.4	rfc-2	4.19	7/92	DNA replication; gametogenesis; locomotory behavior; embryonic development (sensu Metazoa);
5	R10E4.4	mcm-5	4.15	20/92	cytokinesis; DNA replication initiation; embryonic development (sensu Metazoa); embryonic cleavage;
6	F57B10.12	mei-2	4.10	19/92	meiotic spindle organization and biogenesis; microtubule depolymerization; meiosis; embryonic development; embryonic development (sensu Metazoa);
7	F14F3.1	vab-3	4.03	7/92	regulation of transcription, DNA-dependent; multicellular organismal development; anterior/posterior pattern formation; regulation of cell adhesion; tail tip morphogenesis (sensu Nematoda); cell fate commitment; regulation of transcription; positive regulation of transcription from RNA polymerase II promoter;
8	R08C7.3	htz-1	4.02	25/92	larval development (sensu Nematoda); nucleosome assembly; chromosome organization and biogenesis (sensu Eukaryota); locomotory behavior; embryonic development (sensu Metazoa); positive regulation of growth rate; post-embryonic body morphogenesis;
9	Y45F10A.2	puf-3	3.99	19/92	cytokinesis; embryonic development (sensu Metazoa); cellular osmoregulation; pronuclear migration; embryonic cleavage;
10	C28C12.2	na	3.94	16/92	cytokinesis; larval development (sensu Nematoda); chromosome segregation; locomotory behavior; embryonic development (sensu Metazoa); growth; positive regulation of growth rate; embryonic cleavage;

Table 8 WormNet analysis of the genes ranked by highest connectivity. Nuclear component genes down-regulated on valproate exposure identified in regression analysis with a BH corrected p value of 1% are ranked according to the highest connectivity. The top ten genes are mapped in WormNet for their connectivity among each other with a p value of $6.8318e^{-28}$.Refer Table 19 (page 111) for the evidence codes.

Rank	Locus_ ID	Sym bol	Sco re	Evide nces	#_linked _seed / #_valid_s eed	Linked_ seed	GO_P	GO_C	GO_F
1	C39E9. 13	rfc-3	4.2 4	CE-CX:0. 22 SC-CC:0. 16 HS-LC:0.1 2 SC-TS:0.1 0 HS-CC:0. 09 SC-LC:0.0 9 SC-MS:0. 08 CE-PG:0.0 7 SC-GT:0. 06 CE-GN:0. 04	8/10	C28C12 .2 mcm-7 mei-2 rfc-2 htz-1 mcm-5 pcn-1 puf-3	DNA replication; DNA repair; gametogene sis; locomotory behavior; embryonic developmen t (sensu Metazoa); positive regulation of growth rate; hermaphrod ite genitalia developmen t;	protein complex;	DNA binding;
2	W03D2 .4	pcn-1	3.8 0	CE-CX:0. 26 SC-LC:0.1 8 SC-GT:0. 13 HS-LC:0.1 3 HS-CX:0. 12 CE-PG:0.1 0 SC-CC:0. 07	8/10	C28C12 .2 rfc-3 mcm-7 mei-2 rfc-2 htz-1 mcm-5 puf-3	reproductio n; cytokinesis; regulation of DNA replication; embryonic developmen t (sensu Metazoa); embryonic cleavage;	na	DNA binding; DNA polymera se processiv ity factor activity;
3	F58F6. 4	rfc-2	3.7 3	HS-LC:0.1 8 SC-TS:0.1 5 SC-CC:0. 14 HS-	2/10	rfc-3 pcn-1	DNA replication; gametogene sis; locomotory behavior; embryonic developmen	protein complex;	nucleotid e binding; DNA binding; ATP binding; nucleosid

				CC:0.13 SC-MS:0.12 SC-LC:0.11 SC-GT:0.10 CE-GN:0.06			t (sensu Metazoa);		e-triphosphatase activity;
4	F32D1.10	mcm-7	3.61	CE-CX:0.21 SC-CC:0.15 SC-LC:0.14 HS-LC:0.12 SC-GT:0.10 CE-PG:0.09 HS-CX:0.07 SC-CX:0.07 SC-MS:0.05	4/10	rfc-3 htz-1 mcm-5 pcn-1	reproduction; cytokinesis; DNA replication initiation; embryonic development (sensu Metazoa); embryonic cleavage; hermaphrodite genitalia development;	nucleus;	nucleotide binding; nucleic acid binding; DNA binding; ATP binding; DNA-dependent ATPase activity; nucleoside-triphosphatase activity;
5	R10E4.4	mcm-5	3.47	SC-CC:0.18 SC-LC:0.17 HS-LC:0.14 SC-GT:0.12 CE-PG:0.11 SC-CX:0.08 HS-CX:0.08 CE-CX:0.07 SC-MS:0.06	3/10	rfc-3 mcm-7 pcn-1	cytokinesis; DNA replication initiation; embryonic development (sensu Metazoa); embryonic cleavage;	nucleus;	nucleic acid binding; DNA binding; ATP binding; DNA-dependent ATPase activity;
6	C28C12.2	na	3.41	CE-CX:1.00	5/10	rfc-3 mei-2 htz-1 pcn-1	cytokinesis; larval development (sensu	na	na

						puf-3	Nematoda); chromosome segregation; locomotory behavior; embryonic development (sensu Metazoa); growth; positive regulation of growth rate; embryonic cleavage;		
7	Y45F10A.2	puf-3	3.34	CE-CX:1.00	5/10	C28C12.2 rfc-3 mei-2 htz-1 pcn-1	cytokinesis; embryonic development (sensu Metazoa); cellular osmoregulation; pronuclear migration; embryonic cleavage;	na	RNA binding; binding;
8	F57B10.12	mei-2	2.76	CE-CX:1.00	4/10	C28C12.2 rfc-3 pcn-1 puf-3	meiotic spindle organization and biogenesis; microtubule depolymerization; meiosis; embryonic development; embryonic development (sensu Metazoa);	condensed nuclear chromosome; spindle pole;	protein binding;
9	R08C7.3	htz-1	2.59	CE-CX:0.63 HS-CX:0.37	5/10	C28C12.2 rfc-3 mcm-7 pcn-1 puf-3	larval development (sensu Nematoda); nucleosome assembly; chromosome organization and biogenesis (sensu	nucleosome; nucleus;	DNA binding;

			Eukaryota); locomotory behavior; embryonic development (sensu Metazoa); positive regulation of growth rate; post-embryonic body morphogenesis;		
Not connected	F14F3.1	vab-3	regulation of transcription, DNA-dependent; multicellular organismal development; anterior/posterior pattern formation; regulation of cell adhesion; tail tip morphogenesis (sensu Nematoda); cell fate commitment; regulation of transcription; positive regulation of transcription from RNA polymerase II promoter;	nucleus;	DNA binding; transcription factor activity; sequence-specific DNA binding;

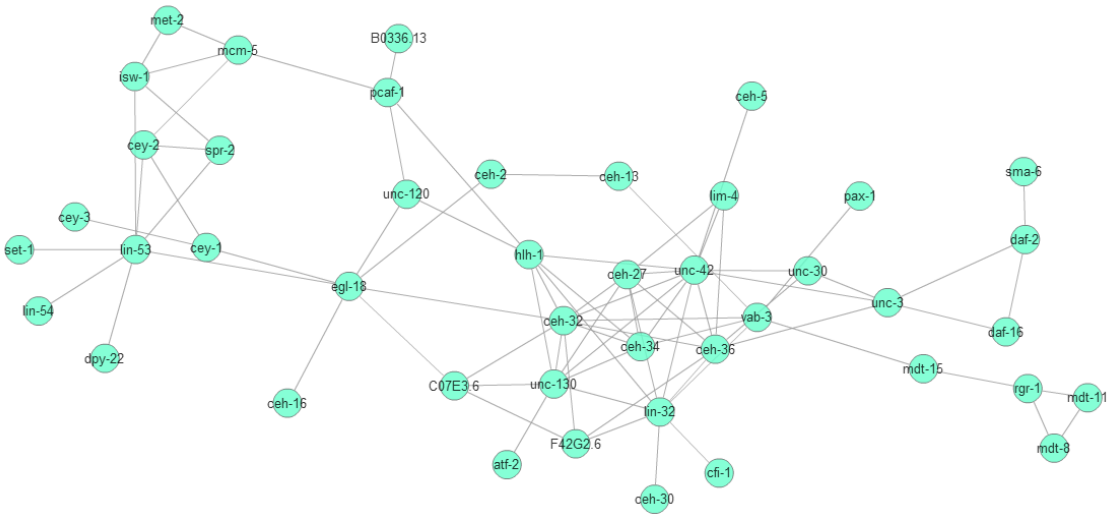

Figure 21 WormNet analysis of transcription factors negatively correlated with valproate exposure and their interaction with the insulin and TGF-β Sma/Mad pathway. Transcription factors significantly negatively correlated with valproate exposure with a BH corrected p value of 1% are mapped in WormNet to identify possible interactions. *daf-2* , *daf-16* and *sma-6* are added to identify their link to these transcription factors. Vab-3 had the highest connectivity score of 3.95. Insulin signalling pathway is connected to these transcription factors via *unc-3*.

4.2.2Comparison of correlation analysis with SAM analysis

Simple correlation analysis identifies only linear relationships. But Significant Analysis of Microarray (SAM) is designed to identify any genes differentially regulated in a number of sample groups. Therefore by applying this approach to the different dose groups we can identify nonlinear relationships as well. Therefore significantly altered gene expression profiles identified by regression analysis at 1% BH corrected p value are compared with significant expression profile identified by SAM analysis at 1% FDR. SAM identified 571 genes not identified by regression analysis (Figure 22, page81). These expression profiles identified only by SAM were enriched in functional terms such as structural constituents of cuticle (Table 9, page81) and muscle development and differentiation and cell signalling (Table 10, page 82).

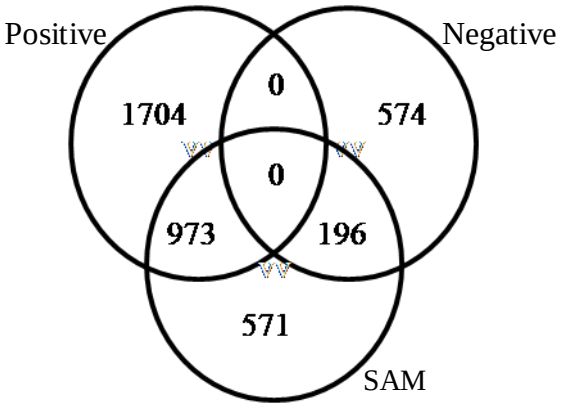

Figure 22 Comparison of significant gene expression profiles identified by regression analysis and SAM analysis. A threshold of 1% BH corrected p value was used in regression analysis and a 1%FDR in SAM analysis. Positively correlated expression profile with valproate identified by regression analysis is given as 'positive' and the negatively correlated expression profile identified by regression analysis is shown as 'negative'.

Table 9 DAVID functional clustering of significant expression profiles with a bell shaped curve with dose identified only by SAM but not by regression analysis. A threshold of 1% BH corrected p value is used in the regression analysis and 1% FDR in SAM analysis.

Cluster	Enrichment Score	Term	Count	Benjamini
1	3.6658165	INTERPRO:Nematode cuticle collagen, N-terminal	8	5.67E-04
		GOMF:structural constituent of cuticle	8	4.29E-04
		INTERPRO:Collagen triple helix repeat	8	0.001144
		GOMF:structural molecule activity	9	0.041234
3	0.740971	GOMF:structural molecule activity	9	0.041234

Table 10 DAVID functional clustering of significant expression profiles with an inverted bell shaped curve with dose identified only by SAM but not by regression analysis. A threshold of 1% BH corrected p value is used in the regression analysis and 1% FDR in SAM analysis.

Cluster	Enrichment Score	Category	Term	Count
1	3.5403603	GOTERM_BP_FAT	GO:0051146~striated muscle cell differentiation	4
		GOTERM_BP_FAT	GO:0055002~striated muscle cell development	4
		GOTERM_BP_FAT	GO:0055001~muscle cell development	4
		GOTERM_BP_FAT	GO:0042692~muscle cell differentiation	4
		GOTERM_BP_FAT	GO:0007517~muscle organ development	4
2	2.127062	SP_PIR_KEYWORDS	alternative splicing	8
3	2.0742409	GOTERM_MF_FAT	GO:0005509~calcium ion binding	8
5	1.5831041	SP_PIR_KEYWORDS	signal	8
		SP_PIR_KEYWORDS	glycoprotein	8
		SP_PIR_KEYWORDS	membrane	11
6	1.4890645	GOTERM_MF_FAT	GO:0005509~calcium ion binding	8

4.2.3Genes correlated with lipid accumulation, egg laying and valproate dose

After getting the significant expression profile, I looked at the overlap between differentially regulated genes in egg laying, lipid mass and valproate exposure on three replicates at a threshold of p value <1% FDR with BH correction for multiple testing (Figure 23, page83). Since lipid mass and valproate dose are highly correlated, most of the genes picked by correlation analysis of lipid mass are identified by correlation analysis of valproate dose except 135 genes. But lipid mass plateaued after 15mM valproate dose resulting in fewer genes that were correlated with lipid mass compared to valproate concentration.

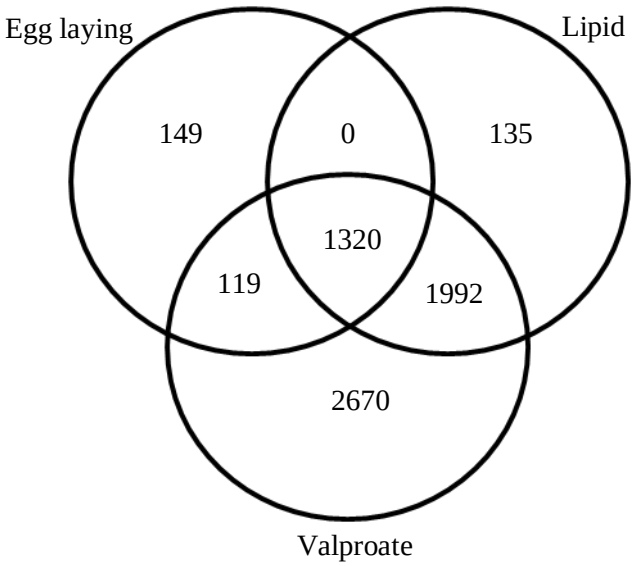

Figure 23 Overlap in expression profiles of egg laying, lipid mass and valproate exposure. Genes correlated to valproate dose captures 92% of the expression profile correlated with lipid mass and egg laying. Expression profile correlated only with lipid mass could explain the nonlinear dose response of lipid mass.

A shift from membrane components to amino acid biosynthesis is a land mark of decrease of lipid at high valproate doses (Figure 24, page86). Down regulation of neuronal function genes is followed by an up-regulation of lipid catabolism genes and G-protein coupled receptors. This also involves down-regulation of histone phosphorylating enzyme *kin-1.ser-4*, serotonin receptor is negatively correlated with lipid level and down regulation of serotonin pathway is known to increase lipid level. *acs-1* codes for acyl CoA synthetase which is involved in fatty acid synthesis in the cytosol(Zhang et al., 2011).*hyl-2* codes for ceramide

synthase which catalyses the transfer of acyl units to sphingosine to make ceramide (Finver et al., 1988). Both *acs-1* and *hyl-2*show a positive correlation with lipid level.

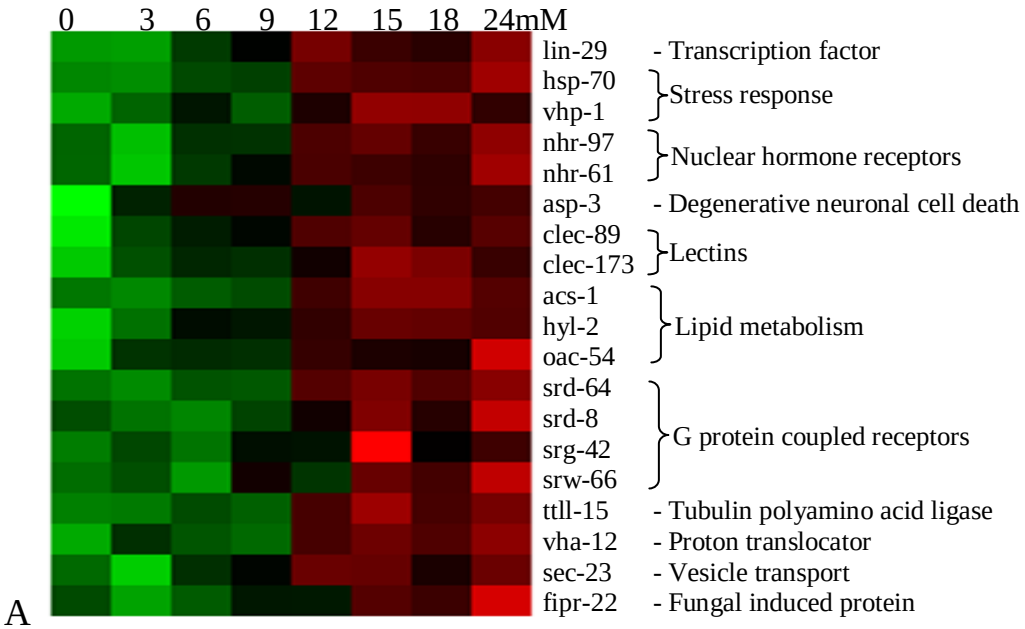

A

Cluste	Enrichment	Category	Term	Coun	Benjami

r	Score			t	ni
1	2.266388	GOTERM_BP_FAT	GO:0008652~cellular amino acid biosynthetic process	3	0.130447
2	0.243229	GOTERM_MF_FAT	GO:0046872~metal ion binding	5	1
3	0.176887	GOTERM_BP_FAT	GO:0040010~positive regulation of growth rate	4	0.999999

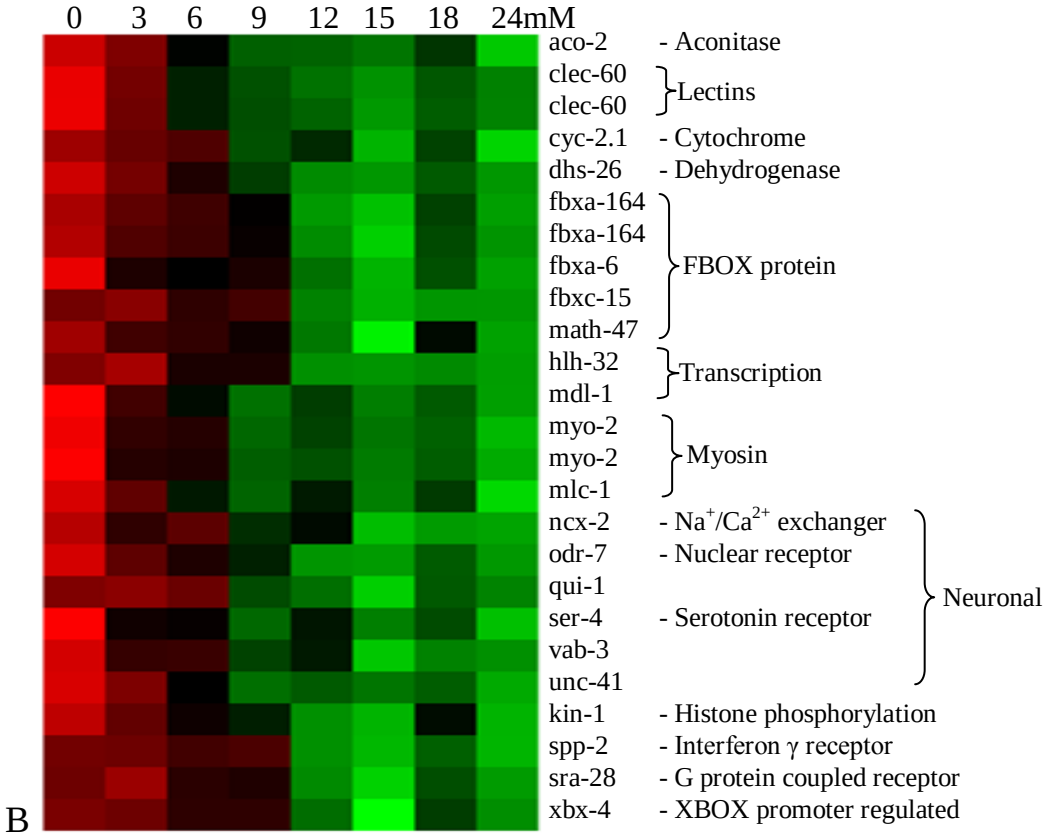

(Numbers across top indicate the valproate concentration.)

Cluster	Enrichment Score	Category	Term	Count	Benjamini
1	1.072365	INTERPRO	IPR002900:Protein of unknown function DUF38, Caenorhabditis species	3	0.816623
2	0.241771	GOTERM_CC_FAT	GO:0016021~integral to membrane	9	1
3	0.22574	GOTERM_MF_FAT	GO:0043169~cation binding	4	1

Figure 24 Figure shows the expression profiles of 135 genes positively (panel A) and negatively correlated with valproate (panel B) unique to lipid metabolism identified in Venn diagram in figure 5.Numbers across top of each heatmap indicate valproate concentration. The degree of expression is indicated with a red to green scale where the higher expression is given by red. Tables below the heatmap show the functional terms enriched in each cluster.

Enrichment of functional terms such as structural molecule activity, detoxification, electron carrier activity and cell signalling characterize the negatively correlated expression profile of valproate exposure with egg laying (Table 11). None of the functional terms were significantly enriched in the expression profile positively correlated with egg laying.

Table 11 Functional terms enriched in negatively correlated expression profile with egg laying on valproate exposure at a threshold of 10% FDR.

Cluster	Enrichment score	Term	Count	Benjamini
1	16.139254	INTERPRO: Nematode cuticle collagen, N-terminal	35	9.34E-19
		INTERPRO: Collagen triple helix repeat	37	8.04E-18
		GOMF:structural molecule activity	41	5.33E-08
2	5.4068484	INTERPRO:Glutathione S-transferase/chloride channel, C-terminal	11	1.43E-04
		INTERPRO:Thioredoxin fold	16	1.90E-04
3	4.2267186	INTERPRO:Protein of unknown function DUF38	23	7.21E-05
		SMART:FBOX	25	0.001636

4	3.127229	SP_PIR:cuticle	7	0.022424
5	3.0397377	INTERPRO:Uncharacterised protein family UPF0376	7	0.012298
6	1.9185696	INTERPRO:UDP-glucuronosyl/UDP-glucosyltransferase	9	0.09126
7	1.7383587	KEGG: Metabolism of xenobiotics by cytochrome P450	4	0.131267
		KEGG: Glutathione metabolism	4	0.148172
8	1.6178212	GOMF: electron carrier activity	15	0.139609
9	1.4996211	UP_SEQ: signal peptide	20	0.102358
		GO_MF: peptidase activity	23	0.156726

Enrichment of functional terms such as structural molecule activity, detoxification, energy balance, lipid metabolism and tryptophan metabolism characterize the expression profile positively correlated with lipid mass on valproate exposure (Table 12). There was no significant enrichment of any functional terms negatively correlated with lipid mass on valproate exposure identified by regression analysis. But SAM analysis identified expression profiles negatively correlated with lipid mass on valproate exposure enriched with functional terms, such as cell adhesion, muscle development and differentiation, lectin, neuronal transmission, EGF-like, cell signalling and calcium binding (Table 13, page 90).

Table 12 Functional terms enriched in positively correlated expression profile with lipid mass on valproate exposure at a threshold of 10% FDR.

Cluster	Enrichment score	Term	Count	Benjamini
1	16.044666	INTERPRO: Nematode cuticle collagen, N-terminal	49	6.15E-

				19
		INTERPRO: Collagen triple helix repeat	54	8.81E-19
		GOMF:structural molecule activity	73	4.03E-09
2	11.800575	SMART:PTPc	31	1.17E-13
		GOMF:phosphatase activity	53	4.57E-13
		SP_PIR:hydrolase	58	0.007092
3	5.367098	INTERPRO:UDP-glucuronosyl/UDP-glucosyltransferase	21	1.13E-05
		GOBP:lipid glycosylation	14	1.67E-05
		GOMF:carbohydrate binding	25	0.042659
4	5.0846709	INTERPRO:Metallophosphoesterase	20	1.17E-06
		SMART: PP2Ac	16	1.49E-06
5	4.4116928	GOBP:phosphorus metabolic process	94	3.57E-17
		GOBP:phosphorylation	58	3.00E-06
		SMART: SH2	17	1.78E-05
6	3.2947023	SP_PIR:cuticle	11	0.00256

				4
7	3.2404504	INTERPRO: Glutathione S-transferase, C-terminal	16	1.77E-05
		INTERPRO:Thioredoxin fold	20	0.010829
		KEGG:Metabolism of xenobiotics by cytochrome P450	6	0.028012
8	2.5528737	INTERPRO: CHK kinase-like	8	0.023515
9	2.4919646	KEGG:Limonene and pinene degradation	7	0.006266
		INTERPRO: Cytochrome P450	15	0.010977
		GOMF: iron ion binding	32	0.07844
		SP_PIR:Monooxygenase	13	0.154439
10	1.6688352	SMART: CLECT	25	0.102393
11	1.4612299	INTERPRO: Major sperm protein	15	0.010977
15	1.3139589	INTERPRO: NADH:flavin oxidoreductase/NADH oxidase, N-terminal	5	0.023884
		GOMF: FMN binding	6	0.096152
17	1.1341216	INTERPRO: Protein of unknown function DUF38	26	0.132932
18	1.1013774	INTERPRO: Phospholipase A2, active site	5	0.174594

19	1.0861378	INTERPRO: Peptidase, metallopeptidases	9	0.155766
21	1.0164771	KEGG:Tryptophan metabolism	6	0.067141
		KEGG:Fatty acid metabolism	7	0.077678

Table 13 DAVID functional clustering of expression profile negatively correlated with lipid mass on valproate exposure. These were identified only in SAM analysis but not in regression analysis.

Cluster	Enrichment Score	Term	Count	Benjamini
1	3.1470645	INTERPRO:EGF-like, type 3	6	0.032117
		GOBP:biological adhesion	5	0.037047
		GOBP:cell adhesion	5	0.037047
2	2.9611154	GOBP:striated muscle cell development	5	0.001132
		GOBP:striated muscle cell differentiation	5	0.001132
		GOBP:muscle cell development	5	7.14E-04
		GOBP:muscle cell differentiation	5	0.001066
		GOBP:actin filament-based process	4	0.102589
		GOBP:actomyosin structure organization	3	0.136371
		GOBP:myofibril assembly	3	0.136371
		GOBP:cellular component assembly involved in morphogenesis	3	0.136371
3	2.7803265	INTERPRO:type lectin, conserved site	5	0.027124

		INTERPRO:type lectin-like	8	0.042207
		SP_PIR:Lectin	6	0.102251
		INTERPRO:C-type lectin	8	0.058599
		SMART:CLECT	8	0.19063
4	2.5607565	INTERPRO:Immunoglobulin subtype	5	0.047875
		INTERPRO:Immunoglobulin-like	6	0.024368
		SMART:IG	5	0.041076
		INTERPRO:Immunoglobulin-like fold	5	0.058698
		INTERPRO:Immunoglobulin	4	0.058254
		INTERPRO:Immunoglobulin I-set	4	0.060697
		INTERPRO:Immunoglobulin V-set	3	0.070281
5	2.2104446	GOBP:cell-cell signaling	6	0.007249
		GOBP:synaptic transmission	4	0.170817
		GOBP:transmission of nerve impulse	4	0.170817
6	2.1595663	INTERPRO:EGF-like, type 3	6	0.032117
		GOMF:calcium ion binding	8	0.071871
		INTERPRO:EGF-like region, conserved site	7	0.055396
		INTERPRO:Laminin G, subdomain 2	3	0.074657
		INTERPRO:Laminin G	3	0.074657
		INTERPRO:EGF	4	0.086806
		INTERPRO:EGF-like	5	0.100631
7	1.612791	UP_SEQ:signal peptide	10	0.166592
		SP_PIR:signal	10	0.088608
10	0.4900507	GOMF:calcium ion binding	8	0.071871

Functional terms such as detoxification, energy balance, structural molecule activity, major sperm protein, cytoskeleton, heat shock protein, fatty acid metabolism and ABC-transporter like were enriched in the expression profile positively correlated with valproate (Table 14).

Table 14 Functional terms enriched in positively correlated expression profile with valproate identified by regression analysis at a threshold of 10% FDR.

Cluster	Enrichment score	Term	Count	Benjamini
1	20.604504	SMART:PTPc	48	2.01E-25
		GOMF:phosphatase activity	79	5.66E-23
		SP_PIR:hydrolase	81	4.71E-04
2	15.848884	INTERPRO:Nematode cuticle collagen, N-terminal	56	6.12E-19
		INTERPRO:Collagen triple helix repeat	61	7.15E-18
		GOMF:structural molecule activity	99	3.80E-12
3	9.3937479	GOBP:phosphate metabolic process	151	3.70E-36

		GOBP:phosphorylation	96	1.11E-15
		SMART:SH2	26	6.30E-10
		GOMF:ATP binding	127	0.003548
		GOMF:adenyl nucleotide binding	134	0.003644
		GOMF:purine nucleotide binding	144	0.06807
4	9.3438724	INTERPRO:Metallophosphoesterase	28	1.28E-10
5	5.380872	SP_PIR:collagen	34	1.46E-09
		SP_PIR:cuticle	13	7.91E-04
6	5.2624126	INTERPRO:Glutathione S-transferase, N-terminal	20	1.83E-06
		INTERPRO:Thioredoxin fold	24	0.01276
7	5.0544358	GOBP:lipid glycosylation	16	3.09E-05
		INTERPRO:UDP-glucuronosyl/UDP-glucosyltransferase	23	5.97E-05
		GOMF:carbohydrate binding	31	0.041588
8	3.8045691	GOMF:iron ion binding	49	5.27E-04
		Cytochrome P450, conserved site	20	6.66E-04

		KEGG:Limonene and pinene degradation	8	0.006625
		GOMF:electron carrier activity	37	0.009878
		SP_PIR:Monooxygenase	19	0.013434
9	3.4384841	INTERPRO:Major sperm protein	27	5.39E-08
		INTERPRO:PapD-like	25	1.55E-07
		SP_PIR:cytoskeleton	21	0.109352
10	2.9954186	SMART:BRCT	11	0.00155
		INTERPRO:Ankyrin	17	0.100955
11	2.2248019	INTERPRO:Protein of unknown function DUF856	5	0.03768
12	2.0831552	SMART:CHK	8	0.054519
13	1.750404	PIR_SUPERFAMILY:glutathione transferase	8	0.15639
		KEGG:Metabolism of xenobiotics by cytochrome P450	6	0.090779
14	1.6786155	SMART:CLECT	32	0.121572
15	1.6736906	INTERPRO:NADH:flavin oxidoreductase/NADH oxidase, N-terminal	5	0.063405
16	1.4671233	PIR_SUPERFAMILY:gliadin	5	0.12707
17	1.431552	SMART:NRF	6	0.142466

18	1.3562886	INTERPRO:Protein of unknown function DUF38	35	0.038335
23	1.1386328	INTERPRO:2Fe-2S ferredoxin, iron-sulphur binding site	6	0.098803
26	0.9791065	INTERPRO:Heat shock protein Hsp20	6	0.166244
28	0.9443988	SMART:ZnMc	10	0.129871
29	0.8904833	KEGG:Fatty acid metabolism	8	0.164282
43	0.3840152	INTERPRO:ABC transporter-like	13	0.048339
		COG:Defense mechanisms	8	0.077149

Functional terms such as reproductive development process, cell division, neuron differentiation, cell cycle, Wnt signalling, glycoprotein and protein-DNA complex assembly were enriched in the expression profile negatively correlated with valproate in regression analysis (Table 15).

Table 15 Functional terms enriched in negatively correlated expression profile with valproate identified by regression analysis at a threshold of 10% FDR.

Cluster	Enrichment score	Term	Count	Benjamini
1	5.418025	GOBP:tissue morphogenesis	50	8.70E-05
		GOBP:morphogenesis of an epithelium	48	1.06E-04
		GOBP:reproductive developmental process	86	0.003037
		GOBP:hermaphrodite genitalia development	74	0.003626

		GOBP:sex differentiation	80	0.003775
2	4.5862188	SP_PIR:cell cycle	18	6.34E-05
		GOBP:cell division	29	0.004132
3	2.7895358	GOBP**:**DNA replication	14	0.006634
		GOBP:DNA metabolic process	21	0.086511
		KEGG:Mismatch repair	6	0.099903
		KEGG:Base excision repair	5	0.198048
4	2.333731	INTERPRO:Immunoglobulin-like fold	13	0.067869
5	2.1367808	SP_PIR:nucleus	80	3.93E-04
		SP_PIR:Homeobox	18	4.73E-04
		GOMF:DNA binding	79	0.087607
		SMART:HOX	18	0.14043
		SP_PIR:dna-binding	47	0.075483
6	2.0183949	GOCC:nucleoplasm	11	0.019123
		GOCC:nuclear lumen	12	0.064516
		GOCC:Srb-mediator complex	5	0.123916
		GOCC:intracellular organelle lumen	14	0.157436
8	1.9788232	GOCC:chromatin	12	0.003851
9	1.9677001	SP_PIR:sh3 domain	8	0.072719
10	1.9072694	GOBP:cellular component morphogenesis	20	0.036085
		GOBP:neuron differentiation	13	0.062106
		GOBP:cell projection organization	14	0.079005
		GOBP:cell motion	15	0.145949
11	1.8748935	GOBP:chromosome organization	24	0.003969
		GOBP:kinetochore assembly	4	0.088987
		GOBP:centromere complex assembly	4	0.088987
13	1.7863499	SP_PIR:tpr repeat	7	0.079355

16	1.7044824	GOBP:cell cycle	42	0.004196
17	1.6861614	SP_PIR:wnt signaling pathway	6	0.076356
19	1.5877662	GOBP:glycosaminoglycan metabolic process	4	0.052188
25	1.345056	SP_PIR:glycoprotein	39	0.037395
		SP_PIR:signal	34	0.150913
27	1.2345633	GOBP:protein-DNA complex assembly	9	0.088448
41	0.9299484	SP_PIR:mitosis	7	0.177892
63	0.5220007	SP_PIR:myristate	6	0.103074

Overall, the expression profile correlated with valproate exposure is enriched with all the functional terms that could explain expression profiles correlated with egg laying and lipid mass (Table 16). It identified nuclear components such as DNA repair, cell cycle, DNA replication, cell division, transcription and nucleotide binding which are not identified by the expression profiles correlated with lipid or egg laying. Therefore it was decided to concentrate only on expression profile correlated with valproate exposure.

Table 16 Summary of DAVID functional clustering of expression profiles correlated with egg laying, lipid mass and valproate concentration identified by regression analysis.

Cellular function	**Egg laying**		**Lipid**		**VPA**	
	positive	negative	positive	negative	positive	negative
Structural molecule activity/Collagen/cuticle/ cytoskeleton	48	84			133	
Cellular detoxification	24	56			75	

Amino acid and protein metabolism/ Peptidase	23	14	35	
Lipid metabolism		26	32	
Tissue morphogenesis				50
Reproductive development		15		86
Cell cycle/DNA replication/DNA repair/Cell division			19	96
Neuron differentiation				31
Chromosome organization				36
Phosphorus metabolism/Phosphatase		175	258	
Carbohydrate binding		50	63	
ion binding		32	55	
Transporter			30	
Cell signalling	20			40
Redox reactions	15	38	42	
Carbohydrate metabolism				43
Transcription				84
Nucleotide binding			144	
Nucleus				143

Regression analysis identified one sixth of the probe IDs in the array to be correlated significantly with valproate dose at a threshold of < 1% BH corrected p value (Table 17, page 99). qPCR verification was not performed as use of low throughput methods to verify highthroughput results is questionable.

SAM analysis identified 1744 significant expression profiles at a threshold of 1% FDR and they all had a fold change > 1 (Figure 25).

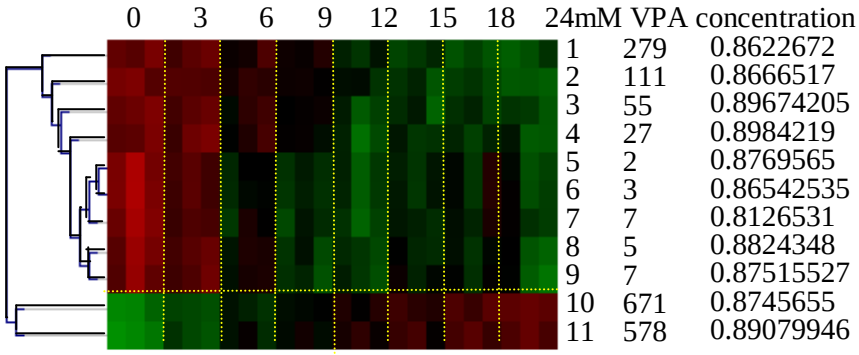

Figure 25 Dendogram of SOTA cluster analysis of significant expression profile identified by SAM at a threshold of 1% FDR. Degree of gene expression is shawn by a scale of red to green with red indicating higher expression. Three replicates were done for each drug concentration.

Table 17 Significant expression profiles identified by regression analysis at different threshold values. Expression profiles correlated with average of three replicates or with replicates are shown for each phenotype. For egg laying, only average of the three replicates were considered as the samples were unpaired with microarray samples.

FDR	1%	5%	10%	15%
Egg laying (Average)			10794	17202
Lipid (Average)			16970	21092

Lipid (Replicates)		2313	5659	8823
Valproate (Average)		6089	18574	21686
Valproate (Replicate)	7002	13503	17321	20004

There were 1742 probe IDs with significant expression profiles at 1% FDR SAM with 1 fold change(S3: Supplementary Material). Out of these only 363 could be converted to Wormbase gene IDs using DAVID gene ID conversion tool. Out of these 363 genes, 97 had a negative correlation with the valproate concentration.

Regression analysis identified down regulation of most of the nuclear components as a remarkable feature of valproate exposure, which was not detected by SAM analysis. In biological systems, a slight change in the concentration of one key gene product could result in the amplification of a downstream cascade of events. Use of a high threshold would eliminate these key genes leaving only the downstream targets.

To concentrate on a highly significant smaller number of expression profiles, it was decided to focus on significant expression profile identified by SAM at 1% FDR. Clustering revealed that this significant expression profile could be summarised in four clusters with four different expression patterns correlated with drug dose.

4.2.4Cluster analysis

After deciding on the significant expression profile to work on, I clustered themin to groups with similar expression patterns because genes showing similar expression patterns normally have common regulatory mechanisms(Sturn et al., 2002). CAST

(Clustering Affinity Search Technique) clustering of this significant expression profile with a threshold affinity value of 0.4 identified four clusters with two main clusters composed of 1249 positive and 485 negatively correlated expression profiles with valproate dose (Figure 26). It also identified two other clusters with a few gene expression profiles with a bell shape curve and an inverted bell shape curve on valproate exposure. In CAST, the user defines an affinity threshold between 0-1 and each expression profile allocated to a specific cluster if its affinity to that cluster exceeds the threshold value. Thresholds near one make many clusters with less variability and threshold values near zero make few clusters with high variability. The advantage is that the number of clusters formed is not predetermined.

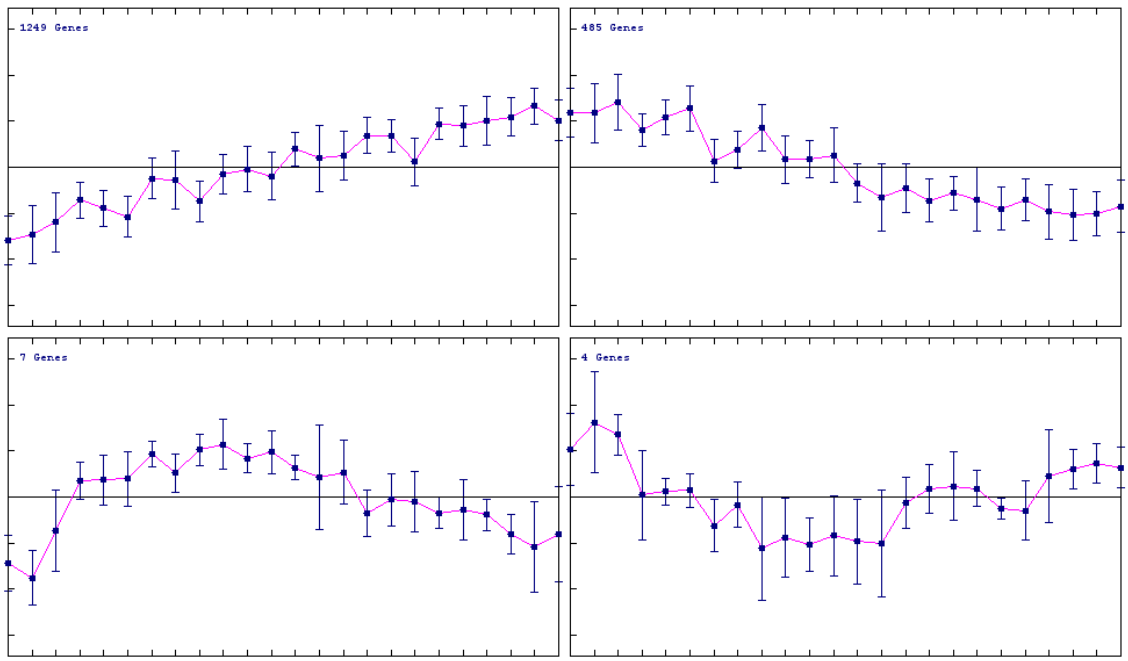

Figure 26Centroid graphs showing CAST clustering of significant expression profile identified by SAM analysis at a threshold of 1% FDR with 1fold change. A threshold affinity value of 0.4 is used in CAST.

4.2.4.1 Expression profile positively correlated with valproate concentration

Out of the 1249 gene expressions positively correlated with valproate concentration, only 263 had known functions. HCL clustering identifies most of these genes in a single cluster indicating positive correlation with dose of these genes to have a common regulatory mechanism (Figure 27). These were enriched with cellular detoxification, transporters, F-box proteins and G-protein coupled receptors. Several nuclear hormone receptors, neuropeptides and genes regulated by DAF-16 are also positively correlated with valproate(Table 18, page 104). Details of these genes are given in Figure 27.

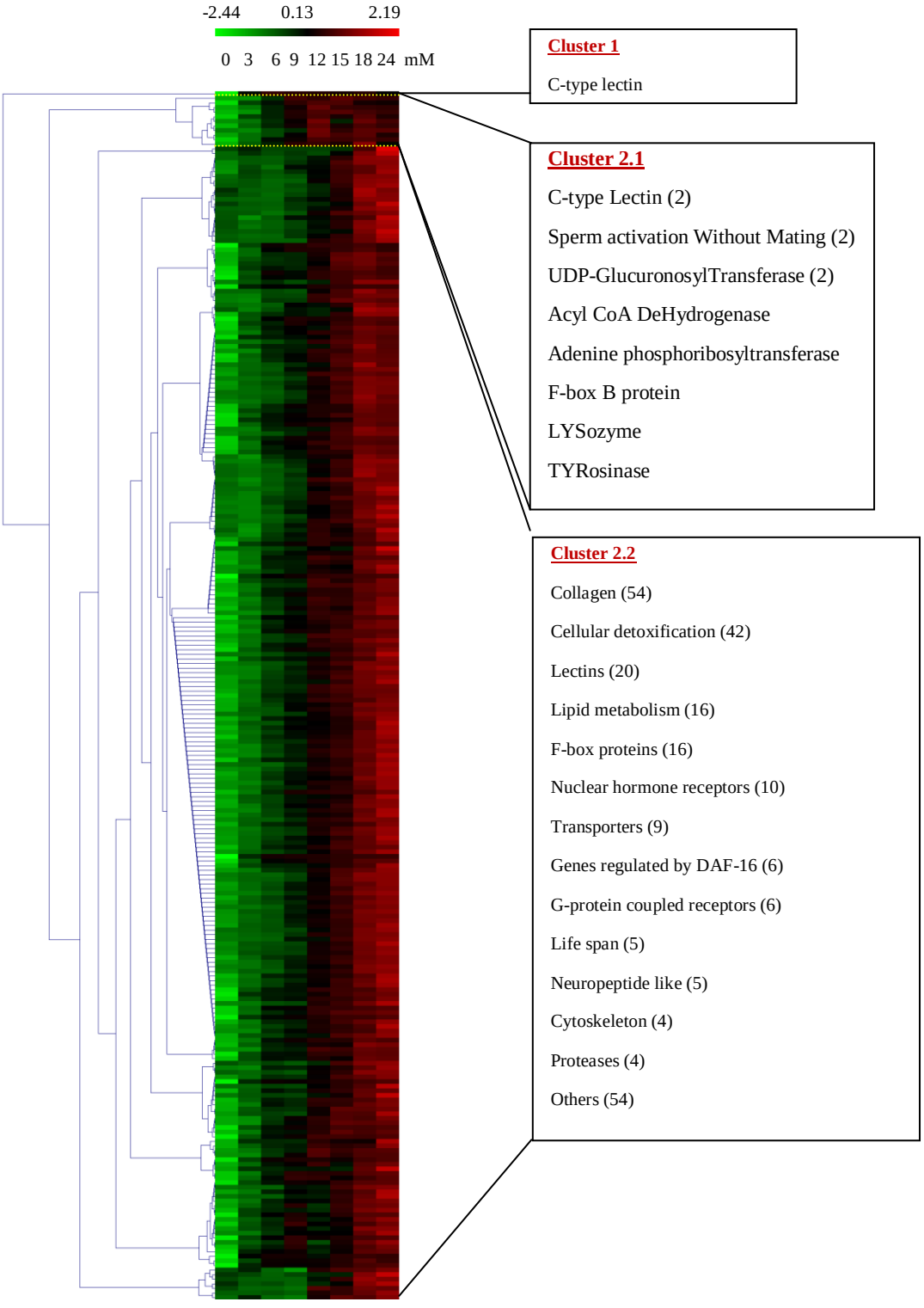

Figure 27 Heat map showing HCL clustering of expression profile positively correlated with valproate dose. Expression profile identified by CAST as positively correlated with valproate dose is shown as a heat map. HCL clustering of these genes identified two clusters with one cluster containing only one gene (cluster 1) and the other cluster containing therest of the genes (cluster 2). This second cluster contains two sub-clusters.

Cluster 2.1 contained only 11 genes and cluster 2.2 contained the rest of the genes. This shows that valproate exposure cause an up-regulation of genes as a single cluster which indicates a common mechanism for the regulation of expression of these genes. Number of genes of each type are given in parentheses.Degree of gene expression is given in a scale of red to green where red indicates higher expression. Valproate concentration is given above the heatmap.

Table 18 David functional clustering of expression profile positively correlated with valproate dose identified by CAST. Expression profiles with a p value of <0.05 are shown.

Cluster	Enrichment Score	Term	Count	PValue	Benjamini
1	41.35963	IPR008160:Collagen triple helix repeat	57	8.86E-55	1.71E-52
2	10.52595	GO:0030246~carbohydrate binding	24	5.70E-11	3.06E-09
		GO:0030259~lipid glycosylation	12	1.14E-10	2.85E-08
3	4.969211	IPR001128:Cytochrome P450	14	8.89E-10	2.86E-08
4	4.747159	IPR004046:Glutathione S-transferase, C-terminal	11	1.48E-08	3.57E-07
5	4.427775	IPR001304:C-type lectin	15	1.66E-04	0.00267324

6	3.838634	GO:0040002~collagen and cuticulin-based cuticle development	9	1.31E-04	0.008099457
7	2.452669	IPR001810:Cyclin-like F-box	15	0.016232595	0.160943813
8	1.634829	GO:0008340~determination of adult life span	10	0.023183073	0.565849655
10	1.128651	SM00276:GLECT	3	0.035408898	0.10712004
9	1.301845	IPR016040:NAD(P)-binding domain	7	0.027971981	0.239498173
11	1.109851	IPR017871:ABC transporter, conserved site	7	3.81E-04	0.005636084

4.2.4.1.1 CAST clustering of expression profile positively correlated with valproate dose

SOTA clustering of expression profile positively correlated with valproate dose identified by CAST is shown as centroids graphs in Figure 28 (page106). It identifies four clusters enriched in different GO functional terms and there is a gradual transfer from one cluster to the next starting from cluster 4 on increasing drug dose. Dendogram of the four clusters shows this gradual up-regulation of the genes of the four clusters (Figure 29, page106). At lower valproate doses, an up-regulation of genes involved in

cellular detoxification, lectins and ABC transporters is seen (Figure 30, page107). Further increase of valproate dose caused an up-regulation of genes coding for FBOX proteins, lipid glycosylation and determination of life span. Much higher valproate dose is required for the up-regulation of genes involved in growth regulation, collagen synthesis, signal peptides and proteolysis.

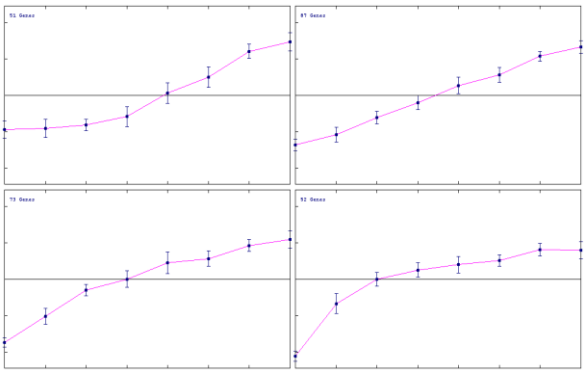

Figure 28 SOTA Four cluster analysis of expression profile positively correlated with valproate dose. SOTA clustering of expression profile positively correlated with valproate dose identified by CAST is shown as centroids graphs.Expression profiles with ≤ 1% FDR in SAM are taken as significant.

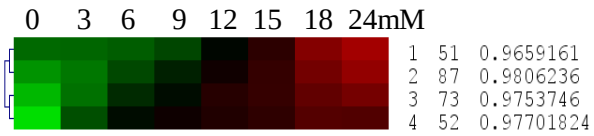

Figure 29 Dendogram of four cluster analysis of expression profile positively correlated with valproate dose. SOTA clustering of expression profile positively correlated with valproate dose identified by CAST is shown in the dendogram. Expression profiles with ≤ 1% FDR in SAM are taken as significant. Numbers across top of heatmap indicate valproate concentration. The degree of expression is indicated with a red to green scale where the higher expression is given by red.

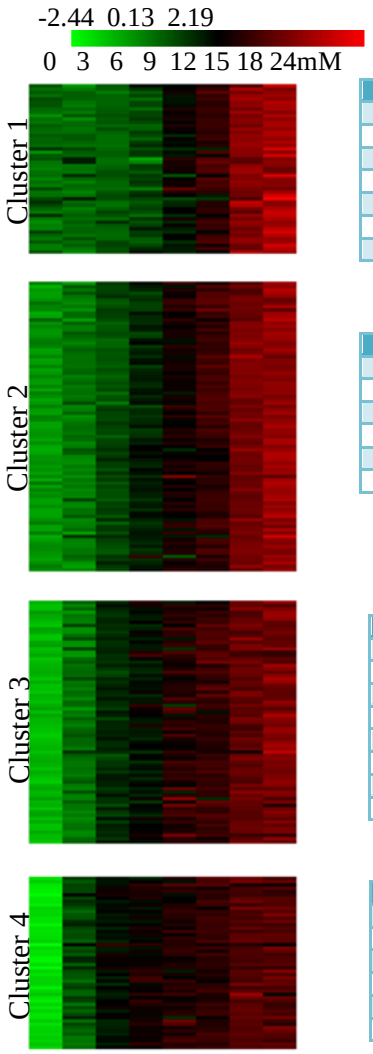

Cluster	Enrichment Score	Term	Count	PValue	Benjamini
1	20.6575	IPR008160:Collagen triple helix repeat	28	1.27E-38	7.38E-37
2	2.259283	GO:0040002~collagen and cuticulin-based	5	2.97E-04	0.013131
3	2.162389	cuticle	4	9.55E-05	0.002812
		signal peptide	6	0.019037687	0.369543
4	1.760744	GO:0010171~body morphogenesis	13	4.03E-07	3.59E-05
6	1.000599	GO:0006508~proteolysis	7	0.010605571	0.211193
7	0.900505	GO:0040008~regulation of growth	13	0.039822552	0.514872

Cluster	Enrichment Score	Term	Count	PValue	Benjamini
1	16.5654	IPR008160:Collagen triple helix repeat	26	7.32E-29	2.56E-27
2	8.889744	collagen	16	4.91E-20	2.60E-18
3	3.641014	IPR001810:Cyclin-like F-box	9	0.001897612	0.032693
4	2.224764	IPR004045:Glutathione S-transferase, N-terminal	4	0.002912604	0.040013
5	1.990804	GO:0030259~lipid glycosylation	4	0.001310132	0.158905
7	0.875629	iron	4	0.048988219	0.412821

Cluster	Enrichment Score	Term	Count	PValue	Benjamini
1	7.803873	IPR002213:UDP-glucuronosyl/UDP-glucosyltransferase	10	2.12E-10	1.63E-08
		GO:0030259~lipid glycosylation	7	5.31E-08	6.21E-06
2	3.83731	IPR004046:Glutathione S-transferase, C-terminal	6	4.40E-06	1.69E-04
3	3.078754	GO:0030246~carbohydrate binding	12	1.52E-08	1.45E-06
4	1.535437	GO:0008340~determination of adult life span	5	0.029145	0.684484
5	1.402542	IPR017973:Cytochrome P450, C-terminal region	4	0.005735	0.084759
6	1.104109	SM00256:FBOX	5	0.033329	0.111871
9	0.586723	IPR003439:ABC transporter-like	3	0.028896	0.221873

Cluster	Enrichment Score	Term	Count	PValue	Benjamini
1	6.034186	IPR016186:C-type lectin-like	9	9.65E-07	1.40E-05
2	5.175213	GO:0055114~oxidation reduction	11	1.14E-07	6.04E-06
		IPR001128:Cytochrome P450	7	3.07E-07	5.94E-06
3	4.713796	GO:0030246~carbohydrate binding	7	1.34E-04	0.001636
4	2.349013	IPR002213:UDP-glucuronosyl/UDP-glucosyltransferase	4	0.003166127	0.030189
7	0.519549	IPR003439:ABC transporter-like	3	0.016079331	0.11088

Figure 30 Four cluster analysis of expression profile positively correlated with valproate exposure. DAVID functional clustering of expression profiles of each cluster is shown next to the heat map of the respective cluster.Numbers across top of heatmaps indicate valproate concentration. The degree of expression is indicated with a red to green scale where the higher expression is given by red.

4.2.4. 1.2 Network analysis of the four clusters positively correlated with valproate exposure

After identifying the separate clusters which could be having common regulatory elements, I did Network Analysis of those clusters to identify those possible common regulatory elements. I used WormNet to identify the underlying gene interactions. Because *daf-2, daf-16* and *sma-6* were found to be involved in valproate induced lipid accumulation in the phenotypic analysis I did, I also generated networks of the genes in these clusters including these three genes to find their role at the molecular level. Network analysis of the four clusters with WormNet shows the first cluster to be mainly involved in collagen synthesis (Figure 31, page110).

The main network of interconnected genes of the second cluster contained *dao-4*, which is connected to dao-6 (Figure 32, page116). Both of these genes are regulated by DAF-16.

The third cluster contains genes known to be regulated by DAF-16, such as *dod-19*, *dod-20* and *dod-24* (Figure 33, page122). *dod-19* is a hub gene and *dod-24* connects several hub genes. Unlike the first two clusters, the network generated with genes of this cluster contains mainly genes involved in cellular detoxification with some genes involved in collagen synthesis and lipid metabolism.

Connected genes in the fourth cluster (Figure 34, page125) made a network of genes with two sub-clusters connected to each other via *daf-36*. *daf-36*is involved in a hormone biosynthetic pathway that produces the ligand for *daf-12*, which regulates the entering of *C.elegans* into high fat dauer stage(Rottiers et al., 2006).

Because *sma-6, daf-2* and *daf-16*are found to affect valproate induced lipid accumulation, I also did the network analysis including those three genes to find their position in the interaction networks. All clusters, except the first cluster, were connected to *daf-2, daf-16* and *sma-6* indicating an involvement of insulin signalling and TGF-β Sma/Mad pathways on valproate exposure. Also this analysis identifies B0286.3 as a key gene which may act upstream of *sma-6*. This is an uncharacterized gene in *C.elegans* and RNAi studies have shown it to cause larval arrest and larval lethality when mutated (WormBase). The human ortholog of this gene is phosphoribosylaminoimidazole carboxylase, a bifunctional enzyme, the activities of which are required for steps 6 and 7, respectively, of purine biosynthesis.

Cluster one is connnected to cluster 2 via *dao-4*, which is connected to *daf-2* and *sma-6* (Figure 35, page131). This indicates an overalll involvement of insulin signalling and *sma-6* on positively correlate expression profile on valproate exposure. This could be tested by analysing the overlap between the positively corelated expression profile on valproate exposure of the wild type *C.elegans* with the negatively correlated expresssion profile of *sma-6* mutants.

When all four clusters positively correlated with valproate are considered, the transcrition factors in or associated with all the four clusters show that most of them are to be associated with steroid hormone mediated signalling pathway (Table 28, page 131).

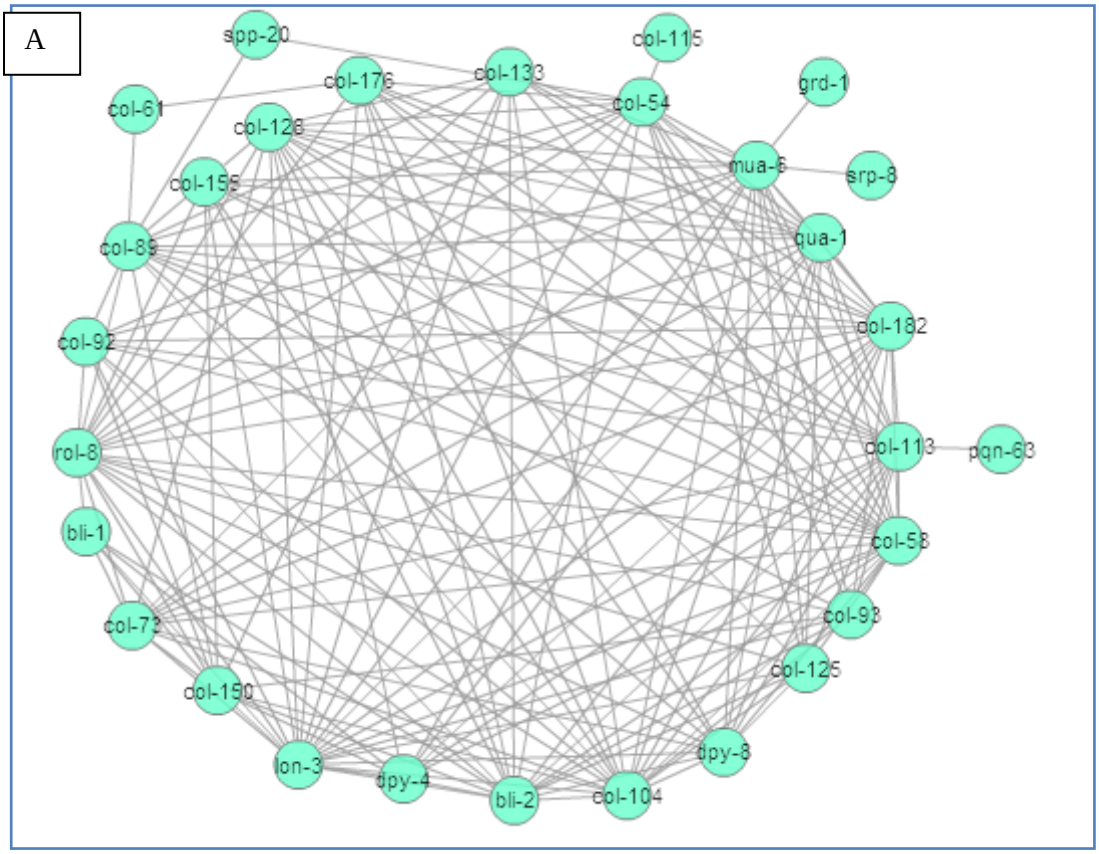

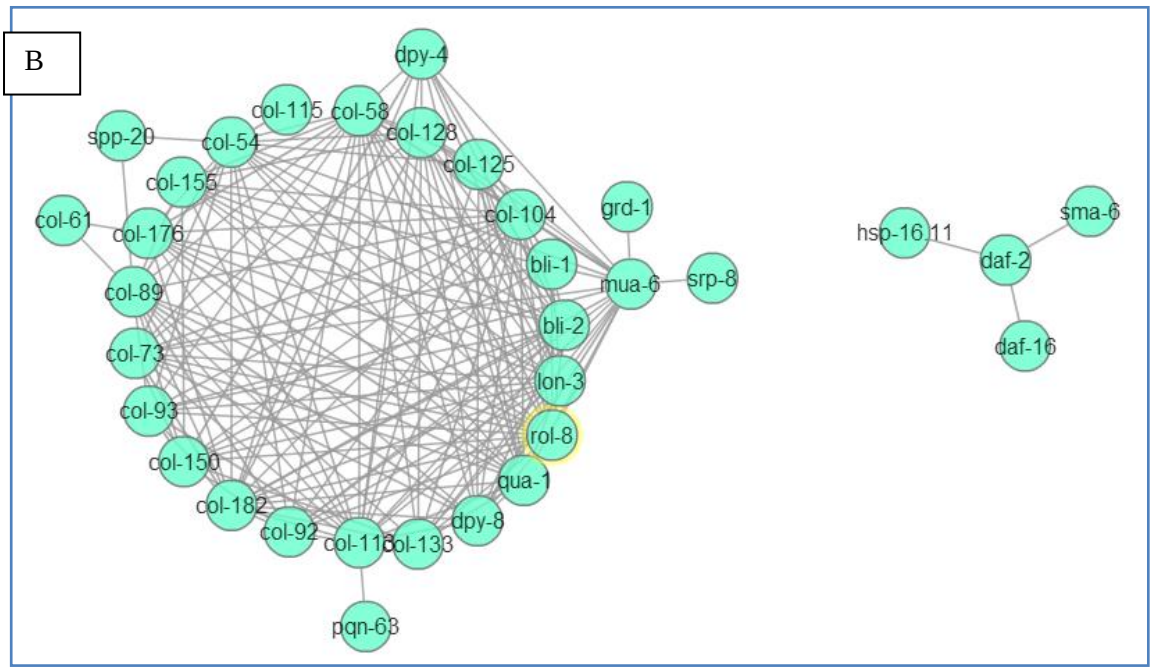

Figure 31Network graph of seed genes of SOTA cluster 1 of positively correlated genes with valproate identified by CAST. (A) Out of 51 genes, 42 genes were mapped in WormNet v. 2. Out of the 42 genes, 29 which were connected to each other are shown in the figure. Transcription factor nhr-203 in this cluster was

not found in WormNet. grd-1 is predicted to be involved in cholesterol dependent hedge-hog like signalling and is shown to be involved in growth, cuticle adhesion and mail tail development. This cluster is mainly composed of genes involved in collagen synthesis. (B) Same cluster with daf-2, daf-16 and sma-6 added. These three genes made a separate cluster from the main cluster. This shows that this expression profile is not directly connected to any of these three genes.

Table 19Evidence codes for 21 types of data sets incorporated in WormNet

Evidence code	Data set description
CE-CC	Co-citation of worm gene
CE-CX	Co-expression among worm genes
CE-GN	Gene neighbourhoods of bacterial and archaeal orthologs of worm genes
CE-GT	Worm genetic interactions
CE-LC	Literature curated worm protein physical interactions
CE-PG	Co-inheritance of bacterial and archaeal orthologs of worm genes
CE-YH	High -throughput yeast two hybrid assays among worm genes
DM-PI	Fly protein physical interactions
HS-CC	Co-citation of human genes
HS-CX	Co-expression among human genes
HS-DC	Co-occurance of domains among human proteins
HS-LC	Literature curated human protein physical interactions
HS-MS	Human protein complexes from affinity purification/mass Spectrometry
HS-YH	High -throughput yeast two hybrid assays among human genes
SC-CC	Co-citation of yeast genes
SC-CX	Co-expression among yeast genes
SC-DC	Co-occurance of domains among yeast proteins
SC-GT	Yeast genetic interactions
SC-LC	Literature curated yeast protein physical interactions
SC-MS	Yeast protein complexes from affinity purification/mass Spectrometry
SC-TS	Yeast protein interactions inferred from tertiary structures of complexes

Table 20Transcription factors in or associated with SOTA cluster 1 of positively correlated genes with valproate identified by CAST. Only genes found in WormNet are given. Refer Table 19 for the evidence codes.

Rank	Locus_ ID	Symbol	Score	Evidence	#_linked_seed / #_valid_seed	Linked_seed	GO_P	GO_C	GO_F
26	ZK180.5	na	4.90	CE-CX:0.99 DM-PI:0.01	23/45	try-2 col-125 dpy-8 col-113 col-73 col-128 col-89 col-58 col-54 col-133 col-155 col-104 bli-2 col-182 qua-1	regulation of transcription, DNA-dependent;	nucleus;	transcription factor activity;

					pqn-63 col-93 col-92 mua-6 dpy-4 col-176 rol-8 lon-3			
Not in Worm net	M02H5.5	nhr-203				regulation of transcription, DNA-dependent;	nucleus;	transcription factor activity; steroid hormone receptor activity; zinc ion binding; sequence-specific DNA binding;

Table 21 Seed genes of SOTA cluster 1 of genes positively correlated with valproate dose identified by CAST ranked by total connectivity. First ten genes are shown in the table. Refer Table 19 for the evidence codes.

Rank	Symbol	Score	Evidences	#_linked_seed / #_valid_seed	Linked_seed	GO_P	GO_C	GO_F
1	col-58	5.27	CE-CX:1.00	20/45	col-125 dpy-8 col-113 col-73 col-128 col-89 col-54 col-133 col-155	phosphate transport;	cytoplasm;	structural constituent of cuticle;

					col-104 bli-2 col-182 qua-1 col-93 col-92 mua-6 dpy-4 col-176 rol-8 lon-3			
2	lon-3	5.06	CE-CX:1.00	21/45	col-150 bli-1 col-125 dpy-8 col-113 col-73 col-128 col-58 col-54 col-133 col-155 col-104 bli-2 col-182 qua-1 col-93 col-92 mua-6 dpy-4 col-176 rol-8	phosphate transport; negative regulation of body size;	cytoplasm;	structural constituent of cuticle;
3	col-104	4.95	CE-CX:1.00	19/45	col-150 col-125 dpy-8 col-113 col-73 col-128 col-89 col-58 col-133 col-155 bli-2 col-182 qua-1 col-93 col-92 mua-6 col-176 rol-8 lon-3	phosphate transport; metabolic process;	cytoplasm;	catalytic activity; structural constituent of cuticle;
4	col-73	4.93	CE-CX:1.00	13/45	col-150 bli-1 dpy-8 col-113 col-128 col-58 col-54 col-104 col-182 qua-1 mua-6 rol-8 lon-3	phosphate transport; positive regulation of body size;	cytoplasm;	structural constituent of cuticle;
5	rol-8	4.89	CE-CX:1.00	20/45	col-150 bli-1 col-125 dpy-8	phosphate transport;	cytoplasm;	structural constituent of cuticle;

					col-73 col-128 col-89 col-58 col-54 col-133 col-155 col-104 bli-2 col-182 qua-1 col-93 col-92 mua-6 col-176 lon-3			
6	col-182	4.71	CE-CX:1.00	18/45	dpy-8 col-113 col-73 col-128 col-89 col-58 col-54 col-133 col-104 bli-2 qua-1 col-93 col-92 mua-6 dpy-4 col-176 rol-8 lon-3	phosphate transport;	cytoplasm;	na
7	dpy-8	4.65	CE-CX:1.00	14/45	col-125 col-113 col-73 col-128 col-89 col-58 col-104 bli-2 col-182 qua-1 mua-6 col-176 rol-8 lon-3	phosphate transport; locomotory behavior; oviposition; cuticle biosynthetic process (sensu Nematoda); positive regulation of body size;	cytoplasm;	structural constituent of cuticle;
8	bli-2	4.61	CE-CX:1.00	18/45	col-150 bli-1 col-125 dpy-8 col-113 col-128 col-58 col-54 col-133 col-155 col-104 col-182 col-93 col-92	phosphate transport; locomotory behavior; metabolic process; cuticle biosynthetic process (sensu Nematoda); cuticular attachment	cytoplasm; external encapsulating structure;	oxidoreductase activity; structural constituent of cuticle; structural constituent of cuticle (sensu Nematoda);

					dpy-4 col-176 rol-8 lon-3	to epithelium (sensu Nematoda);		
9	dpy-4	4.61	CE-CX:1.00	10/45	col-150 bli-1 col-113 col-128 col-58 bli-2 col-182 qua-1 mua-6 lon-3	larval development (sensu Nematoda); phosphate transport; locomotory behavior; positive regulation of body size;	cytoplasm;	structural constituent of cuticle;
10	col-133	4.45	CE-CX:1.00	11/45	col-150 col-128 col-89 col-58 col-104 bli-2 col-182 qua-1 mua-6 rol-8 lon-3	morphogenesis of an epithelium; phosphate transport; embryonic development (sensu Metazoa); positive regulation of growth rate;	cytoplasm;	structural constituent of cuticle;

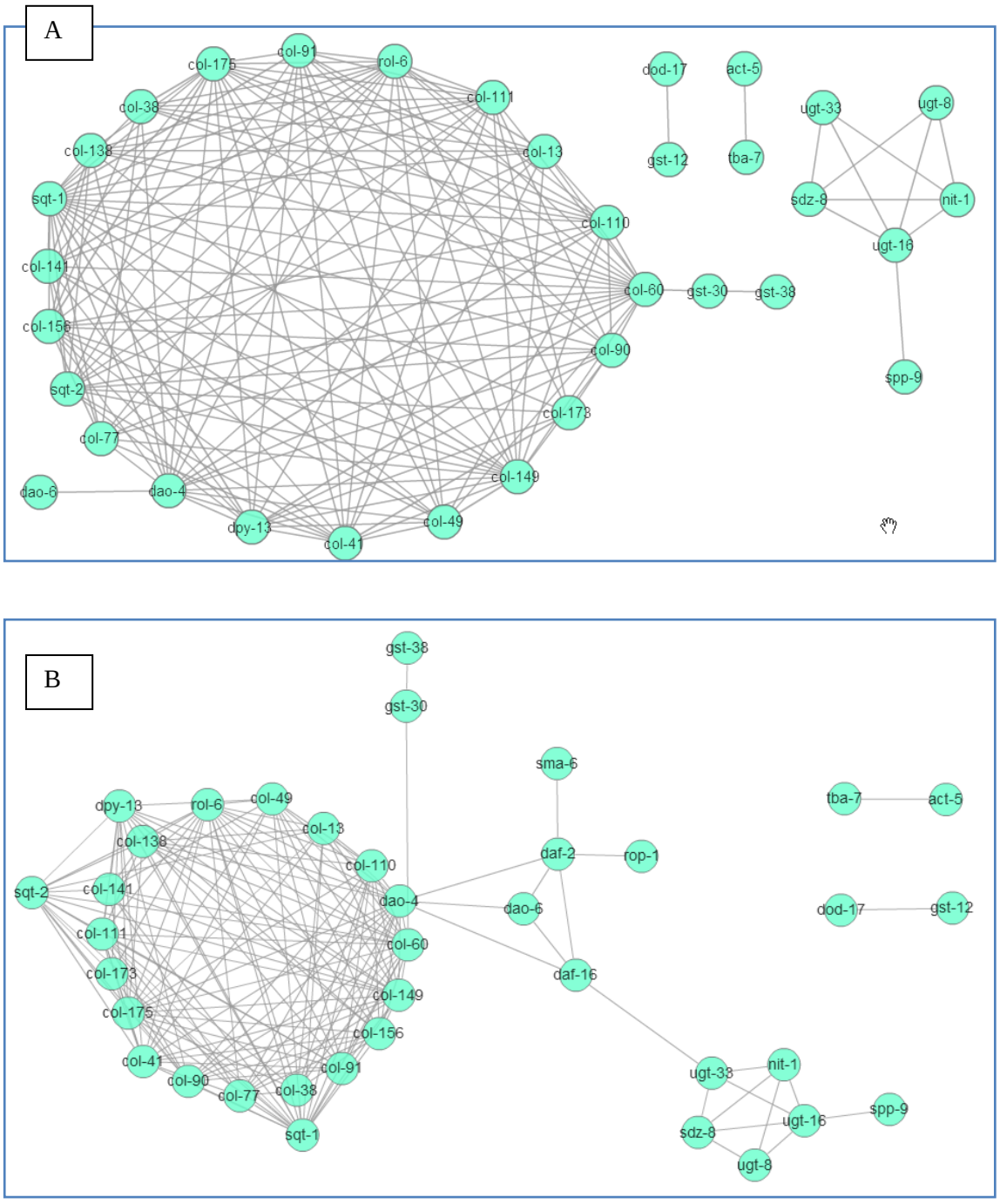

Figure 32 Network graph of seed genes of SOTA cluster 2 of genes positively correlated with valproate identified by CAST. (A)Out of 84 genes, 66 genes were mapped in WormNet v. 2. Out of the 66 genes, 34 which were connected to each other are shown in the figure. Transcription factors nhr-25 and nhr-234were not connected to other genes in the cluster. Transcription factors nhr-245 and nhr-202 are not found in the WormNet. DAF-2 negatively regulates dao-6, which is positively regulated by DAF-16. But*dao-4* is down

regulated in *daf-2* mutants in a DAF-16 dependent manner. sma- 6 mutants show high expression of spp-9. The largest network generated contains genes involved in collagen synthesis and a separate smaller network contains genes involved in cellular detoxification. (B) Same cluster with daf-2, daf-16 and sma-6 added. These three genes were connected to the main cluster. *daf-2* and *daf-16* seems to be downstream of *sma-6* and this sub cluster connects clusters involved in cellular detoxification with cell morphogenesis, mainly collagen synthesis.

Table 22 Transcription factors in or associated with SOTA cluster 2 of genes positively correlated with valproate identified by CAST. These transcription factors either disconnected or are not found in WormNet.

Locus_ID	Symbol	GO_P	GO_C	GO_F
C27C7.8	nhr-259	regulation of transcription, DNA-dependent;	nucleus;	transcription factor activity; steroid hormone receptor activity;
Y38E10A.18	nhr-234	regulation of transcription, DNA-dependent;	nucleus;	transcription factor activity; steroid hormone receptor activity; zinc ion binding; sequence-specific DNA binding;
ZK1025.10	nhr-245	regulation of transcription, DNA-dependent;	nucleus;	transcription factor activity; steroid hormone receptor activity; zinc ion binding; sequence-specific DNA binding;
M02H5.4	nhr-202	regulation of transcription, DNA-dependent;	nucleus;	transcription factor activity; steroid hormone receptor activity; zinc ion binding; sequence-specific

				DNA binding;
ZK180.5	na	col-149 sqt-1 sqt-2 col-90 col-175 col-138 col-91 col-13 col-60 col-111 dpy-13 col-38 col-156 col-77 pqn-54 rol-6 col-41 col-141	regulation of transcription, DNA-dependent;	nucleus;

Table 23 Seed genes of SOTA cluster 2 of genes positively correlated with valproate identified by CAST ranked by total connectivity. First ten genes are shown in the table. Refer Table 19 for the evidence codes.

Rank	Symbol	Score	Evidences	#_linked_seed / #_valid_seed	Linked_seed	GO_P	GO_C	GO_F
1	sqt-1	5.77	CE-CX:0.88 CE-GT:0.08 CE-CC:0.05	20/75	col-149 sqt-2 col-90 col-175 col-138 col-91 col-13 col-110 col-60 col-111 dpy-13 col-173 col-38 col-156 col-49 col-77 rol-6 col-41 col-141 dao-4	phosphate transport; embryonic development (sensu Metazoa); cuticle biosynthetic process (sensu Nematoda); positive regulation of body size;	cytoplasm;	structural constituent of cuticle;
2	rol-6	5.50	CE-CX:0.85 CE-GT:0.09 CE-CC:0.06	18/75	col-149 sqt-1 sqt-2 col-175 col-138 col-91 col-13 col-110 col-60 col-111 col-173 col-38 col-156 col-49 col-77 col-41 col-141	phosphate transport; oviposition; positive regulation of body size; cuticle biosynthetic process during molting (sensu Nematoda);	extracellular matrix (sensu Metazoa); cytoplasm;	structural constituent of cuticle; structural constituent of cuticle (sensu Nematoda);

					dao-4			
3	col-156	5.44	CE-CX:1.00	14/75	col-149 sqt-1 col-90 col-175 col-138 col-110 col-60 dpy-13 col-38 col-49 col-77 rol-6 col-41 dao-4	phosphate transport;	cytoplasm;	structural constituent of cuticle;
4	dpy-13	5.44	CE-CX:1.00	14/75	col-149 sqt-1 sqt-2 col-90 col-175 col-91 col-60 col-111 col-173 col-156 col-49 col-41 col-141 dao-4	phosphate transport; locomotory behavior; positive regulation of body size; post-embryonic body morphogenesis;	cytoplasm;	structural constituent of cuticle;
5	sqt-2	5.41	CE-CX:0.88 CE-GT:0.12	14/75	col-149 sqt-1 col-90 col-175 col-138 col-91 col-13 col-60 col-111 dpy-13 col-173 rol-6 col-41 col-141	phosphate transport;	cytoplasm;	structural constituent of cuticle;
6	col-175	5.25	CE-CX:1.00	18/75	col-149 sqt-1 sqt-2 col-90 col-138 col-91 col-13 col-110 col-60 col-111 dpy-13 col-38 col-156 col-49 rol-6 col-41 col-141 dao-4	phosphate transport;	cytoplasm;	structural constituent of cuticle;
7	col-41	5.10	CE-CX:1.00	14/75	col-149 sqt-1 sqt-2 col-175 col-91 col-13 col-111 dpy-13 col-173 col-156 col-49 col-	phosphate transport;	cytoplasm;	structural constituent of cuticle;

					77 rol-6 dao-4			
8	col-138	5.08	CE-CX:1.00	12/75	col-149 sqt-1 sqt-2 col-175 col-13 col-110 col-60 col-111 col-156 rol-6 col-141 dao-4	phosphate transport;	cytoplasm;	structural constituent of cuticle;
9	col-77	5.05	CE-CX:1.00	11/75	col-149 sqt-1 col-110 col-60 col-111 col-38 col-156 rol-6 col-41 col-141 dao-4	phosphate transport;	cytoplasm;	structural constituent of cuticle;
10	col-90	4.99	CE-CX:1.00	12/75	col-149 sqt-1 sqt-2 col-175 col-91 col-110 col-60 col-111 dpy-13 col-173 col-156 dao-4	phosphate transport; positive regulation of body size;	cytoplasm;	structural constituent of cuticle;

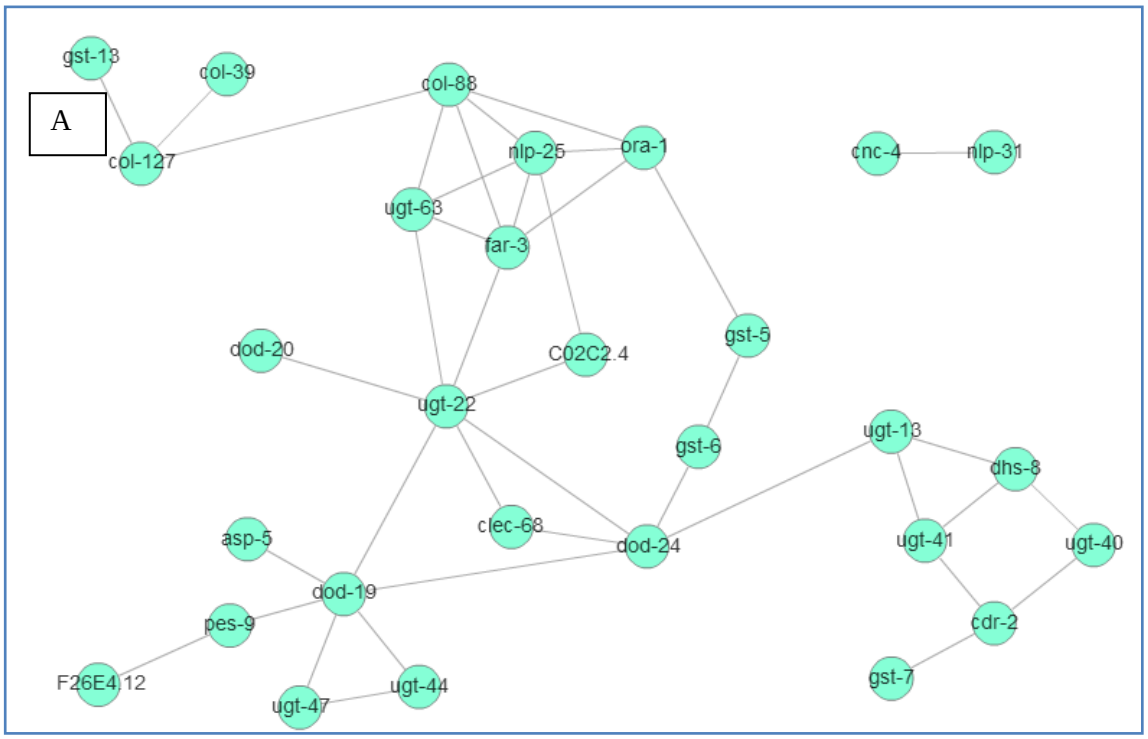
A
gst-13
col-39
col-88
col-127
nlp-25
ora-1
cnc-4
nlp-31
ugt-63
far-3
gst-5
dod-20
C02C2.4
ugt-22
gst-6
ugt-13
dhs-8
clec-68
dod-24
asp-5
ugt-41
ugt-40
dod-19
pes-9
cdr-2
F26E4.12
ugt-47
ugt-44
gst-7

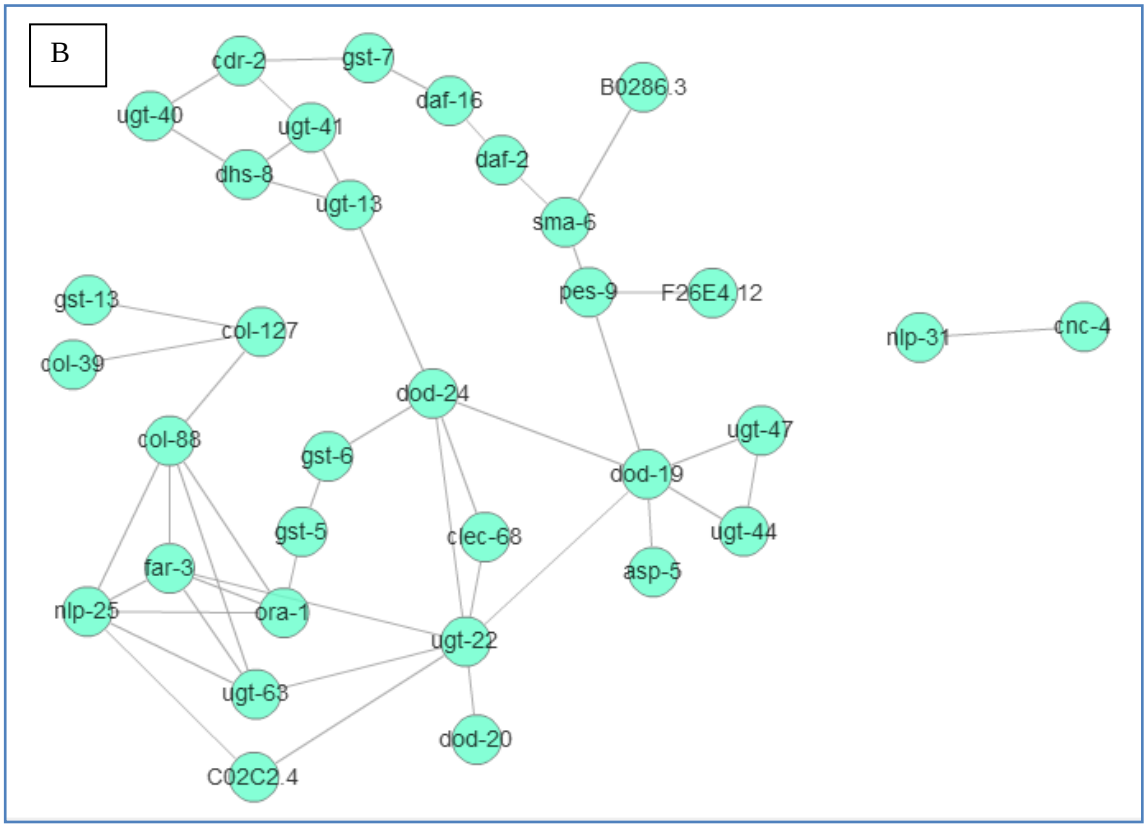

Figure 33 Network graph of seed genes of SOTA cluster 3 of genes positively correlated with valproate identified by CAST. (A)Out of 73 genes, 53 genes were mapped in WormNet v. 2. Out of the 53 genes, 29, which were connected to each other, are shown in the figure.The majority of the genes in this network are involved in cellular detoxification. It also contains some genes involved in collagen synthesis and lipid metabolism. *dod-20 and dod-19* mutants are known to have reduced fat content and is regulated by DAF-16. far-3 codes for a fatty acid binding protein and expression of far-3 is down regulated in sir-2; lin-35 double mutant. dod-24 connects hub genes of several sub clusters and it is also known to be regulated by DAF-16. (B) Same cluster with daf-2, daf-16 and sma-6 added. These three genes were connected to the main cluster. *daf-2* and *daf-16* seems to be downstream of *sma-6* and B0286.3 seems to be upstream to sma-6.

Table 24 Transcription factors in or associated with SOTA cluster 3 of genes positively correlated with valproate identified by CAST. Refer Table 19 for the evidence codes.

Rank	Locus_ID	Symbol	Score	Evidence	#_linked_seed / #_valid_seed	Linked_seed	GO_P	GO_C	GO_F
79	ZK180.5	na	2.93	CE-CX:1.00	3/63	col-39 col-127 col-88	regulation of transcription, DNA-dependent;	nucleus;	transcription factor activity;
156	W02C12.3	hlh-30	2.56	HS-CC:1.00	1/63	tyr-4	regulation of transcription;	nucleus;	transcription regulator activity;

Table 25Seed genes of SOTA cluster 3 of genes positively correlated with valproate identified by CAST ranked by total connectivity. First ten genes are shown in the table. Refer Table 19 for the evidence codes.

Rank	Locus_ID	Symbol	Score	Evidences	#_linked_seed / #_valid_seed	Linked_seed	GO_P	GO_C	GO_F
1	F54D1.3	col-127	3.64	CE-CX:1.00	3/63	col-39 gst-13 col-88	phosphate transport;	cytoplasm;	structural constituent of cuticle;
2	W05G11.3	col-88	3.38	CE-CX:1.00	5/63	ugt-63 far-3 col-127 ora-1 nlp-25	phosphate transport;	cytoplasm;	structural constituent of cuticle;
3	C09G5.4	col-39	2.87	CE-CX:1.00	1/63	col-127	phosphate transport;	cytoplasm;	structural constituent of cuticle;
4	C08F11.8	ugt-22	2.30	CE-CX:1.00	7/63	dod-20 C02C2.4 ugt-63 dod-24 far-3 clec-68 dod-19	metabolic process;	na	transferase activity, transferring hexosyl groups;
5	K10H10.3	dhs-8	2.28	CE-CX:1.00	3/63	ugt-41 ugt-40 ugt-13	metabolic process;	na	oxidoreductase activity;
6	Y43F8C.1	nlp-25	2.16	CE-CX:1.00	5/63	C02C2.4 ugt-63 far-3 ora-1 col-88	na	na	na
7	F10D2.11	ugt-41	2.16	CE-CX:1.0	3/63	cdr-2 ugt-13	metabolic process;	na	transferase activity,

				0		dhs-8			transferring hexosyl groups;
8	C32H11.12	dod-24	1.91	CE-CX:1.00	5/63	ugt-22 gst-6 clec-68 ugt-13 dod-19	determination of adult life span;	na	na
9	F15B9.1	far-3	1.91	CE-CX:1.00	5/63	ugt-63 ugt-22 ora-1 col-88 nlp-25	na	na	na
10	C04F5.7	ugt-63	1.78	CE-CX:1.00	4/63	ugt-22 far-3 col-88 nlp-25	metabolic process;	na	transferase activity, transferring hexosyl groups;

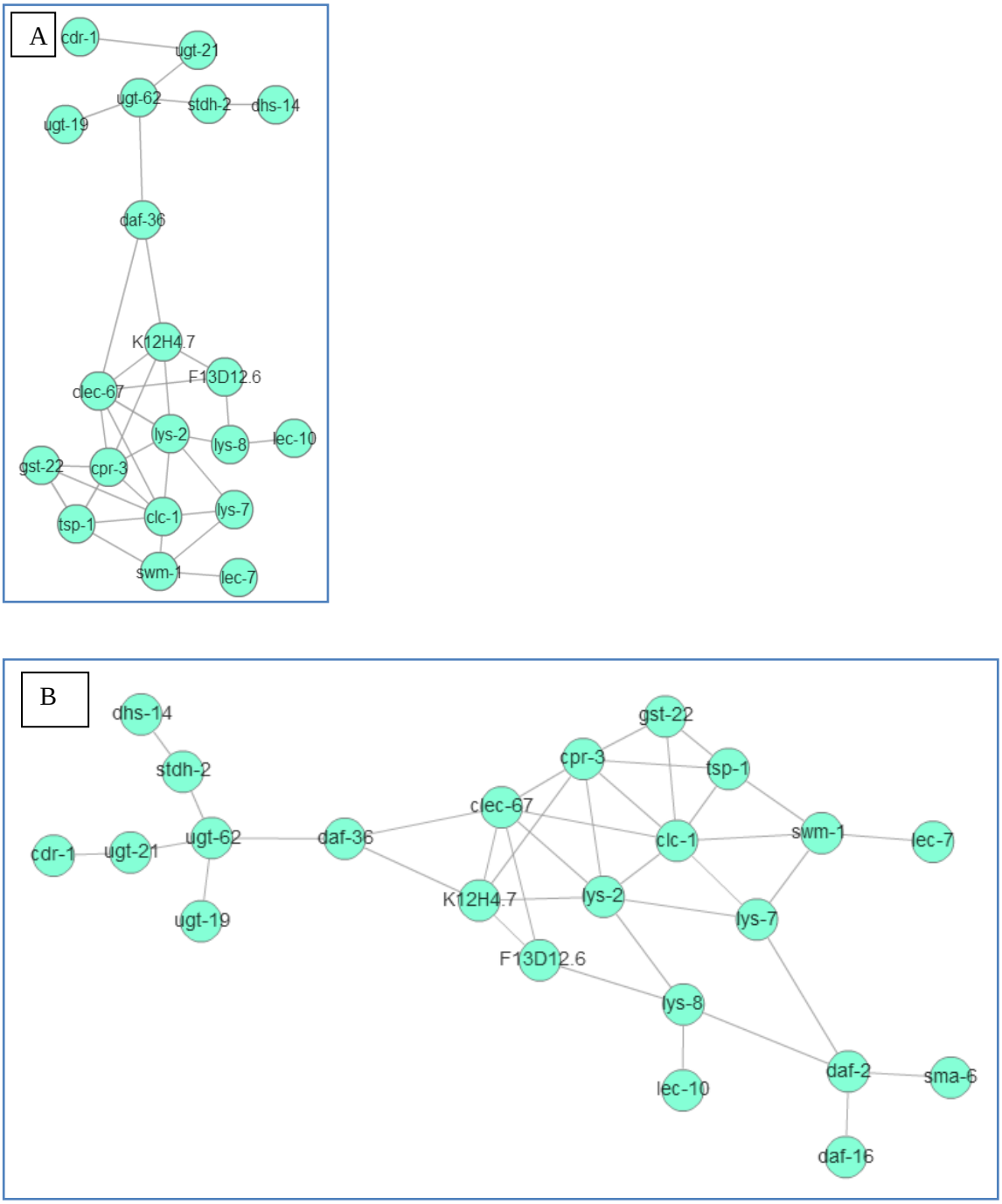

Figure 34Network graph of seed genes of SOTA cluster 4 of genes positively correlated with valproate identified by CAST. (A) Out of 51 genes, 32 genes were mapped in WormNet v. 2. Out of the 32 genes, 20 which were connected to each other are shown in the figure. These genes were clustered into two network modules connected via daf-36, which functions in a hormone biosynthetic pathway and produce the ligand for daf-12 nuclear receptor which regulates the decision between reproductive development and dauer formation,

lipid metabolism as well as lifespan. DAF-36 is a cholesterol 7- desaturase and is a key enzyme in steroidogenesis. (B) Same cluster with daf-2, daf-16 and sma-6 added. These three genes were connected to the main cluster. *daf-2* and *daf-16* seems to be downstream of *sma-6* , which is connected to a second smaller cluster via *daf-36*.

Table 26Transcription factors/ regulators of transcription factors in or associated with SOTA cluster 4 of genes positively correlated with valproate identified by CAST. Refer Table 19 for the evidence codes.

Rank	Locus_ID	Symbol	Score	Evidence	#_linked_seed / #_valid_seed	Linked_seed	GO_P	GO_C	GO_F
Disconnected seed gene	F44E7.8	nhr-142					regulation of transcription, DNA-dependent;	nucleus;	DNA binding; transcription factor activity; steroid hormone receptor activity; ligand-dependent nuclear receptor activity; zinc ion binding; sequence-

									specific DNA binding;
Not found in Wormnet	Y70C5C.6	nhr-112					reproduction; regulation of transcription, DNA-dependent;	nucleus;	transcription factor activity; steroid hormone receptor activity; zinc ion binding; sequence-specific DNA binding;
17	F33A8.3	cey-1	3.06	CE-CX:0.50 HS-CC:0.50	3/35	lys-8 F13D12.6 pgp-1	regulation of transcription, DNA-dependent;	na	nucleic acid binding; DNA binding;
101	Y55D5A.5	daf-2	2.38	CE-GT:1.00	2/35	lys-7 lys-8	reproduction; protein amino acid phosphorylation; locomotory behavior; determination of adult life span; ATP synthesi	integral to plasma membrane; membrane; proton-transporting two-sector ATPase complex;	protein kinase activity; protein-tyrosine kinase activity; transmembrane

	s coupled proton transport; dauer larval development; negative regulation of transcription factor import into nucleus; dauer exit;	receptor protein tyrosine kinase activity; epidermal growth factor receptor activity; insulin receptor activity; ATP binding; peptide hormone binding; SH2 domain binding; hydrogen ion transporting ATP synthase activity, rotational mechanism; hydrogen

									ion transporting ATPase activity, rotational mechanism;
111	F02E9.4	pqn-28	2.34	SC-CC:1.00	1/35	pgp-1	DNA repair; regulation of transcription, DNA-dependent;	nucleus;	na
183	Y49A3A.1	na	2.08	CE-CX:0.50 SC-LC:0.50	3/35	lys-8 stdh-2 F13D12.6	regulation of transcription, DNA-dependent; phospholipid biosynthetic process; embryonic development (sensu Metazoa); negative regulation of body size;	nucleus;	sequence-specific DNA binding; protein dimerization activity;

Table 27 Seed genes of SOTA cluster 4 of genes positively correlated with valproate identified by CAST ranked by total connectivity. First ten genes are shown in the table.Refer Table 19 for the evidence codes.

Rank	Locus_ID	Symbol	Score	Evidences	#_linked_seed / #_valid_seed	Linked_seed	GO_P	GO_C	GO_F
1	C09F12.1	clc-1	2.86	CE-CX:1.00	7/35	lys-7 tsp-1 swm-1 gst-22 clec-67 cpr-3 lys-2	na	na	na
2	Y22F5A.5	lys-2	2.80	CE-CX:1.00	6/35	lys-7 clc-1 lys-8 clec-67 K12H4.7 cpr-3	peptidoglycan catabolic process; cell wall catabolic process;	na	lysozyme activity;
3	K12H4.7	na	2.69	CE-CX:1.00	5/35	daf-36 F13D12.6 clec-67 cpr-3 lys-2	proteolysis;	na	catalytic activity; serine-type peptidase activity;
4	F11A5.12	stdh-2	2.63	SC-TS:0.74 HS-CX:0.26	2/35	ugt-62 dhs-14	metabolic process; determination of adult life span;	na	oxidoreductase activity;
5	F13D12.6	na	2.54	CE-CX:1.00	3/35	lys-8 clec-67 K12H4.7	proteolysis;	na	catalytic activity; serine carboxypeptidase activity;
6	R05D8.8	dhs-14	2.42	SC-TS:1.00	1/35	stdh-2	metabolic process;	na	oxidoreductase activity;
7	T10H4.12	cpr-3	2.00	CE-CX:1.00	6/35	tsp-1 clc-1 gst-22 clec-67 K12H4.7 lys-2	proteolysis; embryonic development (sensu Metazoa);	na	cysteine-type endopeptidase activity; cysteine-type peptidase activity;
8	C17G10.5	lys-8	1.69	CE-CX:1.00	3/35	F13D12.6 lec-10 lys-2	peptidoglycan catabolic process; cell wall catabolic process;	na	lysozyme activity;
9	C12D8.5	daf-36	1.63	CE-CX:1.00	3/35	clec-67 K12H4.7 ugt-62	electron transport;	na	oxidoreductase activity;
10	F56D6.	clec-	1.59	CE-	6/35	clc-1 daf-	na	na	sugar

2	67	CX:1.00	36 F13D12.6 K12H4.7 cpr-3 lys-2	binding;

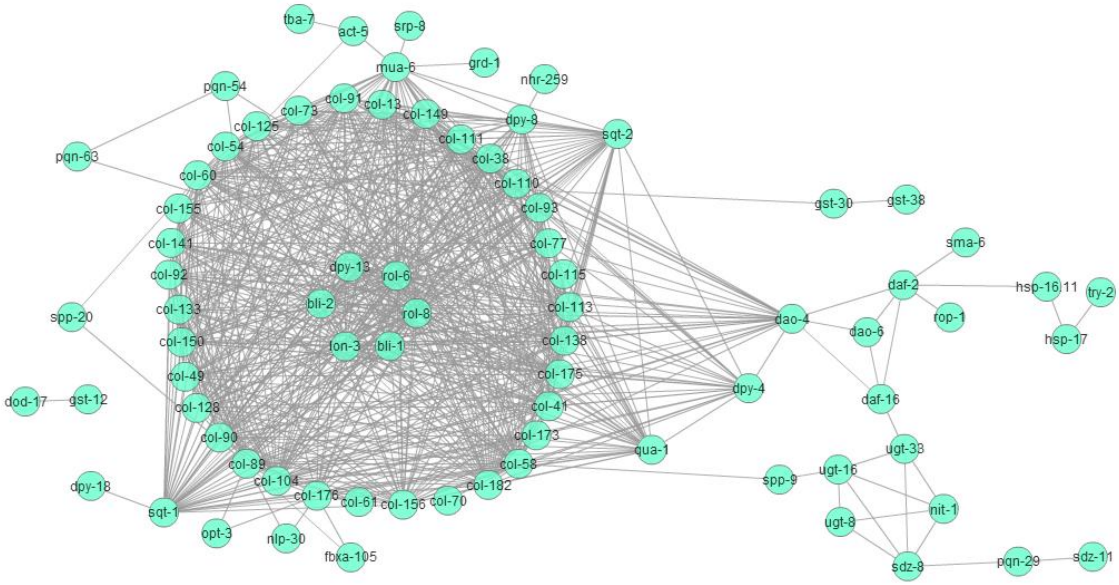

Figure 35 Network graph of seed genes of SOTA cluster 1 and 2 together of genes positively correlated with valproate identified by CAST with daf-2, daf-16 and sma-6 added. (A) Out of 138 genes, 111 genes were mapped in WormNet v. 2. Out of the 111 genes, 79 which were connected to each other are shown in the figure. This shows that cluster 1 which was not connected to *daf-2*is actually connected to it indirectly via *dpy-4*.

Table 28 Analysis of transcription factors in or associated with all the four clusters of genes positively correlated with valproate exposure.

Locus ID	Symbol	Regulator type	Biological process	RNAi Phenotypes
M02H5.5	nhr-203		Steroid hormone mediate signalling pathway	

ZK180.5				
C27C7.8	nhr-259		Steroid hormone mediate signalling pathway	
Y38E10A.18	nhr-234		Steroid hormone mediate signalling pathway, lipid storage	
ZK1025.10	nhr-245		Steroid hormone mediate signalling pathway	
	nhr-202		Steroid hormone mediate signalling pathway	
ZK180.5	na			
	na			
W02C12.3	hlh-30	Activator	Lipid storage, reproduction	Fat content reduced, reduced brood size
	nhr-142		Steroid hormone mediate signalling pathway, lipid storage	
Y70C5C.6	nhr-112			Fat content increased
F33A8.3	cey-1			
Y55D5A.5	daf-2	repressor	Dauer entry and exit, dauer larval development, determination of adult lifespan, insulin receptor signalling pathway,	Fat content increased

		lipid storage, locomotion, nematode larval development, organ senescence, positive regulation of multicellular organism growth, protein aotophosphorylation, regulation of response to reactive oxigen species, reproduction, response to heat, transmembrane receptor protein tyrosine kinase signalling pathway.	
F02E9.4	pqn-28		
Y49A3A.1	na	Lipid storage, phospholipid biosynthesis process	Fat content reduced

4.2.4.2 Expression profile negatively correlated with valproate concentration

After showing that the positive correlation with valproate exposure is via insulin and TGF-β Sma/Mad pathways probably through steroid hormone signalling, I then looked at the expression profile negatively correlated with valproate exposure. CAST clustering identified 485 expression profiles negatively correlated with valproate exposure. Only 90 of these had a known function on gene ID conversion and functional annotation done by DAVID gene ID conversion tool and functional annotation tool. HCL clustering of these known genes separated them into several different clusters shown in Figure 36.

Unlike the positively correlated expression profile, which had several similar genes, this negatively correlated expression profile had dissimilar genes (Table 29, page 135). Cluster 1.1 contains rab family member, a family of proteins known to associate with lipid droplets in mammals. Cluster 2.1 contains BBS (Bardet-Biedl Syndrome) protein, a syndrome associated with obesity(Forsythe and Beales, 2012).

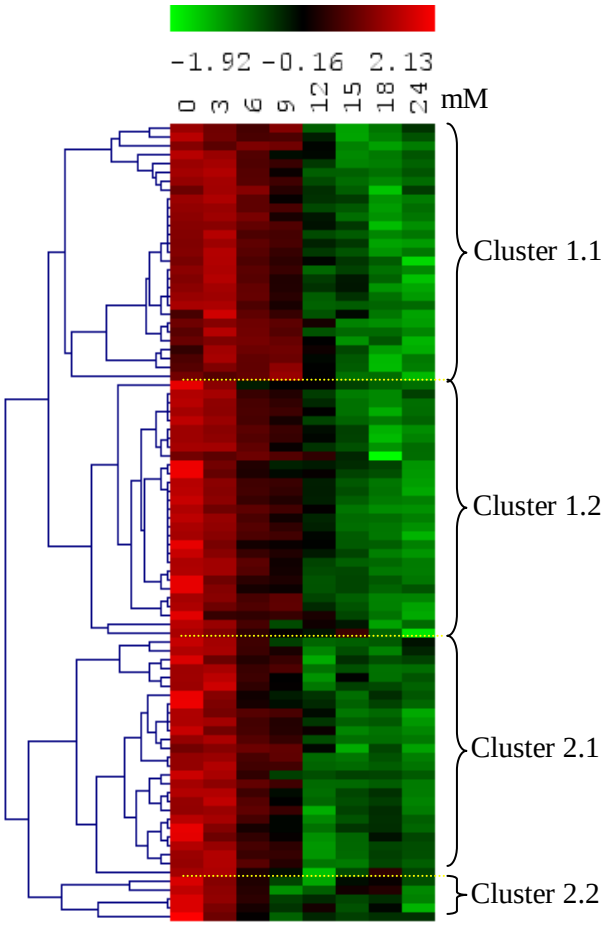

Figure 36 Heat map showing HCL clustering of expression profile negatively correlated with valproate dose. Expression profile identified by CAST as negatively correlated with valproate dose is shown as a heat map. HCL clustering of these genes identified several clusters and the genes in these clusters are shown in Table 29.Numbers across top of heatmap indicate valproate concentration. The degree of expression is indicated with a red to green scale where the higher expression is given by red.

Table 29This table shows the genes in each cluster in Figure 36. Number of genes of each type are given in parentheses.

Cluster 1.1	Cluster 1.2	Cluster 2.1	Cluster 2.2
C-type lectin (5)	C-type lectin (5)	C-type lectin (4)	Uncoordinated (2)
ARF-Like (2)	Collagen (3)	Groundhog (2)	Coronin
Cutclin (2)	THaumatiN family (2)	Helix Loop Helix (2)	Slowpoke potassium channel family
Acetylcholinesterase	Acetylcholinesterase	Glutamate Receptor family (AMPA)	Myosin Light Chain
neuronal ceroid lipofuscinosis related	Blistered cuticle	Resistance to Inhibitors of Cholinesterase	
Enhancer of unc-40 Ventral Axon guidance defects	Cyclin-Dependent Kinase family	Dehydrogenases, Short chain	
SynaptoGenesis abnormal	Carnitine Palmitoyl Transferase	Dystrobrevin homolog	
Homeobox	Cuticlin	GalactoFuranose synthesis (UGM, UDP-galactopyranose mutase)	
FriZzled homolog	Fatty acid desaturase	Collagen	
Dumpy	F-box B protein	Hexosaminidase	
Dynein Light chain	FerroPortiN	Lipase related	
Gamma Butyrobetaine Hydroxylase	Intermediate Filament, C	Insulin related	
Intermediate Filament, A	Invertebrate LYSozyme	L1 CAM Adhesion molecule homolog	
Insulin related	INneXin	Suppressor/Enhancer of Lin-12	
Jun N-terminal Kinase	Nematode AStacin protease (only	Slit (Drosophila)	

	BMP-1/Tolloid homolog in C. elegans)	homolog
RAB family	abnormal NUClease	Syntrophin
Rho GTPase Activating protein	PHAryngeal gland Toxin-related	Uncoordinated
TransThyretin-Related family domain	PLeXin	D-amino-acid oxidase 2
Uncoordinated	SCP-Like extracellular protein	Probable galactose-1-phosphate uridylyltransferase
Others (4)	TropoNin T	Amino acid Transporter Glycoprotein subunit
	2 (Zwei) IG-domain protein	BBS (Bardet-Biedl Syndrome) protein
		Calcium Binding protein homolog

DAVID functional clustering identified this negatively correlated expression profile to be enriched in lectins and signal peptides (Table 30).

Table 30 David functional clustering of expression profile negatively correlated with valproate dose identified by CAST. Expression profiles with a p value of <0.05 are shown.

Cluster	Enrichment Score	Term	Count	PValue	Benjamini
1	6.172376	IPR016186:C-type lectin-like	18	3.13E-08	9.71E-06
2	3.096296	signal peptide	20	4.32E-06	8.56E-04
3	2.993274	IPR008139:Saposin B	5	5.73E-04	0.043417
4	2.969779	Lectin	11	6.19E-06	7.05E-04
5	2.65101	GO:0055002~striated muscle cell development	4	0.001472	0.146283
6	2.399801	GO:0010259~multicellular organismal ageing	10	0.003983	0.167714
7	1.991721	IPR013032:EGF-like region, conserved site	11	3.78E-04	0.038273
8	1.662147	IPR003599:Immunoglobulin subtype	5	0.003555	0.11543
9	1.583614	GO:0008378~galactosyltransferase activity	4	0.004067	0.27968
10	1.48891	GO:0045111~intermediate filament cytoskeleton	3	0.012568	0.53181

11	1.349825	GO:0007267~cell-cell signaling	6	0.00272	0.160903
		GO:0007268~synaptic transmission	4	0.045464	0.607968
12	1.289882	IPR003961:Fibronectin, type III	4	0.029945	0.336199
13	1.116414	GO:0070011~peptidase activity, acting on L-amino acid peptides	12	0.0272	0.67043
15	0.774528	GO:0010171~body morphogenesis	19	3.99E-04	0.120598
16	0.774119	GO:0044459~plasma membrane part	9	0.032601	0.630033

Transcription factors *unc-86* and *unc-120*are negatively correlated with valproate exposure (Table 31, page 139). Down regulation of *unc-86*cause fat accumulation due to low serotonin levels which cause nuclear localization of DAF-16. (Liang et al., 2006). *unc-120* is a member of MADS-box family and is required for expression of actin and myosin.

Several genes involved in neurotransmission are negatively correlated with valproate exposure. These include genes coding for acetyl choline esterase, *ric-3*; which is required for maturation and function of four different nicotinic acetylcholine receptors, genes involved in axon navigation/guidance, synapse formation, K^+ channel and glutamate receptor(Halevi et al., 2002, Ben-Ami et al., 2005, Shteingauz et al., 2009).

The expression profiles of several genes involved in lipid metabolism including dehydrogenases, fatty acid desaturases, lipases and insulin were also negatively

correlated with valproate exposure. GTPases, genes involved in WNT signalling, CDK andjun kinases are also among the expression profiles negatively correlated with valproate. A number of genes coding for C-type lectins, intermediate filaments and collagen are also negatively correlated with valproate dose.

Table 31 Known genes with expression profiles negatively correlated with valproate dose identified by CAST.

	Gene name	Description
Insulin related	ins-23, ins-8	INSulin related
Transporters	aqp-2	AQuaPorin or aquaglyceroporin related
	atgp-2	Amino acid Transporter GlycoProtein subunit
	C41D11.9	TM2 domain-containing protein C41D11.9
	cbn-1	Calcium BiNding protein homolog
Kinases	cdk-5	Cyclin-Dependent Kinase family
	jnk-1	Jun N-terminal Kinase
Neuronal	unc-41	UNCoordinated
	ACE-1, ace-3	abnormal ACEtylcholinesterase
	ric-3	Resistance to Inhibitors of Cholinesterase
	Y69A2AR.5	D-amino-acid oxidase 2
	arl-3, arl-6	ARF-Like
	cln-3.2	human CLN (neuronal ceroid lipofuscinosis) related
	zig-8	2 (Zwei) IG-domain protein

	cdh-6	CaDHerin family
	lad-2	L1 CAM ADhesion molecule homolog
	slt-1	SLiT (Drosophila) homolog
	plx-2	PLeXin
	eva-1	Enhancer of unc-40 Ventral Axon guidance defects
	syg-2	SYnaptoGenesis abnormal
	slo-1	SLOwpoke potassium channel family
	glr-1	GLutamate Receptor family (AMPA)
	bbs-5	BBS (Bardet-Biedl Syndrome) protein
	unc-86	UNCoordinated
	cfz-2	Caenorhabditis FriZzled homolog
	ceh-13	Homeobox
	grd-16	GRounDhog (hedgehog-like family)
	grl-11	GRound-Like (grd related)
	sel-7	Suppressor/Enhancer of Lin-12
Collagen	col-135, col-165, col-184, col-74	COLlagen
	dpy-17	DumPY : shorter than wild-type
Cytoskeleton/muscle related	unc-120, unc-52	UNCoordinated
	cut-3, cut-5	CUTiclin
	cutl-13	CUTiclin-Like
	bli-4	BLIstered cuticle
	cor-1	CORonin

	dyb-1	DYstroBrevin homolog
	stn-1	SynTrophiN
	dylt-2	DYnein Light chain (Tctex type]
	ifa-3	Intermediate Filament, A
	ifc-1	Intermediate Filament, C
	mlc-1	Myosin Light Chain
	tnt-4	TropoNin T
Lectins	clec-140, clec-160, clec-24, clec-26, clec-31, clec-33, clec-35, clec-43, clec-48, clec-49, clec-51, clec-52, clec-54, clec-60	C-type LECtin
Lipid metabolism	cpt-3	Carnitine Palmitoyl Transferase
	dhs-21	DeHydrogenases, Short chain
	fat-6	FATty acid desaturase
	gbh-2	Gamma Butyrobetaine Hydroxylase
	lips-4	LIPaSe related
	fbxb-114	F-box B protein
	fpn-1.2	FerroPortiN
	glf-1	GaLactoFuranose synthesis (UGM, UDP-galactopyranose mutase)
	hex-5	HEXosaminidase
	rab-28	RAB family
	rga-2	Rho GTPase Activating protein
	hlh-13, hlh-32	Helix Loop Helix
	ifta-2	IntraFlagellar Transport Associated
	ilys-3	Invertebrate LYSozyme

	inx-8	INneXin
	nas-39	Nematode AStacin protease (only BMP-1/Tolloid homolog in C. elegans)
	nspc-9	Nematode Specific Peptide family, group C
	nuc-1	abnormal NUClease
	phat-5	PHAryngeal gland Toxin-related
	scl-3	SCP-Like extracellular protein
	thn-1, thn-2	THaumatiN family
	ttr-1	TransThyretin-Related family domain
	ZK1058.3	Probable galactose-1-phosphate uridylyltransferase

SOTA clustering showed the negatively correlated expression profile to be a single cluster. This also suggests a common down regulatory mechanism of genes on valproate exposure.

4.2.4.2.1 Network analysis ofexpression profilesdown-regulated with valproate dose

After showing that the negatively correlated expression profile of valproate exposure is involved in lipid accumulation and acts as a single cluster, I then set to identify any regulatory mechanisms. For that I did Network analysis using WormNet. Only 68 genes out of 90 known genes mapped in WormNet (Figure 37, page149). Thirty seven of these

genes were connected to each other making three networks with 7 genes and another larger network with the rest of the connected genes. It comprised of two sub-clusters connected to each other via *tnt-4*. Smaller sub cluster contains several genes involved in G-protein coupled receptor activity. Larger sub cluster contains several genes involved in cuticle development including some collagen synthesis genes. *fat-6*, which has stearoyl-CoA 9-desaturase activity, is a key gene in fat metabolism found in this cluster. *hlh-13* and *dyb-1* are transcription factors found connected to each other in a smaller network.

To find the role played by insulin signalling and TGF-β pathways on negatively correlated expression profile on Valproate exposure, I reconstructed the networks adding *daf-2, daf-16* and *sma-6*. When the networks were reconstructed after adding *daf-2, daf-16* and *sma-6*, it showed *sma-6* to act as a key gene which connects acetylcholine esterase genes with the insulin signalling and it also connected them with the two clusters of the largest network via *tnt-4* (Figure 38, page150).

Transcription factor analysis identified several transcription regulators involved in reproduction to be negatively correlated with valproate exposure. These include *egl-5*, a gene, which causes egg laying defective in mutant and *unc-86*(Table 32, page 144). *unc-86* codes for a transcription factor required for correct fate determination and differentiation of neuronal lineages including egg laying neurons(Horvitz and Sulston, 1980).It is also required for *tph-1* and *cat-1* expression in serotonergic neurons and for neutrite outgrowth(Sze et al., 2002).

Genes with the highest connectivity included several cuticle components, GTP-binding, Calcium and Zinc ion binding and acetylcholine esterase (Table 33, page 147).

Analysis of transcription factors in or associated with expression profile negatively correlatedwith valproate identified most of them to be regulated by RNA polymerase II promoter (Table 34, page 150). This indicates RNA polymerase II promoter to be a target of valproate exposure, which results in selective down regulation of expressions.

Table 32 Transcription factors/ regulators of transcription factors in or associated with down-regulated genes identified by CAST

Locus_ID	Symbol	GO_P	GO_C	GO_F
W10D5.1	mef-2	regulation of transcription, DNA-dependent;	nucleus;	transcription factor activity; sequence-specific DNA binding;
Y48C3A.17	efl-2	regulation of progression through cell cycle; regulation of transcription, DNA-dependent;	transcription factor complex;	transcription factor activity;
C25A1.11	aha-1	regulation of transcription, DNA-dependent; signal transduction; locomotory behavior; response to xenobiotic stimulus; intracellular receptor-mediated signaling pathway; positive regulation of growth rate; positive regulation of locomotion; positive regulation of body size; regulation of transcription;	intracellular; nucleus;	DNA binding; transcription factor activity; signal transducer activity; aryl hydrocarbon receptor nuclear translocator activity; transcription regulator activity;
F46G10.6	mxl-3	regulation of transcription;	nucleus;	transcription regulator activity;

Y75B8A.1	php-3	regulation of transcription, DNA-dependent; regulation of transcription;	nucleus;	DNA binding; transcription factor activity; sequence-specific DNA binding;
F16H11.4	ceh-1	regulation of transcription, DNA-dependent; regulation of transcription;	nucleus;	DNA binding; transcription factor activity; sequence-specific DNA binding;
F33D11.4	ceh-12	regulation of transcription, DNA-dependent; regulation of transcription;	nucleus;	DNA binding; transcription factor activity; sequence-specific DNA binding;
C08C3.1	egl-5	negative regulation of transcription from RNA polymerase II promoter; regulation of transcription, DNA-dependent; anterior/posterior pattern formation; oviposition; regulation of cell adhesion; tail tip morphogenesis (sensu Nematoda); regulation of transcription;	nucleus;	DNA binding; transcription factor activity; sequence-specific DNA binding;
B0304.1	hlh-1	larval development (sensu Nematoda); regulation of transcription from RNA polymerase II promoter; muscle development; locomotory behavior; embryonic development (sensu	nucleus;	RNA polymerase II transcription factor activity, enhancer binding; transcription

		Metazoa); positive regulation of growth rate; post-embryonic body morphogenesis; regulation of transcription; protein heterooligomerization;		regulator activity; bHLH transcription factor binding;
F01D4.6	mec-3	regulation of transcription, DNA-dependent; mechanosensory behavior; response to mechanical stimulus; regulation of transcription; neuron development;	nucleus;	DNA binding; transcription factor activity; zinc ion binding; sequence-specific DNA binding;
F48D6.3	hlh-13	larval development (sensu Nematoda); locomotory behavior; embryonic development (sensu Metazoa); growth; regulation of transcription;	nucleus;	transcription regulator activity;
D1081.2	unc-120	regulation of transcription, DNA-dependent; gametogenesis; locomotory behavior; embryonic development (sensu Metazoa); positive regulation of growth rate; locomotion;	nucleus;	transcription factor activity; sequence-specific DNA binding;
R13A5.5	ceh-13	larval development (sensu Nematoda); regulation of transcription, DNA-dependent; locomotory behavior; embryonic development; cell-cell adhesion; growth; positive regulation of body size; post-embryonic body morphogenesis; regulation of transcription;	nucleus; cytoplasm;	DNA binding; transcription factor activity; sequence-specific DNA binding;

C30A5.7	unc-86	regulation of transcription, DNA-dependent; locomotory behavior; mechanosensory behavior; response to mechanical stimulus; oviposition; positive regulation of locomotion; regulation of transcription; neuron development;	nucleus;	DNA binding; transcription factor activity; sequence-specific DNA binding;

Table 33 Seed genes of down-regulated genes identified by CAST ranked by total connectivity. First ten genes are shown in the table

Rank	Symbol	Score	#_linked_seed / #_valid_seed	GO_P	GO_C	GO_F
1	col-165	4.25	7/76	phosphate transport;	cytoplasm;	structural constituent of cuticle;
2	col-74	4.18	6/76	phosphate transport;	cytoplasm;	na
3	cut-3	3.58	9/76	positive regulation of body size;	na	na
4	dpy-17	3.30	4/76	phosphate transport; cuticle biosynthetic process (sensu Nematoda);	cytoplasm;	structural constituent of cuticle;

				positive regulation of body size; hermaphrodite genitalia development;		
5	phat-5	3.08	5/76	na	na	na
6	dyb-1	2.92	2/76	na	na	calcium ion binding; zinc ion binding;
7	arl-3	2.81	5/76	rRNA processing; small GTPase mediated signal transduction; ribosome biogenesis and assembly;	intracellular;	GTP binding;
8	thn-2	2.77	6/76	na	na	na
9	clec-60	2.73	5/76	na	na	sugar binding;
10	ace-3	2.50	1/76	acetylcholine catabolic process in synaptic cleft; larval development (sensu Nematoda); acetylcholine catabolic process; hatching; regulation of backward locomotion;	na	catalytic activity; acetylcholinesterase activity; cholinesterase activity; protein dimerization activity;

organismal movement;

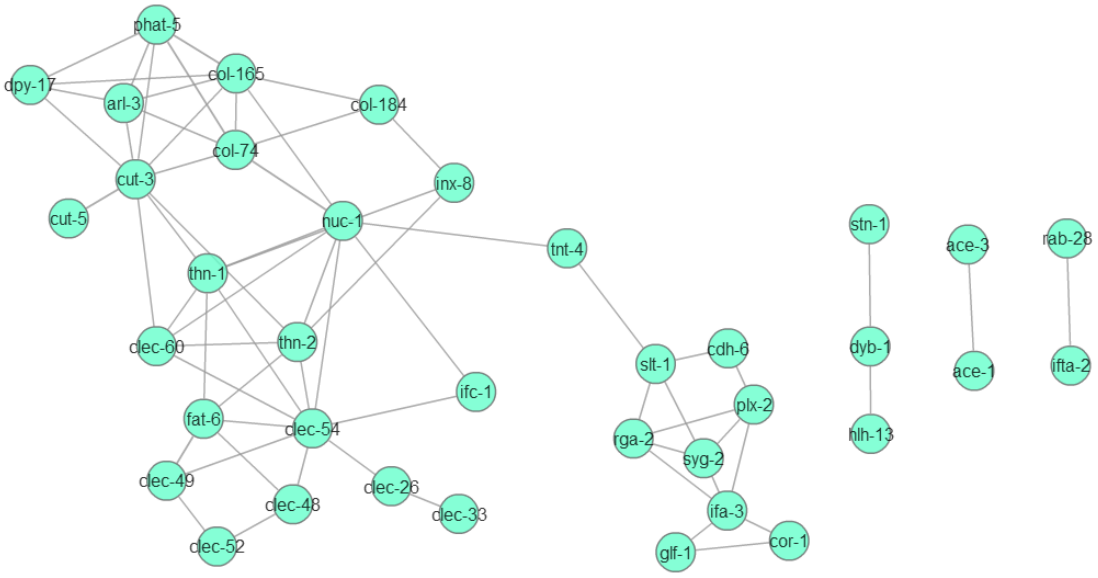

Figure 37 Network graph of seed genes that show negative correlation with increasing valproate dose identified by CAST.(A) Out of 90 genes, 68 genes were mapped in WormNet v. 2. Out of the 68 genes, 37 of which were connected to each other are shown in the figure.

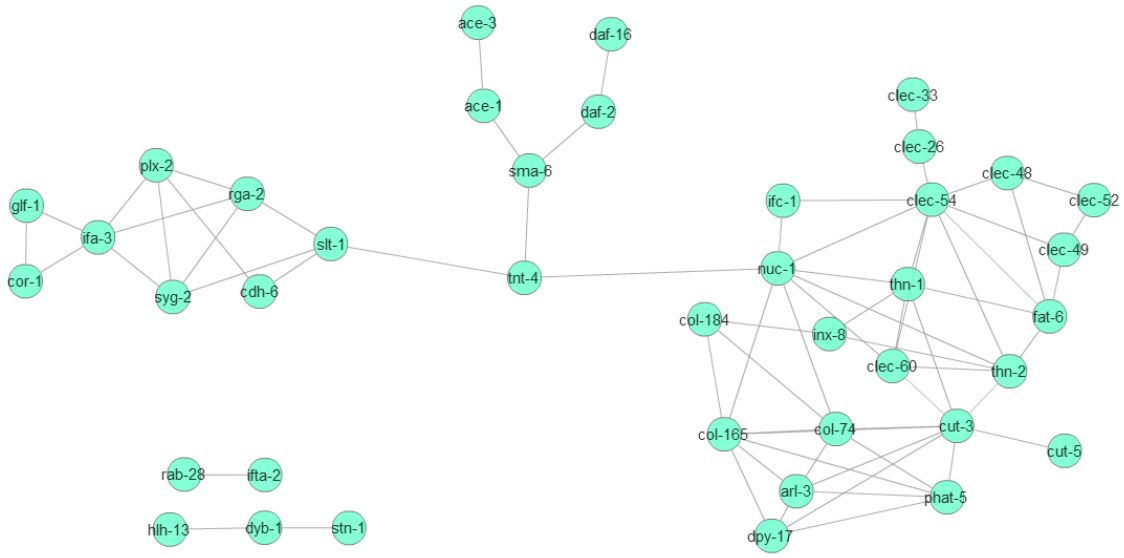

Figure 38 Network graph of seed genes showing negative correlation with valproate, identified by CAST with *daf-2, daf-16* and *sma-6* added. (A) Out of 93 genes, 71 genes were mapped in WormNet v. 2. This shows an involvement of sma-6 in connecting ace-1 and 3, which are acetylcholine esterases with the cellular metabolism via daf-2 and daf-16. Also it connects this neuronal and metabolic signals via *tnt-4* to the other two subclusters identified in the expression profile negatively correlated with valproate exposure.

Table 34 Analysis of transcription factors in or associated with cluster of genes down-regulated on valproate exposure.

Locus ID	**Symbol**	**Biological process**	**RNAi phenotypes**
W10D5.1	mef-2	Regulation of acetylcholine secretion, neurotransmission, negative and positive regulator of transcription from RNA polymerase II promoter	
Y48C3A.	efl-2	Negative regulation of vulval	Multivulva

17		development	
C25A1.11	aha-1	Positive regulation of transcritption from RNA polymerase II promoter, body morphogenesis, intracellular receptor signalling pathway, locomotion, nematode larval development, response to xenobiotic stimulus	
F46G10.6	mxl-3	Transcription from RNA polymerase II promoter	slow growth
Y75B8A.1	php-3	Regulation of transcription	Posterior body morphology variant
F16H11.4	ceh-1	Regulation of transcription	
F33D11.4	ceh-12	Regulation of transcription	
C08C3.1	egl-5	Negative regulation of transcritption from RNA polymerase II promoter, anterior posterior pattern specification, oviposition, protein catabolic process, regulation of cell adhesion, tail tip morphogenesis	Coiler, ectopic neuron, egg laying defective, HSN migration variant, male mating defective, serotonin deficient
B0304.1	hlh-1	Positive regulation of transcritption from RNA polymerase II promoter, body morphogenesis, locomotion, muscle organ development, nematode larval development, protein oligomerization, reproduction	dumpy, embroyonic arrest, embroyonic lethal, locomotion variant, lumpy, reduced brood size, slow growth, sterile

F01D4.6	mec-3	Positive regulation of transcritption from RNA polymerase II promoter, mechanosensory behavior, neuron differentiation, neurone development,	dendrite development variant, neuron development variant, neuronal outgrowth variant, sluggish, touch resistant
F48D6.3	hlh-13	Locomotion, nematode larval development, embroyo development ending in birth	Embroyonic lethal, larval arrest, locomotion variant, protein aggregation variant
D1081.2	unc-120	Body morphogenesis, locomotion, reproduction, protein catabolic process, nematode larval development	Dumpy, egg laying defective, embroyonic lethal, locomotion reduced, paralysed, reduced brood size, slow growth, sluggish, sterile, thin
R13A5.5	ceh-13	Axon guidance, axonal fasciculation, body morphogenesis, cell-cell adhesion, dendrite development, embroyo development, locomotion, nematode larval development, regulation of transcription	Axon fasciculation variant, backward locomotion variant, axon midline crossing variant, body elongation defective, dumpy, embroyonic development variant, locomotion variant, small
C30A5.7	unc-86	Positive regulation of transcritption from RNA polymerase II promoter, Axon extension, dendrite development, locomotion, neuron development, meiotic chromosome segregation, oviposition, response to mechanical stimulus	Egg laying defective, axon outgrowth variant, bag of worms, cell differentiation variant, locomotion variant, neurone degradation, reduced brood size, touch resistant

4.2.4.3Network analysis of transcription factors in or associated with valproate expression profile

After showing that probably up-regulation of genes on valproate exposure is via steroid hormone signalling and the down-regulated expression profile of valproate exposure is through RNA polymerase II promoter and both of these expression profiles are known to be regulated by insulin and TGF-β Sma/Mad signalling pathways, I then set to analyse the link between these two expression profiles. For that, I developed a network of the transcription factors in (or associated with) these two expression profiles to find the key regulators. Network analysis of expression profiles positively and negatively correlated with valproate of transcription factors in or associated with valproate exposure identified by WormNet shows most of these transcription regulators to be associated with the insulin signalling pathway (Figure 39, page154). *daf-2* connects the two main sub-clusters of transcription factors positively and negatively correlated with valproate exposure.

pqn-28 codes for a histone acetylase. *hlh-30* codes for a transcription factor and is known to result in reduced fat storage when silenced by RNAi. Y49A3A.1 codes for a homolog of choline/ethanolaminephosphotransferase. *egl-5* mutant has a egg laying defective, coiler, serotonin deficient phenotype, phenotypes also observed on valproate exposure. As explained earlier, *unc-86* is required for the expression of *cat-1* and *tph-1* in serotonergic neurotransmission.

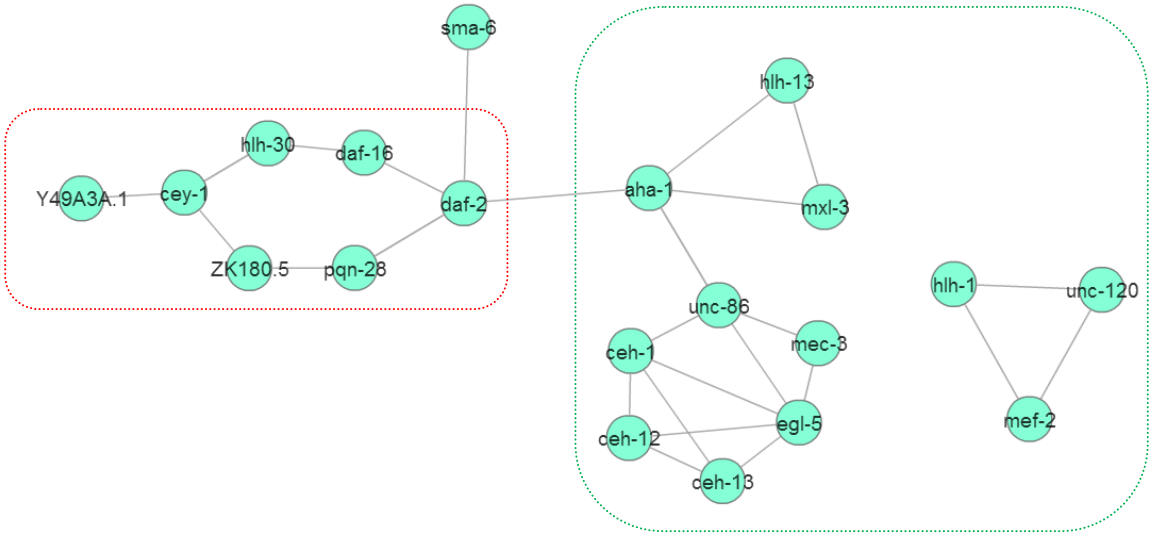

Figure 39 Network analysis of transcription factors in, or associated with, positively(red box) and negatively(green box) correlated expression profiles of valproate exposure identified by WormNet analysis. Networkwas generated by adding *sma-6* and *daf-16* to the transcription factors in or associated with valproate exposure expression profile.

4.2.4.4 Expression profiles showing a bell shape and an inverted bell shapendistributions

There were 7 genes showing an expression profile of bell curve and 4 genes showing an inverted bell curve. *ins-7*, which codes for one of the insulin like peptides in *C.elegans* shows a bell shaped expression profile with valproate exposure. INS-7is known to act as an agonist for DAF-2receptor and makes a positive feedback loop to amplify DAF-2 activity.*daf-2* mutants are known to have high lipid mass and therefore this could not explain the increase of lipid mass on valproate exposure(Pierce et al., 2001, Murphy et al., 2003, Husson et al., 2007).

mup-2, which encodes muscle contractile protein, troponin-c, shows an inverted bell shaped expression profile. This gene product affects muscle contraction, epidermal morphogenesis and is required for growth and fertility (Myers et al., 1996, McArdle et al., 1998, Simmer et al., 2003).

4.3 Discussion

4.3.1 Correlation analysis

Expression profiles that correlate with valproate dose show an increase in the expression of several genes involved in lipid biosynthesis and catabolism. Steroid synthesis is expected to increase on exposure to valproate with an increase in the expression of hydroxysteroid dehydrogenases. The gene coding for glycerol-3-phosphate dehydrogenase(*gpdh-1*) which links carbohydrate metabolism with lipid metabolism by converting dyhydroxyacetone phosphate to glycerol-3-phosphate is also positively correlated with valproate. This enzyme is involved in lipid biosynthesis by providing glycerol-3-phosphate for the formation of glycerol by dephosphorylation. Guanylate cyclase is involved in the synthesis of cGMP, which signals for insulin secretion. Insulin helps in lipid synthesis by increasing the uptake of glucose into adipocytes and increasing fatty acid synthesis in the liver and reducing breakdown of fat in adipose tissue. Choline kinase B, which catalyzes the committed step of the formation of phosphocholine for phosphatidyl choline synthesis, the main phospholipid found in eukaryotic membranes is also positively correlated with valproate under this category.

Therefore, an increase in phospholipids is also expected on valproate exposure. UDP-glucuronosyl transferases, which are involved in lipid glycosylation are also positively correlated with valproate. It also contains glucose-6-phosphate dehydrogenase, which catalyses the rate limiting step in pentose phosphate pathway and makes NADPH required for lipid synthesis. Cellular detoxification also depends on NADPH and is one of the functional terms enriched in the expression profile positively correlated with valproate dose.Since cell division is found to show a negative correlation with valproate dose, the purpose of activation of pentose phosphate pathway would be to provide NADPH required for cellular biosynthesis and for detoxification rather than the production of pentoses.

As a result synthesis of lipids, especially steroids, phospholipids and glycophospholipids are expected to increase on valproate exposure.

Gene coding for phytanoyl-CoA dioxygenase, which is involved in alpha-oxidation of fatty acids is positively correlated with valproate. The enzymes that catalyse the first three steps of β-oxidation Acyl-CoA dhydrogenase, enoyl-CoA hydratase and 3-hydroxyacyl-CoA dehydrogenase are all positively correlated with valproate. Therefore an increase in the fatty acid degradation is expected due to an increase in both alpha and beta oxidation of fatty acids.

As a result some lipid synthesis and degradation of fatty acid pathways are expected to increase with valproate.

Glycogen synthase kinase inhibits glycogen synthesis by phosphorylating glycogen synthase enzyme. Glycogen synthase kinase shows a positive correlation with valproate dose and as a result,a depletion of glycogen stores on exposure to valproate is expected.

Since oxidation of fatty acids and a reduction in glycogen synthesis expected on exposure to valproate, an overall reduction in energy storage may occur.

Down regulation of nuclear components is a key feature of valproate exposure. A DNA replication factor, *rfc-3* could be a key gene of this down regulation of nuclear components and is the gene with the highest connectivity to other nuclear components down-regulated on valproate exposure. The second gene with the highest connectivity which is also directly connected to *rfc-3*is *pcn-1*. *pcn-1* codes for the *C.elegans* ortholog of proliferating cell nuclear antigen (PCNA)(Piano et al., 2000). It is an essential component of DNA repair and replication machinery and serves as a processivity factor for DNA polymerase delta (Boulton et al., 2002) . It directly interacts with CKI-2, a cyclin dependent kinase inhibitor homolog that may be required for cell cycle progression and play a role in DNA damage check point pathway. Valproate could be acting via RNA polymerase II promoter to bring this down regulation of genes and a key regulator of that could be *vab-3*, a transcription factor (Figure 40, page157).

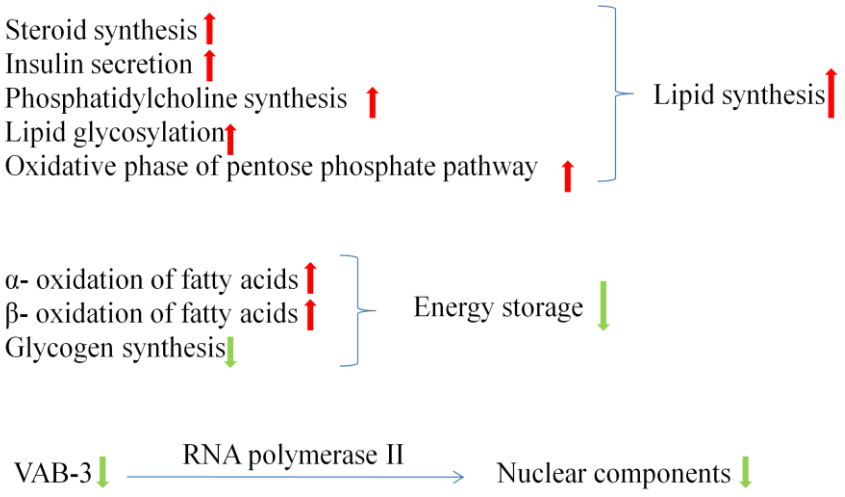

Figure 40 Summary of the findings of the correlation analysis. Cellular functions expected to upregulate due to valproate are indicated with red and downregulated in green arrows.

Correlation analysis helps to identify linear relationships in gene expression but it cannot identify genes coregulated. It also fails to identify gene interactions. Spearman rank correlation was used in this study as it can identify nonmonotonous relationships. SAM analysis can identify nonlinear relationships. To understand the key genes involved in regulation of genes, which interact with each other, I also performed clustering and network analysis.

4.3.2 Clustering and network analysis

In the four cluster analysis of the positively correlated expression profile on valproate exposure, there is a gradual increase in the concentration of valproate where a rapid increase in the up-regulation of gene sets is observed in each cluster. This clearly shows that based on valproate dosage different gene sets could be positively correlated with valproate, which could bring different clinical outcomes. The first cluster is connected to *grd-1* gene. *grd-1* gene is predicted to be involved in cholesterol dependent hedge-hog like signalling and is known to be involved in growth, cuticle adhesion and mail tail development. It is mainly composed of collagen genes indicating valproate to play a role in morphogenesis.

The other three clusters give some indication that insulin signalling pathway could play an important role in the up-regulation of genes on valproate exposure. For examplethe second, third and fourth clusters are directly connected to *daf-2* or connected to *daf-2* via *sma-6*. In the phenotypic characterization of lipid accumulation on valproate exposure, it is shown that accumulation of lipid on valproate exposure requires *sma-6* and *daf-2*. DAVID functional clustering identifies second and third clusters to be

enriched in lipid glycosylation. In cluster one, which is not directly linked to *daf-2*, *daf-16* or *sma-6*, the expression profile shows a rapid up-regulation at 18mM of valproate. At this valproate dose, both lipid level and lifespan starts to decrease on increasing valproate concentration. This cluster is mainly composed of collagen genes. Therefore lack of direct involvement of insulin signaling pathway and *sma-6* could be a possible reason for the decrease of lipid level and lifespan on valproate concentrations above 18mM. This disconnection from insulin signaling pathway could be the reason for the shift from membrane components to amino acid biosynthesis at valproate doses above 18mM, where amino acids synthesized would be utilized to make collagen. Different valproate concentrations up-regulate different sets of gene networks indicating the presence of some valproate dose sensitive molecular switches that regulate the gene expression on valproate exposure. The fourthcluster, which is associated with *daf-2* has two subnetworks, which are connected with each other via *daf-36*. *daf-36* is involved in the production of ligand for *daf-12,* which regulates the entering of *C.elegans* into high fat dauer stage. Therefore lipid accumulation on exposure to valproate could be via *daf-36* under the control of *daf-2*.

Network analysis of the four clusters identified by SOTA clustering of the expresssion profile positively correlated with valproate exposure indicates all clsuters except cluster 1 to be directly connneted to insulin signalling via *daf-16* (Figure 41, page160). Cluster 1 is indirectly connected to the rest of the clusters via *dao-4*, which is known to be regulated by *daf-16*. It also identified B0286.3 as a key gene, uncharacterized gene in *C.elegans,* which is known to cause larval arrrest and larval lethality on mutation. The human homologue is known to be involved in purine biosynthesis.

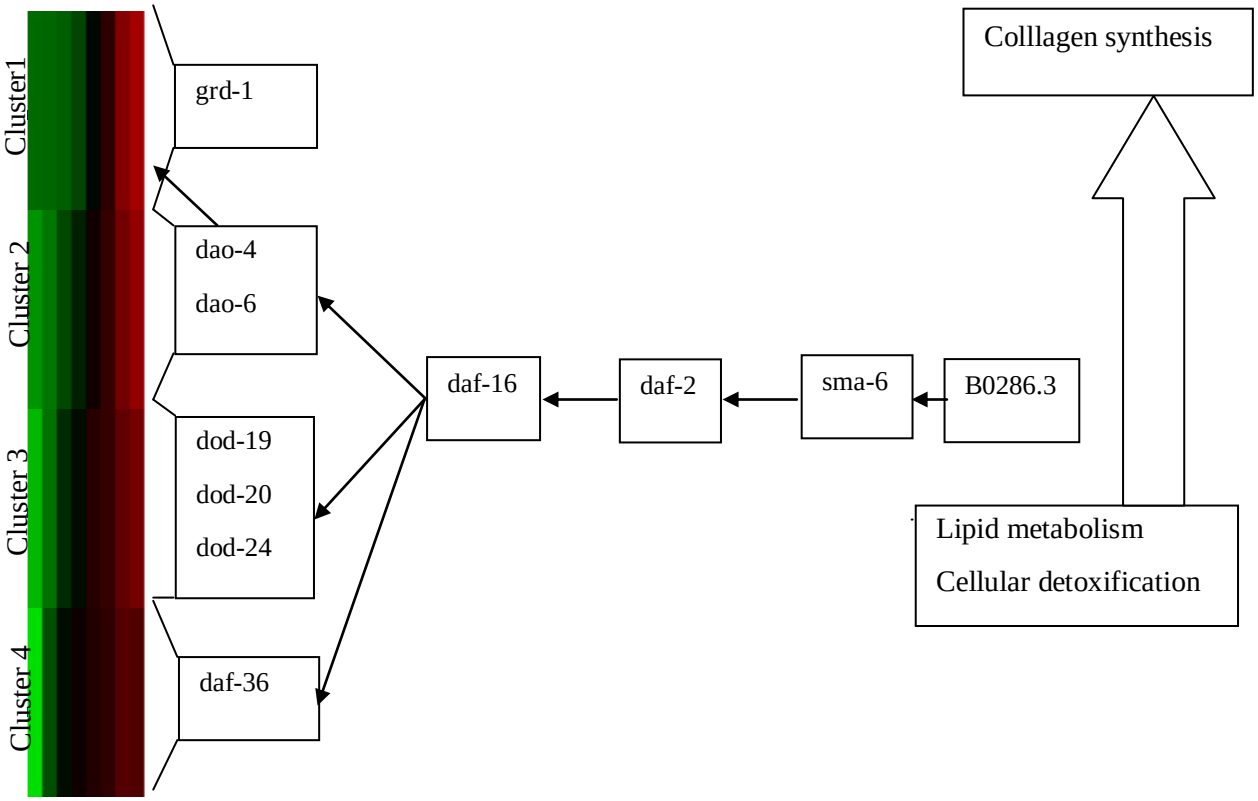

Figure 41 Figure showing the summary of the analysis of the expression profile positively correlated with valproate exposure identified by CAST clustering and separated into four clusters by SOTA. Genes known to be involved in insulin signalling in each cluster are shown with their connection to daf-16. Green shows low expression and red indicates high expression level of each cluster.

Several genes involved in lipid metabolism are negatively correlated with valproate.fat-6, a key gene in lipid metabolism is down-regulated. Down regulation of *fat-6* cannot explain the increase of lipid level by valproate as this is known to decrease the lipid level by increasing β- oxidation. *unc-86* is required for the fate determination and differentiation in diverse neuronal lineages, including egg laying neurons,

mechanosensory neurons and chemosensory neurons. *unc-86* is also required for the expression of *tph-1* and *cat-1* in serotonergic neurons and for neutriteoutgrowth. *tph-1*encodes tryptophan hydroxylase ,the key enzyme in serotonin biosynthesis. Down regulation of it cause *C.elegans* to have low serotonin levels. Serotonin up-regulate a subset of peroxisomal and mitochondrial β- oxidation genes (Mullaney and Ashrafi, 2009b). Reduced serotonin levels cause fat accumulation, dauer formation and reduced egg laying in *C.elegans.* It also cause down regulation of insulin and TGF-β pathways (Sze et al., 2000). Down regulation of *unc-86* may contribute to the changes in lipid content, neuronal and egg laying on valproate exposure.

Therefore both lipid synthesis and degradation pathways are affected on valproate exposure and fat accumulation observed on valproate exposure could be the net result of both pathways.

Transcription factor analysis show steroid hormone signalling to be a main target of valproate, which results in up-regulation of genes and down regulation of genes by valproate to be via the RNA polymerase II promoter.

The main objective of studying model organisms is to understand the human biology in an ethically accepted way. Studying worm networks gives a lot of information related to worm biology but how much of that information is valid for mammalian system could be understand only by relating it to mammalian systems at ortholog level.To understand the overlap of *C.elegans* expression data with mammalian systems, I performed Ingenuity Network Analysis, which maps *C.elegans* data to mammalian gene networks at ortholog level.

5.0 INGENUITY NETWORK ANALYSIS OF TRANSCRIPTIONAL RESPONSE OF *C. ELEGANS* TO SODIUM VALPROATE

5.1 Summary

Pathway analysis, in the context of this project can be defined as the bioinformatics analysis used to identify, biological networks linking genes that share a given property (eg. correlated to increasing doses of a drug treatment)(Viswanathan et al., 2008). The approaches used to reconstruct these pathways can be either data or knowledge driven. In the data driven approach, gene to gene relationships are generated from observational data, such as microarray experiments, where as in a knowledge driven approach genes are linked because of pre-existing knowledge and the bioinformatics approach aims at identifying the connections that are consistent with some criteria (e.g. protein protein interaction or transcriptional link).

Here we describe the network analysis of the gene expression signatures identified in the previous chapters performed using the knowledge management system Ingenuity Pathway Analysis (IPA). IPA map the gene identifiers provided to the gene objects in the Ingenuity Pathway Knowledge Base. Then it generates networks by overlaying these focus genes on to a global network in the Knowledge Base. The specificity of connectivity of these focus genes were calculated by the percentage of connectivity to other focus genes. Then the networks are generated starting with the focus gene with the highest specific connectivity. Each network is limited to 35 focus genes for easier visualization and analysis.

IPA analysis revealed a negative correlation of NFkB signalling and MYC with valproate dose (Figure 42, page 163). In lipid metabolism, a positive correlation withβ-

oxidation of fatty acids, steroid and phospholipid synthesis, as well as cholesterol and phospholipid transport are found with valproate dose.

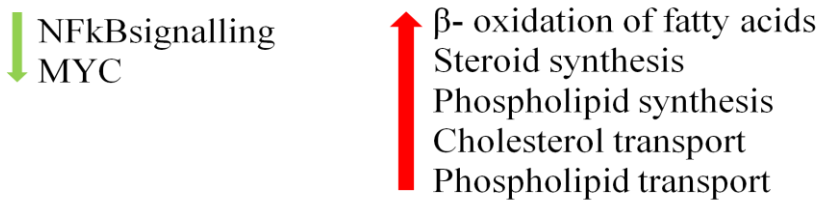

Figure 42 Diagram showing the cellular functions correlated with valproate dose identified by Ingenuity Pathway Analysis. Cellular functions with positive correlation are shown in red and the negative correlation are shown in green.

5.2 Results

After identifying the significant expression profile and the functional terms associated with valproate exposure, I then set to assess the possible homology in mammalian system to this expression profile identified in *C.elegans*. For that I mapped the *C.elegans* gene signatures associated with valproate exposure on IPA knowledgebase. First the genes which do not show a monotonic relationship were identified by SAM analysis (significance <1% FDR) and were pooled together with the genes from the correlation analysis with a threshold of BH corrected p value < 1% and mapped to Ingenuity knowledgebase. Ingenuity pathway analysis generated 11 significant networks with a score >30 (Figure 43, page164). Except network 3, all the other significant networks were interconnected.

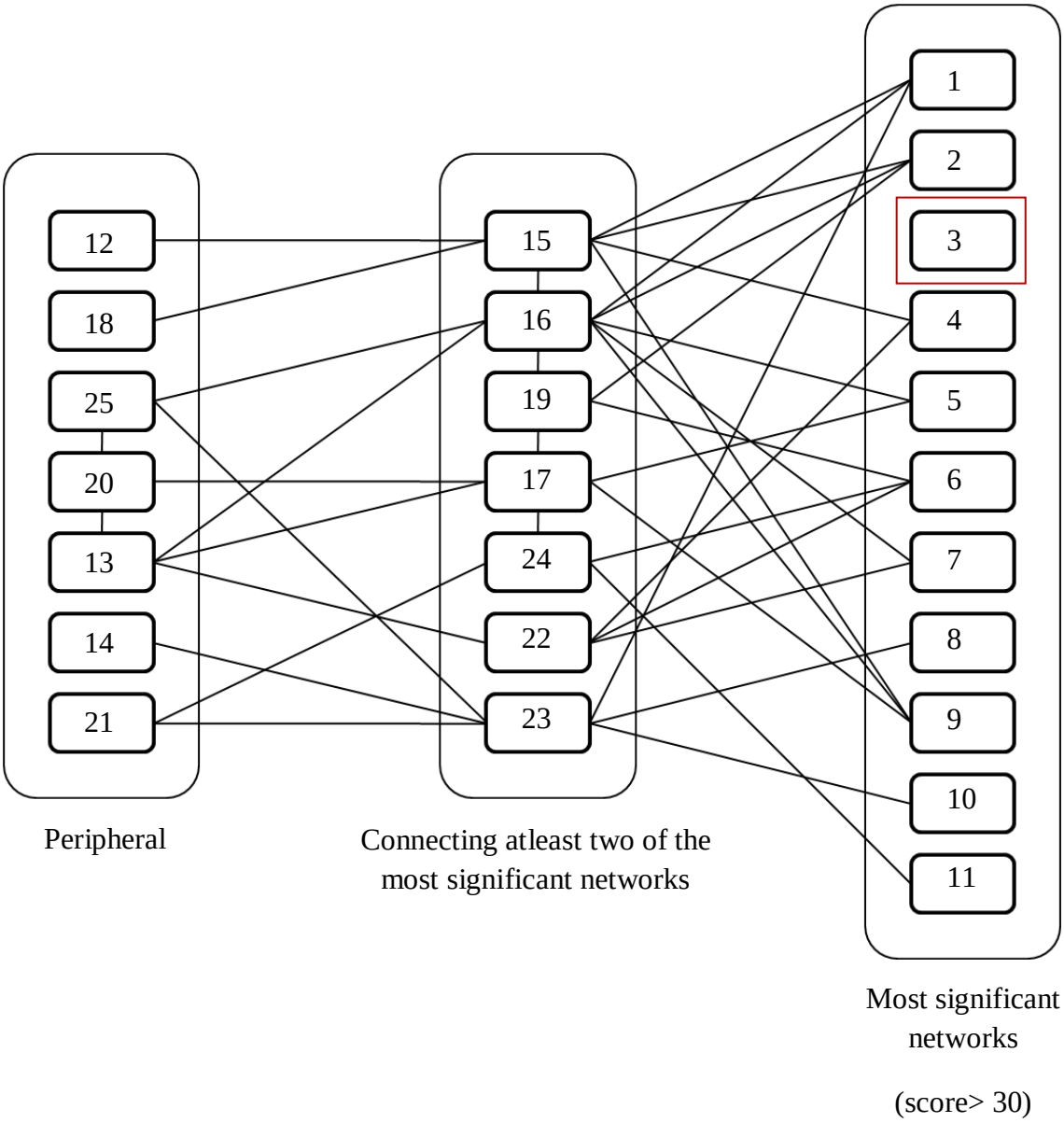

Figure 43 Interactions between networks identified by Ingenuity analysis. Gene identifiers associated with valproate exposure with a significance level of 1% BH corrected p value in correlation analysis were pooled with the gene identifiers with a significance level of 1% FDR in SAM analysis. Networks were generated by mapping these gene identifiers to gene objects in a global network in Ingenuity Pathway Knowledge Base giving priority to the ones with highest specific connectivity. Each network is limited to 35 focus molecules for

easier visualization. Networks generated with a score of > 30 are shown in the diagram with their connectivity to other networks generated.

Table 35 gives a summary of the ingenuity analysis. The significance score of each network isdetermined by Fisher's exact test using the whole database as a reference set. The most significant network was involved in development disorder, Genetic disorder and neurological disease with a score of 50 and 32 focus molecules.

Table 35Summary of the functions of the networks identified by Ingenuity Pathway analysis. Threshold used was p value < 1% with BH correction for multiple testing pooled with nonmonotonic expression profiles identified by SAM analysis

ID	Molecules in Network	Score	Focus Molecu	Top Functions
1	3-hydroxyacyl-CoA dehydrogenase, ↑ABCD3, ↑ACY1, ↓ANKFY1, ↓AP3D1, ↓ATG7*, ↓BBS2, ↓BBS5*, ↓BBS7, ↓CLN3*, ↓FLCN, ↓FUBP1, ↑GANAB, ↓GFPT2, ↑HADH, ↑HSD17B4, ↑HSD17B8*, ↑HSD17B12, ↑HSD17B14*, HSD17B, NFkB (complex), ↑NPEPPS, ↑PGRMC1, ↓PPP1R16A, ↓PUF60*, ↓RTKN, ↑SARM1, ↓SLC11A2, ↑SLC15A2, ↓SLC3A1, ↓SLIT2, ↑TFG, ↓TRAPPC9, ↑TROVE2, ↓TXNRD1	50	32	Developmental Disorder, Genetic Disorder, Neurological Disease
2	↓ACLY, ↓AGRN, ↑ATIC*, ↓ATP1A3*, ↓BTBD9, ↓CDC5L, ERK1/2, ↑GART, ↑GIPC1*, ↑HERC3*, ↓LOC100130109, ↓LSM3, ↓MO8KL3*, ↑MYO6*, Ndpk, ↓NME2*, ↓NTN1, ↑PAICS, ↑PDIA6, ↓PLRG1, ↑PPP1R7, ↓PPP1R8, ↓PRPF19, ↓PRPF31, ↓PRPF38A*, ↓RAPGEF2*, ↑SLC2A1, ↓SMNDC1, ↓SNRNP40, snRNP, ↓SNRPB2, ↓SNRPD2, ↓SNRPD3, ↓SNRPF*, ↓UNC5A	50	32	RNA Post-Transcriptional Modification, DNA Replication, Recombination, and Repair, Nucleic Acid Metabolism
3	↑ACTG1*, Actin, ↓AIP, Alpha Actinin, Alpha catenin, ↓ARRDC3, ↑CAP1, ↓CASK, ↓CDC73, ↓CNTNAP2, ↓CTNNA2, ↓CTR9, ↓CUTC*, ↓DCTN6, ↓DIAPH2*, ↑ECHS1*, ↓FBXO45, ↑FER, G-Actin, ↓KARS, ↓Macf1, ↓MAGI1, ↓NPHS1, ↓PAM16, ↑PDCD6IP*, PI3K (complex), ↑PLB1 (includes EG:151056)*, ↑SLC25A6*, ↓STARD3, ↓TJP1, ↑TNNI3K, ↓TOMM20, ↓UBE2A, ↑WBP2, ↑WWOX*	45	30	Cellular Assembly and Organization, Cellular Movement, Cell Morphology
4	↑Abcb1b, Akt, ↑BMP5, ↓CDK5*, ↓CELF1*, ↓DBH, ↓EXOSC7, ↓FAM192A, ↑FOLH1, ↓GABARAP, ↓GBE1, ↓GIT2, Glutathione peroxidase, glutathione transferase, ↑GOLGA2, ↑GSTP1*, ↑GSTZ1, ↑HPGDS*, ↑HYOU1*, ↓IP6K1, ↑ITSN1, Laminin, ↑MGAT1, Pak, ↓PNN, ↓PRDX6, ↓RAB33B, ↓RABGAP1, ↓RBM5, ↓SMPD1*, ↑SOD2, Sod, ↑TOE1, ↑UGCG, ↓UXS1*	43	29	Lipid Metabolism, Small Molecule Biochemistry, Free Radical Scavenging
5	↑ABCB1, ↑ABCC3, ↑ACOT4*, ↑ACOT8*, ↑ACOT9*, ↑AHCY*, ↓AKAP17A*, ↑ALDH3A2*, Ces, ↑Ces1c*, ↑CYP3A7*, ↓EIF2C2, ↓EIF3E, ↓EIF3I, ↓EIF4A3*, ↓KIF23*, ↓LIPA*, ↓MYLPF*, Myosin, ↓NCBP1, Ncoa-Nr1i2-Rxra, ↓NKAP, palmitoyl-CoA hydrolase, ↑PDIA4, Pkc(s), ↑PNPLA7, PXR ligand-PXR-Retinoic acid-RXRα, ↓RBM25, ↓RBM8A*, ↓RNPS1, ↓SFSWAP*, ↑SH3D19, ↓SRSF7, ↑TTN*, ↓UPF3B*	43	29	RNA Damage and Repair, Molecular Transport, RNA Trafficking
6	20s proteasome, ↑ABCC1*, ↓ACTL6B, ↓ATG5*, ATPase, ↓CEBPZ, ↓CLPX*, ↑CMPK1, ↓DNA2, ↑GDI1, ↓GRIA3, ↓HEXB*, HSP, ↑HSPA5*, ↑IDE*, ↓KIF15*, ↓MAP1LC3A, ↓MYH7*, P38 MAPK, ↓PABPN1, ↓PSMA3, ↑PSMD4, ↓PTCH1*, ↓RBPJ, ↓RRM1*, ↓RRM2*, ↓SLC31A1, ↓SMARCA4, ↓SMARCD3*, ↑SOD1*, ↓SPOP, ↓STUB1, SWI-SNF, ↓TIAL1, Trypsin	43	29	Cell Cycle, DNA Replication, Recombination, and Repair, Energy Production
7	26s Proteasome, ↓ANK2, ↓Aph1a, ↑BRP44L*, ↑C20orf54, Cdk, ↓CHEK1, ↓COPS5, ↓CPSF3L, ↑CTSZ, ↓CYB5R2, ↓DHRS1, ↓EFNB2, ↓EXT1, ↑FAIM2*, ↓GALT, ↑HAL, Hsp90, ↑IFI30, Immunoglobulin, Interferon alpha, ↓LPHN2*, ↓MELK*, ↓NOP2, ↓NRCAM, ↑PLSCR1*, ↓PLXDC2, ↓PSENEN, ↓RPL23A, Secretase gamma, ↓SKP2, ↑SMC6, ↓TRIP13, Ubiquitin, Vegf	37	27	Cellular Development, Cellular Growth and Proliferation, Cell Death
8	↓ANAPC10*, ↑ANXA7*, Ap2 alpha, APC, ↓AURKA, ↓CDC14A*, ↓CDK1*, ↓CHD4*, ↑CKS2, Clathrin, ↑CRYZ, Cyclin B, ↓DDX6*, Dynamin, ↓HIST1H1A*, ↑ICMT, ↓INCENP*, ↓KCNMA1, ↓KDM1A, ↓MAD2L1, Mapk, ↑MAT2A, Mi2, ↓MIER1, ↓MTA3*, ↓PAX6, ↓PBRM1*, ↓PFKFB3*, Ppp2c, PRKAC, ↑PTS*, ↓RBBP4, ↓RPS6KA1, ↓SMARCE1, ↑TMLHE	36	26	Cell Cycle, Cellular Compromise, Cellular Movement
9	14-3-3, ↑ABCG1, ↑ABCG4, ↓ACAT1, ↓ADA, Adaptor protein 2, ↑AGXT, ↑BIN1, ↑CHP2, ↓CYP24A1, ↑CYP2J2*, ↑DUSP8*, ↑FABP4*, G protein beta gamma, ↓GNAI1, ↓GNB5*, Growth hormone, Jnk, LDL, MAP2K1/2, ↓MAPK10*, ↑NAPEPLD*, ↓PLD3, Pld, ↑POR, ↓PTGR2, ↓RGS7, Rxr, Sapk, ↓SFRP2, ↑SLC9A3*, ↓TLL1, TSH, ↓WNT5B*, ↑XDH	32	24	Lipid Metabolism, Small Molecule Biochemistry, Molecular Transport
10	↑ACAD8, alcohol group acceptor phosphotransferase, Alp, ↓CDK7, ↓CDK8, Creb, ↑DECR1*, DNA-directed RNA polymerase, ↑GGT1*, ↓GTF2E1, ↓GTF2F2, ↓HCFC1*, Holo RNA polymerase II, ↓HOXA1, Hsp70, IFN Beta, IL1, ↓KAT2B, ↓MED8, ↓MED12, Mediator, ↓MEIS1*, ↑OGT, ↓POLR2G, ↓POLR3C, ↑POLR3G, ↓PQBP1, Pro-inflammatory Cytokine, RNA polymerase II, ↓RNGTT, ↓TAF3, ↓TAF11, ↑TDO2*, ↓VPS39, ↓ZW10	32	24	Gene Expression, Amino Acid Metabolism, Cell Morphology
11	Basc, ↓CDC6, Cdc25, ↓CDC45, ↓CHEK2, ↓CHTF18, ↓CLSPN, ↑CTH*, Cyclin A, Cyclin E, DNA-directed DNA polymerase, E2f, ERK, ↓HELQ, ↓LIG1, ↓MAPK15, ↓MCM2*, ↓MCM5*, ↓MCM7*, ↓MCM10, Mcm, ↓MRE11A, ↓ORC2, ↑PCYT1A, ↓PMS2, ↓POLE, ↓POLH, ↓RFC1*, ↓RFC2, ↓RFC3*, ↓RFC5, Rfc, RPA, ↓SMARCB1, ↑TUBA1B	31	25	DNA Replication, Recombination, and Repair, Cell Cycle, Nucleic Acid Metabolism
12	Ap1, ↓ARL6, ↓ARL6IP5*, ↓ATAD2, ↓ATG16L1, ↓C12orf44, Calpain, ↓CAPN9, ↓CHAF1A, ↓EPC2, FSH, ↑G6PD, ↓GK, ↓GUSB, ↓H2AFV*, hCG, HISTONE, Histone h3, Histone h4, ↓HSPG2, ↓IK*, IL12 (complex), Lh, ↓MORF4L1*, ↑PGK1, ↑PPIA, ↓PYGM, Rb, ↓SET, ↓SMARCA1, ↑TALDO1, Tgf beta, ↓UNG*, ↓USP46*, ↓WDR1	30	24	Drug Metabolism, Endocrine System Development and Function, Lipid Metabolism
13	↑AACS*, ↓ACHE, ADCY, ↓AGPAT6, ↓AQP9*, ↓ARRB1, Beta Arrestin, ↓CELSR1, Estrogen Receptor, ↓FZD1*, ↓FZD8*, G protein alpha, G protein alphai, G-protein beta, Gpcr, Gsk3, ↑IGF1R*, Insulin, ↓KCTD3, ↓KIAA1409, ↓KIF3A, ↑LHCGR*, ↓MT-ND1, ↓MT-ND4*, ↓NPY1R, ↑NUCB2, p85 (pik3r), ↑PCSK5, ↑PKM2, Rac, ↓Rims2, ↓SAE1*, ↓Scd2*, Shc, ↓UBA2	30	23	Carbohydrate Metabolism, Lipid Metabolism, Small Molecule Biochemistry
14	↑ABRA, Alpha tubulin, ↓ARL2, Beta Tubulin, Calcineurin A, Calcineurin protein(s), ↓CAMK2D, CaMKII, ↑CREM, ↓ELP3, F Actin, ↓FAT1, ↓GAPDH*, ↓HDAC6*, Hdac, ↓HEXDC*, Histone H1, ↑KCNK18*, ↓KDM6A, ↓MAP3K7*, MEF2, Nfat (family), ↓NPHP1, ↓PARK2, Pka, ↑RAB32*, ↓SLC8A3, ↓SMEK1, ↑STX1A*, ↓TBX2, ↑TCP11L1, ↓TIPRL, ↓TUBB2C, Tubulin, ↓WDR5	24	23	Cell-To-Cell Signaling and Interaction, Nervous System Development and Function, Gene Expression
15	↑ABCG1, ↑AMY2A, ANXA11, ↓CDC40, ↓CHSY3*, dihydrotestosterone, Gapdh (includes others), GPD2, Gsta4, ↑HPGDS*, ↓HSD17B6, IL6, IL36B, ↓MT-CYB, NKX3-1, ↓NTN1, ↑PAFAH2*, Pbsn, ↑PHGDH, SAT1, SELS, SEPP1, ↑SLC39A14, ↓SLC4A7, ↓SLC7A7, SLC7A8, SMURF1, ↑SP5, ↑Srsf4*, ↑TALDO1, ↑TCF25, ↓TMEM98, TNF, ↓TXNRD1, ↓WLS	24	20	Connective Tissue Development and Function, Skeletal and Muscular System Development and Function, Tissue Morphology
16	↑ABCB1, ↓ABCD4, ACPP, ATOH7, ↓BARHL2, ↓CNDP2, COL5A2, ↑CRIM1, ↑CTSA, ↓ERAP2, ↑FAH*, FGF9, ↑GGCT, GLB1, HLA-G, ↑HSD17B4, IFNG, ↓MAN8A, ↓MINK1, MYCN, ↓NME2*, ↓NPY1R, NR2E1, PEA15, ↑PHGDH, POU4F2, ↓POU4F3, progesterone, RAB11FIP5, ↓RPL23A, RPLP1, SCNN1B, SCNN1G, ↓SLC37A4, ↑XDH	22	19	Lipid Metabolism, Molecular Transport, Small Molecule Biochemistry
17	↑ABCA3, ↑ABCG1, ↓ABHD5*, ↑ACAA2, ↑ACADM, ACADVL, ARNT2, beta-estradiol, CACNA1G, ↓COG3, COG6, CTSH, CXCR7, DNAJC3, ↓DNASE2*, ETFB, ↑ETNK1*, GPX3, IL13, ↓LIPA*, ↓MAB21L1, MAOA, ↓MGAT2, norepinephrine, ↓NPY1R, ↑OXCT1*, ↑PDIA4, SELENBP1, SLC17A1, ↑SLC26A6, ↑SRM, SSR1, ↓TINAGL1, ↑TSSK2, XBP1	20	18	Energy Production, Lipid Metabolism, Small Molecule Biochemistry
18	↓ARHGAP1, Collagen type I, Collagen type IV, ↓CPD, ↓DTNA*, ↓FGFRL1, ↓FHL2, ↓FLT1, Focal adhesion kinase, ↓GRB2, growth factor receptor, Integrin, ↑KCNQ1, ↓LAMA2, ↓LCP1, Mlc, ↓MYL1, Pdgf (complex), PDGF BB, Pdgfr, ↓PITX2*, PLC gamma, PP1 protein complex group, PP1-C, PP2A, ↓PPP1R3B, ↓Ppp1r9a*, Ras, Ras homolog, ↓RPS6KB1, ↓SLC7A7, SMOOTH MUSCLE ACTIN, ↓SNTB1*, ↓TRIO*, ↓UGDH	20	19	Cellular Movement, Cellular Assembly and Organization, Cellular Function and Maintenance
19	↑AMD1, BRF1 (includes EG:2972), ↓C14orf169, CDCA5, ↓CEBPZ, CHRNB1, ECM1, F7, FN1, ↑GART, ↓IMPACT*, ↓KLHL3, LCN1, LCN1L1, ↑LGMN*, ↓METTL9, ↓MTAP, MYC, NFYB, ↓NME2*, PDS5A, ↓PDS5B, ↑POFUT1, PPI, RAD21, RND3, ↓RRM2*, STAG1, ↓STAG2, ↑TSTA3, ↓UBE3B, USP13, ↓VANGL1, ↓WAPAL*, ZFP42	19	18	Cellular Assembly and Organization, Cell Cycle, Cellular Movement
20	ABLIM1, ADAM22, BAI1, ↓BAIAP3, ↑BEST4*, ↓CCNY, ↓CDK17, ↓CELSR1, CPSF3, ↓CPSF4, CPSF7, DLG4, ↓EPT1, EWSR1, FIP1L1, ↑FZD1*, FZD7, ↓GIT2, KIF1B, ↑LASS5*, MARK3, NCKIPSD, ↓RBM26, SEPT5, ↓SEPT11, ↑SFXN3*, SUV39H2, ↓SUV420H1, TACC2, TRA2A, ↑TTYH2, USP21, YWHAG, ↓ZDHHC3, ↓ZDHHC6	19	17	RNA Post-Transcriptional Modification, Cell Morphology, Cellular Development
21	BCOR, BHMT, CKS1B, ↓CORO1C*, ↓CPN2, DLX2, ↓ELMO2, ↓FBXW9, HPRT1, HSD11B2, ↓KAL1, LOC728622/SKP1, MEST, miR-124, MITF, ↓MTHFD1, ↓MTX1, NFIC, NR3C1, PAX3, RHOG, ↑SGPL1, ↓SLC17A5, ↓SLC27A4*, ↑SLC50A1*, ↓SMARCE1, STOM, SURF4, TJP2, ↑TKTL2, ↓TM2D3, ↑TMBIM4, ↓TRPM1, TYRP1, ZFP36L2	17	16	Cellular Development, Hair and Skin Development and Function, Dermatological Diseases and Conditions
22	↓ALG3, ↑APRT, ↓ARL5A, ↑BCAT2, ↑CISD1, ↓CRELD2, ↓DDX46, ↓Eif4e2, EIF4EBP1, EIF4EBP2, EIF4EBP3, ↓GBE1, GBP7, GBP2 (includes EG:14469), ↑Grtp1 (mouse), ↓HEXB*, ↑IFI30, IFNA2, IL4, IL5, KLHDC2, Ku, LFNG, LRRC8C, ↑MBOAT2*, ↓MRPS10, MTORC2, PDK1, RAC3, ↓RWDD1, ↓Scd2*, ST7, STAT4, Trim30a/Trim30d, UCHL3	17	16	Protein Synthesis, Respiratory System Development and Function, Antigen Presentation
23	↓ALKBH7, ATF2, ATF4, ATF7, ATF6B, ↓B9D2, ↓BCS1L, ↓BUD31*, CEBPA, CEBPB, ↑CPA2*, ↓DHX35, FOSL2, ↓GPATCH3, ↓HBS1L, HNF4A, JUN, JUNB, ↓MITD1, ↑MOCOS, ↓MRM1, NFkB (complex), Pka, RASA1, RB1, RNA polymerase II, ↓RPRD1B, ↓SLC25A40, TAOK3, TGFB1, ↓TMTC4, ↓UTP11L	16	15	Gene Expression, Infectious Disease, Cellular Development
24	↓ADPGK, AHCYL1, AHCYL2, AKT3, ↑AMACR*, ↓B4GALT5, CDKN1A, ↑CECR5*, CHAF1B, ↑CTH*, ↓DDO, Dgk, ↓DGKD, EGF, EZH1, ↓GALNT11, ↓JOSD2, ↑MGAM*, ↑P4HA1*, ↓PCGF3, PEX5, ↓RRM1*, ↓RRM2*, SMARCA2, SP4, SPHK2, TACC3, TADA3, ↑TAT, TERT, TRAPPC2, TYSND1, ZFP36, ZFP36L2, ZMYND11	16	15	Cell Cycle, Cellular Growth and Proliferation, Protein Synthesis
25	↓AGPAT1, ↓C5orf44*, ↓C6orf211, CEBPB, ↓CHERP, DBI, GH1, ↓GLCE, GSTK1, HNF1A, HNF4A, ↑HPD*, Insulin, ↓MRPL43, ↓MRPS35, ONECUT1, PPARA, PPARD, PPARG, ↓PPCDC, progesterone, ↓RIOK1, SAP18, ↑SLC22A18, ↓SLC39A1, ↑SQRDL*, SREBF1, SREBF2, TRAPPC3, TRAPPC8, ↑TXNDC12, ↓UTP3, WBP4, YWHAB	16	15	Cellular Development, Connective Tissue Development and Function, Tissue Development

Similar to the DAVID analysis originally applied to the genes identified by the correlation analysis, this pathway analysis also shows an obvious down regulation of genes coding for nuclear components (Figure 44, page167).

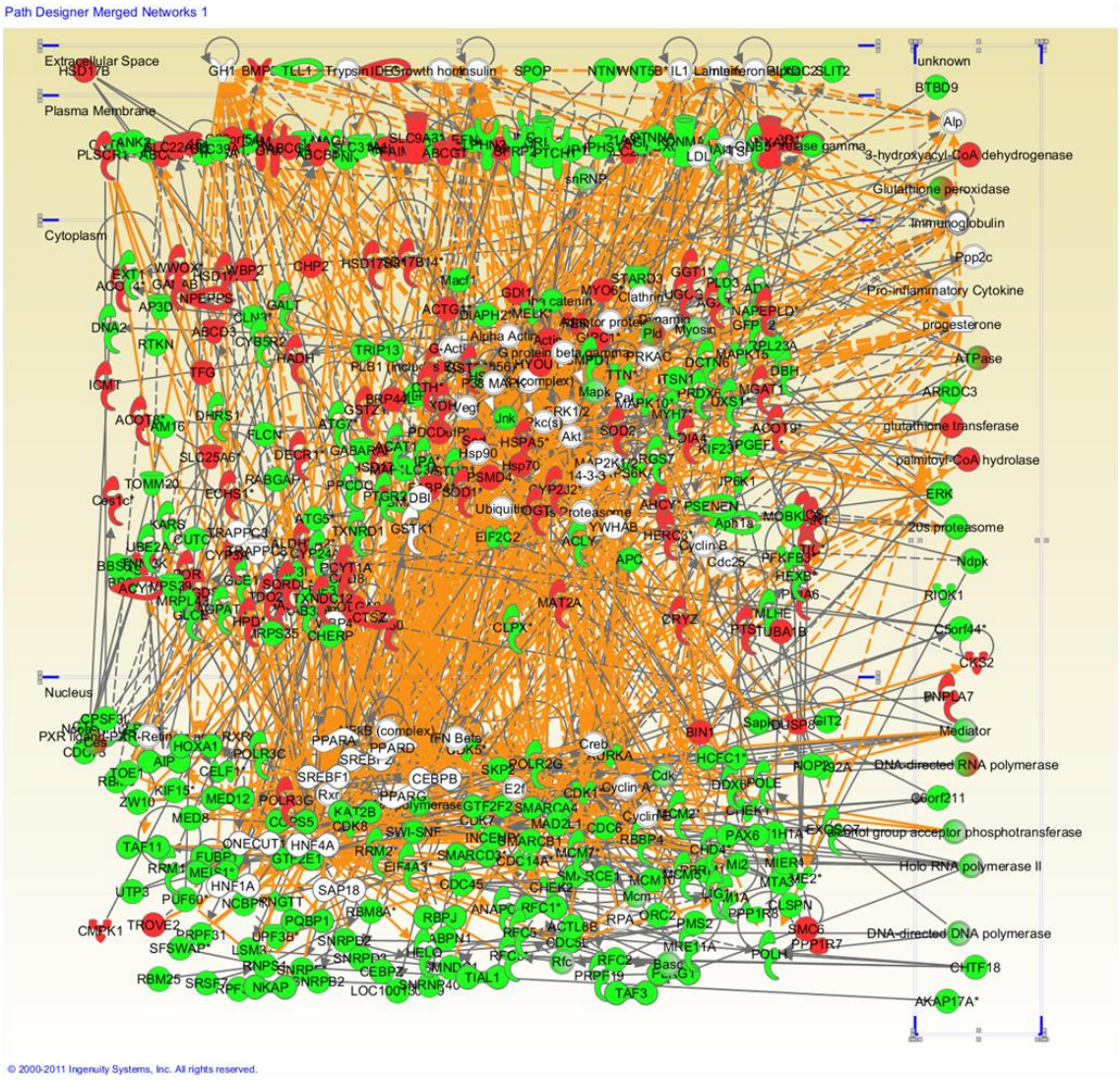

Figure 44Combination of all the genes mapped by Ingenuity shows a clear down regulation of nuclear components. Genes which do not show a monotonic relationship were identified by SAM analysis (significance <1% FDR) and were pooled together with the genes from the correlation analysis with a threshold of BH corrected p value < 1%. Genes in all the significant networks generated are pooled together to identify cellular localization of protein products of expression profile associated with valproate exposure. Focus molecules corresponding to gene expression profiles negatively (green) and positively (red) correlated with valproate dose are shown with the focus molecules identified by the IPA which are connected to the network but not found in the data set (white).

Figure 45 (page177) to Figure 55 (page187) show the most significant networks generated by Ingenuity on the pooled expression profiles identified by Correlation analysis and SAM with a threshold of corrected 1% FDR with BH correction for multiple testing. After generating those significant networks I identified different functions associated with it to generate hypothesis to explain the affects of valproate.

5.2.1 NFkB signalling may be downregulated on valproate exposure

IPA identified an NFkB signature associated to valproate exposure. This is found to be negatively correlated with valproate due to a negative correlation found with TXNRO1, thioredoxindisulfide reductase, a cytoplasmic component, which activates NFkB and NKAP.NFkB requires thioredoxine reduction for DNA binding(Arnér and Holmgren, 2000).As expected SLIT2, whose expression is increased by NFkB and SLC11A2 and SLC3A1 transporters, which require NFkB for expression show negative correlation with valproate dose. SARM1, a negative regulator of NFkB, shows a positive correlation with valproate, which further supports the hypothesis that NFkB pathway is down-regulated on valproate exposure. Network 1 generated by Ingenuity Pathway Analysis (Figure 45, page 177) identified NFkB to be the most connected gene.

5.2.2 Downregulation of c-myc is expected on valproate exposure

Both PUF60 and FUBP1, a helicase, show a negative correlation with valproate dose. PUF60 is known to repress the activation of c-myc by FUBP1. c-myc regulates the expression of 15% of genes by recruiting histone acetyl transferase. NME2 , which is

required for the activation of MYC also shows a negative correlation with valproate dose. Therefore, a down regulation of c-myc is expected on valproate exposure.

5.2.3 B-oxidation is expected to increase on valproate exposure

Several genes involved in β-oxidation including HSD17B4, HSD17B8, HSD17B14, 3-hydroxyacyl-CoA dehydrogenase and HADH are positively correlated with valproate dose. In network 5, ACOT8, involved in oxidation of fatty acids is positively correlated with valproate. In network 3 Phospholipase B (PLB1), which hydrolyse phospholipids and ECHS1, involved in β-oxidation are also positively correlated with valproate. In network 5 carboxy esterase, lipase involved in cholesterol ester hydrolysis, phospholipase and ALDH3A2 involved in oxidation of long chain aliphatic aldehydes to fatty acids are positively correlated with valproate. In network 10 DECRT; which is involved in β-oxidation show positive correlation with valproate. In contrast HSD17B12 which is involved in fatty acid elongation also show positive correlation with valproate. In network 9 Rxr, a co-repressor that induce histone acetylation and chromatin condensation and activate fatty acid oxidation genes is identified by the pathway analysis, a gene not present in the dataset. These data suggest a hypothesis where valproate would increase lipid oxidation, mainly β-oxidation.

5.2.4 Phospholipid level is expected to increase on valproate exposure

In network 11 expression of cytoplasmic phosphate cytidyltransferase choline (PCYT1A); the rate limiting enzyme in phosphatidylcholine biosynthesis is positively correlated with valproate dose. This is the most abundant phospholipid in animals and plants.Therefore an increase in phospholipids is expected on exposure to valproate.

5.2.5 Steroid synthesis is expected to increase with an increase in lipid mobilization on exposure to valproate

In network 5(Figure 49, page 181), palmitoyl-CoA hydrolase, CYP3A7, involved in the formation of estriol shows a positive correlation with valproatedose.In network 9, T POR involved in steroidogenes is also shows a positive correlation with valproate. In network 3STARD3 involved in lipid trafficking has a negative correlation with valproate. Two cell membrane transporters ABCG4, which is involved in cholesterol transport and ABCG1, which is involved in both cholesterol and phospholipid transport are positively correlated with valproate.

Expression of insulin degrading enzyme (IDE), which terminates insulin activity is also positively correlated with valproate. Network 9 (Figure 53, page 185) identified several cytoplasmic proteins involved in lipid metabolism. They include POR involved in steroidogenesis, FABP4 a transporter involved in fatty acid metabolism, CYP2J2, which cause epoxidation of arachidonic acid are all positively correlated with valproate dose, while phospholipase D and prostaglandin reductase expression is negatively correlated with valproate. These observations supports the hypothesis that both steroid synthesis and lipid mobilization are increased by valproate.

5.2.6 Chromatin remodelling is expected to be downregulated on valproate exposure

In network 6 (Figure 50, page182) several nuclear components involved in RNA processing and chromatin remodelling are negatively correlated with valproate. These include the key mediator of Notch signalling, RBPJ, transcription stimulator, CEBPZ, poly(A) binding protein PABPN1, RNA binding TIAL1, co-repressor complex SPOP and chromatin remodelling components ACTL6B and SWI-SNF. Network 8 (Figure 52, page 184) reveals the expression of a number of nuclear components involved in chromatin remodelling by histone deacetylation and cell cycle control to be negatively correlated with valproate. These include PBRM1 and SMARCE1, components of chromatin remodelling complex SWI/SNF, KDM1A and CHD4, RBBP4 , MTA3 components of histone deacetylase complex and Mi2, a component of nucleosome deacetylase complex. These data supports a hypothesis where chromatin remodelling is decreased on exposure to valproate.

5.2.7 DNA replication, progression through cell cycle and DNA damage repair are decreased on valproate exposure

In network 7 (Figure 51, page183) several nuclear components involved in cell cycle control and transcription are negatively correlated with valproate. Helicase and ribonucleotide reductase are also among the negatively correlated nuclear components. In network 8 other nuclear components negatively correlated with valproate include cell cycle control proteins such as the metaphase promoting factor (CDK-1), mitosis spindle assembly checkpoint protein (MAD2L1), anaphase promoting complex (ANAPC10), cell cycle regulated kinase involved in microtubule formation at spindle pole in

chromosome segregation (AURKA) and CDC14A which dephosphorylate p53 and regulate DNA replication. These are connected to APC in the wnt signalling pathway. In network 9 cell membrane components WNT5B and SFRP2 in wnt signalling are negatively correlated with valproate dose. In network 9, expression of DUSP8, which inactivate SAPK is positively correlated with valproate. SAPK , a nuclear component is stress activated protein kinase, which recruit general transcription factors.Network 11(Figure 55, page 187) reveals a remarkable negative correlation of nuclear proteins with valproate dose involved in DNA damage repair, DNA replication factor C and DNA replication initiation. DNA damage repair genes include CLSPN; the upstream regulator of CHECK1 that trigger checkpoint arrest in response to DNA damage which is required for efficient DNA replication in normal S phase, PMS2 that do DNA mismatch repair by binding to MLH1, POLH; the polymerase specialized in replicating UV-damaged DNA, ligase (LIG1) and CHECK2; which inhibit CDC25C phosphatase and prevent entry into mitosis when DNA damaged or replication is blocked.HELQ; helicase, CRC2; the origin recognition complex, MCM2 and MCM5, MCM7 and MCM10; components of pre-replication complex, SMARCB1; a SWI/SNF related actin dependent regulator of chromatin transcription, CDC45; which load DNA polymerase α into chromatin and DNA polymerase are among the components of DNA replication initiation which are negatively correlated with valproate. This supports a hypothesis that DNA replication, progression through cell cycle and DNA damage repair are decreased on valproate exposure.

5.2.8 Transcription is expected to be downregulated by valproate

Network 10 (Figure 54, page186) reveals a remarkable negative correlation of the expression of nuclear genes involved in transcription, mainly the mediator complex with valproate dose. Mediator, MED8; mediator complex essential for the activation of CDK8 and CDK8; the component of RNA polymerase II holoenzyme complex, which links mediator and general transcription machinery are negatively correlated with valproate. Expression of RNA polymerase II, RNA polymerase III, TAF3;which helps to recognize the promoter, general transcription factor GTF2F2, GTF2E1;which recruit TFIIH to initiation complex, CDK7;an essential component of TF11H transcription factor, HCFC1; a transcription regulator, are all negatively correlated with valproate. Network 3 (Figure 47, page179) shows the negative correlation of components of RNA polymerase II complex and AIP, which is also a nuclear component involved in the regulation of many xenobiotic metabolizing enzymes. These findings suggest a hypothesis that transcription is decreased mainly via the mediator complex when exposed to valproate.

5.2.9 Translation is also expected to be downregulated by valproate

The second network generated (Figure 46, page178) shows a remarkable negative correlation of components of the spliceosome. This network is connected to network 5 where the components of the translation initiation factor, post splicing complex are shown to be negatively correlated with valproate dose.

5.2.10 Valproate may affect neuronal function

The second(Figure 46, page 178) network shows negative correlation of several cell membrane components involved in neurotransmission with valproate dose. These include AGRN, a protein involved in the aggregation of post synaptic proteins(Misgeld et al., 2005), NTN1, which is involved in axon guidance and cell migration, ATP1A3, a Na+/K+ pump and ACLY , required for acetylcholine biosynthesis. In network four (Figure 48, page180), several cytoplasmic components involved in neurotransmission are also negatively correlated with valproate. These include DBH, which converts dopamine to norepinephrine, ITSN1, which is involved in synaptic vesicle recycling and GABARAP, which helps to cluster GABA receptors. Glutamate carboxy peptidase expression is increased. Plasmamembrane components glutamate receptor, which is involved in excitatory neurotransmission is positively correlated with valproate. In network 7(Figure 51, page 183) several plasma membrane components involved in nervous system development and notch signalling are negatively correlated with valproate. These include PLXDC2 , a signalling molecule in proliferation and differentiation of the nervous system, NRCAM, involved in neuronal cell adhesion and EFNB2 , involved in nervous system development. In network 8(Figure 52, page184) there is also negative correlation of the expression of growth factor induced transcription regulator MIER1 and PAX6, which regulate transcription in developing nervous system with valproate. In network 8 expression of a cell membrane component KCNMA1 , a voltage and Ca^{2+} sensitive K^{+} channel is also negatively correlated with valproate dose. Expression of ANXA7, a voltage sensitive Ca^{2+} channel is positively correlated with valproate. PTS, a cytoplasmic component involved in the biosynthesis of tetrahydrobiopterin, the irreversible step in the formation of the cofactor for serotonin

biosynthesis and NO synthase activity is positively correlated with valproate dose. Therefore valproate is predicted to affect neural functioning.

5.2.11 mRNA processing may bedecreased by valproate

In network 4 (Figure 48, page 180), several RNA processing components are negatively correlated with valproate including CELF1, which is involved in mRNA splicing, and EXOSC7, involved in mRNA degradation. GIT2, a protein required for receptor internalization TOE1 which inhibit cell growth and cell cycle are also nuclear components that are negatively correlated with valproate exposure.

5.2.12 Cellular detoxification is predicted to increase on valproate exposure

Several cytoplasmic components involved in detoxification are positively correlated with valproate. These include glutathione transferase, HPGDS, SOD2, GSTP1, Sod, GSTZ1 and membrane component Abcb1b. UGCG, which is involved in glycosphingo lipid biosynthesis. In network 5 (Figure 49, page181) several membrane bound ABC transporters involved in xenobiotic transport are positively correlated with valproate. In network 11(Figure 55, page187), expression of cytoplasmic cystathionase; which converts cystathione to cysteine that is required for glutathione synthesis is also positively correlated with valproate supporting a hypothesis that cellular detoxification to increase on valproate exposure.

5.2.13 Jun signalling may decrease on valproate exposure

In network 8(Figure 52, page 184) cytoplasmic component mitogen activated protein kinase (Mapk) in Jun signalling is also negatively correlated with valproate. In network 9(Figure 53,185) several components including jnk, MAPK10 and SAPK in the Jnk pathway are negatively correlated with valproate dose.

5.2.14 G protein coupled signal transduction is also expected to decrease with valproate

In network 9(Figure 53, page 185) in addition, expression of several cytoplasmic components of G protein signal transduction including GNB5, which regulate GNA signal transduction, RGS7, which inhibit signal transduction by increasing GTPase activity of GNA and GNAI1 which inhibit cyclase controlled cAMP level are negatively correlated with valproate.

5.2.15 Tryptophan metabolism may increase with valproate

In network 10 expression of cytoplasmic acyl CoA dehydrogenase (ACAD8);an enzyme that is involved in catabolism of branched chain amino acids is positively correlated with valproate. The expression of Tryptophan 2,3-dioxygenase (TDO2) which catalyzes the rate limiting step in the kynurenine pathway, the major pathway of tryptophan metabolism, is also positively correlated with valproate dose.

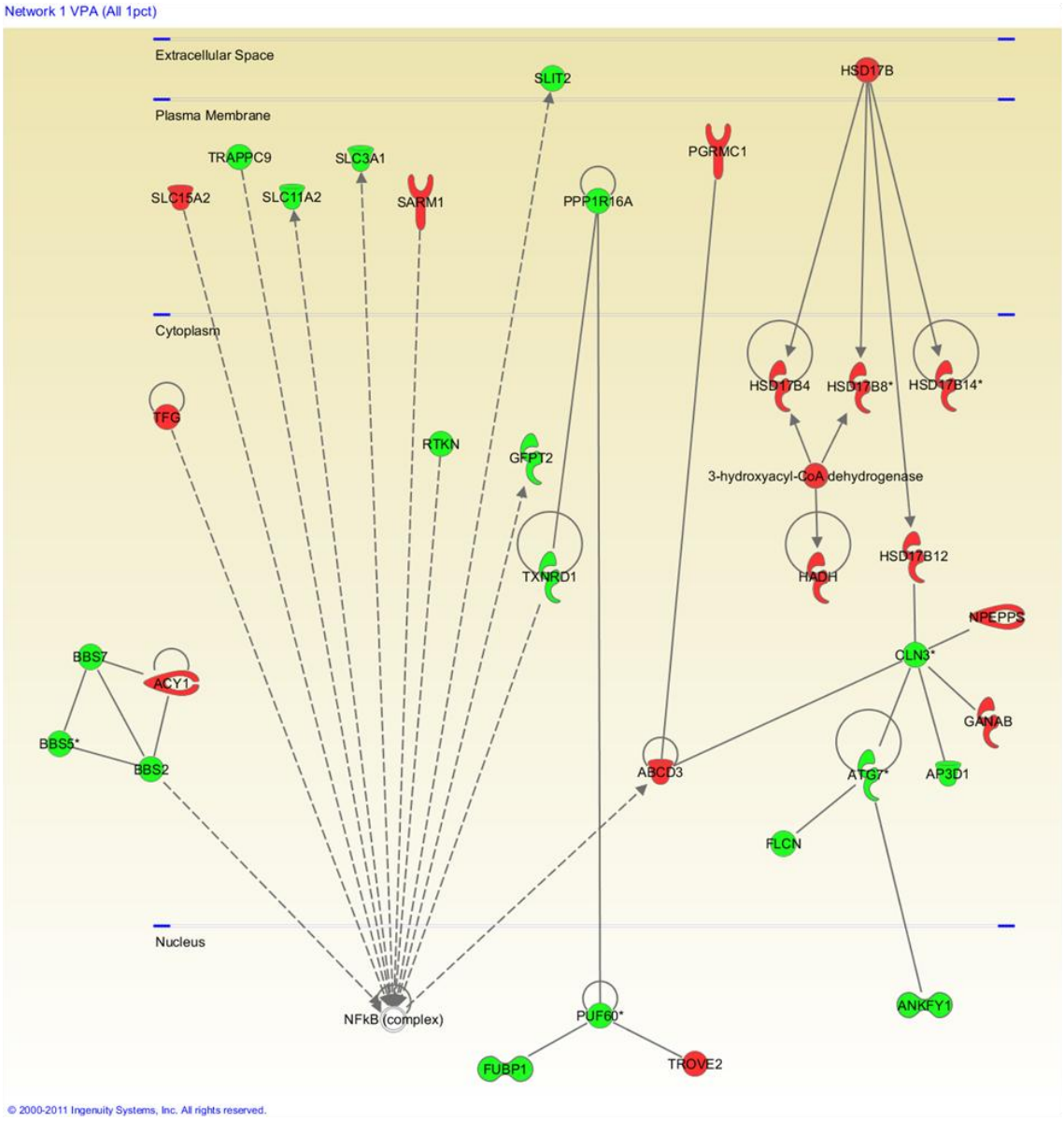

Figure 45 1st most significant network identified by Ingenuity pathway analysis on pooled expression profiles identified by correlation analysis and SAM with a threshold of 1% FDR with BH correction for multiple testingon microarray data on *C.elegans* wild type strain exposed to valproate.Focus molecules corresponding to gene expression profiles negatively (green) and positively (red) correlated with valproate dose are shown with the focus molecules identified by the IPA which are connected to the network but not found in the data set (white).

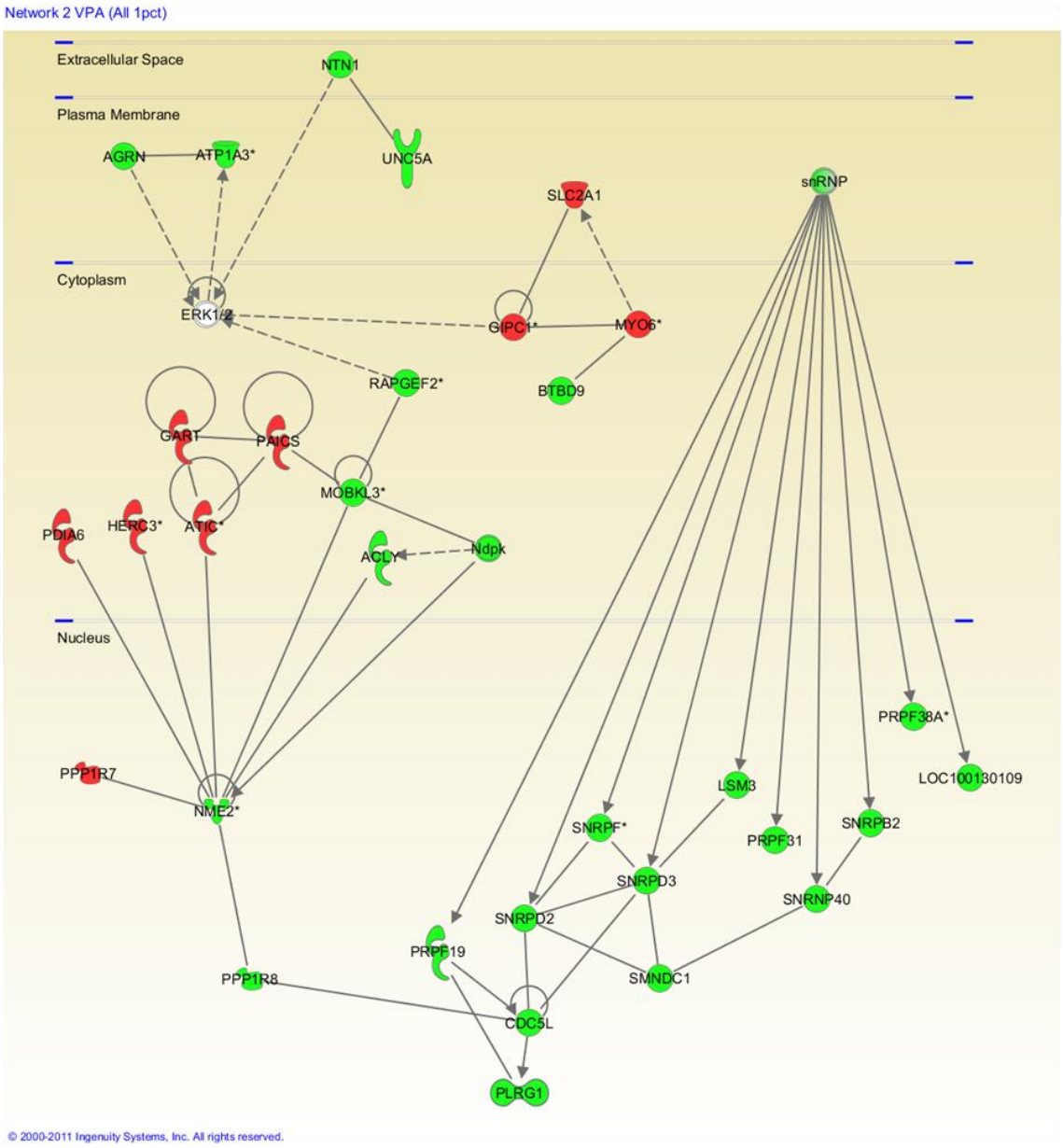

Figure 46 2nd most significant network identified by Ingenuity pathway analysis on pooled expression profiles identified by correlation analysis and SAM with a threshold of 1% FDR with BH correction for multiple testingon microarray data on *C.elegans* wild type strain exposed to valproate.Focus molecules corresponding to gene expression profiles negatively (green) and positively (red) correlated with valproate dose are shown with the focus molecules identified by the IPA which are connected to the network but not found in the data set (white).

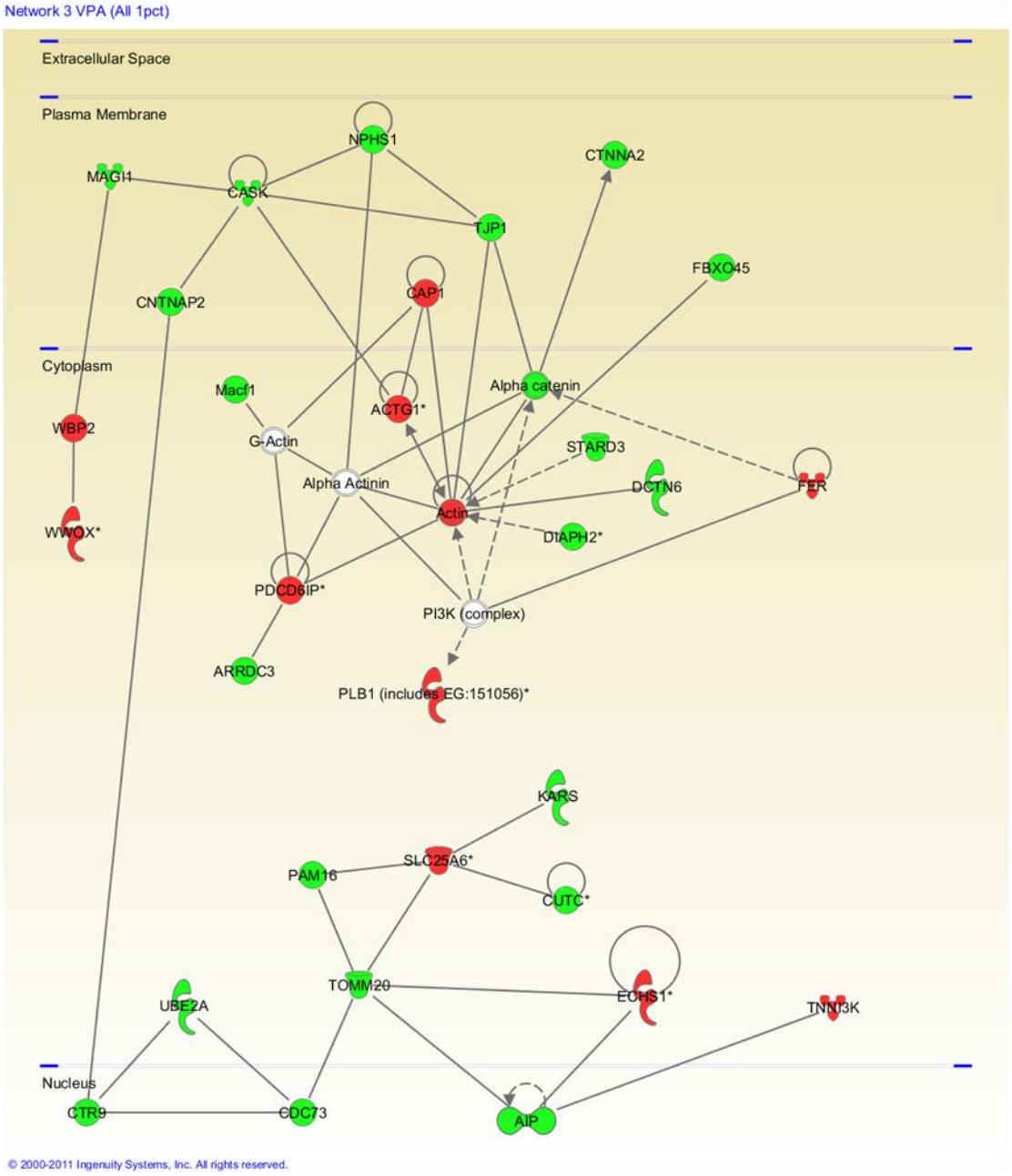

Figure 47 3rd most significant network identified by Ingenuity pathway analysis on pooled expression profiles identified by correlation analysis and SAM with a threshold of 1% FDR with BH correction for multiple testingon microarray data on *C.elegans* wild type strain exposed to valproate.Focus molecules corresponding to gene expression profiles negatively (green) and positively (red) correlated with valproate dose are shown

with the focus molecules identified by the IPA which are connected to the network but not found in the data set (white).

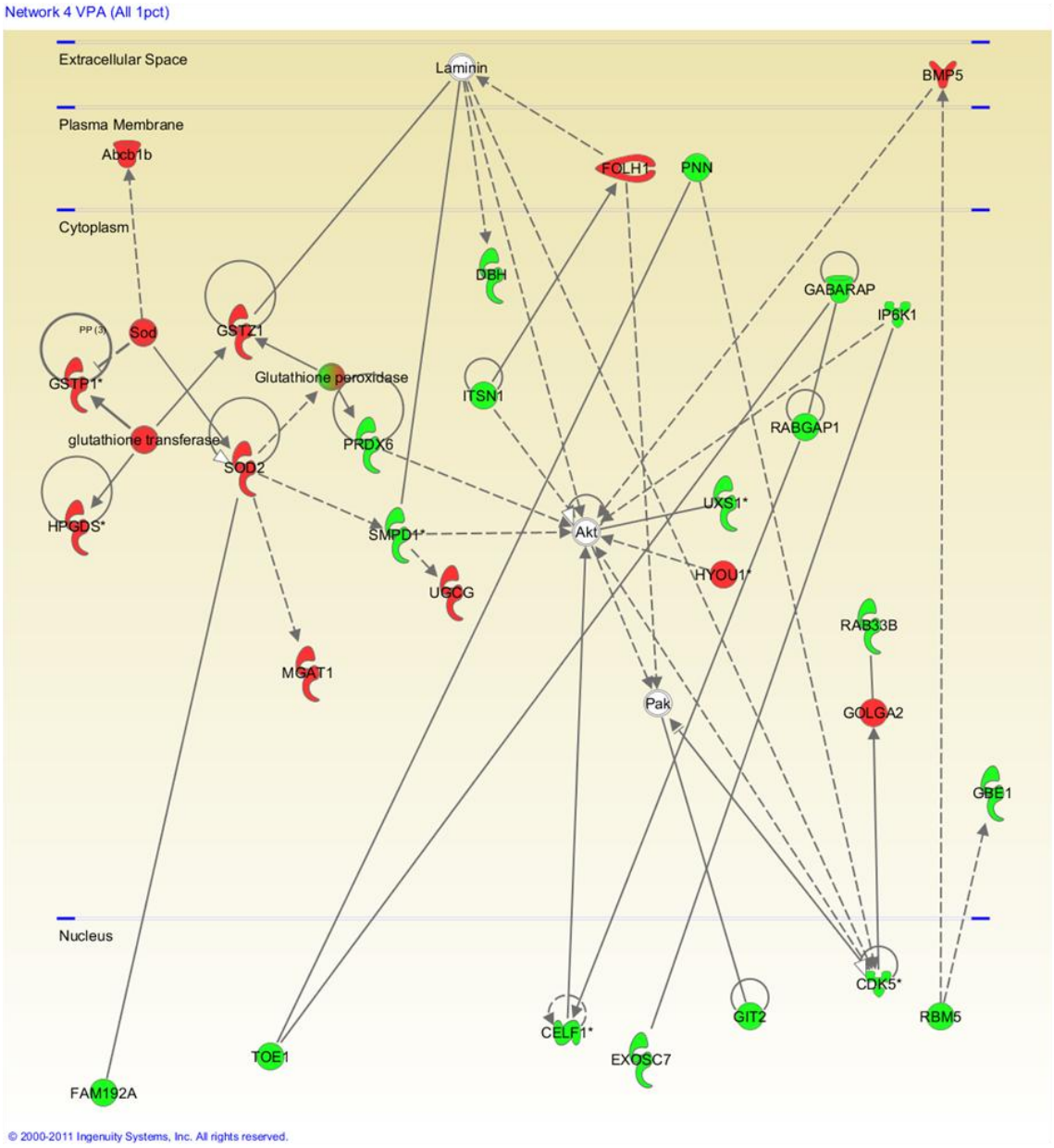

Figure 48 4th most significant network identified by Ingenuity pathway analysis on pooled expression profiles identified by correlation analysis and SAM with a threshold of 1% FDR with BH correction for multiple testingon microarray data on *C.elegans* wild type strain exposed to valproate.Focus molecules corresponding to gene expression profiles negatively (green) and positively (red) correlated with valproate dose are shown

with the focus molecules identified by the IPA which are connected to the network but not found in the data set (white).

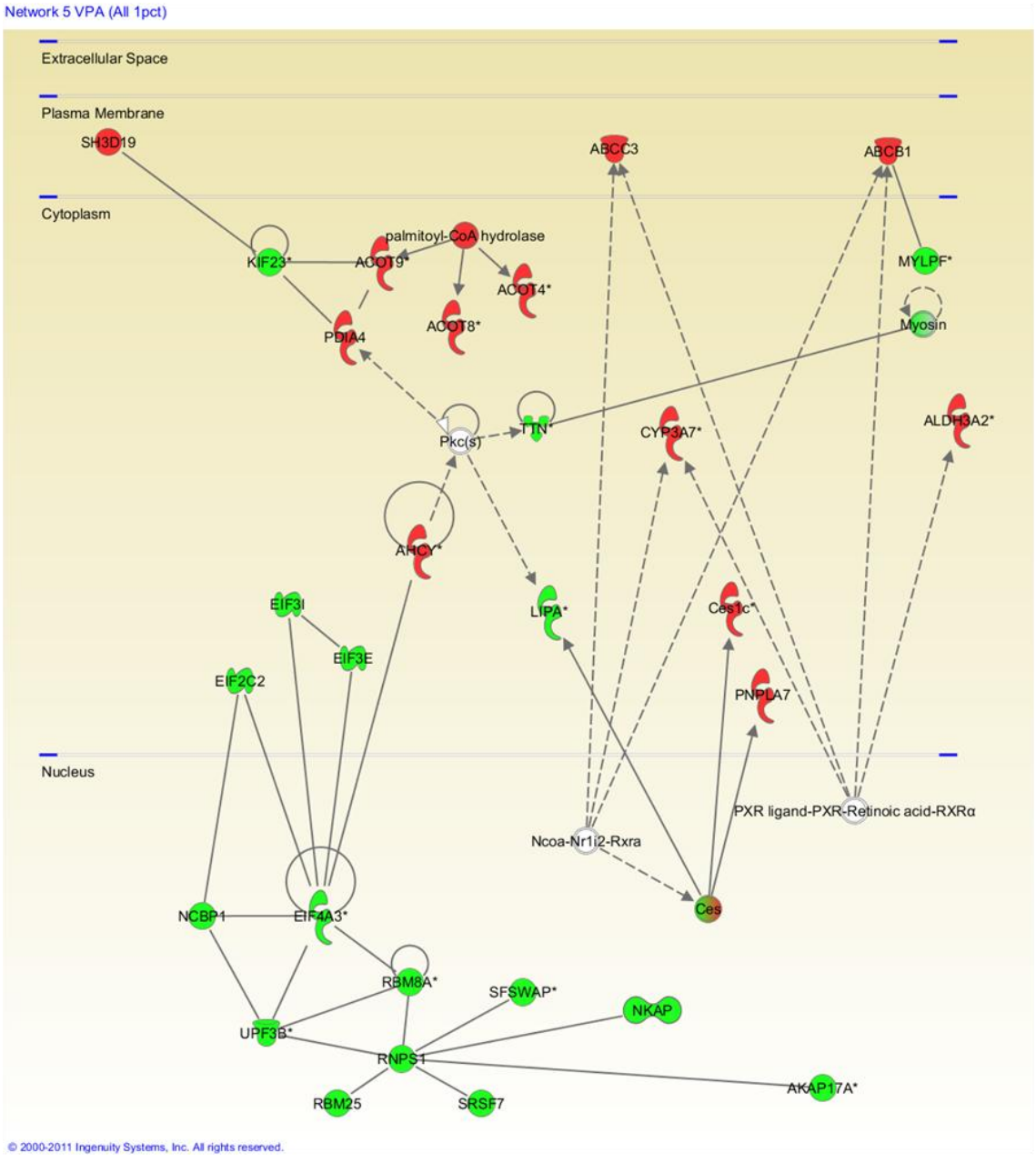

Figure 49 5th most significant network identified by Ingenuity pathway analysis on pooled expression profiles identified by correlation analysis and SAM with a threshold of 1% FDR with BH correction for multiple testingon microarray data on *C.elegans* wild type strain exposed to valproate.Focus molecules corresponding

to gene expression profiles negatively (green) and positively (red) correlated with valproate dose are shown with the focus molecules identified by the IPA which are connected to the network but not found in the data set (white).

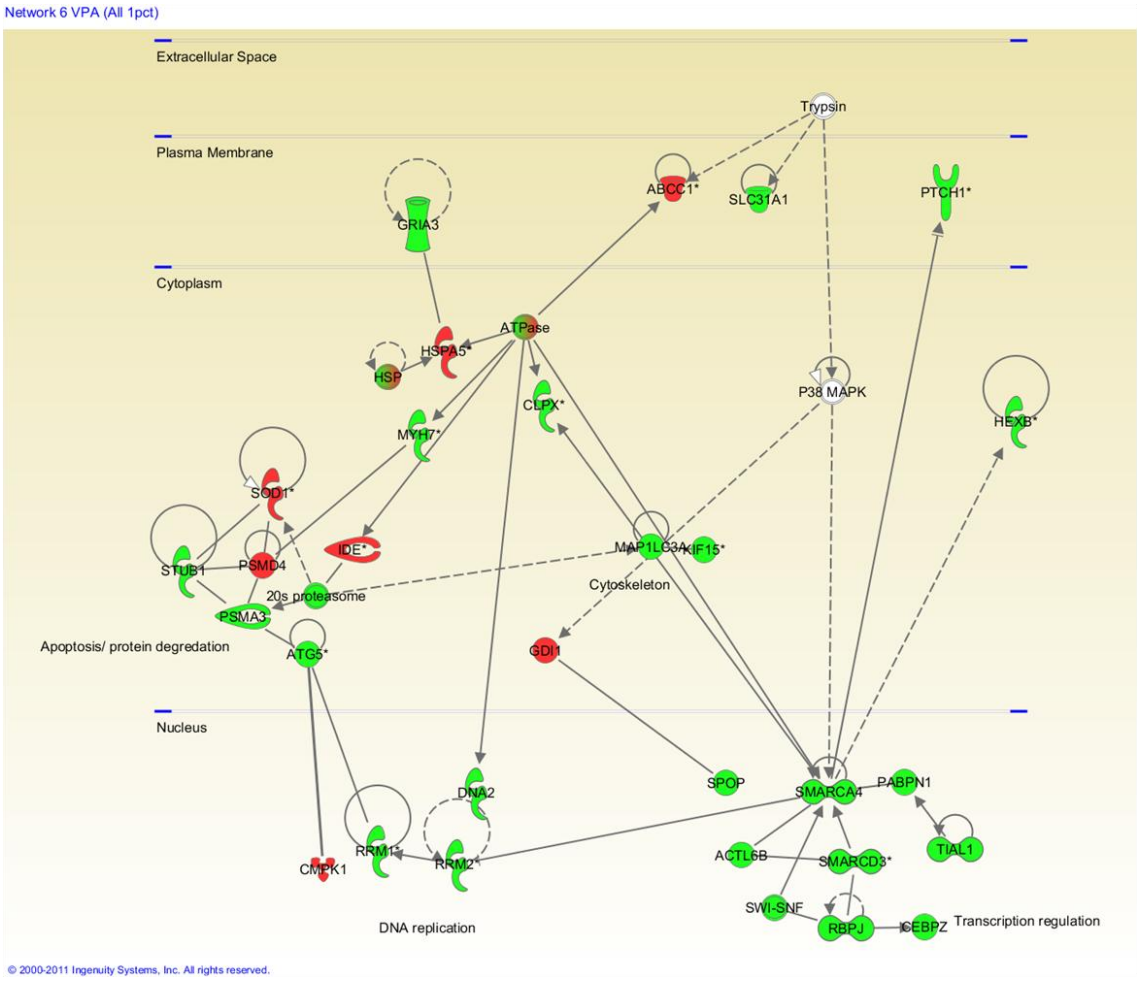

Figure 50 6th most significant network identified by Ingenuity pathway analysis on pooled expression profiles identified by correlation analysis and SAM with a threshold of 1% FDR with BH correction for multiple testingon microarray data on *C.elegans* wild type strain exposed to valproate.Focus molecules corresponding to gene expression profiles negatively (green) and positively (red) correlated with valproate dose are shown with the focus molecules identified by the IPA which are connected to the network but not found in the data set (white).

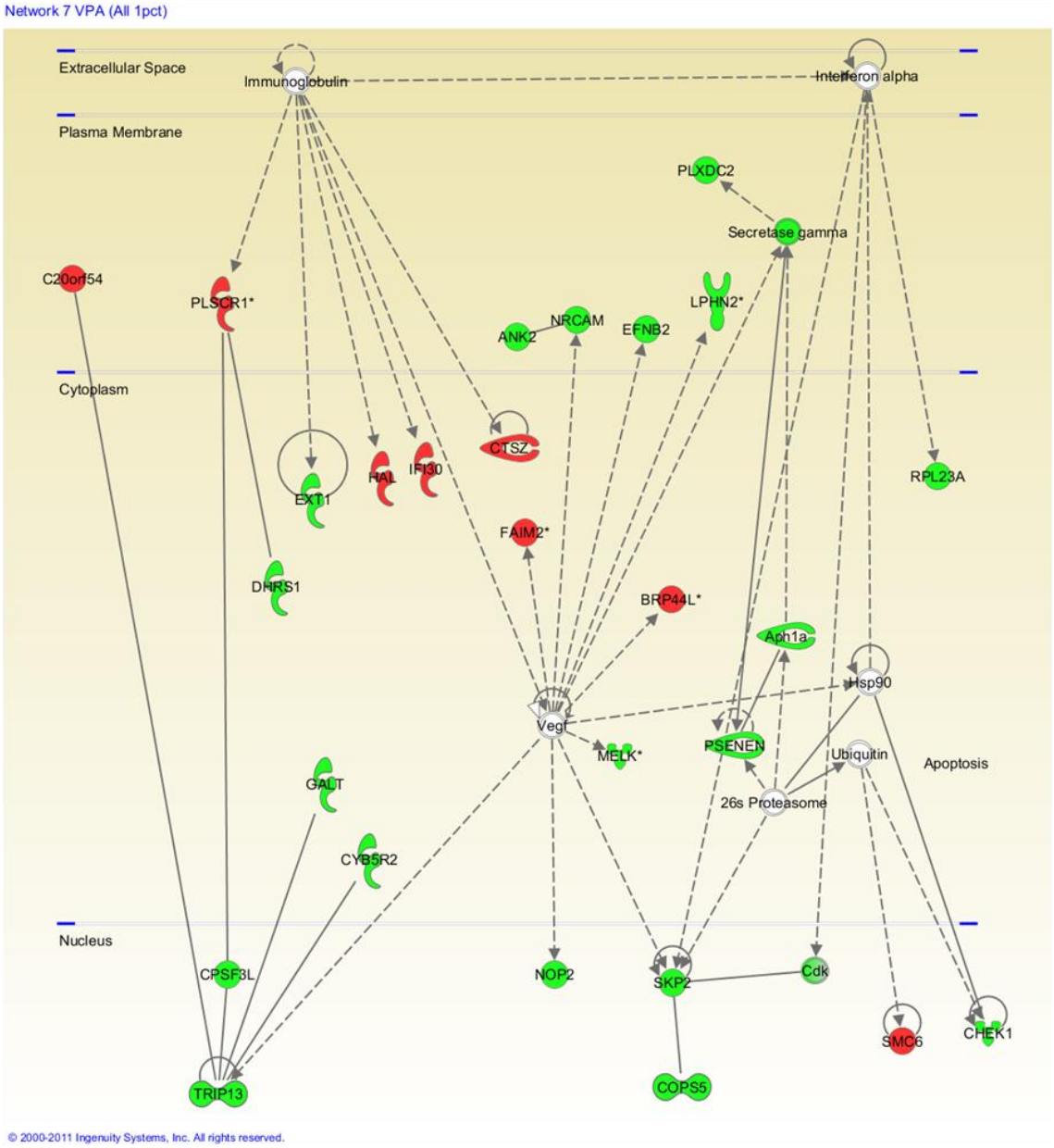

Figure 51 7th most significant network identified by Ingenuity pathway analysis on pooled expression profiles identified by correlation analysis and SAM with a threshold of 1% FDR with BH correction for multiple testingon microarray data on *C.elegans* wild type strain exposed to valproate.Focus molecules corresponding to gene expression profiles negatively (green) and positively (red) correlated with valproate dose are shown with the focus molecules identified by the IPA which are connected to the network but not found in the data set (white).

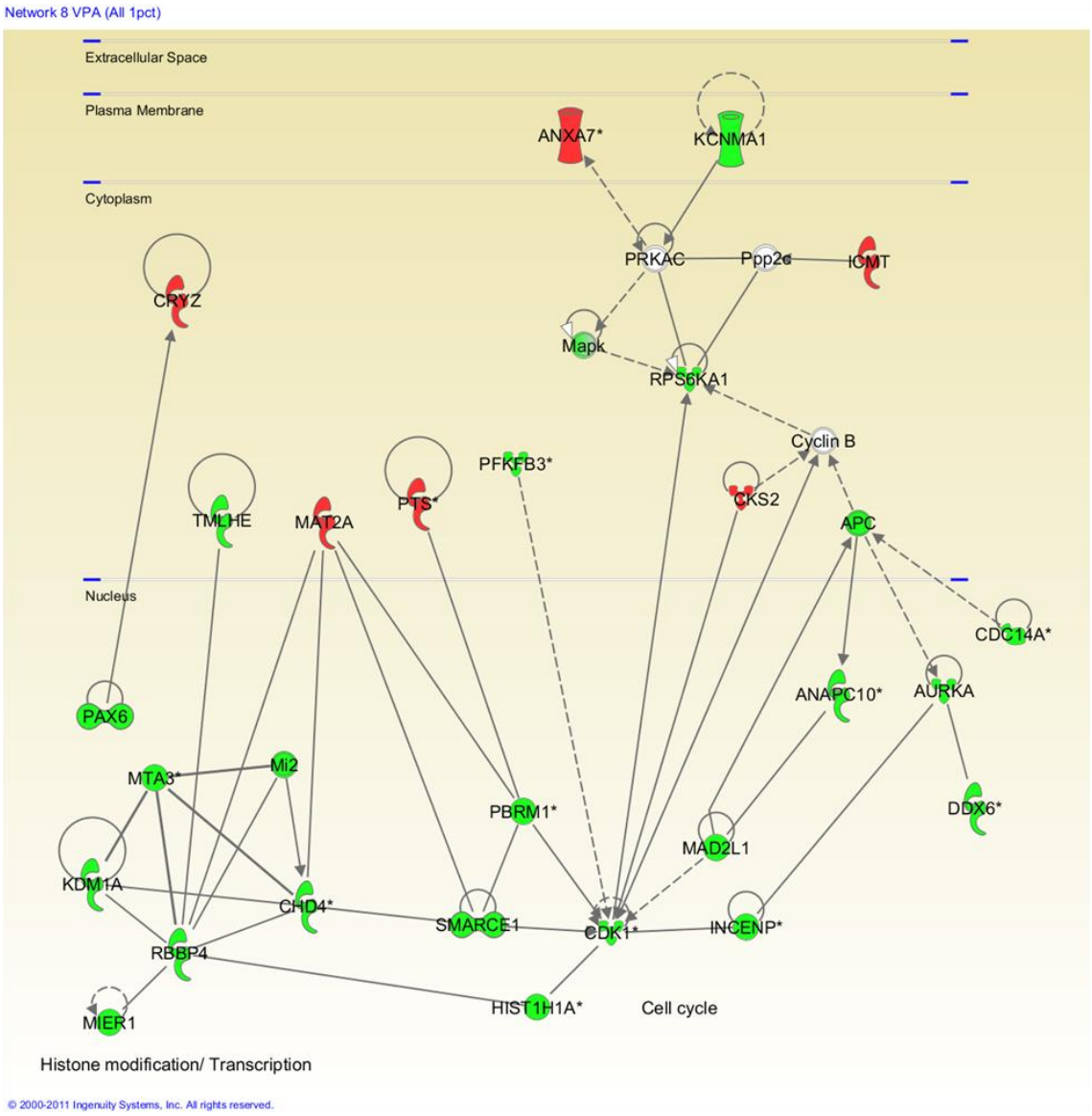

Figure 52 8th most significant network identified by Ingenuity pathway analysis on pooled expression profiles identified by correlation analysis and SAM with a threshold of 1% FDR with BH correction for multiple testingon microarray data on *C.elegans* wild type strain exposed to valproate.Focus molecules corresponding to gene expression profiles negatively (green) and positively (red) correlated with valproate dose are shown with the focus molecules identified by the IPA which are connected to the network but not found in the data set (white).

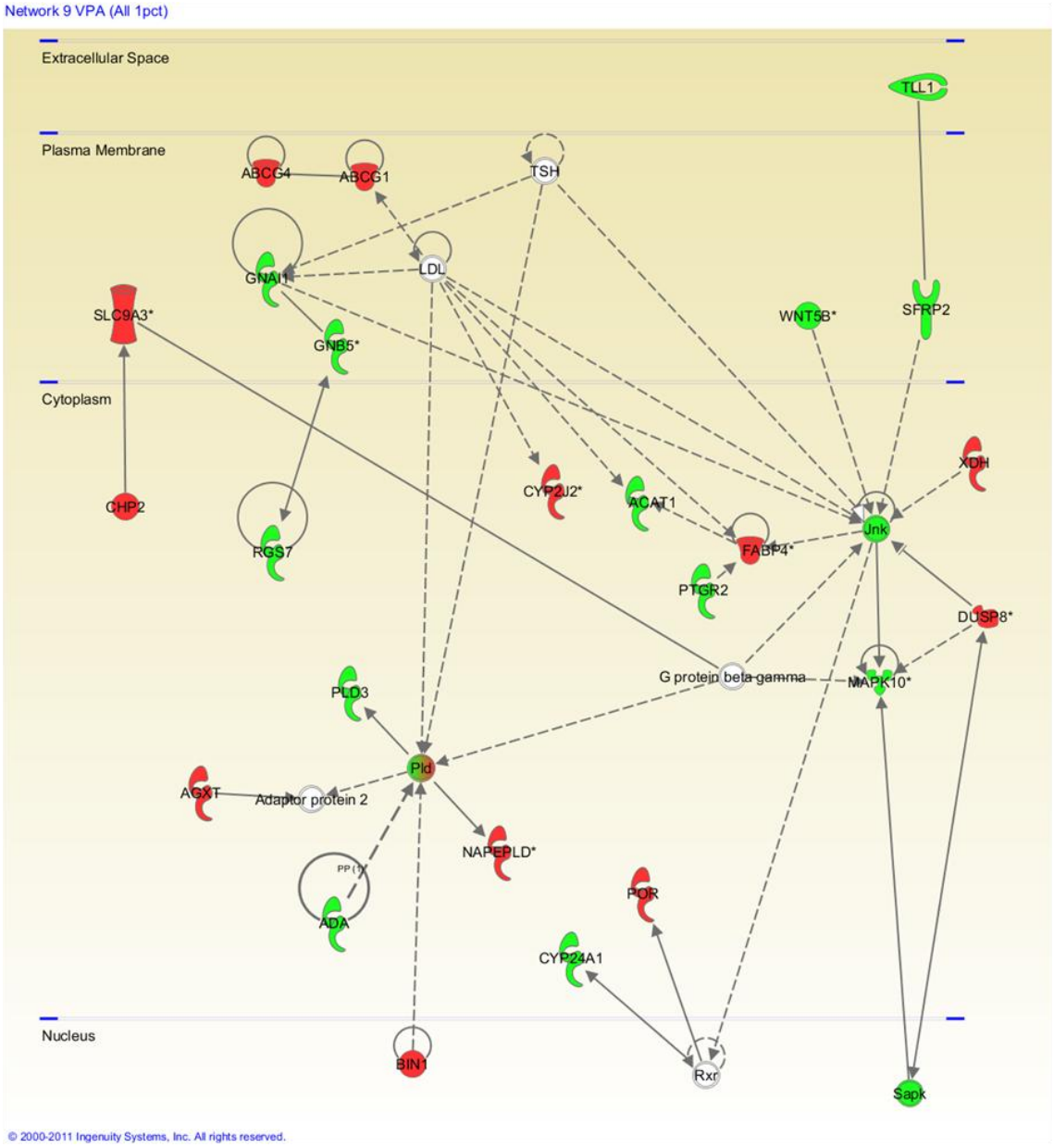

Figure 53 9th most significant network identified by Ingenuity pathway analysis on pooled expression profiles identified by correlation analysis and SAM with a threshold of 1% FDR with BH correction for multiple testingon microarray data on *C.elegans* wild type strain exposed to valproate.Focus molecules corresponding to gene expression profiles negatively (green) and positively (red) correlated with valproate dose are shown with the focus molecules identified by the IPA which are connected to the network but not found in the data set (white).

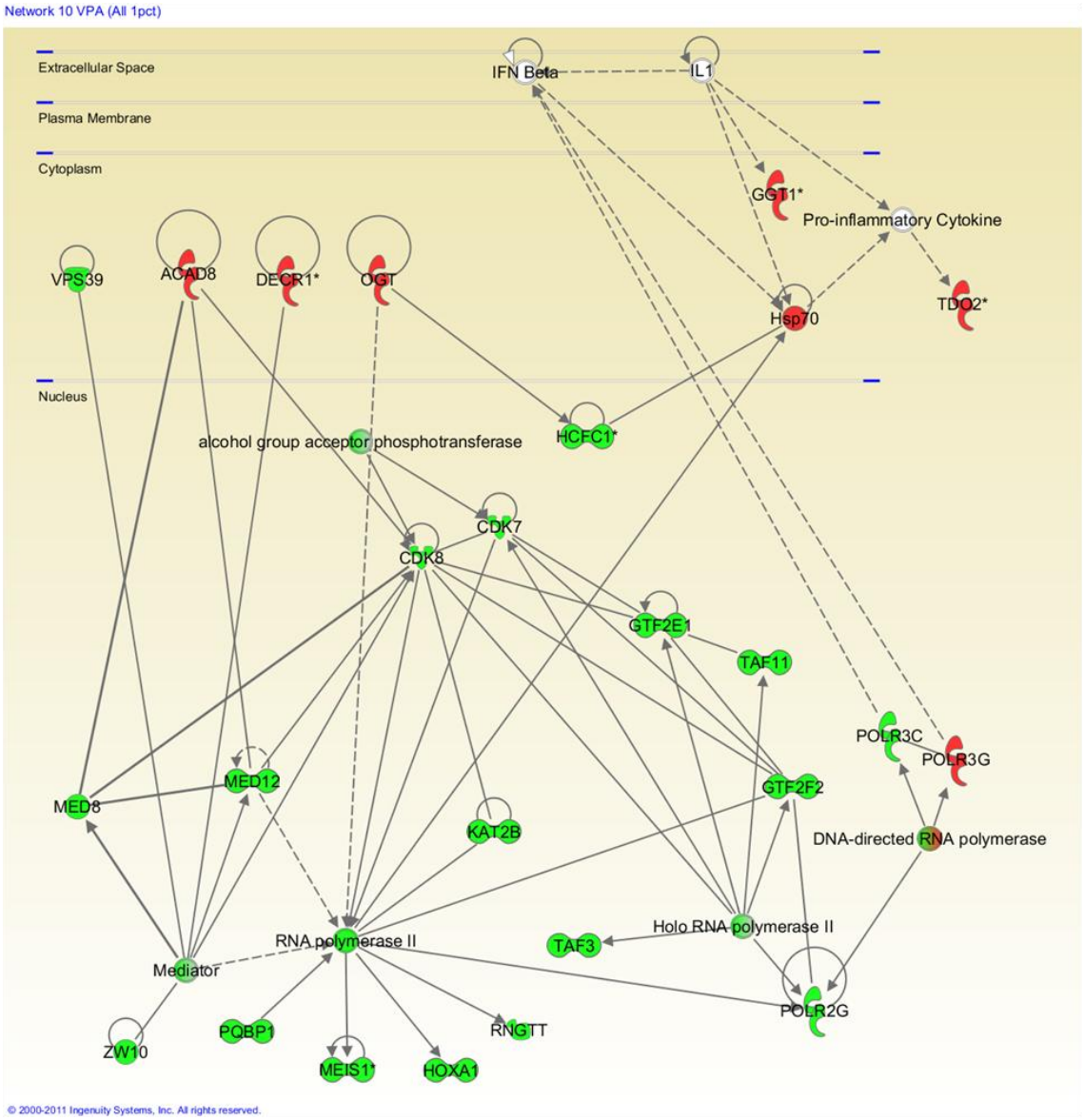

Figure 54 10th most significant network identified by Ingenuity pathway analysis on pooled expression profiles identified by correlation analysis and SAM with a threshold of 1% FDR with BH correction for multiple testingon microarray data on *C.elegans* wild type strain exposed to valproate.Focus molecules corresponding to gene expression profiles negatively (green) and positively (red) correlated with valproate dose are shown with the focus molecules identified by the IPA which are connected to the network but not found in the data set (white).

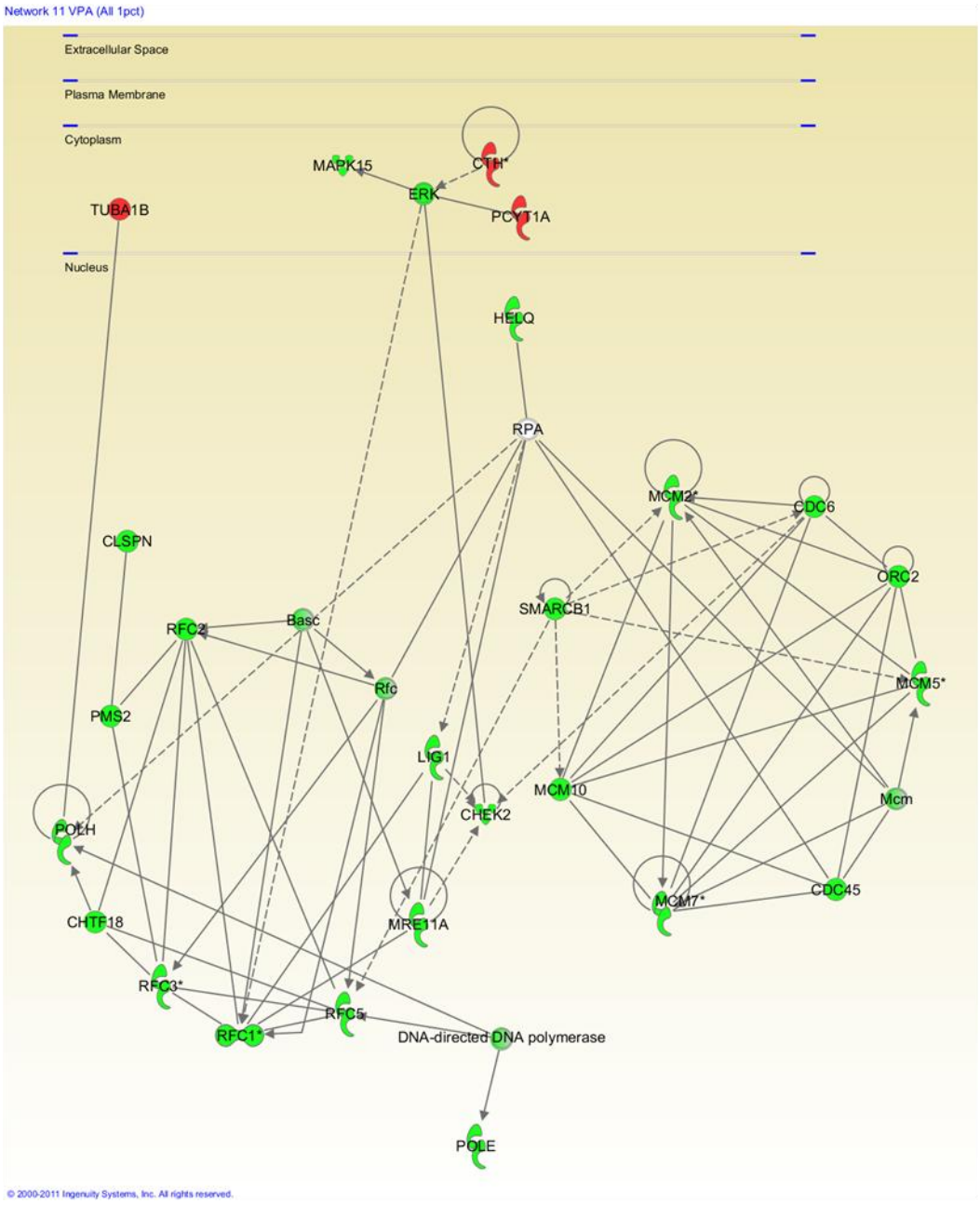

Figure 55 11th most significant network identified by Ingenuity pathway analysis on pooled expression profiles identified by correlation analysis and SAM with a threshold of 1% FDR with BH correction for multiple testingon microarray data on *C.elegans* wild type strain exposed to valproate.Focus molecules corresponding to gene expression profiles negatively (green) and positively (red) correlated with valproate dose are shown with the focus molecules identified by the IPA which are connected to the network but not found in the data set (white).

5.3 Discussion

Ingenuity Pathway Analysis also identified expression of genes related to nuclear functions to be down-regulated. These include chromatin remodelling, DNA replication, progression through cell cycle, DNA damage repair, transcription and mRNA processing. These functions mainly related to functions required for the progression through cell cycle and valproate expected to decrease cell division. Since these mapped on ortholog level to mammalian system, in mammalian system also these nuclear functions are expected to be down-regulated, which could be tested by studying the cell division in human cell lines exposed to valproate.

Network 1 generated by Ingenuity Pathway Analysis (Figure 45, page 177) identified NFkB to be the most connected gene. Even though NFkB homolog not found in *C.elegans*(Kurz and Ewbank, 2003), this finding suggests valproate to act via NFkB in mammalian system. Further supporting this hypothesis, valproate decreases NFkB binding to DNA in rat(Rao et al., 2007). NKAP, which activates NFkB is also negatively correlated with valproate in network 5 further supporting the hypothesis that valproate decreases NFkB signalling.

In the second network generated NME2, which is required for the activation of MYC is negatively correlated with valproate supporting the hypothesis that MYC is down-regulated by valproate. Valproate is known to down-regulate *myc* in neuroblastoma cell line BE[2]-C too(Cinatl et al., 2002). MYC is a promising target for anticancer drugs and this finding suggest a possible anticancer effect of valproate through down-regulation of *myc*.

Ingenuity Pathway Analysis also predicts β-oxidation to be increased on valproate exposure. HSD17B4 expression is increased on valproate exposure. It is a bifunctional enzyme involved in β-oxidation of fatty acids with enoyl-CoA hydratase, D-3-hydroxyacyl –CoA dehydrogenase and 3-ketoacyl-CoA thiolase activities. HSD17B8, 3-hydroxyacyl-CoA dehydrogenase and HADH are also positively correlated with valproate. HADH has 3-hydroxyacyl-CoA dehydrogenase activity. Expression of cytoplasmic acyl CoA dehydrogenase (ACAD8), an enzyme that is involved in catabolism of branched chain amino acids and fatty acid β-oxidation is positively correlated with valproate. Expression of ECHS1which catalyse the second step of fatty acid β-oxidation by hydrating 2-trans-enoyl-coenzyme A (CoA) intermediates to L-3-hydroxyacyl-CoAs is also positively correlated with valproate. Expression of ACOT8 and palmitoyl-CoA hydrolase which are thioesterases, which catalyse the last step of fatty acid β-oxidation, is positively correlated with valproate. Phopholipase B (PLB1), which hydrolyze phospholipids and release fatty acids is also positively correlated with valproate. Valproate treated patients show higher concentrations of serum triglycerides implying catabolism of lipids and release of fatty acids(Pylvänen et al., 2006). Therefore, an increase in β-oxidation is expected on valproate exposure. Thishypothesis could be tested by a similar test to what is done by Franz Knoop in 1904 where he showed that fatty acids are degraded by sequential removal of two carbon units. Can feed *C.elegans* with straight chain fatty acids labelled at ω- carbon atom and test for the rate of production of acetic acid in the presence and absence of sodium valproate.

STARD3 involved in lipid trafficking is negatively correlated with valproate. FABP4 a transporter involved in fatty acid metabolism is positively correlated with valproate. Two cell membrane transporters ABCG4, which is involved in cholesterol transport and

ABCG1, which is involved in both cholesterol and phospholipid transport are positively correlated with valproate. Therefore an increase in cholesterol and phospholipid transport is expected on exposure to valproate.

Ingenuity Pathway Analysis also show activation of several genes involved in steroid synthesis due to the up-regulation of CYP3A7, involved in the synthesis of estriol; cholesterol; steroids and other lipids. POR involved in steroidogenesis and membrane component Abcb1b UGCG, which is involved in glycosphingo lipid biosynthesis is positively correlated with valproate. HSD17B12, which is involved in fatty acid elongation is also positively correlated with valproate. Expression of cytoplasmic phosphate cytidyltransferase choline (PCYT1A); the rate limiting enzyme in phosphatidylcholine biosynthesis is positively correlated with valproate.This is the most abundant phospholipid in animals and plants. As a result, an increase in steroid synthesis, especially cholesterol, glycosphingo lipids and phosphatidylcholine are expected on exposure to valproate. Further supporting this hypothesis, valproate increases androgen levels in human(Rättyä et al., 2001).

Expression of carboxy esterase, lipase involved in cholesterol ester hydrolysis, phospholipase and ALDH3A2 involved in oxidation of long chain aliphatic aldehydes to fatty acids are also positively correlated with valproate. Expression of Phospholipase D, which hydrolyse phosphatidylecholine to phosphatidic acid and prostaglandin reductase involved in arachidonic acid metabolism is down-regulated.Further supporting this finding, valproate treatment reduces arachidonate cascade in platelets of human (Kis et al., 1999). Rxr, a co-repressor that induce histone acetylation and chromatin condensation and activate fatty acid oxidation genes is identified by the pathway analysis, a gene not present in the dataset. These results suggest valproate to

modulate lipid level and the net result would be an increase in total lipids as seen in phenotypic analysis.

Expression of insulin degrading enzyme (IDE), which terminates insulin activity is positively correlated with valproate, which may explain the activation of DAF-16. Valproate causes hyperinsulinemia in human, which contradict with this finding (Pylvänen et al., 2002). But our correlation analysis identified insulin secretion to increase on exposure to valproate.

Therefore valproate may decrease lipid accumulation by increasing β-oxidation of fatty acids. But it may increase cholesterol and other steroid synthesis, glycosphingolipid and phosphatidylcholine biosynthesis resulting in an overall accumulation of lipids. Phenotypic changes predicted to occur on exposure to valproate are summarised in Figure 56.

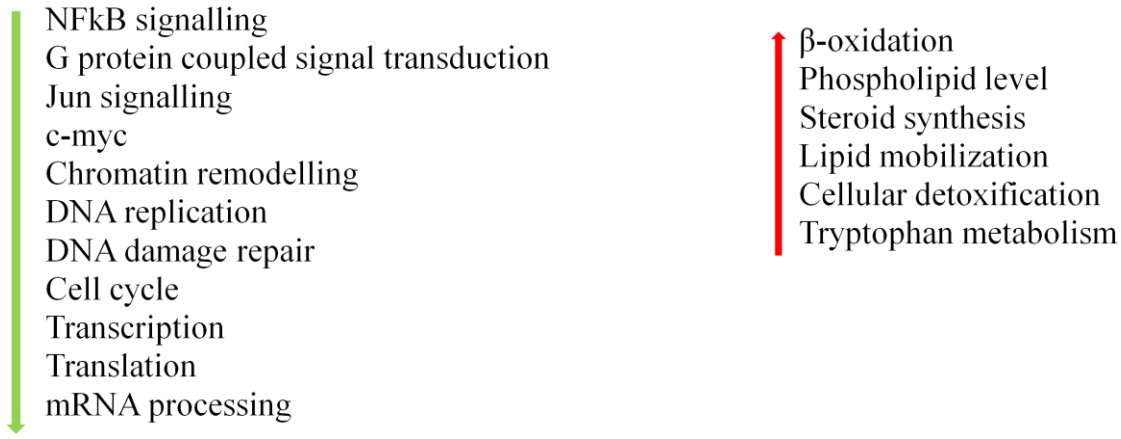

Figure 56 Phenotypic changes predicted to occur on exposure to valproate. Phenotypic changes expected to increase on exposure to valproate are indicated with a red arrow and down regulated with a green arrow.

6.0 INSULIN MEDIATED RESPONSE TO VALPROATE EXPOSURE

6.1 Summary

As discussed in the previous chapters valproate causes lifespan extension and dauer formation probably via the insulin signalling pathway. Therefore we thought this pathway may also play a role in the lipid accumulation on valproate exposure. To assess this I compared the expression profile associated with valproate exposure and the expression profiles of insulin signalling pathway mutants. Specifically I compared the expression profile of wild type *C.elegans* exposed to valproate with the *daf-2* insulin receptor mutant and with *daf-2;daf-16* double mutant where both insulin receptor and the gene coding for FOXO transcription factor *daf-16* are mutated. This analysis revealed most of the gene expression changes associated with valproate exposure to be insulin independent.

6.2 Results

One major limitation of Ingenuity Pathway analysis is the smaller percentage (<15%) of genes mapped to Ingenuity pathways. Therefore genes of interesting pathways were checked for their expression patterns in heatmaps in TMev. TMev is a set of microarray data analysis tools including tools to cluster, visualize, classify, statistically analyse data and helps to discover biological themes. This is performed to identify any trends in expression patterns of pathways by visualization because general patterns in an expression profile associated with a specific pathway is not expected in random noise

and would reveal a biological theme. Expression profiles with <1% FDR in SAM analysis were considered significant. Significantly altered Gene expressions from insulin receptor *daf-2* up to *daf-16* is shown in Figure 57 (page 194). As expected, when the inhibitory effect of receptor is relieved, most of the genes downstream of *daf-16*were positively correlated with valproate exposure (Figure 58, page194). This could explain the plateau effect of lipid level obtained at higher valproate doses. Valproate increases expression of *daf-16* down- stream genes and they exert an inhibitory effect on the increase of lipid by valproate bringing the plateau effect. If this is true, then valproate should be increasing lipid levels by some other means other than via the insulin signalling pathway. None of the genes in the TGF-β dauer pathway show significant changes in the expression profile and only two genes, *unc-129* and *sma-3*, in the sma-mab pathway were significantly changed on valproate exposure (Figure 59, page 195). *unc-129* encodes a growth factor signalling molecule that functions as a dorsalward axonal guidance cue(Colavita and Culotti, 1998) and *sma-3* encodes a smad protein, which interacts with *lin-31* transcription factor. Genes in the SIRT1 pathway are negatively correlated with valproate (Figure 60, page195). Down regulation of *hcf-1* relieves its inhibitory action on *daf-16*. This shows that when the inhibitory action on *daf-16* is relieved, its mRNA level increases. There was no significant change in the gene expressions in the GABA pathway. AMPK phosphorylate *daf-16* directly(Greer et al., 2007). Some genes coding for the 20 different possible *C.elegans* AMPK subunits were positively correlated with valproate(Figure 61, page196). This could partly explain the lifespan extension of *C.elegans* on valproate exposure but cannot explain the changes in lipid content. *daf-15/let-363*, the *C.elegans* TOR pathway components, did not show any significant changes in expression profile. *daf-15* and *let-363* mutants are

known to have high lipid content (Jia et al., 2004). This complex is known to interact with insulin signalling as *daf-16* negatively regulates *daf-15* expression.

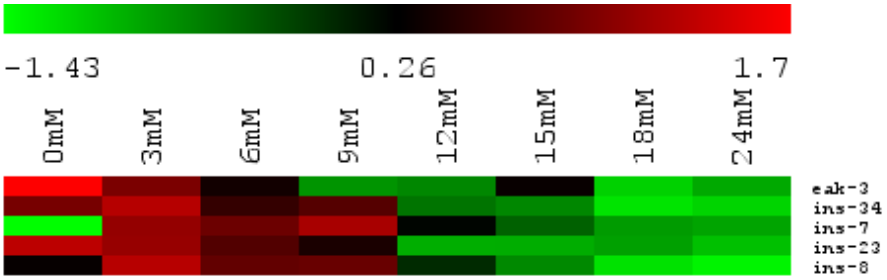

Figure 57Heatmap of significant expression profiles of genes from *daf-2* insulin receptor upto *daf-16* on exposure to valproate. This shows a down regulation of this part of the insulin signalling pathway.Expression profiles with <1% FDR in SAM analysis were considered significant.Numbers across top of heatmap indicates valproate concentration. The degree of expression indicated with a red to green scale where the higher expression is given by red.

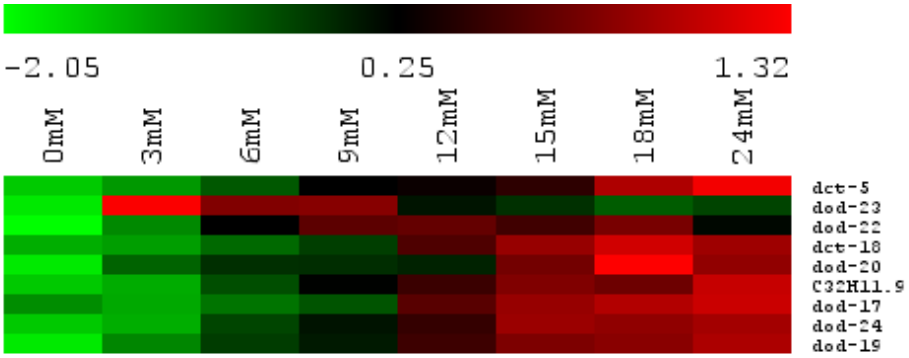

Figure 58Heatmap of expression profile of genes down stream of daf-16 and daf-16. This shows an upregulation of most of the daf-16 downstream genes.Expression profiles with <1% FDR in SAM analysis were considered significant.Numbers across top of heatmap indicates valproate concentration. The degree of expression indicated with a red to green scale where the higher expression is given by red.

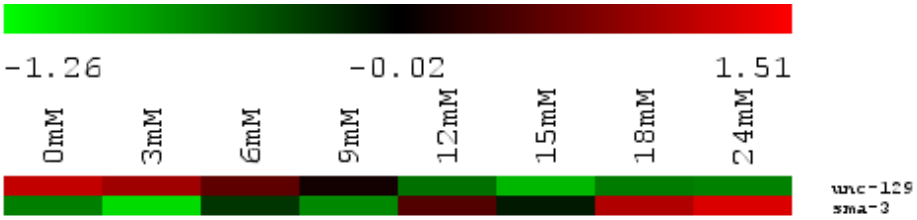

Figure 59Heatmap of significant expression profile of genes in TGF-β sma/mad pathway. Expression profiles with <1% FDR in SAM analysis were considered significant.Numbers across top of heatmap indicates valproate concentration. The degree of expression indicated with a red to green scale where the higher expression is given by red.

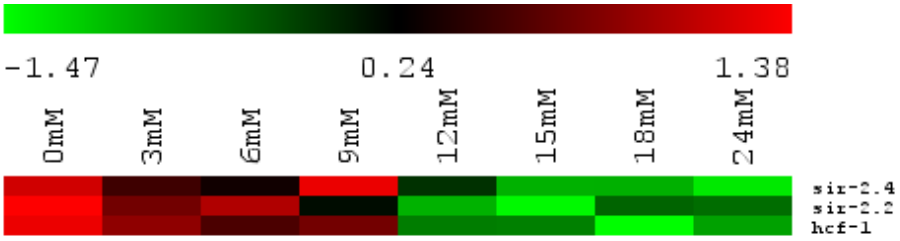

Figure 60Heatmap of significant expression profile of genes from *sir-2* to *daf-16*. This shows a down regulation of sir-2 pathway. Expression profiles with <1% FDR in SAM analysis were considered significant.Numbers across top of heatmap indicates valproate concentration. The degree of expression indicated with a red to green scale where the higher expression is given by red.

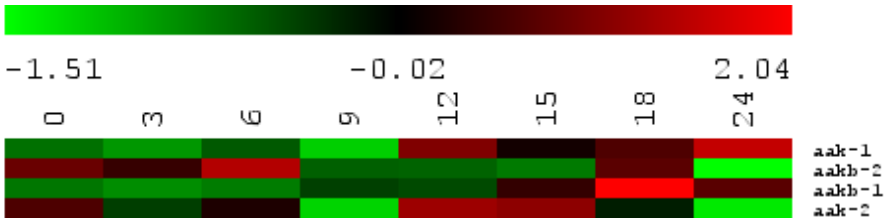

Figure 61Heatmap of significant expression profile of amp kinase genes. Expression profiles with <1% FDR in SAM analysis were considered significant.Numbers across top of heatmap indicates valproate concentration. The degree of expression indicated with a red to green scale where the higher expression is given by red.

Then I assessed the GO functional terms linked to the expression profile dependent on insulin on valproate exposure by DAVID analysis.

Three genes downstream of *daf-16*, a steroid dehydrogenase, lysozyme and a UDP-glucuronosyl transferase are associated with the functional term ‘determination of adult life span’ and are positively correlated with valproate. These were identified as the DAF-16 dependent expression profile positively correlated with valproate(Figure 62, page197).

DAF-16 dependent negatively correlated expression profile of valproate exposure had *bbs-5*, which is required for regulation of insulin secretion. Mutants of this gene are known to have increased levels of insulin, biogenic amines and neuropeptides (Figure 63, page 197).

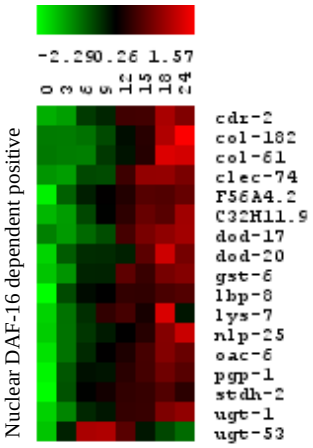

Cluster	Enrichment Score	Term	Count	PValue	Benjamini
1	4.358941	GO:0008340~determination of adult life span	6	4.38E-05	0.002884

Figure 62 Nuclear DAF-16 dependent expression profile positively correlated with valproate exposure. Numbers across top of heatmap indicates valproate concentration. The degree of expression indicated with a red to green scale where the higher expression is given by red.

Cluster	Enrichment Score	Term	Count	PValue	Benjamini
1	2.045856	GO:0008340~determination of adult life span	3	0.008998	0.110862

Figure 63 Nuclear DAF-16 dependent expression profile down-regulated on valproate exposure. Numbers across top of heatmap indicates valproate concentration. The degree of expression indicated with a red to green scale where the higher expression is given by red.

DAF-2 dependent expression profile positively correlated with valproate had several collagen genes and glutathione transferase genes associated with functional terms

'structural constituent of cuticle' and 'glutathione transferase activity'. DAF-2 dependent negatively correlated expression profile with valproate had several lectins.

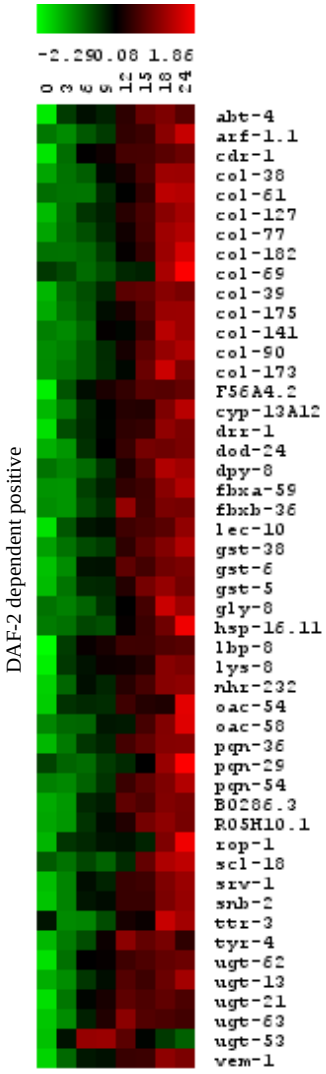

Cluster	Enrichment Score	Term	Count	PValue	Benjamini
1	6.221541	GO:0042302~structural constituent of cuticle	14	1.28E-10	1.30E-08
2	2.289343	GO:0004364~glutathione transferase activity	3	0.007771	0.232971

Figure 64 DAF-2 dependent expression profile positively correlated with valproate exposure. Numbers across top of heatmap indicates valproate concentration. The degree of expression indicated with a red to green scale where the higher expression is given by red.

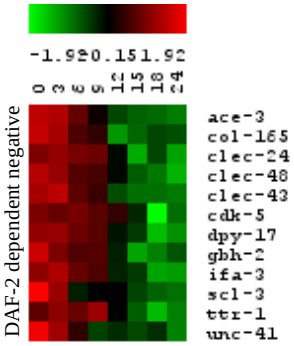

Cluster	Enrichment Score	Term	Count	PValue	Benjamini
1	2.019904	IPR016186:C-type lectin-like	4	0.007155	0.331105

Figure 65 DAF-2 dependent expression profile downregulated on valproate exposure. Numbers across top of heatmap indicates valproate concentration. The degree of expression indicated with a red to green scale where the higher expression is given by red.

Analysis of the insulin dependent expression profile of valproate exposure revealed only a few functional terms to be associated with the insulin dependent part of the expression profile. It shows that determination of adult life span to be associated with DAF-16 and cellular detoxification, collagen and lectins to be associated with the receptor DAF-2. Therefore most of the response to valproate exposure is insulin independent.

Ingenuity pathway analysis revealed lipid metabolism and amino acid metabolism to be dependent on nuclear DAF-16 (Figure 66,). HSD17B12 involved in fatty acid elongation, haematopoetic prostaglandin D synthase (HPDGS), fatty acid binding proteins (FABP) which is involved in fatty acid uptake, transport and metabolism and ABHD4 involved in the biosynthesis of N-acyl ethanol amine are all positively correlated with valproate which are dependent on DAF-16.

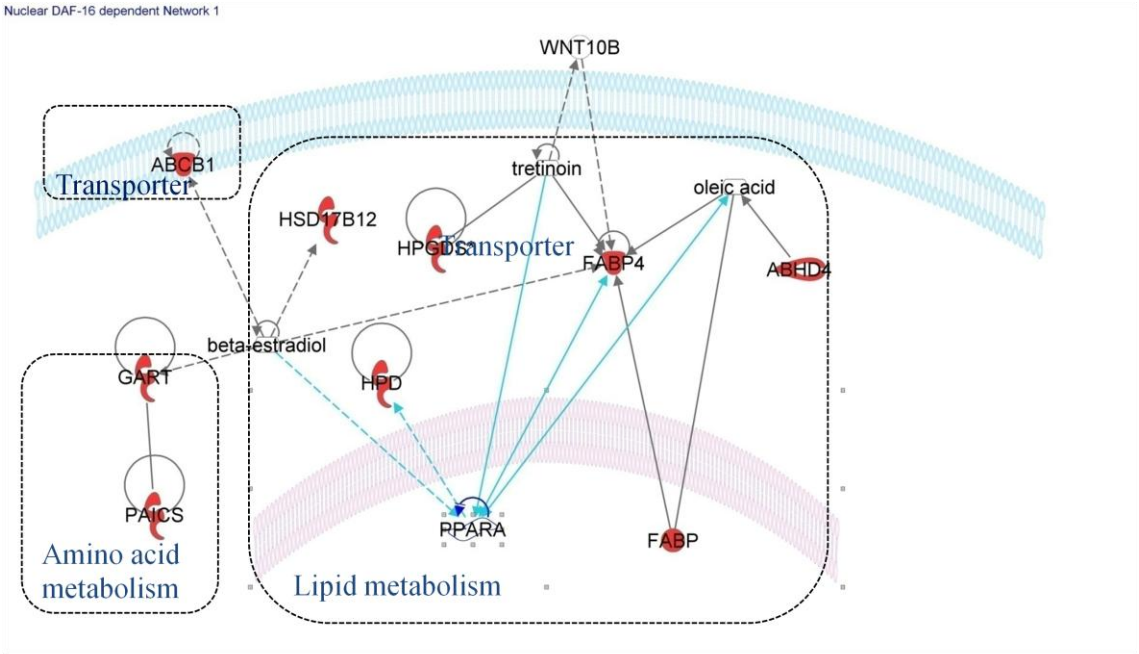

Figure 66 Ingenuity system pathway analysis of nuclear DAF-16 dependent expression profile of valproate exposure. Focus molecules corresponding to gene expression profiles .positively (red) correlated with valproate dose are shown with the focus molecules identified by the IPA which are connected to the network but not found in the data set (white).

The expression of DAF-16 dependent valproate exposure genes are compared with a dataset of daf-16;daf-2 double mutant with daf-2. This reveals an inhibitory effect of DAF-16 on valproate induced lipid accumulation genes (Table 36, page 201). This would explain the increase of lipid mass on valproate treated *daf-16* mutants compared to valproate treated wild type.

Table 36 Lipid metabolism related DAF-16 dependent expression profile of valproate exposure. Expression of DAF-16 dependent valproate gene expressions are identified in daf-16(mu86);daf-2(e1370) vs daf-2(e1370 (PUMA database Shaw *et al*. 2007)

Gene symbol	Gene	Agilent ID	Mean expression
lbp-8	Lipid Binding Protein	A_12_P119973	-0.35926
stdh-2	STeroid DeHydrogenase family	A_12_P119903	0.103837
oac-6	O-ACyltransferase homolog	A_12_P101511	-0.07638
bbs-5	BBS (Bardet-Biedl Syndrome) protein	A_12_P101884	-0.00507

DAF-2 dependent expression profile of valproate exposure was analysed by Ingenuity Systems Pathway Analysis (Figure 67). This shows lipid metabolism, amino acid metabolism, cellular detoxification and transport to be dependent on DAF-2. Gene coding for prostaglandin-D synthase (HPGDS) which is involved in prostaglandin synthesis and detoxification is positively correlated with valproate and AGPAT-6 which transferes acyl groups to lysophosphatidic acid and convert it into phoaphatidic acid is negatively correlated with valproate. Phosphatidic acid is the common metabolite found in phospholipid and triacylglycerol synthesis.

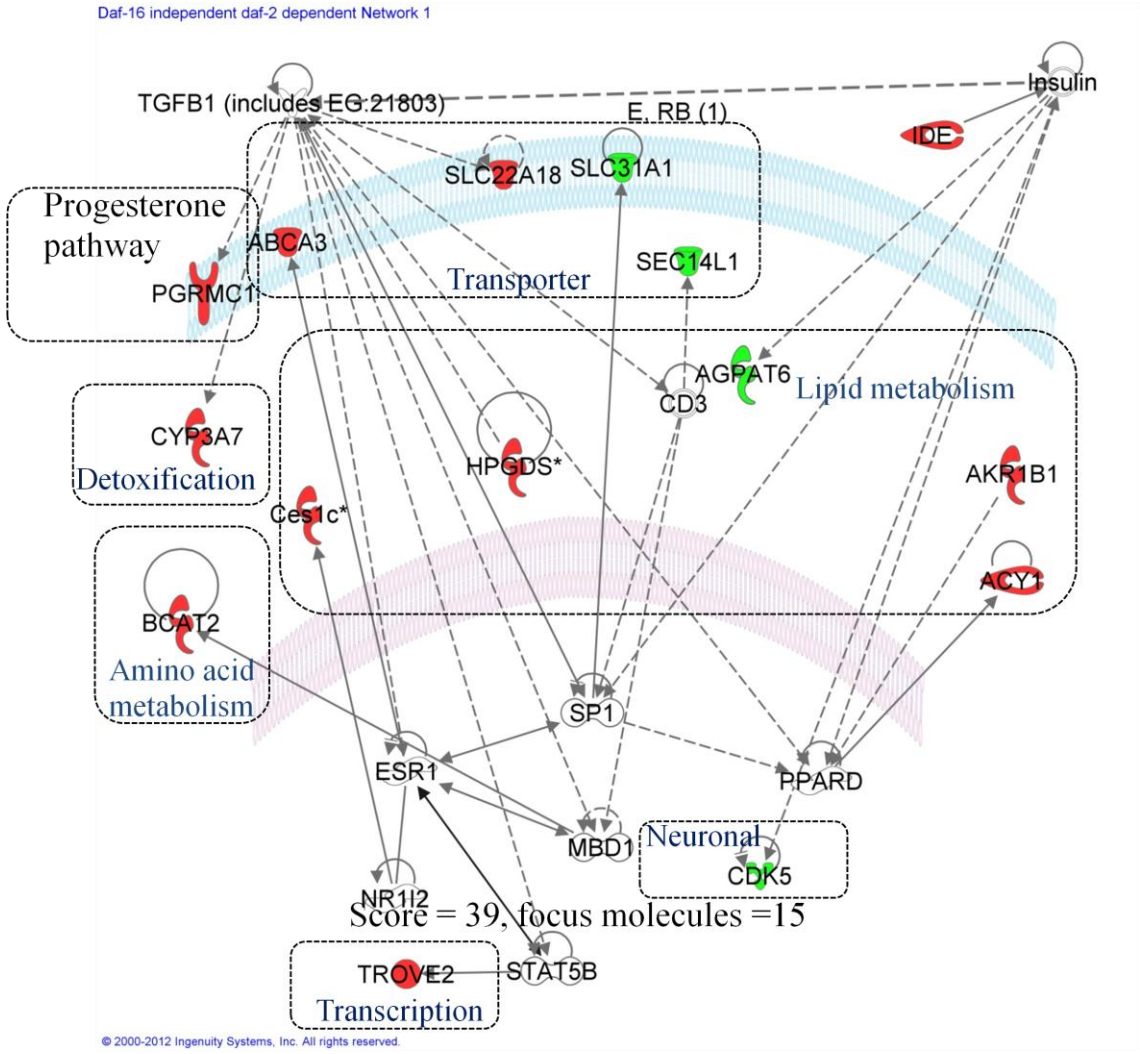

Figure 67 Ingenuity system pathway analysis of DAF-16 independent DAF-2 dependent expression profile of valproate exposure. Focus molecules corresponding to gene expression profiles negatively (green) and positively (red) correlated with valproate dose are shown with the focus molecules identified by the IPA which are connected to the network but not found in the data set (white).

6.2.1 Identification of a few functions to be dependent on daf-16 is not due to inefficient inactivation of daf-16 by RNAi

Only a few functional terms were associated with DAF-16 dependent expression profile of valproate exposure. The possibility of this to be due to inefficient inactivation of genes by RNAi is tested by analysing another data set of *daf-2; daf-16* double mutant vs *daf-2* (Available in PUMAdb by Show *et al*. 2007 Exp. ID 105871, 105873 and 105845)(Shaw et al., 2007). The null mutant *daf-16*(mu86) was compared with the double mutant *daf-16*(mu86);*daf-2*(e1370). Only a few genes negatively correlated with valproate were identified as significant expression profile with a 1% FDR 1fold in SAM analysis in this comparison (Table 37). Therefore the few functions associated with DAF-16 dependent component identified cannot be due to inefficient inactivation of*daf-16* by RNAi.

Table 37 DAVID gene ID conversion of the significant expression profile identified in *daf-16*(mu86) compared with *daf-16*(mu86); *daf-2*(e1370)

Agilent ID	Official gene symbol	Gene Name
A_12_P111479	taf-3	TAF (TBP-associated transcription factor) family
A_12_P101622	nhr-225	Nuclear Hormone Receptor family
A_12_P105555	vit-5	VITellogenin structural genes (yolk protein genes)
A_12_P105555	vit-4	VITellogenin structural genes (yolk protein genes)

A_12_P112365	Y53F4B.24	Y53F4B.24
A_12_P113081	C10A4.2	C10A4.2
A_12_P110918	Y17G7B.13	Y17G7B.13
A_12_P100622	npp-16	Nuclear Pore complex Protein
A_12_P116716	ZK1128.3	Uncharacterized protein ZK1128.3

6.3 Discussion

Since lifespan extension and dauer formation in *C.elegans* depend on insulin signalling pathway(Evason et al., 2008), we hypothesised that lipid accumulation on valproate exposure too could depend on insulin pathway. But the observation of expression profiles of mutants of the insulin signalling pathway reveal that most of the molecular changes associated with valproate to be insulin independent.DAF-16 dependent expression profile of valproate exposure is expected to be involved in steroid synthesis, fatty acid elongation, prostaglandin D synthesis, fatty acid uptake and acylated ethanol amine production. It is also expected to increase insulin secretion by decreasing the expression of *bbs-5* resulting in lipid synthesis. Valproate treated patients show low estradiol levels but increased testesterone and delta-4-androstenedione levels implying valproate to modulate steroid levels(Murialdo et al., 1998).Therefore valproate induced lipid accumulation is partially affected by DAF-16 (Figure 68). It also reveals that prostaglandin synthesis to be positively correlated with valproate and phosphatidate formation to be decreased in a DAF-2 dependent manner. Prostaglandins have anticonvulsant effects and anticonvulsant effects of valproate suggested to be due to

prostaglandins(Srivastava and Gupta, 2001). Supporting this hypothesis current study reveals valproate to induce prostaglandin synthesis.

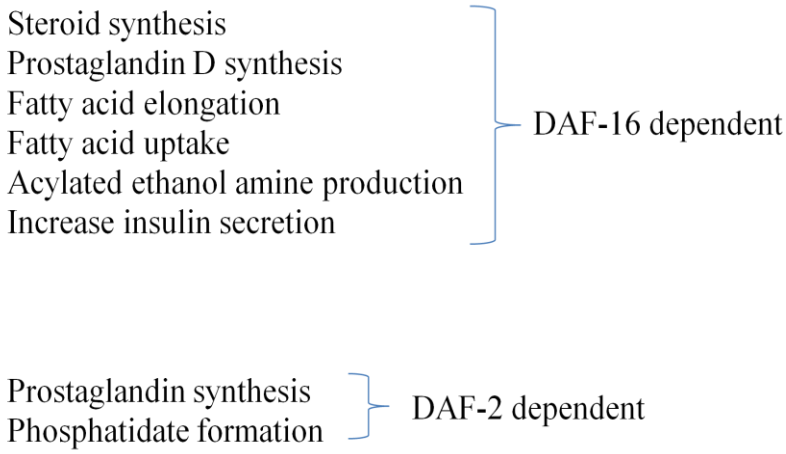

Figure 68 Summary of the functions associated with lipid metabolism which depend on insulin signalling pathway.

7.0 INSULIN INDEPENDENT RESPONSE TO VALPROATE EXPOSURE

7.1 Summary

In the previous chapter I showed that most part of the expression profile associated with valproate exposure is insulin independent. Therefore I set to assess how much of the lipid accumulation of valproate exposure could be explained by insulin independent component. To achieve this, I analysed the insulin independent component of the expression profile of valproate exposure. Also by comparing with TGF-β pathway mutants I also assessed the possible role played by that pathway on valproate induced lipid accumulation.

7.2 Results

The insulin independent component of expression profile associated with valproate exposure is tested by DAVID functional clustering to identify the functional terms associated with insulin independent component .

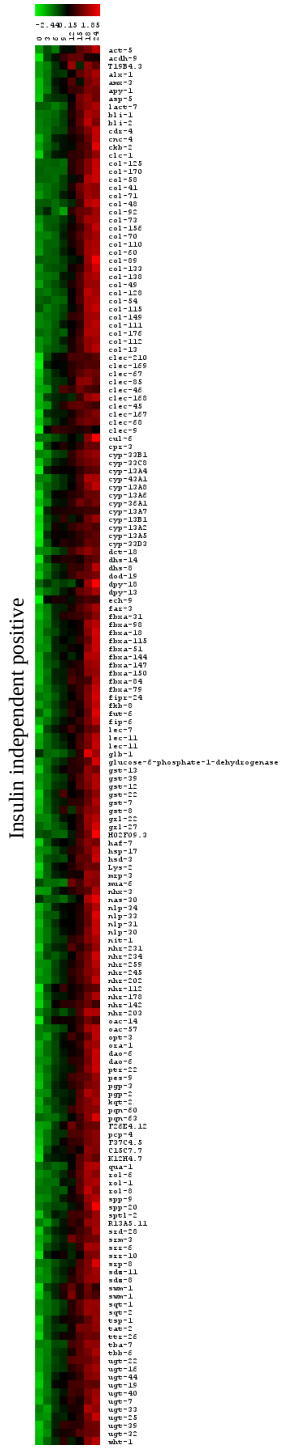

Cluster	Enrichment Score	Category	Term	Count	PValue	Benjamini
1		GOTERM_MF_FAT	GO:0042302~structural constituent of cuticle	32	1.74E-18	3.64E-16
2	8.197562	SP_PIR_KEYWORDS	collagen	22	1.24E-14	1.41E-12
3	5.291014	GOTERM_MF_FAT	GO:0030246~carbohydrate binding	21	1.09E-07	7.61E-06
4	4.710013	SMART	SM00587:CHK	8	4.28E-07	2.23E-05
5	4.377202	KEGG_PATHWAY	cel00903:Limonene and pinene degradation	8	8.52E-08	2.05E-06
		INTERPRO	IPR001128:Cytochrome P450	12	5.68E-06	2.07E-04
		GOTERM_MF_FAT	GO:0009055~electron carrier activity	18	6.99E-05	0.003662
		GOTERM_BP_FAT	GO:0055114~oxidation reduction	22	1.32E-04	0.010495
6	2.559407	GOTERM_MF_FAT	GO:0005529~sugar binding	11	5.97E-04	0.024751
		SMART	SM00034:CLECT	13	0.003338	0.056304
7	1.79217	INTERPRO	IPR012335:Thioredoxin fold	11	0.001753	0.046832

Figure 69 Expression profile positively correlated with valproate exposure which is independent of insulin is shown as a heat map. DAVID functional clustering is shown in the adjacent table. Numbers across top of heatmap indicates valproate concentration. The degree of expression indicated with a red to green scale where the higher expression is given by red.

Several collagen genes are identified under the functional terms ‘structural constituent of cuticle’ and ‘collagen’ (Figure 69). Lectins and UDP-glucuronosyl transferases are identified as ‘carbohydrate binding’. Several checkpoint kinases and cytochrome P450 are also identified as independent of insulin signalling. Acyl CoA dehydrogenase which catalyzes the first step in β-oxidation and cytochrome P450 are identified as electron carrier activity. Several glutathione transferases are identified under the functional term ‘thioredoxine fold’. These are all positively correlated with valproate exposure and is independent of insulin signalling.

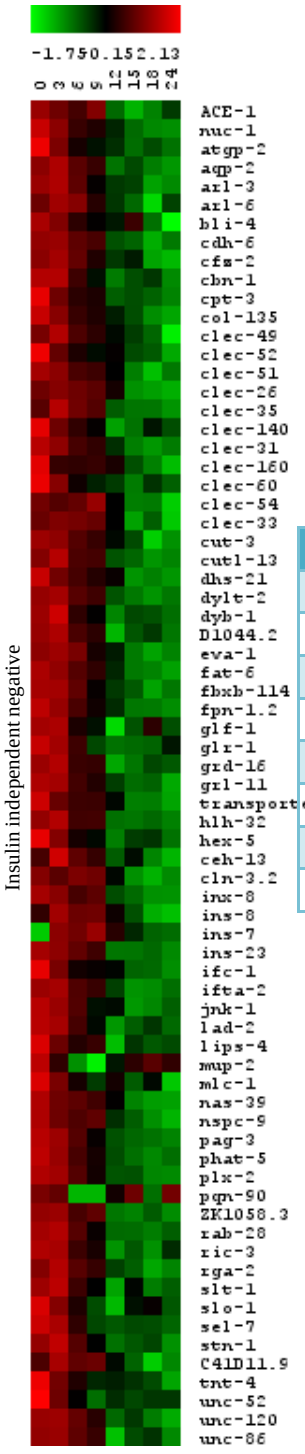

Cluster	Enrichment Score	Category	Term	Count	PValue	Benjamini
1	5.131848	INTERPRO	IPR016186:C-type lectin-like	15	3.23E-07	8.52E-05
2	2.788663	GOTERM_MF_FAT	GO:0005529~sugar binding	6	0.007677	0.423652
		GOTERM_MF_FAT	GO:0030246~carbohydrate binding	6	0.062878	0.787281
3	2.60259	INTERPRO	IPR011001:Saposin-like	4	6.75E-04	0.029262
4	2.556274	UP_SEQ_FEATURE	signal peptide	17	2.29E-05	0.003883
		GOTERM_CC_FAT	GO:0005576~extracellular region	8	0.066307	0.800569
5	2.546035	GOTERM_BP_FAT	GO:0055002~striated muscle cell development	5	2.90E-05	0.009299
6	2.321131	INTERPRO	IPR013032:EGF-like region, conserved site	11	5.47E-05	0.004807

Figure 70 Expression profile down-regulated on valproate exposure which is independent of insulin is shown as a heat map. DAVID functional clustering is shown in the adjacent table.Numbers across top of heatmap indicates valproate concentration. The degree of expression indicated with a red to green scale where the higher expression is given by red.

After assessing the functional terms associated with the insulin independent positively correlated expression profile with valproate, I then set to assess the functional terms associated with negatively correlated expression profile of insulin independent component of valproate exposure. Several lectins, eva-1 a gene whose function is required for axon migration, an acid sphingomyelinase which is required for the conversion of sphingomyelin to ceramide are identified under the functional terms 'C-type lectin like', 'sugar binding', 'carbohydrate binding', and saposine like (Figure 70, page 209). Several neuronal genes are identified under 'signal peptide' including acid sphingomyelinase, glutamate receptor, *unc-52*, and an abnormal acetylcholine esterase. These are identified as down-regulated expression profile on valproate exposure independent of insulin. Two insulin related genes *ins-7* and *ins-23* are also identified as signal peptide. *dyb-1* involved in cholinergic transmission and *slo-1*; a Ca^{2+} activated K^{+} channel and *unc-52* involved in myofilament assembly are identified under striated muscle cell development.

7.2.1 Ingenuity Pathway Analysis of expression profile of valproate exposure independent of insulin signalling

Out of the 1460 expression profiles of insulin independent component identified in comparison with the RNAi study (Murphy *et al.*, 2003), which is uploaded into Ingenuity Systems Pathway Analysis, only 202 could be mapped to Ingenuity database. To make predictions on the possible phenotypic changes associated with the insulin independent expression profile, I did a transcription factor analysis. Transcription factor

analysis helps to predict the upstream activation or inhibition of transcription factors by mapping uploaded genes to Ingenuity Knowledge Base and considering the changes in the expression pattern of the downstream target genes of a given transcription factor (Figure 71, page 212).

Ingenuity systems pathway analysis predicts lipid quantity to increase independent of insulin pathway due to an increase in metabolism, biosynthesis, transport and a decrease in efflux and hydrolysis of lipids (Figure 72, page 213). Table 38 (page 214) gives the details of the genes involved in fatty acid metabolism and the rationale for predicting it to increase.

Table 39 gives the details of the genes involved in increase of lipid quantity and rationale for predicting it to increase. Figure 73 to Figure 80 (page 215 to 218) shows the details of the types of lipids predicted to be increased, types of lipids predicted to have an increase in synthesis and mobilization resulting in an overall increase in lipid quantity. Phospholipids and cholesterol is expected to increase (Figure 73, page 215) with an increase of metabolism of membrane lipids and glycosphingolipids (Figure 74, page 215). *C.elegans* does not have a cholesterol synthesis pathway. Therefore, its increase should be via a decrease in efflux and/or decrease in hydrolysis. Glycolipid synthesis is expected to rise with a decrease in ceramide synthesis (Figure 75, page 216). Efflux of sterols and cholesterol is predicted to decrease (Figure 76, page 216) with an accumulation of sphingolipids (Figure 77, page 216). Sterol transport (Figure 78, page 217) and lipid hydrolysis (Figure 80, page 218) are expected to decrease with an increase in synthesis of glycosphingolipids (Figure 79, page 217).

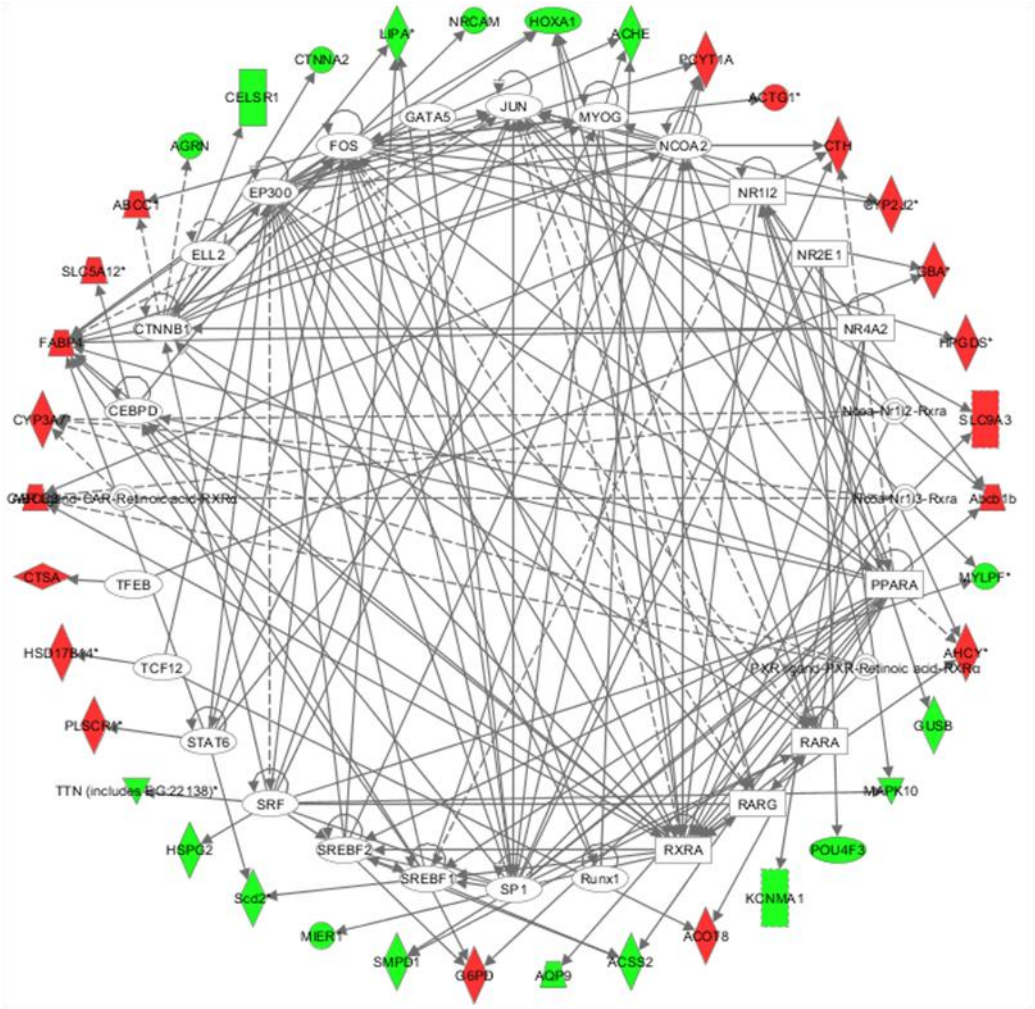

Figure 71 Transcription analysis of insulin independent expression profile by Ingenuity Pathway Analysis software. Transcription factors predicted to be involved are shown with their direct targets. Positively correlated genes with valproate are shown in red and genes negatively correlated with valproate are shown in green.Focus molecules corresponding to gene expression profiles negatively (green) and positively (red) correlated with valproate dose are shown with the focus molecules identified by the IPA which are connected to the network but not found in the data set (white).

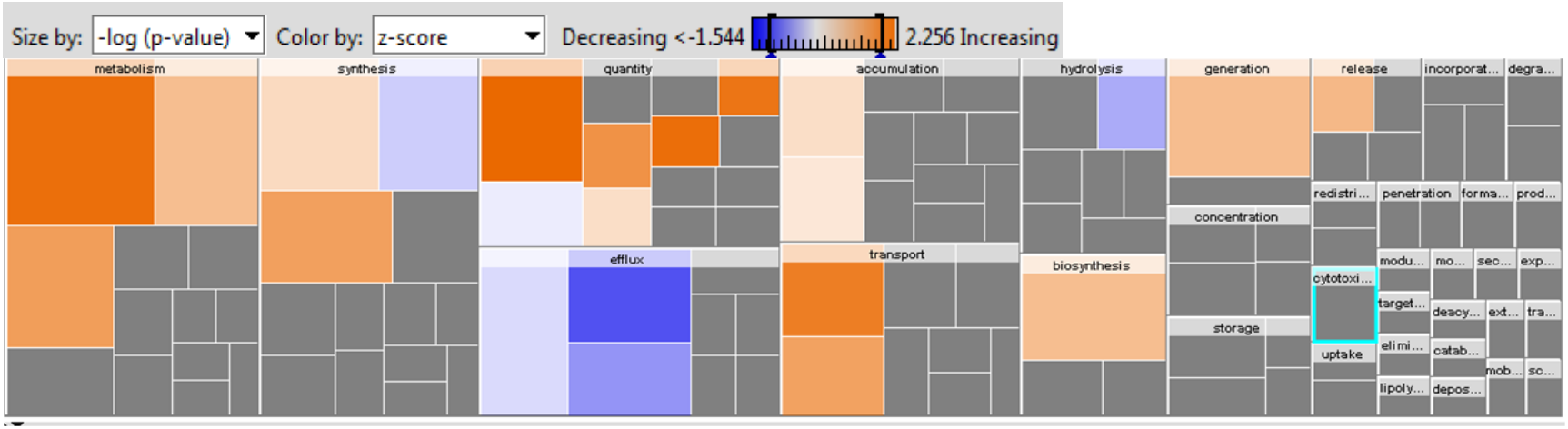

Figure 72 Ingenuity Pathway Analysis of insulin independent component of expression profiles associated with valproate exposure. In this figure, the expression profiles independent of insulin are predicted to increase lipid quantity via decreasing efflux and hydrolysis.

Table 38 Ingenuity systems pathway analysis prediction of insulin independent valproate exposure expression profile. This predicts valproate exposure to increase fatty acid metabolism independent of insulin signalling.

fatty acid metabolism predicted to be increased (z-score 2.095). Overlap p-value **3.52E-11**

10 of 23 genes have expression direction consistent with increased in fatty acid metabolism.

ADD TO MY PATHWAY | ADD TO MY LIST | CUSTOMIZE TABLE | Provide Feedback | More Info

ID	Genes in dataset	Prediction (based on expression direction)	Fold Change	Findings
A_12_P114586	GBA	Increased	↑2.000	Increases (2)
A_12_P109695	PCYT1A	Increased	↑2.000	Increases (2)
A_12_P113372	ABCC3	Increased	↑2.000	Increases (8)
A_12_P155500	FABP4	Increased	↑2.000	Increases (7)
A_12_P105447	PLA2G6	Increased	↑2.000	Increases (6)
A_12_P103569	HPGDS	Increased	↑2.000	Increases (8)
A_12_P114730	CLN3 (includes EG:1201)	Increased	↓-2.000	Decreases (1)
A_12_P112362	Abcb1b	Increased	↑2.000	Increases (4)
A_12_P157796	ABCC1	Increased	↑2.000	Increases (16)
A_12_P161317	CERS5	Increased	↑2.000	Increases (5)
A_12_P109152	SMPD1	Decreased	↓-2.000	Increases (15)
A_12_P102374	MAPK10	Decreased	↓-2.000	Increases (1)
A_12_P109680	ACOT4		↑2.000	Affects (8)
A_12_P104273	DEGS2		↑2.000	Affects (1)
A_12_P112374	AQP9		↓-2.000	Affects (1)
A_12_P111807	FAR2		↓-2.000	Affects (1)
A_12_P156881	PLSCR1		↑2.000	Affects (1)
A_12_P114885	LIPA		↓-2.000	Affects (1)
A_12_P119599	SPTLC2		↑2.000	Affects (2)
A_12_P166284	ACSS2		↓-2.000	Affects (1)
A_12_P151995	Scd2		↓-2.000	Affects (1)
A_12_P117324	ACOT8		↑2.000	Affects (1)
A_12_P118382	CYP2J2		↑2.000	Affects (1)

Table 39 Ingenuity systems pathway analysis prediction of insulin independent valproate exposure expression profile. This predicts valproate exposure to increase lipid quantity independent of insulin signalling.

quantity of lipid predicted to be increased (z-score 2.335). Overlap p-value **2.96E-05**

12 of 15 genes have expression direction consistent with increased in quantity of lipid.

ADD TO MY PATHWAY | ADD TO MY LIST | CUSTOMIZE TABLE | Provide Feedback

ID	Genes in dataset	Prediction (based on expression direction)	Fold Change	Findings
A_12_P114586	GBA	Increased	↑2.000	Increases (1)
A_12_P109695	PCYT1A	Increased	↑2.000	Increases (9)
A_12_P109152	SMPD1	Increased	↓-2.000	Decreases (12)
A_12_P120294	WWOX	Increased	↑2.000	Increases (1)
A_12_P139485	PDCD6IP	Increased	↑2.000	Increases (1)
A_12_P155500	FABP4	Increased	↑2.000	Increases (6)
A_12_P105447	PLA2G6	Increased	↑2.000	Increases (11)
A_12_P103569	HPGDS	Increased	↑2.000	Increases (2)
A_12_P119599	SPTLC2	Increased	↑2.000	Increases (3)
A_12_P114885	LIPA	Increased	↓-2.000	Decreases (1)
A_12_P112362	Abcb1b	Increased	↑2.000	Increases (1)
A_12_P112374	AQP9	Increased	↓-2.000	Decreases (1)
A_12_P100691	KCNMA1	Decreased	↓-2.000	Increases (1)
A_12_P151995	Scd2	Decreased	↓-2.000	Increases (3)
A_12_P158720	CYP3A7		↑2.000	Affects (1)

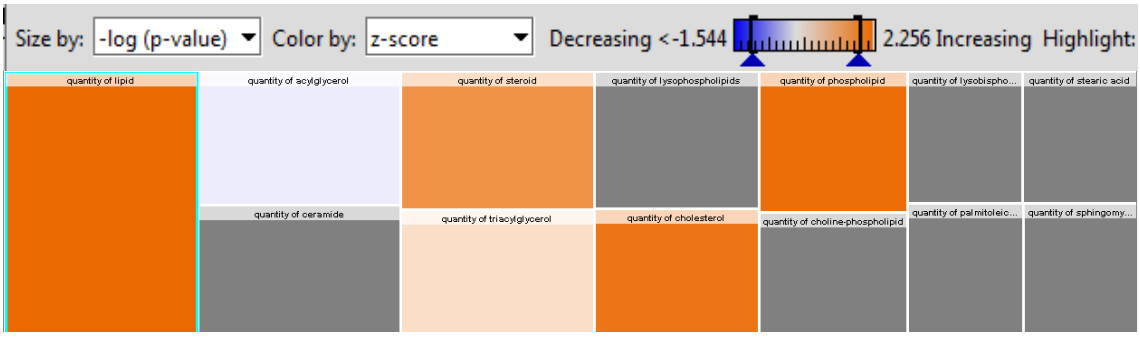

Figure 73 Ingenuity systems pathway analysis prediction of insulin independent valproate exposure expression profile. This predicts valproate exposure to increase lipid quantity independent of insulin signalling by increasing mainly phospholipids and cholesterol levels.

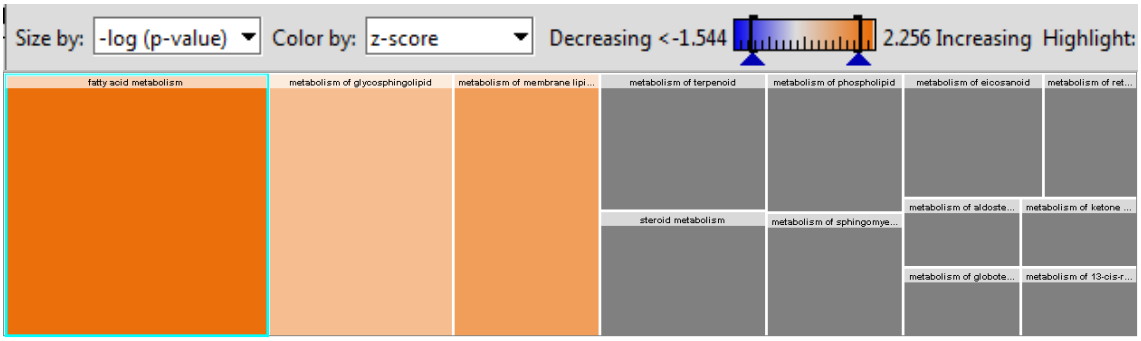

Figure 74 Ingenuity systems pathway analysis prediction of insulin independent valproate exposure expression profile. This predicts valproate exposure to increase lipid quantity independent of insulin signalling by increasing metabolism of membrane lipids and glycosphingolipids.

Figure 75 Ingenuity systems pathway analysis prediction of insulin independent valproate exposure expression profile. This predicts valproate exposure to increase lipid quantity independent of insulin signalling by increasing synthesis of lipids and glycolipids. Synthesis of ceramide is predicted to decrease.

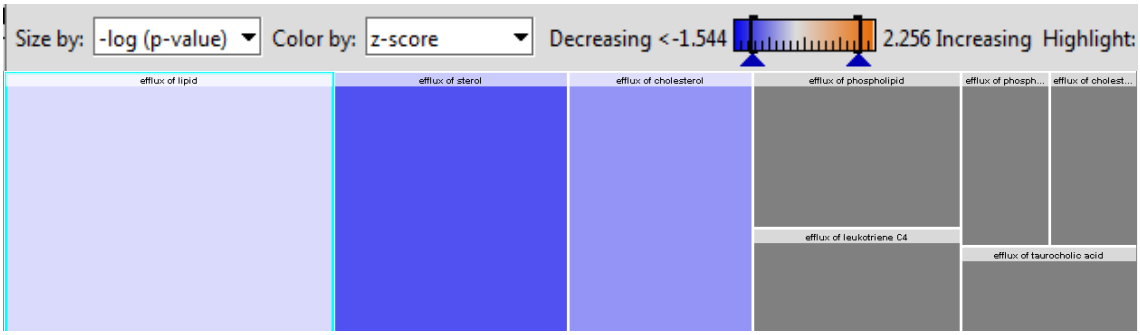

Figure 76 Ingenuity systems pathway analysis prediction of insulin independent valproate exposure expression profile. This predicts valproate exposure to increase lipid quantity independent of insulin signalling by decreasing efflux of cholesterol and sterols.

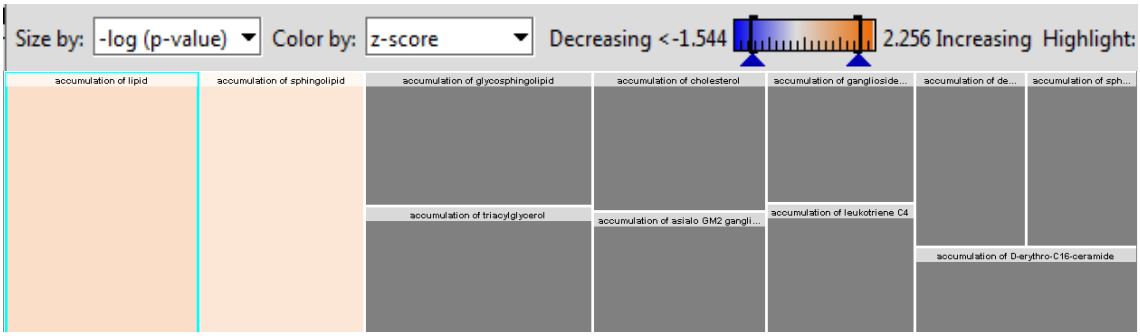

Figure 77 Ingenuity systems pathway analysis prediction of insulin independent valproate exposure expression profile. This predicts valproate exposure to increase lipid quantity independent of insulin signalling by increasing accumulation of sphingolipids.

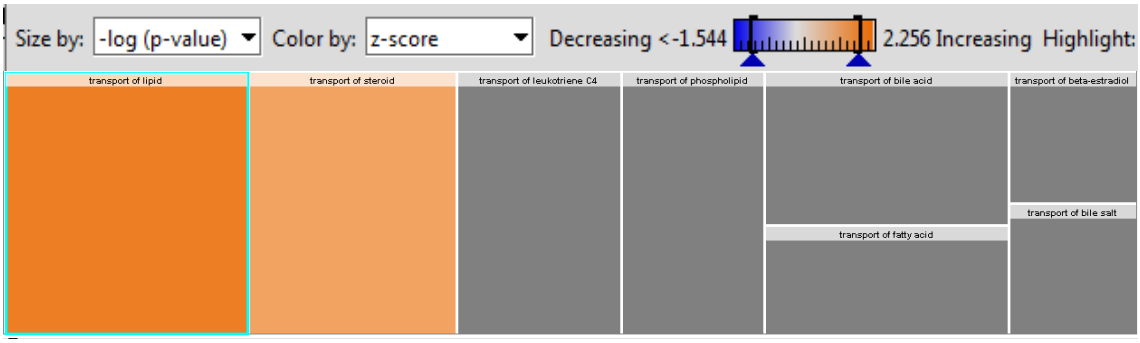

Figure 78 Ingenuity systems pathway analysis prediction of insulin independent valproate exposure expression profile. This predicts valproate exposure to increase lipid quantity independent of insulin signalling by increasing transport of steroids.

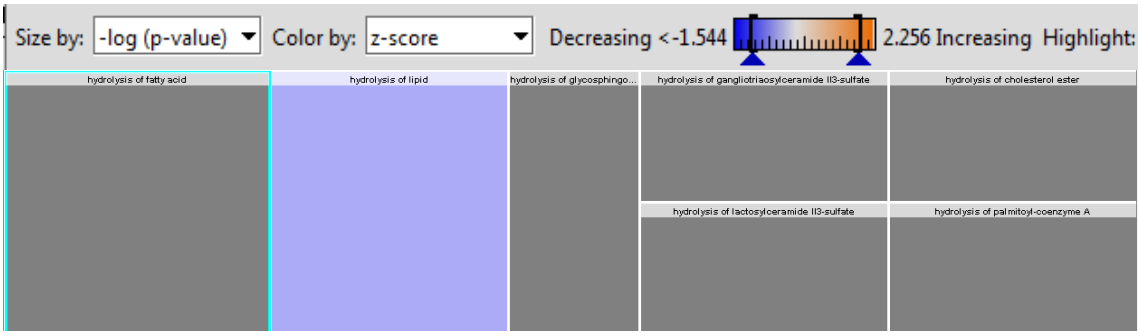

Figure 79 Ingenuity systems pathway analysis prediction of insulin independent valproate exposure expression profile. This predicts valproate exposure to increase lipid quantity independent of insulin signalling by decreasing lipid hydrolysis.

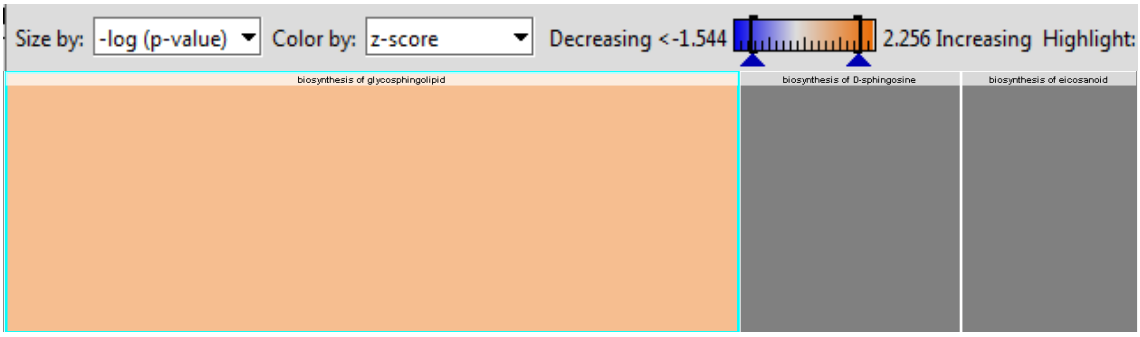

Figure 80 Ingenuity systems pathway analysis prediction of insulin independent valproate exposure expression profile. This predicts valproate exposure to increase lipid quantity independent of insulin signalling by increasing synthesis of glycosphingolipids.

Main limitation of this study is the use of mutants from an RNAi study which may not as good as a null mutant. Network analysis by Ingenuity systems pathway revealed an indirect link to insulin signalling in this insulin independent expression profile of valproate exposure (Figure 81). The second most significant network shows cellular phosphorylation to be a key feature of valproate exposure (Figure 82).

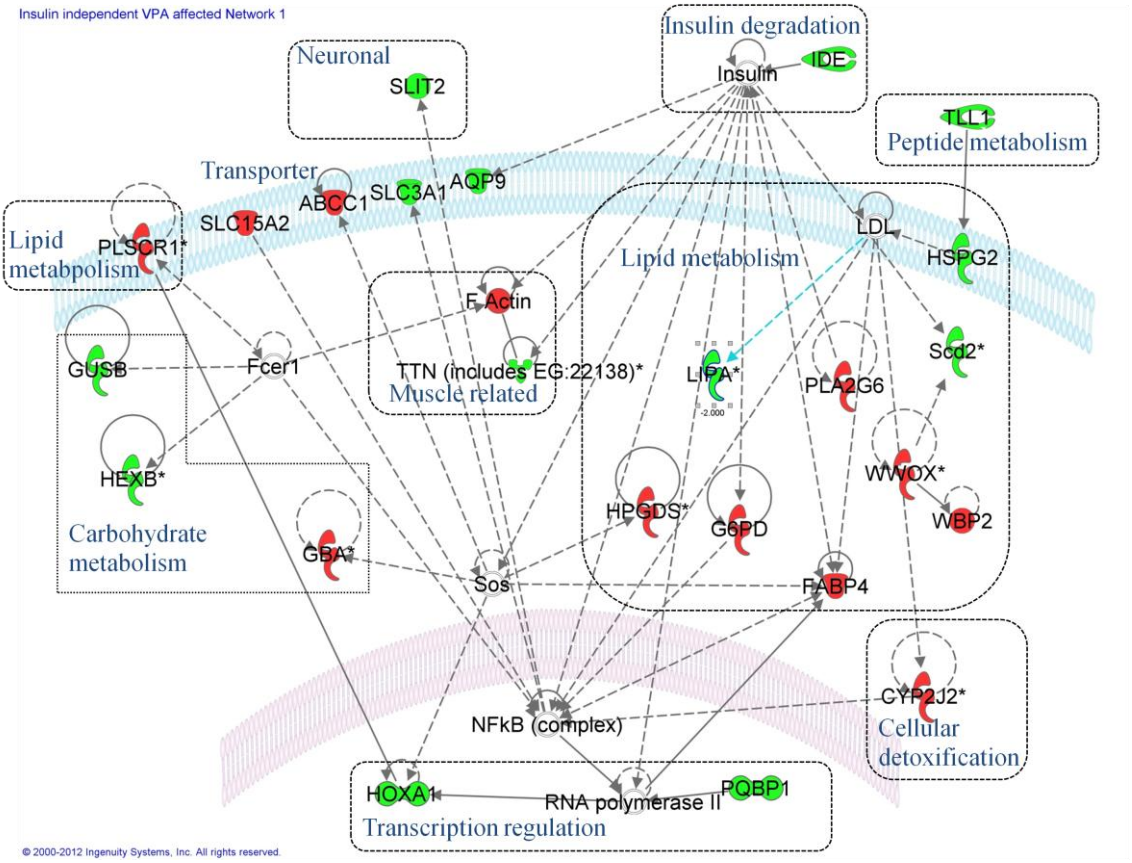

Figure 81 Ingenuity systems pathway analysis of insulin independent valproate affected gene expression profile. This most significant network derived shows an indirect insulin signalling.Focus molecules corresponding to gene expression profiles negatively (green) and positively (red) correlated with valproate dose are shown with the focus molecules identified by the IPA which are connected to the network but not found in the data set (white).

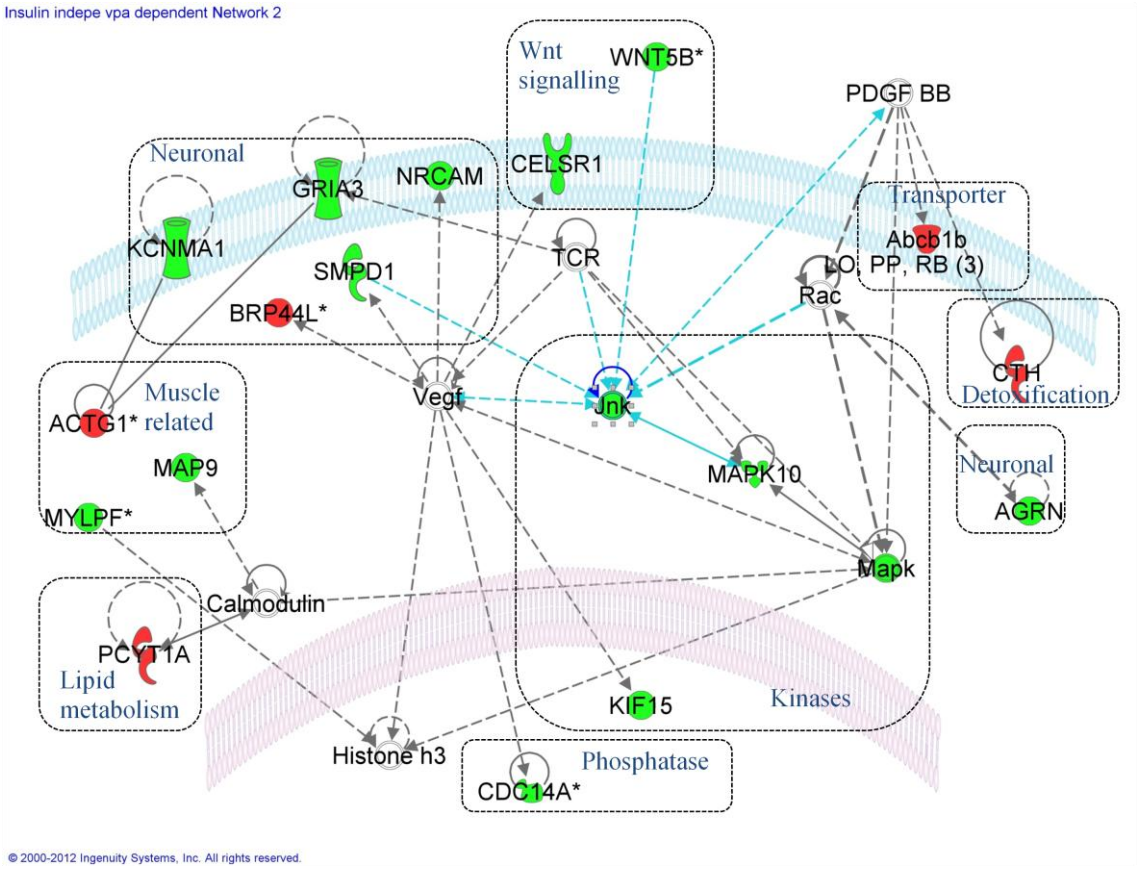

Figure 82 Ingenuity systems pathway analysis of insulin independent expression profile of valproate exposure. This shows cellular phophorylation to be a key feature of valproate exposure. Focus molecules corresponding to gene expression profiles negatively (green) and positively (red) correlated with valproate dose are shown with the focus molecules identified by the IPA which are connected to the network but not found in the data set (white).

7.2.2 Valproate induced lipid accumulation could be partially due to TGFβ Sma/Mab pathway

TGFβ dependent expression profile of valproate exposure was identified by comparing the expression profile of valproate exposure with a microarray dataset of a dbl-1 over-expressing strain (BW1940) and a null mutant of *sma-6 (sma-6(wk7))* from GEO database (accession number GSE15527). SMA-6 and DBL-1 are the type I receptor and the ligand of the Sma/Mab TGFβ related pathway (Figure 83, page 222). This comparison identified 43 genes that positively correlated with valproate and 10 negatively correlated with valproate expression profiles to be dependent on Sma/Mab TGFβ related pathway (Figure 84, page 222). The expression profile positively correlated with valproate identified several genes regulated by *daf-16*, lectins, lysozyme (Table 40, page 223). It also contained O-acyltransferase, which is involved in glycerophospholipid synthesis. Expression profile negatively correlated with valproate was not involved in lipid biosynthesis (Table 41, page 224).

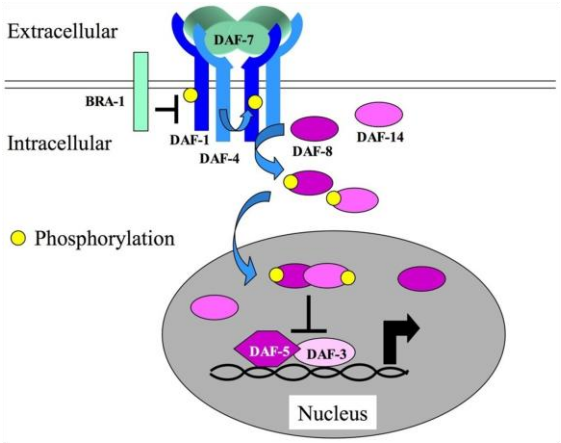

The Dauer TGF-β-related pathway . DAF-7 promotes continuous, nonDauer development. The DAF-7 signal is transduced by DAF-1 type I receptor, DAF-4 type II receptor, and DAF-8 and DAF-14 Smads. These components, when activated, inhibit the functions of DAF-3 Smad and DAF-5 Sno/Ski, which promote Dauer development. BRA-1 is a negative regulator of DAF-1.

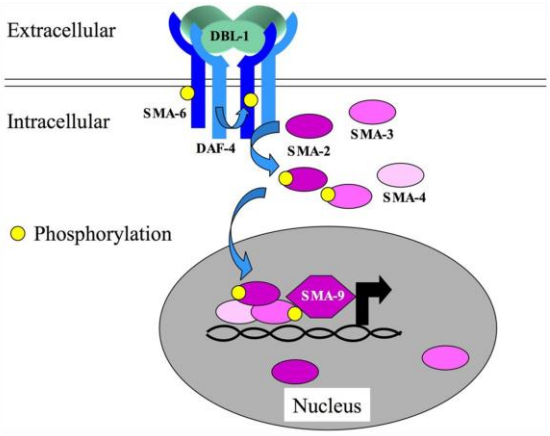

**The Sma/Mab TGFβ-related pathway . ** DBL-1 regulates body size and male tail morphogenesis. The DBL-1 signal is transduced by SMA-6 type I receptor, DAF-4 type II receptor, SMA-2, SMA-3, and SMA-4 Smads, and SMA-9 Schnurri.

Figure 83 TGFβ dauer and Sma/Mab pathways

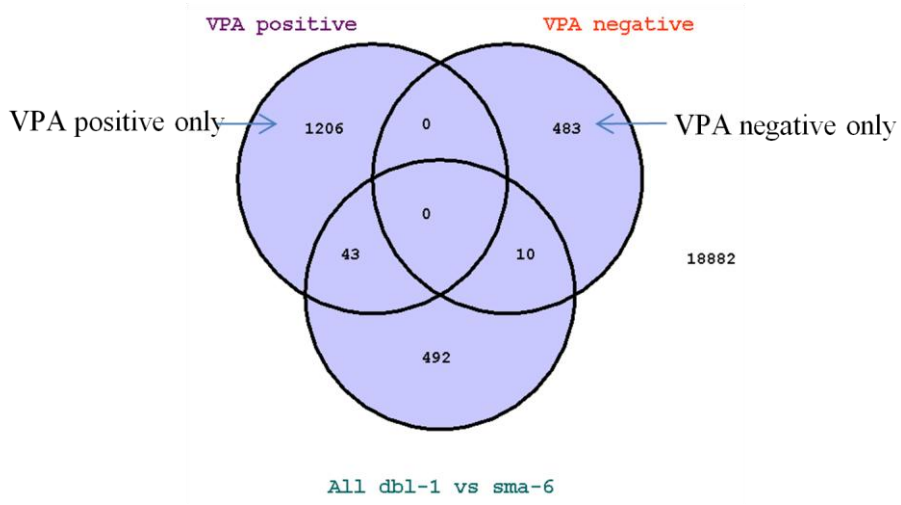

Figure 84 Comparison of the expression profile of valproate exposure with the expression profile dependent on Sma/Mab TGFβ related pathway

Table 40Known up regulated expression profile of valproate exposure that is dependent on Sma/Mab TGFβ related pathway

Agilent ID	Gene	Gene Name
A_12_P117774	col-90	COLlagen
A_12_P120298	clec-67	C-type LECtin
A_12_P115146	F56A4.2	C-type LECtin
A_12_P115146	clec-209	C-type LECtin
A_12_P119327	dod-17	Downstream Of DAF-16 (regulated by DAF-16)
A_12_P118504	dod-24	Downstream Of DAF-16 (regulated by DAF-16)
A_12_P110068	Lys-2	LYSozyme
A_12_P117943	oac-58	O-ACyltransferase homolog
A_12_P103686	pes-9	Patterned Expression Site
A_12_P108210	F26E4.12	Probable glutathione peroxidase F26E4.12
A_12_P102462	C15C7.7	Putative GDP-fucose protein O-fucosyltransferase 1
A_12_P114080	spp-21	SaPosin-like Protein family
A_12_P107929	ZK1320.3	Uncharacterized protein ZK1320.3

Table 41 Known negatively correlated expression profile of valproate exposure that is dependent on Sma/Mab TGFβ related pathway

Agilent ID	Gene	Gene Name
A_12_P110147	bli-4	BLIstered cuticle
A_12_P115388	clec-26	C-type LECtin
A_12_P109821	phat-5	PHAryngeal gland Toxin-related

7.3 Discussion

Comparison of insulin pathway mutants with wild type *C.elegans* treated with valproate reveals that major component of the gene changes associated with valproate exposure are independent of insulin. Ingenuity System pathway analysis predicts valproate induced lipid accumulation to be partly due to this insulin independent component. This increase of lipid level is expected to be due to an increase in metabolism, biosynthesis, transport and a decrease in efflux and hydrolysis of lipids. Specifically, phospholipids and cholesterol is expected to increase with an increase of metabolism of membrane lipids and glycosphingolipids. Supporting this finding, supplementation with radioactively labaled phosphorus of valproate treated Saccharomyces cereviseae show modifications in phospholipid synthesis (Ju and Greenberg, 2003). Rats treated with valproate show abnormalities in muscle mitochondrial cistae and microvesicular lipid deposition in muscle(Melegh and Trombitás, 1997). This also suggest an abnormality in lipid mobilization caused by valproate and an effect of valproate on membranes. *C.elegans* does not have a cholesterol synthesis pathway. Therefore its increase should

be via a decrease in efflux and/or decrease in hydrolysis. In contrast to this observation, valproate has not affected total cholesterol levels in human(Franzoni et al., 1992). Glycolipid synthesis is expected to rise with a decrease in ceramide synthesis. Efflux of sterols and cholesterol is predicted to decrease with an accumulation of sphingolipids. Sterol transport and lipid hydrolysis are expected to decrease with an increase in synthesis of glycosphingolipids (Figure 85).

Figure 85 Functions associated with lipid metabolism, which are independent of insulin signalling pathway.

TGF-β pathway could be linked to glycerophospholipid synthesis on valproate exposure causing an increase of lipid accumulation.

In addition to be involved in valproate induced lipid accumulation, theSma/Mab pathway could have a neuronal phenotype, which is shown by the paralysis of *sma-6* mutants on exposure to valproate. But *daf-4* type II receptor of both dauer and Sma/Mab pathway was not paralysed on exposure to valproate. But *daf-1*mutants get paralysed on exposure to valproate. Therefore this could be a phenotype of TGF-β type I receptors rather than a function of either pathway. In the next chapter I assess this novel neuronal phenotype to generate a hypothesis to explain this novel paralysis phenotype.

8.0 SMA-6 -INTERGRATES CENTRAL METABOLISM AND NEURONAL SIGNALLING

8.1 Summary

Valproate is a drug known to inhibit GABA inhibitory neurotransmission. It is currently the most widely used antiepileptic drug (Duncan et al., 2006). It is also used to treat bipolar disorder and schizophrenia. Recently its therapeutic effects have been extended to other illnesses such as cancer, migraine, Alzheimers disease and HIV. With the exception of cancer and HIV, valproate is used in the treatment of diseases caused by a dysfunction in the nervous system (Lloyd, 2013). The therapeutic effects of valproate are thought to be a result of the reduction in excitatory neurotransmission, modification of monoamines (Morland et al., 2012) or inhibition of sodium and potassium conductance (VanDongen et al., 1986). Its histone deacetylase inhibitory activity and interference with respiratory chain and acceleration of oxidative damage has been implicated in teratogenicity (Lloyd, 2013) including malformation of the nervous system.

There is no record of paralysis caused by valproate in *C.elegans*. In this chapter I report for the first time a paralysis caused by valproate on *C.elegans* TGF-β Sma/Mad pathway type I receptor mutant, *sma-6*. The TGF-β pathway is involved in lipid metabolism. After performing several paralysis assays I have developed a model to explain this neuronal phenotype of SMA-6 on valproate exposure where SMA-6 has a regulatory role on neurotransmission. This shows integration between metabolism and neuronal signalling via SMA-6.

8.2 Results

8.2.1 *sma-6* mutants get paralysed by sodium valproate

When we tested the TGF-β pathway mutants on valproate induced lipid accumulation, we saw that the TGF-β Sma/mad pathway type I receptor mutant, *sma-6*, gets paralysed by sodium valproate in a dose dependent manner (Figure 86). Similar to *sma-6*, *unc-25* the GABA mutant and *unc-38* the acetylcholine receptor mutant also gets paralysed by sodium valproate in a dose dependent manner (Figure 87 and Figure 88). Because this indicates a novel neuronal function for *sma-6*, we performed several paralysis assays to confirm this finding.

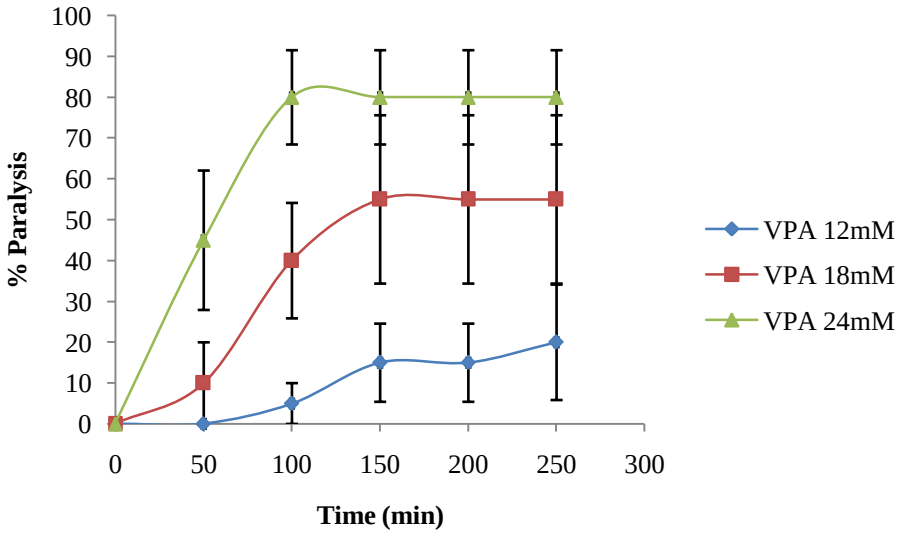

Figure 86 Paralysis of *sma-6* mutant *C.elegans* by sodium valproate. *sma-6* mutant get paralysed on exposure to valproate in a dose dependent manner.Error bars = ± SEM of four independent trials. n=30

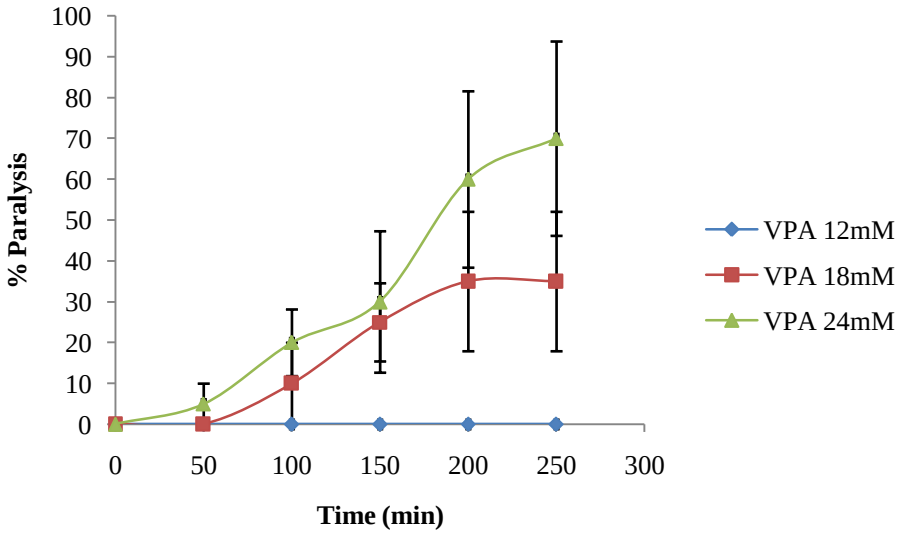

Figure 87 Paralysis of *unc-38* mutant *C.elegans* by sodium valproate. The acetylcholine receptor mutant unc-38 gets paralysed on exposure to valproate in a dose dependent manner.Error bars = ± SEM of four independent trials. n=30

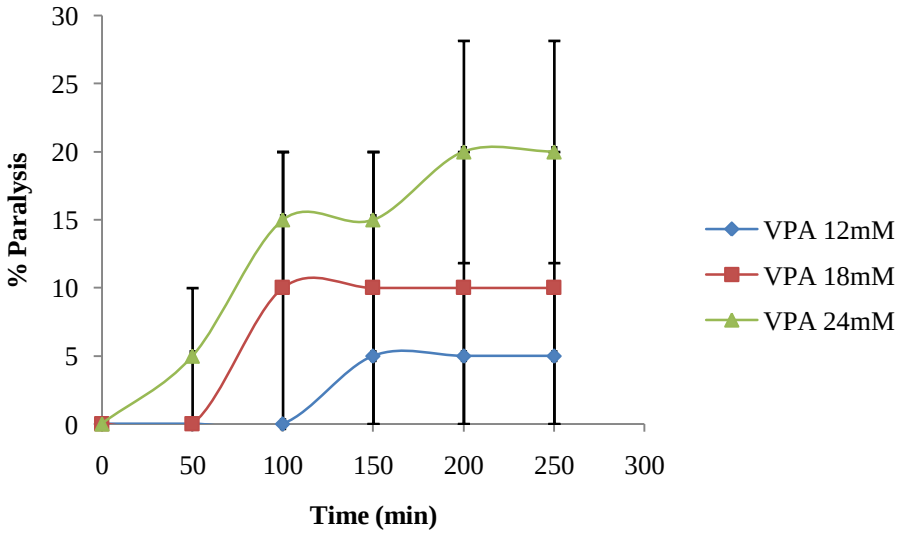

Figure 88Paralysis of *unc-25* mutant *C.elegans* by sodium valproate. The GABA mutant unc-25 gets paralysed on exposure to valproate in a dose dependent manner.Error bars = ± SEM of four independent trials. n=30

8.2.2 *sma-6* has a neuronal phenotype

To test whether *sma-6* has a neuronal phenotype, we tested the sensitivity of *a sma-6* mutantto the acetylcholine esterase inhibitor, Aldicarb, and the acetylcholine receptor agonist, levamisole. The*sma-6*mutantwas hypersensitive to both drugs (Figure 89 and Figure 90). Having shown that mutation of*sma-6*can affect neuronal processes, we compared this hypersensitivity with mutants of both excitatory and inhibitory neurotransmission. Specifically, we compared *sma-6* with the acetylcholine receptor mutant, *unc-38* and the GABA defective mutant, *unc-25*. Our data show that *sma-6* resembles *unc-25* more than *unc-38*. As expected *unc-38*, being a acetylcholine receptor mutant, is resistant to both drugs. Like *sma-6*, *unc-25* is also hypersensitive to both drugs.

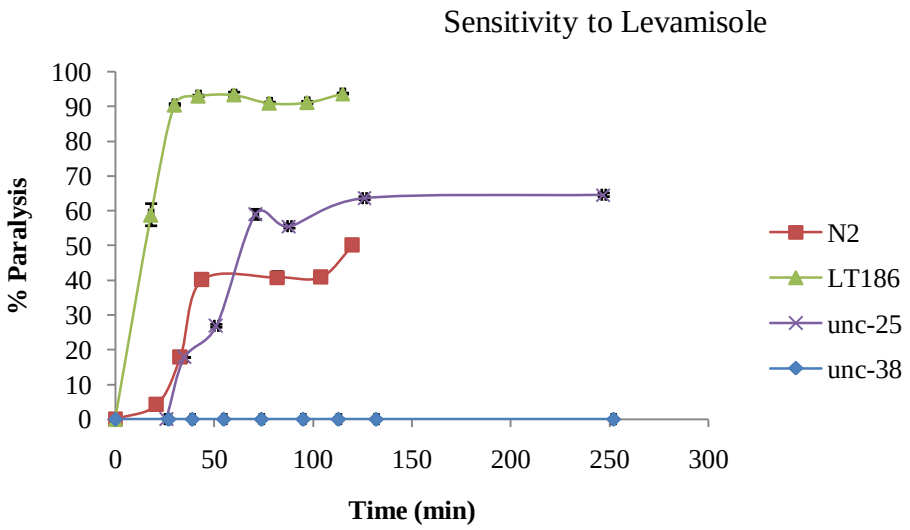

Figure 89Sensitivity to the acetylcholine receptor agonist, Levamisole. Wild type (N2) and *sma-6, unc-25, unc-38* mutant *C.elegans*were treated with 100µM Levamisole.TGF-β Sma/Mad pathway mutant, *sma-6,* and

GABA mutant *unc-25* show hypersensitive to Levamisole. The acetylcholine receptor mutant, *unc-38* is resistant to Levamisole. Error bars = ± SEM of three independent trials. n=30

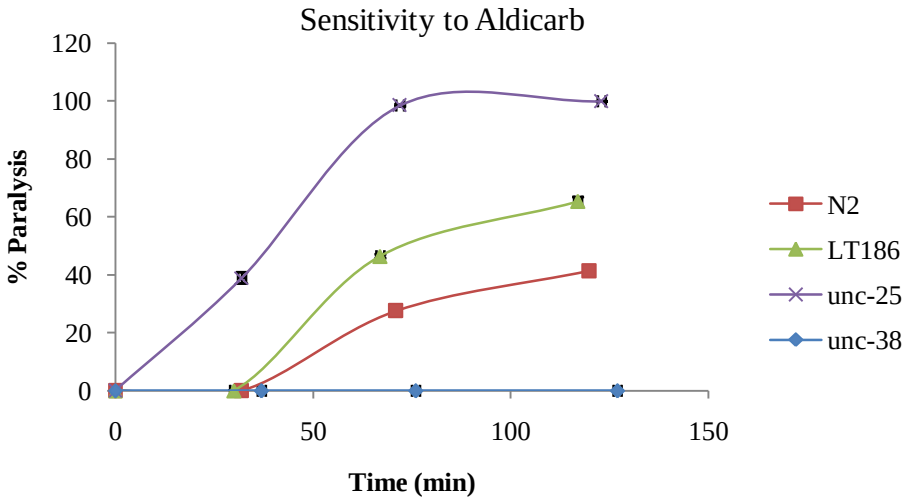

Figure 90Sensitivity to the acetylcholine esterase inhibitor, Aldicarb. Figure shows the paralysis of wild type (N2) and the GABA mutant *unc-25*, the acetylcholine receptor mutant*unc-38* and TGF- β Sma/Mad pathway mutant *sma-6*on 1mM Aldicarb. Both *sma-6* and *unc-25* show hypersensitivity to Aldicarb but *unc-38* is resistant to Aldicarb. Error bars = ± SEM of three independent trials. n=30

8.2.3 *sma-6* affects somatic nerve function and is post synaptic

In *C.elegans*, the pharynx is anearly autonomous organ with its own neuronal system, muscles, and epithelium (Altun and Hall, 2011). After showing that valproate does cause paralysis on *sma-6* mutant, we wanted to see whether this involves somatic or pharyngeal nervous system. To assess this,*sma-6* mutant worms were exposed to valproate and observed under the microscope. Significantly paralysed worms retain pharyngeal pumping. The posterior region of worms showed early paralysis is which then spread to anterior regions. Therefore, the somatic nervous system and/or obliquely

striated body wall muscles may be involved in paralysis of *sma-6* treated with valproate. Therefore*sma-6* should be residing on the somatic nervous system or associated muscles to bring these neuronal effects. SMA-6 is expressed in dorsal and ventral hypodermis, pharyngeal muscle and the intestine (Altun and Hall, 2011). This shows that SMA-6 could be acting post synaptically. The hypersensitivity shown by *sma-6* mutants for the acetylcholine receptor agonist, levamisole, compared to the wild type further supports the idea that *sma-6* could be post synaptic.

8.2.4 Valproate cause hyperparalysis on *sma-6* before causing death

After showing that *sma-6* has a neuronal phenotype, we wanted to clarify whether valproate cause paralysis of *sma-6* mutants or whether it cause death without paralysis. Valproate treated *sma-6* mutants died, which is confirmed by tissue degradation seen after 24hrs on staining for lipids (data not shown). But*sma-6* showed shortening of body length by ~50% on exposure to valproate (data not shown), which is a phenotype observed on hyperparalysis.

8.2.5 Neuronal phenotype observed in *sma-6* is a character of TGF-β type I receptors but not a feature of the TGF-β whole pathway or insulin signalling pathway

After showing that valproate does cause paralysis of *sma-6* mutants, I then tested whether this could be an attribute of the TGF-β pathway or associated insulin signalling pathway. To assess this, I tested the effect of valproate on TGF-β pathway mutants and insulin signalling pathway mutants. Specifically, I tested the effect of valproate

exposure on *daf-1*, the common type II receptor in TGF-β dauer and Sma/mad pathways. It did not show any paralysis (data not shown). After showing that this neuronal phenotype is not a feature of the TGF-β pathway, I then tested the effect of valproate on the *daf-1*, the type I receptor in TGF-β dauer pathway. Like*sma-6*, the TGF-β Sma/mad pathway type I receptor, daf-1 also showed paralysis (data not shown) indicating that this neuronal phenotype is a feature of type I receptors on TGF-β pathways. To identify whether this also involves insulin signalling pathway, I tested the effect of valproate exposure on insulin receptor mutant, *daf-2*. *daf-2* did not show any paralysis on exposure to valproate (data not shown).

8.2.6 Paralysis observed on *sma-6* treated with valproate is via either cholinergic neurotransmission or GABAergic neurotransmission but not via other mechanism

After confirming the hyperparalysis of *sma-6*mutant on valproate exposure, I then wanted to see whether this could be via different mechanisms other than a reduction in GABA inhibitory neurotransmission and activation of acetylcholine mediated excitatory neurotransmission. This was assessed by treating the GABA mutant, *unc-25* with a saturating concentration of Aldicarb. This is done to bring the strongest possible paralysis that can be achieved by inhibiting GABA neurotransmission and activating the acetylcholine mediated excitatory neurotransmission simultaneously. Valproate could not increase paralysis of *sma-6*treated with Aldicarb more than what is achieved in this *unc-25* mutant. This shows that *sma-6* could not increase the paralysis caused by the dual action of acetylcholine build-up and inhibition of GABAergic neurotransmission

confirming that *sma-6* acts through one or both of these mechanisms but not some other mechanism(Figure 91).

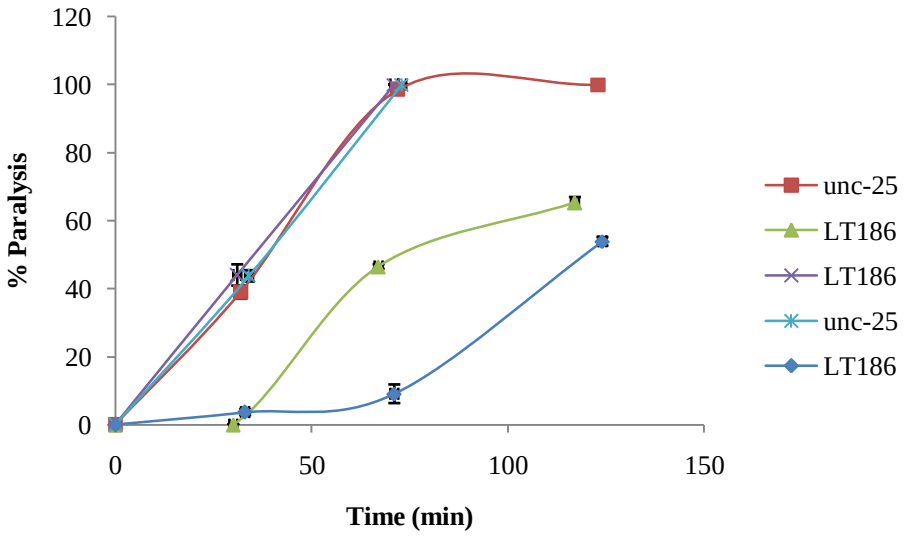

Figure 91The maximum paralysis obtained by simultaneous activation of excitatory cholinergic neurotransmission and inactivation of inhibitory GABAergic neurotransmission is similar to the paralysis obtained on activation of cholinergic neurotransmission in *sma-6* treated with 15mM Sodium Valproate (VPA). GABA mutant *unc-25* or TGF-β Sma/Mad pathway type I receptor mutant *sma-6* were treated with the 1mM acetylcholine esterase inhibitor Aldicarb or 15mM Sodium Valproate or both. Error bars = ± SEM of three independent trials. n=30

8.2.7 *sma-6* mutant has inhibitory neurotransmission intact

After showing that valproate cause paralysis of *sma-6* either via inhibition of GABAergic neurotransmission or by increasing cholinergic neurotransmission, we then tested whether inhibitory neurotransmission is intact in *sma-6*. To test this I looked at the paralysis caused by Aldicarb on *sma-6* and compared that with the paralysis caused by Aldicarb on the GABA mutant, *unc-25* (Figure 91). In both cases, the saturating

concentration of Aldicarb would bring the maximum effect of excitatory neurotransmission but the paralysis of *sma-6* on Aldicarb was not as intense as the *unc-25* on Aldicarb supporting the hypothesis that inhibitory neurotransmission is intact in *sma-6*. Also*sma-6* shows hypersensitivity to levamisole than *unc-25* and *unc-25* shows hypersensitivity to Aldicarb than *sma-6*(Figure 92) further supporting the idea that *sma-6* may be acting via different mechanisms compared to *unc-25*.

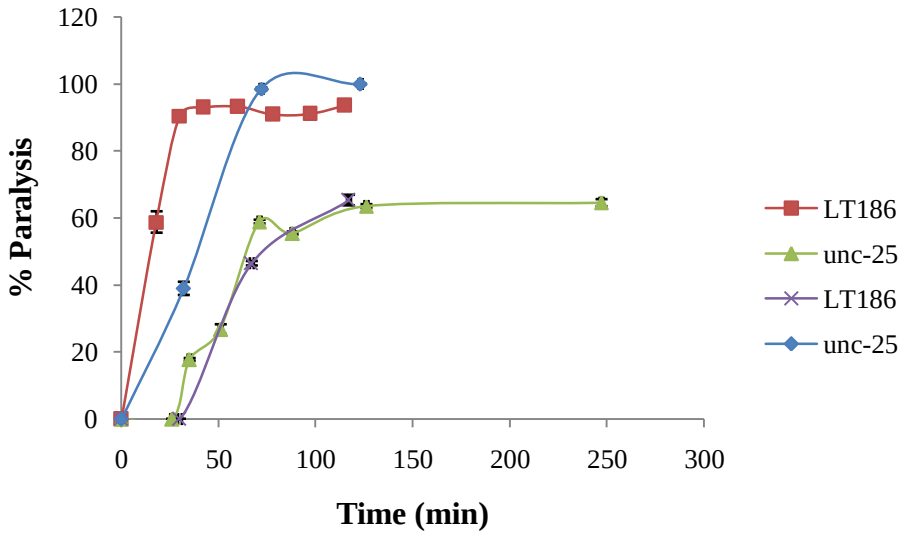

Figure 92*sma-6* with 1mM Aldicarb show similar paralysis with *unc-25* on levamisole. TGF-β Sma/Mad type I receptor mutant *sma-6* shows highest paralysis on Levamisole when the GABA mutant *unc-25* shows highest paralysis on Aldicarb. *sma-6* on Aldicarb and *unc-25* on Levamisole show similar paralysis. Error bars = ± SEM of three independent trials. n=30

8.2.8 Evidence from microarray data that valproate affects both cholinergic and GABAergic neurotransmission

After looking at the phenotypes and finding that valproate could be paralysing *sma-6* mutants by either increasing cholinergic neurotransmission or by decreasing GABAergic neurotransmission, I then looked at the expression profile of valproate exposure to see whether that would also support the same hypothesis. The expression profile positively correlated with valproate show that it would cause quick termination of action potentials but the negatively correlated expression profile shows that cholinergic neurotransmission is increased on exposure to valproate and GABAergic neurotransmission is diminished.

8.2.9 Expression signature positively correlated tovalproate exposure on neuronal function

There were several genes positively correlated with valproate, which are involved in neuronal function that shows it would cause a quick termination of action potential (Figure 93). These include *eat-2* which codes for a ligand gated ion channel subunit closely related to nicotinic acetylcholine receptor that works post synaptically on pharyngeal muscle and regulates the rate of pharyngeal pumping. The Na^+ Ca^{2+} exchangers positively correlated with valproate help to restore Ca^{2+} concentrations after an action potential. *kqt-2* and *twk-1* codes for K^+ channels which help to restore resting membrane potential after an action potential. *snf-8, snf-7, snf-10, snf-5* and *snf-4*code for members of sodium: neurotransmitter symporter family, which reuptake released neurotransmitters from the synaptic cleft. Up-regulation of these genes would result in the quick termination of action potentials. *snb-5* and *snb-2* codes for synaptobrevin

which is part of the SNARE complex that facilitates binding of vesicles to presynaptic membrane on exocytosis in neurotransmission.

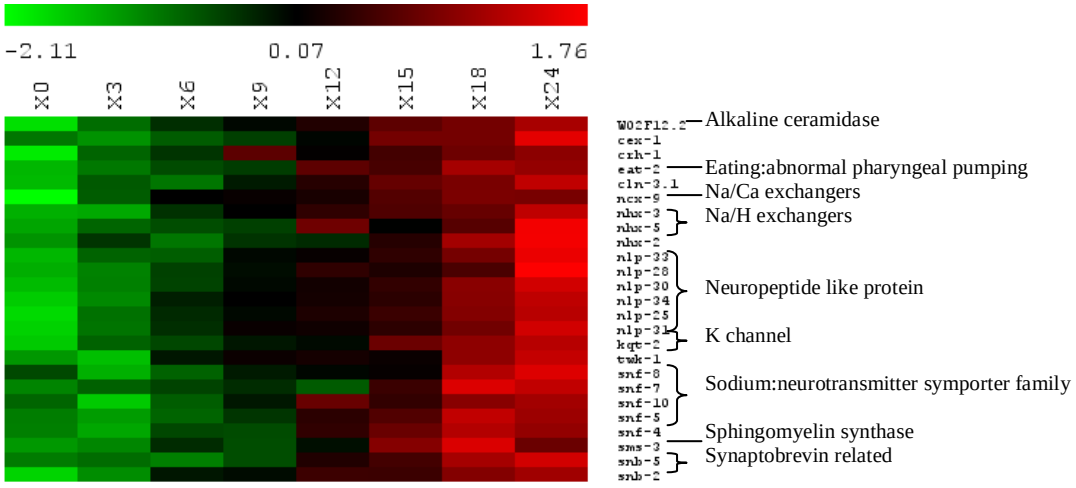

Figure 93Expression profile Positively correlated with valproate on neuronal function. Numbers across top of heatmap indicates valproate concentration. The degree of expression indicated with a red to green scale where the higher expression is given by red.

8.2.10 Expression signature negatively correlated to valproate on neuronal function

Several genes involved in neuronal function are down-regulated on exposure to valproate which shows an increase of cholinergic neurotransmission and decrease in GABAergic neurotransmission (Figure 94, page 238). *lev-8* and acr-17 encode nAChR subunits. The protein coded by *lev-8* is required for egg laying and muscle contraction. Expression of this protein is strongest in the anterior, consistent with increased levamisole resistance of head and anterior muscles of *lev-8* mutants. *ric-3* is required for the maturation and function of four nicotinic acetylcholine receptor types. *ace-3* and *ace*-1 encodes two of the four *C.elegans'* acetylcholine esterases. This indicates that

exposure to valproate would decrease nicotinic acetylcholine receptors but increase acetylcholine level in the synaptic cleft.

dgk-4 encodes a diacylglycerol kinase which converts DAG to phosphatidic acid. DAG binds to C1 domain of *unc-13* which primes vesicle binding to presynaptic membrane by forming SNARE complex. Down regulation of *dgk-4* would result in an enhanced synaptic transmission. *unc-10* encodes a protein which is probably involved in the priming of presynaptic vesicles.

unc-30 encodes a transcription factor which controls terminal differentiation of all 19 type D-GABA-ergic motor neurones by directly regulating the expression of *unc-25* which codes for GAD which synthesises GABA and *unc-47* , which codes for VGAT, the protein which loads GABA into synaptic vesicles. Therefore valproate is expected to decrease GABA inhibitory neurotransmission.

8.2.11 Expression profiling suggests a decrease in dopaminergic and serotonergic neurotransmission on exposure to valproate

After showing that valproate affects cholinergic neurotransmission and GABAergic neurotransmission, I then assessed its effects on other neurotransmitters. I found both serotonergic neurotransmission and dopaminergic neurotransmission to be decreased as a result of valproate exposure.

ast-1 encodes a transcription factor which is required for maintenance of dopamine neuronal fate. It positively regulates the expression of several dopamine neuron specific genes such as *dat-1* and *cat-2* which encodes dopamine transporter and tyrosine

hydroxylase respectively. This shows that exposure to valproate may decrease dopamine neurotransmission.

unc-86 encodes a transcription factor that is required for fate determination and differentiation in diverse neuronal lineages and is also required for the expression of *tph-1* and *cat-1* in seretonergic neurones. TPH-1 catalyzes the rate limiting step of serotonin biosynthesis and interacts with TGF-β and insulin like signalling pathways. *cat-1* codes for a synaptic vesicular monoamine transporter that is required for the presence of serotonin and dopamine in nerve terminals. Therefore in addition to dopamine neurotransmission, serotonergic neurotransmission is also expected to decrease on valproate exposure.

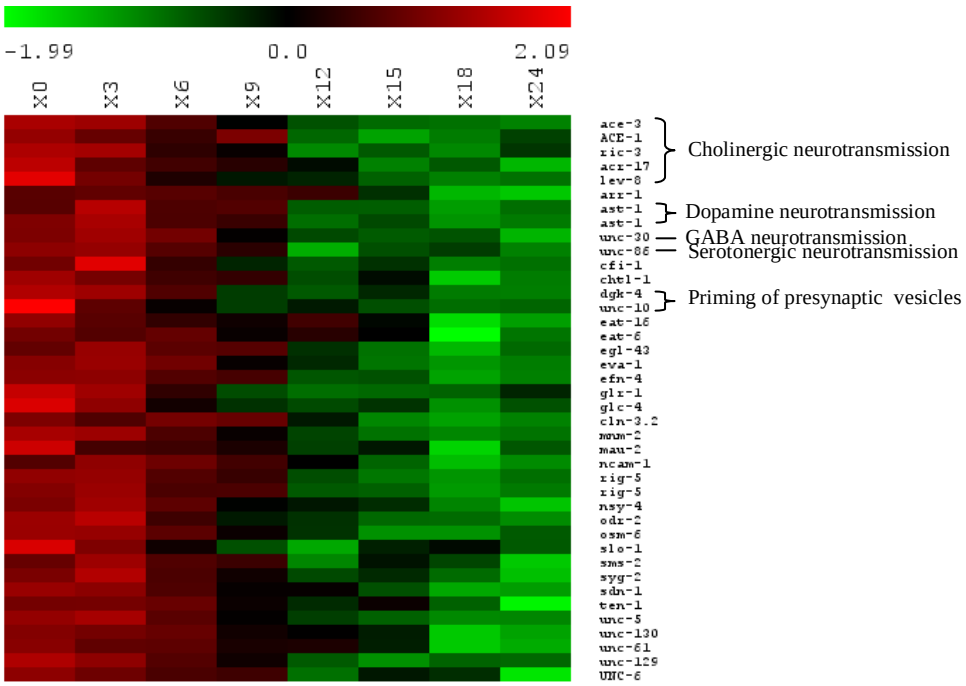

Figure 94 Down-regulated expression profile of valproate exposure on neuronal function. Numbers across top of heatmap indicates valproate concentration. The degree of expression indicated with a red to green scale where the higher expression is given by red.

8.2.12 Sodium valproate acts on both cholinergic and GABAergic neurotransmission

After showing that valproate exposure profile also suggest a down regulation of GABAergic neurotransmission and an increase in cholinergic neurotransmission, we then checked whether that could explain the observed paralysis phenotypes on exposure to valproate.

Sodium valproate can increase paralysis observed in wild type *C.elegans* treated with saturation concentration of Aldicarb(Figure 95, page 240). Therefore, sodium valproate should be causing paralysis in a different mechanism other than, or in addition to, paralysis by build-up of acetylcholine in the synaptic cleft. The paralysis caused by treatment of wild type with Aldicarb and sodium valproate is similar to the paralysis observed on *unc-25* treated with Aldicarb. Therefore, valproate may be acting similar to *unc-25* mutation by inhibiting GABAergic neurotransmission. Sodium Valproate does not increase paralysis of *unc-25* by Aldicarb further and this could be explained by the fact that acetylcholine esterase is fully inhibited by the saturation concentration of Aldicarb and inhibitory effect of GABA is relieved by *unc-25* mutation. This shows that valproate causes paralysis via either or both of these two mechanisms. Therefore, increase of paralysis of untreated *unc-25* mutant by sodium valproate should be due to build-up of acetylcholine in the synaptic cleft. Also the increased paralysis of Aldicarb treated wild type by sodium valproate should be due to inhibition of GABA mediated inhibitory neurotransmission. Aldicarb is more potent than sodium valproate on paralysing *unc-25*.

Wild type *C.elegans* does not get paralysed by sodium valproate. nAchR mutant *unc-38* is also resistant to Aldicarb but treatment of Aldicarb treated *unc-38* with sodium

valproate causes paralysis (Figure 96). The paralysis of *unc-38* with and without Aldicarb treatment could be explained by decrease of GABA mediated neurotransmission by sodium valproate. Wild type *C.elegans* may be resistant to valproate effect on decrease of GABA because its acetylcholine mediated excitatory neurotransmission is intact.

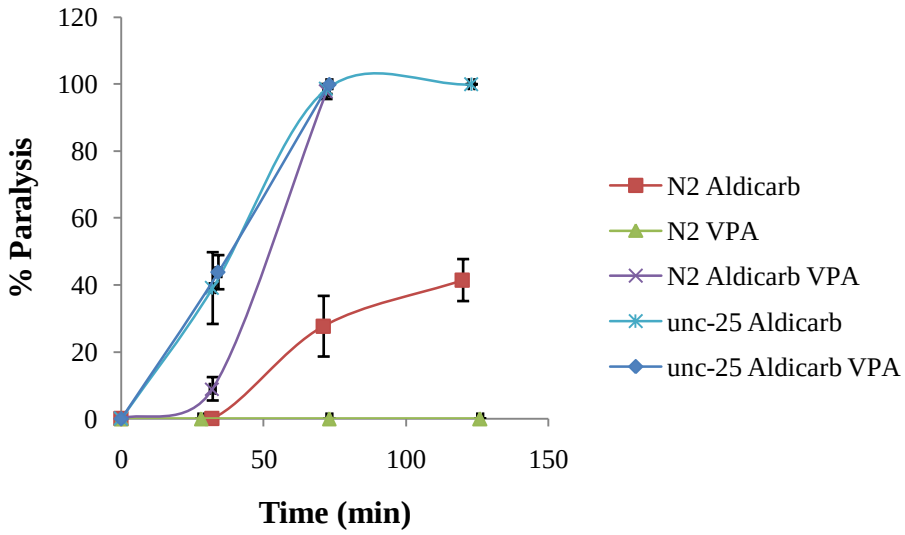

Figure 95 Synergistic effect of Valproate on Aldicarb seen in wild type *C.elegans* but not in *unc-25* mutant. Wild type (N2) or *unc-25* mutants were treated with 1mM Aldicarb or 15mM Sodium Valproate (VPA) or both. Error bars = ± SEM of three independent trials. n=30

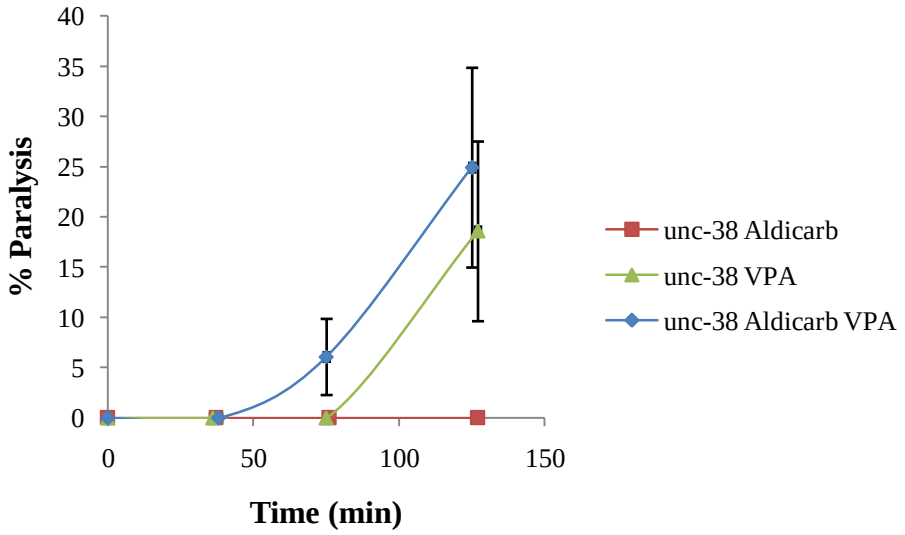

Figure 96Sodium valproate has a positive synergistic effect with Aldicarb on *unc-38* mutant. Acetylcholine receptor mutant *unc-38* were treated with either 1mM Aldicarb or 15mM Sodium Valproate (VPA) or both. Error bars = ± SEM of three independent trials. n=30.

8.2. 13 SMA-6 has a regulatory role in excitatory neurotransmission

After showing that *sma-6* has a neuronal phenotype and *sma-6* is post synaptic, I then tried to develop a model which could explain the observed phenotypes. I hypothesise that the function of SMA-6 would be to inactivate acetylcholine bound receptor.

*sma-6*mutant is hypersensitive to both Aldicarb and levamisole (Figure 97, page 242) SMA-6 is a membrane protein (Greer et al., 2008) and considering the tissues it is expressed in it is found to be postsynaptic as explained earlier. *sma-6* mutant is more sensitive to levamisole than to Aldicarb when compared with *unc-25* mutant, which is more sensitive to Aldicarb than to levamisole. Treatment with levamisole as well as Aldicarb causes paralysis by activating acetylcholine receptor. The only difference is acetyl choline is natural but levamisole is synthetic. Therefore there can be mechanisms

to reverse the acetylcholine bound receptor back to normal. But there will be no mechanism to convert levamisole bound receptor back to the original state. If it is something to do with the muscle after receptor, both should have the mechanisms to convert back to the original state in equal level. Therefore, the only possible thing that can cause paralysis more intensely in *sma-6* treated with levamisole is the inability of the receptor to convert back to its "unbound" original state. Therefore *sma-6* should be coding for something that facilitates conversion of acetylcholine bound receptor back to the original state. Considering the location of SMA-6 and its kinase activity the most probable model is that SMA-6 inactivates acetylcholine bound receptor. Therefore lack of SMA-6 would make the nematode hypersensitive to both Aldicarb and levamisole but will be more prone to levamisole induced paralysis. *sma-6* mutant without any treatment may not show any paralysis due to the presence of other mechanisms such as the presence of choline esterase to inactivate acetylcholine.

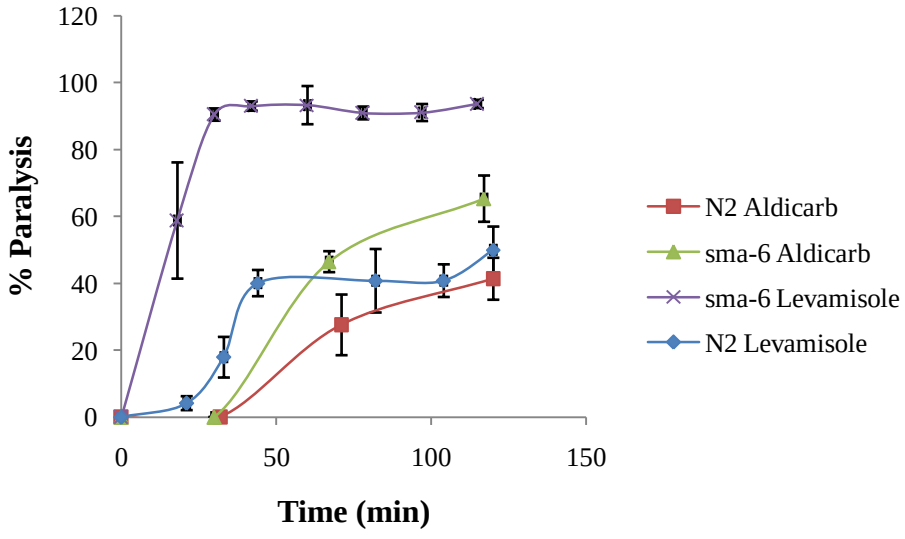

Figure 97*sma-6* mutant is hypersensitive to both Aldicarb and Levamisole. Wild type (N2) or TGF-β Sma/Mad pathway mutant *sma-6*were treated with either 100µM acetylcholine receptor agonist Levamisole or the 1mM acetylcholine esterase inhibitor Aldicarb. Error bars = ± SEM of three independent trials. n=30

8.3 Discussion

In The present study, I looked at the paralysis of TGF-β Sma/Mad pathway type I receptor mutant *sma-6*by Sodium Valproate. The paralysis assays performed goes in line with a novel neuronal function for SMA-6 where SMA-6 acts post synaptically to inactivate acetylcholine bound receptor probably via phosphorylation.

Valproate does not paralyse wildtype *C.elegans* but it does paralyse *sma-6* mutant. *sma-6* null mutant wk-7 is nicotine hypersensitive (Almedom et al., 2009) and Almedom *et al* have suggested this to be due to a cuticle defect considering the short time taken for paralysis. But my results suggest it to have a neuronal function. This is confirmed by the finding that *sma-6* is hypersensitive to the acetylcholine receptor agonist levamisole and acetylcholine esterase inhibitor Aldicarb.

SMA-6 has not co-purified with nicotinic acetylcholine receptor extracts (Gottschalk et al., 2005). A membrane component is shown to cause aggregation of acetylcholine receptors and acetylcholine esterase (Wallace et al., 1985). This suggest that SMA-6 may not be directly associated with acetylcholine receptor or acetylcholine esterase. But it may fascilitate this aggregation probably via phosphorylation to inactivate activated acetylcholine receptor (Figure 98, page 244).*sma-6* mutants and wild type *C.elegans* treated with sodium valproate show sinusoidal movement of the body on locomotion. *sma-6* mutants treated with Sodium Valproate gets shortened indicating a contraction of muscles of both sides of the body, an observation also made in animals lacking D-type neurones which release GABA. Like sma-6 mutants, these nematodes lacking D-type neurones also show sinusoidal body movement(Jorgensen, 2005). This also goes in line with the hypothesis that SMA-6 has an inhibitory effect on excitatory

neurotransmission.SMA-6 is a membrane protein with kinase activity. DBL-1, the ligand of TGF-β Sma/Mad pathway is secreted from cholinergic neurones (Duerr et al., 2008). Hypersensitivity of muscle cells to levamisole and Aldicarb is caused by mutations which increase acetylcholine secretion or decrease inhibitory GABAergic synaptic signalling (Gumienny and Savage-Dunn, 2013). Loss of the ligand of SMA-6, DBL-1 cause defects in pre and post GABAergic synapses indicating that this hypersensitivity is due to a defect in GABAergic neurotransmission (Vashlishan et al., 2008). Therefore, the hypersensitivity of *sma-6* mutants for these drugs also could be attributed to a defect in GABAergic neurotransmission or some other inhibitory neurotransmission effect. GABA also serves a metabolic role in the citric acid cycle(Jorgensen, 2005) and these findings suggest SMA-6 to be a key link between neuronal regulation and metabolism.

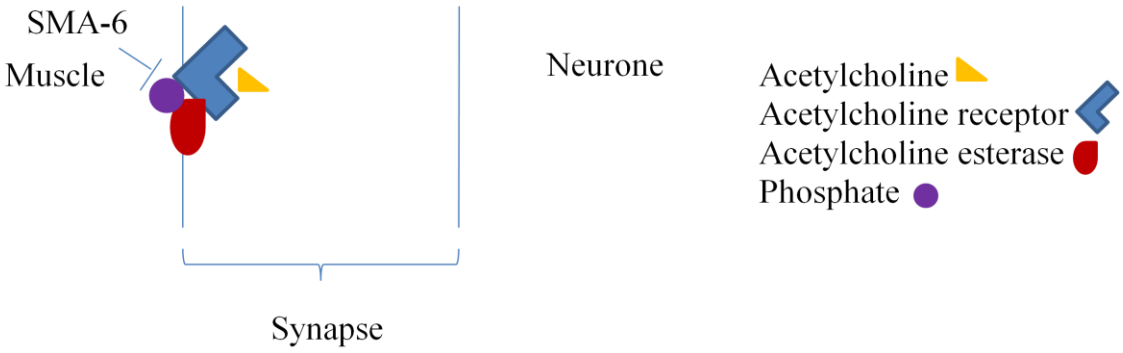

Figure 98 Diagram showing the possible mechanisms of SMA-6 neuronal function in the neuromuscular junction. SMA-6 acts post synaptically and inactivate acetylcholine receptor which is bound to its ligand. This could be either via phosphorylation of activated acetylcholine receptor or by fascilitation of aggregation of acetylcholine esterase to activated acetylcholine receptor.

To explain the paralysis of sma-6 on Sodium Valproate, I looked at the expression profile of *C.elegans* on valproate exposure. Sodium valproate increase Acetylcholine level in synaptic cleft by decreasing transcription of Acetyclcholine Esterases. It also

decreases GABA inhibitory neurotransmission by acting on *unc-30*. Valproate could induce the paralysis of *sma-6* mutants due to inability to decrease cholinergic neurotransmission and inhibition of GABA inhibitory neurotransmission.

9.0 SUMMARY

There is a marked decrease in nuclear components on valproate exposure probably via *vab-3*. In addition, valproate increases lipid in a dose dependent manner up to 15mM. Plateau effect seen in dose response of lipid accumulation suggests valproate to induce lipid accumulation via a receptor mediated pathway where saturation leads to the plateau effect. Transcription profile following valproate exposure suggest itaffects both lipid synthesis and degradation pathways. Valproate induced lipid accumulation is found to be partially dependent on DAF-16, DAF-2 and TGF-β Sma/Mab pathways.

Valproate may decrease lipid accumulation by increasing β-oxidation of fatty acids. But It may increase cholesterol and other steroid synthesis, glycosphingolipid, glycophospholipids and phosphatidylcholine biosynthesis resulting in an overall accumulation of lipids.

DAF-16 dependent expression profile of valproate exposure is expected to be involved in steroid synthesis, fatty acid elongation, prostaglandin D synthesis, fatty acid uptake and acylated ethanol amine production. It is also expected to increase insulin secretion by decreasing the expression of bbs-5 resulting in lipid synthesis. These genes are down regulated in the*daf-16* mutant resulting in an inhibitor effect by DAF-16 on lipid accumulation by valproate exposure. Therefore, the plateau effect of lipid mass on high valproate exposure could be due to the over expression of *daf-16*. Therefore, valproate induced lipid accumulation is partially dependent on DAF-16. It also reveals prostaglandin synthesis to be positively correlated with valproate and phosphatidate formation to be negatively correlated with valproate in a DAF-2 dependent manner.

TGF-β Sma/Mab pathway may be responsible for the glycerophospholipid synthesis.

Decrease of lipid mass by valproate in *daf-2* and *sma-6* mutants could be due to a decrease in prostaglandin synthesis and glycerophospholipid synthesis respectively.

During the phenotypic analysis to see whether *sma-6* plays a role in valproate induced lipid accumulation, I found valproate to cause paralysis of sma-6 mutants. In the last chapter, I have developed a model to explain this neuronal function and suggest a model in whichsma-6 may act postsynaptically to inhibit acetylcholine receptors, which could be possibly via phosphorylation.

10.0 FUTURE WORK

During this study I have performed phenotypic analysis and expression profiling to develop several hypothesis to explain the valproate induced lipid accumulation and paralysis of *sma-6* mutants. These hypotheses now need to be tested experimentally. For example, in a future study the expression profile of the*vab-3* mutant on exposure to valproate could be compared with the negatively correlated expression profile of wild type *C.elegans* following valproate exposure to confirm the role played by *vab-3* in down-regulating nuclear components on valproate exposure. Also, lipid profiling of mutants of the insulin signalling pathway and TGF-β pathway, as well as wild type on valproate exposure would confirm the predictions made on insulin dependent and independent components of valproate induced lipid accumulation of valproate exposure. Solvent extraction of lipids followed by assaying for different lipid types would confirm how valproate affects the levels of different lipid types. This could be done by assaying a given number of age-synchronized worms on valproate plates. Biosynthesis of lipid types can study by using radio actively labelled precursors. For example, incorporation of ^{32}P as $AT^{32}P$ on valproate plates could be use to study phospholipid synthesis. Profiling lipids and fatty acids in human blood could test applicability of these findings to human. Characterization of proteins that are phosphorylated by SMA-6 would support the hypothesis developed for the neuronal phenotype of SMA-6. Separating proteins of *sma-6* mutants followed by analysis of phosphorylation by Mass Spectrometry and comparing with the wild type could do this. Also proteins that interact with SMA-6 should be identified. Determination of structure of the wild type and mutant acetylcholine receptor in wild type and *sma-6* mutant would reveal any molecular changes, which would be predicted if the given hypothesis is valid. Since

sma-6 mutants show a paralysis phenotype on exposure to valproate, any toxic effect of valproate on the people mutant for *sma-6* homologue, born morphogenic protein, should be tested.

In addition to these, repeat of the lipid assay tests by performing a different assay for lipid quantification such as Oil RedO method or Sudan Black assay would validate the results. Microarray data too could validate by performing QPCR for a selected number of genes.

In addition to these findings, I also found that MSG and exercise decrease lipid level. When the interaction between exercise and MSG was studied, it is found that exercise could further decrease the lipid level decreased due to MSG. It is possible to find whether MSG and exercise decrease lipid level via the same or different mechanisms by identifying the highest MSG concentration that would bring the minimum lipid level and letting those worms exercise to see whether it could further decrease the lipid level. If exercise can further decrease the lipid level, that indicates that exercise and MSG act via different mechanisms to decrease lipid level.

REFERENCES

ABRÀMOFF, M. D., MAGALHÃES, P. J. & RAM, S. J. 2004. Image processing with ImageJ. *Biophotonics international,* 11**,** 36-42.

ALMEDOM, R. B., LIEWALD, J. F., HERNANDO, G., SCHULTHEIS, C., RAYES, D., PAN, J., SCHEDLETZKY, T., HUTTER, H., BOUZAT, C. & GOTTSCHALK, A. 2009. An ER-resident membrane protein complex regulates nicotinic acetylcholine receptor subunit composition at the synapse. *The EMBO journal,* 28**,** 2636-2649.

ALTUN, Z. & HALL, D. 2011. Nervous system, general description.

ANDERSEN, E. C., LU, X. & HORVITZ, H. R. 2006. C. elegans ISWI and NURF301 antagonize an Rb-like pathway in the determination of multiple cell fates. *Development,* 133**,** 2695-2704.

ANDRES, R. H., DUCRAY, A. D., SCHLATTNER, U., WALLIMANN, T. & WIDMER, H. R. 2008. Functions and effects of creatine in the central nervous system. *Brain research bulletin,* 76**,** 329-343.

ANTOSHECHKIN, I. & HAN, M. 2002. The< i> C. elegans evl-20</i> Gene Is a Homolog of the Small GTPase ARL2 and Regulates Cytoskeleton Dynamics during Cytokinesis and Morphogenesis. *Developmental cell,* 2**,** 579-591.

APFELD, J., O'CONNOR, G., MCDONAGH, T., DISTEFANO, P. S. & CURTIS, R. 2004. The AMP-activated protein kinase AAK-2 links energy levels and insulin-like signals to lifespan in C. elegans. *Genes & development,* 18**,** 3004-3009.

ARNÉR, E. S. & HOLMGREN, A. 2000. Physiological functions of thioredoxin and thioredoxin reductase. *European Journal of Biochemistry,* 267**,** 6102-6109.

ASHRAFI, K. 2007. Obesity and the regulation of fat metabolism.

AVERY, L. & HORVITZT, H. R. 1989. Pharyngeal pumping continues after laser killing of the pharyngeal nervous system of C. elegans. *Neuron,* 3**,** 473-485.

BALEN, A. H. & ANDERSON, R. A. 2007. Impact of obesity on female reproductive health: British fertility society, policy and practice guidelines. *Human Fertility,* 10**,** 195-206.

BARAN, R., ARONOFF, R. & GARRIGA, G. 1999. The C. elegans homeodomain gene unc-42 regulates chemosensory and glutamate receptor expression. *Development,* 126**,** 2241-2251.

BEN-AMI, H. C., YASSIN, L., FARAH, H., MICHAELI, A., ESHEL, M. & TREININ, M. 2005. RIC-3 affects properties and quantity of nicotinic acetylcholine receptors via a mechanism that does not require the coiled-coil domains. *Journal of Biological Chemistry,* 280**,** 28053-28060.

BEN-DOR, A., SHAMIR, R. & YAKHINI, Z. 1999. Clustering gene expression patterns. *Journal of computational biology,* 6**,** 281-297.

BÉNARD, C. Y., KÉBIR, H., TAKAGI, S. & HEKIMI, S. 2004. mau-2 acts cell-autonomously to guide axonal migrations in Caenorhabditis elegans. *Development,* 131**,** 5947-5958.

BENNION, L. J. & GRUNDY, S. M. 1975. Effects of obesity and caloric intake on biliary lipid metabolism in man. *Journal of Clinical Investigation,* 56**,** 996.

BERKOWITZ, L. A. & STROME, S. 2000. MES-1, a protein required for unequal divisions of the germline in early C. elegans embryos, resembles receptor tyrosine kinases and is localized to the boundary between the germline and gut cells. *Development,* 127**,** 4419-4431.

BERRI, S., BOYLE, J. H., TASSIERI, M., HOPE, I. A. & COHEN, N. 2009. Forward locomotion of the nematode C. elegans is achieved through modulation of a single gait. *HFSP journal,* 3**,** 186-193.

BHAMIDIPATI, A., LEWIS, S. A. & COWAN, N. J. 2000. ADP ribosylation factor-like protein 2 (Arl2) regulates the interaction of tubulin-folding cofactor D with native tubulin. *The Journal of cell biology,* 149**,** 1087-1096.

BOULTON, S. J., GARTNER, A., REBOUL, J., VAGLIO, P., DYSON, N., HILL, D. E. & VIDAL, M. 2002. Combined functional genomic maps of the C. elegans DNA damage response. *Science,* 295**,** 127-131.

BRENNER, S. 1974. The genetics of Caenorhabditis elegans. *Genetics,* 77**,** 71-94.

BROCK, T. J. & WATTS, J. L. 2006. Genetic regulation of unsaturated fatty acid composition in C. elegans. *PLoS genetics,* 2**,** e108.

BROCKIE, P. J., MADSEN, D. M., ZHENG, Y., MELLEM, J. & MARICQ, A. V. 2001. Differential expression of glutamate receptor subunits in the nervous system of Caenorhabditis elegans and their regulation by the homeodomain protein UNC-42. *The Journal of Neuroscience,* 21**,** 1510-1522.

BÜRGLIN, T. R. & KUWABARA, P. E. 2006. Homologs of the Hh signalling network in C. elegans.

BURNETT, C., VALENTINI, S., CABREIRO, F., GOSS, M., SOMOGYVÁRI, M., PIPER, M. D., HODDINOTT, M., SUTPHIN, G. L., LEKO, V. & MCELWEE, J. J. 2011. Absence of effects of Sir2 overexpression on lifespan in C. elegans and Drosophila. *nature,* 477**,** 482-485.

CASTRO, A. A., GHISONI, K., LATINI, A., QUEVEDO, J., TASCA, C. I. & PREDIGER, R. D. 2012. Lithium and valproate prevent olfactory discrimination and short-term memory impairments in the intranasal 1-methyl-4-phenyl-1, 2, 3, 6-tetrahydropyridine (MPTP) rat model of Parkinson's disease. *Behavioural Brain Research,* 229**,** 208-215.

CHAN, J. M., RIMM, E. B., COLDITZ, G. A., STAMPFER, M. J. & WILLETT, W. C. 1994. Obesity, fat distribution, and weight gain as risk factors for clinical diabetes in men. *Diabetes care,* 17**,** 961-969.

CHEESEMAN, I. M., NIESSEN, S., ANDERSON, S., HYNDMAN, F., YATES, J. R., OEGEMA, K. & DESAI, A. 2004. A conserved protein network controls assembly of the outer kinetochore and its ability to sustain tension. *Genes & development,* 18**,** 2255-2268.

CHEN, Z. & HAN, M. 2001. Role of C. elegans lin-40 MTA in vulval fate specification and morphogenesis. *Development,* 128**,** 4911-4921.

CHIEN, S.-C., BRINKMANN, E.-M., TEULIERE, J. & GARRIGA, G. 2013. Caenorhabditis elegans PIG-1/MELK Acts in a Conserved PAR-4/LKB1 Polarity Pathway to Promote Asymmetric Neuroblast Divisions. *Genetics,* 193**,** 897-909.

CHOPRA, A., KOLLA, B. P., MANSUKHANI, M. P., NETZEL, P. & FRYE, M. A. 2012. Valproate-induced hyperammonemic encephalopathy: an update on risk factors, clinical correlates and management. *General hospital psychiatry,* 34**,** 290-298.

CINATL, J., KOTCHETKOV, R., BLAHETA, R., DRIEVER, P. H., VOGEL, J.-U. & CINATL, J. 2002. Induction of differentiation and suppression of malignant phenotype of human neuroblastoma BE (2)-C cells by valproic acid: enhancement by combination with interferon-α. *International journal of oncology,* 20**,** 97-106.

CLARK-MAGUIRE, S. & MAINS, P. E. 1994. mei-1, a gene required for meiotic spindle formation in Caenorhabditis elegans, is a member of a family of ATPases. *Genetics,* 136**,** 533-546.

COLAVITA, A. & CULOTTI, J. G. 1998. Suppressors of Ectopic UNC-5 Growth Cone Steering Identify Eight Genes Involved in Axon Guidance in< i> Caenorhabditis elegans</i>. *Developmental biology,* 194**,** 72-85.

COLLISON, K. S., MAQBOOL, Z., SALEH, S. M., INGLIS, A., MAKHOUL, N. J., BAKHEET, R., AL-JOHI, M., AL-RABIAH, R., ZAIDI, M. Z. & AL-MOHANNA, F. A. 2009. Effect of dietary monosodium glutamate on trans fat-induced nonalcoholic fatty liver disease. *Journal of lipid research,* 50**,** 1521-1537.

COMUZZIE, A. G. & ALLISON, D. B. 1998. The search for human obesity genes. *Science,* 280**,** 1374-1377.

COWDEN, J., PADNOS, B., HUNTER, D., MACPHAIL, R., JENSEN, K. & PADILLA, S. 2012. Developmental exposure to valproate and ethanol alters locomotor activity and retino-tectal projection area in zebrafish embryos. *Reproductive Toxicology,* 33**,** 165-173.

CROWDER, C. M., WESTOVER, E. J., KUMAR, A. S., OSTLUND, R. E. & COVEY, D. F. 2001. Enantiospecificity of cholesterol function in vivo. *Journal of Biological Chemistry,* 276**,** 44369-44372.

DA WEI HUANG, B. T. S. & LEMPICKI, R. A. 2008. Systematic and integrative analysis of large gene lists using DAVID bioinformatics resources. *Nature protocols,* 4**,** 44-57.

DANIELS, S. A., AILION, M., THOMAS, J. H. & SENGUPTA, P. 2000. egl-4 acts through a transforming growth factor-β/SMAD pathway in Caenorhabditis elegans to regulate multiple neuronal circuits in response to sensory cues. *Genetics,* 156**,** 123-141.

DAVID, D. C., OLLIKAINEN, N., TRINIDAD, J. C., CARY, M. P., BURLINGAME, A. L. & KENYON, C. 2010. Widespread protein aggregation as an inherent part of aging in C. elegans. *PLoS biology,* 8**,** e1000450.

DE BARTOLOMEIS, A., TOMASETTI, C., CICALE, M., YUAN, P.-X. & MANJI, H. K. 2012. Chronic treatment with lithium or valproate modulates the expression of< i> Homer1b/c</i> and its related genes< i> Shank</i> and< i> Inositol 1, 4, 5-trisphosphate receptor</i>. *European Neuropsychopharmacology,* 22**,** 527-535.

DECHENES, C. J., VERCHERE, C. B., ANDRIKOPOULOS, S. & KAHN, S. E. 1998. Human aging is associated with parallel reductions in insulin and amylin release. *American Journal of Physiology-Endocrinology And Metabolism,* 275**,** E785-E791.

DENT, J. A., SMITH, M. M., VASSILATIS, D. K. & AVERY, L. 2000. The genetics of ivermectin resistance in Caenorhabditis elegans. *Proceedings of the National Academy of Sciences,* 97**,** 2674-2679.

DESAI, A., RYBINA, S., MÜLLER-REICHERT, T., SHEVCHENKO, A., SHEVCHENKO, A., HYMAN, A. & OEGEMA, K. 2003. KNL-1 directs assembly of the microtubule-binding interface of the kinetochore in C. elegans. *Genes & development,* 17**,** 2421-2435.

DESAI, C., GARRIGA, G., MCLNTIRE, S. L. & HORVITZ, H. R. 1988. A genetic pathway for the development of the Caenorhabditis elegans HSN motor neurons.

DILLIN, A., HSU, A.-L., ARANTES-OLIVEIRA, N., LEHRER-GRAIWER, J., HSIN, H., FRASER, A. G., KAMATH, R. S., AHRINGER, J. & KENYON, C. 2002. Rates of behavior and aging specified by mitochondrial function during development. *Science,* 298**,** 2398-2401.

DONG, Y., BOGDANOVA, A., HABERMANN, B., ZACHARIAE, W. & AHRINGER, J. 2007. Identification of the C. elegans anaphase promoting complex subunit Cdc26 by phenotypic profiling and functional rescue in yeast. *BMC developmental biology,* 7**,** 19.

DOPAZO, J. & CARAZO, J. M. 1997. Phylogenetic reconstruction using an unsupervised growing neural network that adopts the topology of a phylogenetic tree. *Journal of Molecular Evolution,* 44**,** 226-233.

DUERR, J. S., HAN, H. P., FIELDS, S. D. & RAND, J. B. 2008. Identification of major classes of cholinergic neurons in the nematode Caenorhabditis elegans. *Journal of Comparative Neurology,* 506**,** 398-408.

DUKES, I. D., MCINTYRE, M. S., MERTZ, R. J., PHILIPSON, L. H., ROE, M. W., SPENCER, B. & WORLEY, J. 1994. Dependence on NADH produced during glycolysis for beta-cell glucose signaling. *Journal of Biological Chemistry,* 269**,** 10979-10982.

DUNCAN, J. S., SANDER, J. W., SISODIYA, S. M. & WALKER, M. C. 2006. Adult epilepsy. *The Lancet,* 367**,** 1087-1100.

ESTEVEZ, M., ATTISANO, L., WRANA, J. L., ALBERT, P. S., MASSAGUÉ, J. & RIDDLE, D. L. 1993. The daf-4 gene encodes a bone morphogenetic protein receptor controlling C. elegans dauer larva development.

EVASON, K., COLLINS, J. J., HUANG, C., HUGHES, S. & KORNFELD, K. 2008. Valproic acid extends Caenorhabditis elegans lifespan. *Aging Cell,* 7**,** 305-317.

FAN, Z., BERESFORD, P. J., OH, D. Y., ZHANG, D. & LIEBERMAN, J. 2003. Tumor suppressor NM23-H1 is a granzyme A-activated DNase during CTL-mediated apoptosis, and the nucleosome assembly protein SET is its inhibitor. *Cell,* 112**,** 659-672.

FIELENBACH, N. & ANTEBI, A. 2008. C. elegans dauer formation and the molecular basis of plasticity. *Genes & development,* 22**,** 2149-2165.

FINVER, S. N., NISHIKURA, K., FINGER, L. R., HALUSKA, F. G., FINAN, J., NOWELL, P. C. & CROCE, C. M. 1988. Sequence analysis of the MYC oncogene involved in the t (8; 14)(q24; q11) chromosome translocation in a human leukemia T-cell line indicates that putative regulatory regions are not altered. *Proceedings of the National Academy of Sciences,* 85**,** 3052-3056.

FLAMES, N. & HOBERT, O. 2009. Gene regulatory logic of dopamine neuron differentiation. *nature,* 458**,** 885-889.

FORSYTHE, E. & BEALES, P. L. 2012. Bardet–Biedl syndrome. *European Journal of Human Genetics,* 21**,** 8-13.

FRANZONI, E., GOVONI, M., D'ADDATO, S., GUALANDI, S., SANGIORGI, Z., DESCOVICH, G. C. & SALVIOLI, G. P. 1992. Total cholesterol, high-density lipoprotein cholesterol, and triglycerides in children receiving antiepileptic drugs. *Epilepsia,* 33**,** 932-935.

FRASER, A. G., KAMATH, R. S., ZIPPERLEN, P., MARTINEZ-CAMPOS, M., SOHRMANN, M. & AHRINGER, J. 2000. Functional genomic analysis of C. elegans chromosome I by systematic RNA interference. *nature,* 408**,** 325-330.

GEORGI, L. L., ALBERT, P. S. & RIDDLE, D. L. 1990. daf-1, a C. elegans gene controlling dauer larva development, encodes a novel receptor protein kinase. *Cell,* 61**,** 635-645.

GOMCELI, Y., KUTLU, G., CAVDAR, L., SANIVAR, F. & INAN, L. 2007. Different clinical manifestations of hyperammonemic encephalopathy. *Epilepsy & Behavior,* 10**,** 583-587.

GÖNCZY, P., ECHEVERRI, C., OEGEMA, K., COULSON, A., JONES, S. J., COPLEY, R. R., DUPERON, J., OEGEMA, J., BREHM, M. & CASSIN, E. 2000. Functional genomic analysis of cell division in C. elegans using RNAi of genes on chromosome III. *nature,* 408**,** 331-336.

GOODWIN, P. R., SASAKI, J. M. & JUO, P. 2012. Cyclin-dependent kinase 5 regulates the polarized trafficking of neuropeptide-containing dense-core vesicles in Caenorhabditis elegans motor neurons. *The Journal of Neuroscience,* 32**,** 8158-8172.

GÖTTLICHER, M., MINUCCI, S., ZHU, P., KRÄMER, O. H., SCHIMPF, A., GIAVARA, S., SLEEMAN, J. P., COCO, F. L., NERVI, C. & PELICCI, P. G. 2001. Valproic acid defines a novel class of HDAC inhibitors inducing differentiation of transformed cells. *The EMBO journal,* 20**,** 6969-6978.

GOTTSCHALK, A., ALMEDOM, R. B., SCHEDLETZKY, T., ANDERSON, S. D., YATES, J. R. & SCHAFER, W. R. 2005. Identification and characterization of novel nicotinic receptor-associated proteins in Caenorhabditis elegans. *The EMBO journal,* 24**,** 2566-2578.

GREENSPAN, P., MAYER, E. P. & FOWLER, S. D. 1985. Nile red: a selective fluorescent stain for intracellular lipid droplets. *The Journal of cell biology,* 100**,** 965-973.

GREER, E. L. & BRUNET, A. 2009. Different dietary restriction regimens extend lifespan by both independent and overlapping genetic pathways in C. elegans. *Aging Cell,* 8**,** 113-127.

GREER, E. L., DOWLATSHAHI, D., BANKO, M. R., VILLEN, J., HOANG, K., BLANCHARD, D., GYGI, S. P. & BRUNET, A. 2007. An AMPK-FOXO Pathway Mediates Longevity Induced by a Novel Method of Dietary Restriction in< i> C. elegans</i>. *Current Biology,* 17**,** 1646-1656.

GREER, E. R., PÉREZ, C. L., VAN GILST, M. R., LEE, B. H. & ASHRAFI, K. 2008. Neural and Molecular Dissection of a< i> C. elegans</i> Sensory Circuit that Regulates Fat and Feeding. *Cell metabolism,* 8**,** 118-131.

GUMIENNY, T. L. & SAVAGE-DUNN, C. 2013. TGF-β signaling in C. elegans. *WormBook: the online review of C. elegans biology***,** 1.

GURVICH, N. & KLEIN, P. S. 2002. Lithium and valproic acid: parallels and contrasts in diverse signaling contexts. *Pharmacology & therapeutics,* 96**,** 45-66.

HALEVI, S., MCKAY, J., PALFREYMAN, M., YASSIN, L., ESHEL, M., JORGENSEN, E. & TREININ, M. 2002. The C. elegans ric-3 gene is required for maturation of nicotinic acetylcholine receptors. *The EMBO journal,* 21**,** 1012-1020.

HANSEN, M., CHANDRA, A., MITIC, L. L., ONKEN, B., DRISCOLL, M. & KENYON, C. 2008. A role for autophagy in the extension of lifespan by dietary restriction in C. elegans. *PLoS genetics,* 4**,** e24.

HASHMI, S., WANG, Y., PARHAR, R. S., COLLISON, K. S., CONCA, W., AL-MOHANNA, F. & GAUGLER, R. 2013. A C. elegans model to study human metabolic regulation. *Nutrition & metabolism,* 10**,** 31.

HEKIMI, S., BOUTIS, P. & LAKOWSKI, B. 1995. Viable maternal-effect mutations that affect the development of the nematode Caenorhabditis elegans. *Genetics,* 141**,** 1351-1364.

HELLERER, T., AXÄNG, C., BRACKMANN, C., HILLERTZ, P., PILON, M. & ENEJDER, A. 2007. Monitoring of lipid storage in Caenorhabditis elegans using coherent anti-Stokes Raman scattering (CARS) microscopy. *Proceedings of the National Academy of Sciences,* 104**,** 14658-14663.

HERMAN, T., HARTWIEG, E. & HORVITZ, H. R. 1999. sqv mutants of Caenorhabditis elegans are defective in vulval epithelial invagination. *Proceedings of the National Academy of Sciences,* 96**,** 968-973.

HERRERO, J., VALENCIA, A. & DOPAZO, J. 2001. A hierarchical unsupervised growing neural network for clustering gene expression patterns. *Bioinformatics,* 17**,** 126-136.

HODGKIN, J. 2005. Introduction to genetics and genomics.

HOLLOSZY, J. O. 1998. Longevity of exercising male rats: effect of an antioxidant supplemented diet. *Mechanisms of ageing and development,* 100**,** 211-219.

HORVITZ, H. R. & SULSTON, J. E. 1980. Isolation and genetic characterization of cell-lineage mutants of the nematode Caenorhabditis elegans. *Genetics,* 96**,** 435-454.

HSU, A.-L., MURPHY, C. T. & KENYON, C. 2003. Regulation of aging and age-related disease by DAF-16 and heat-shock factor. *Science,* 300**,** 1142-1145.

HU, Y., XIAO, S.-H. & AROIAN, R. V. 2009. The new anthelmintic tribendimidine is an L-type (levamisole and pyrantel) nicotinic acetylcholine receptor agonist. *PLoS neglected tropical diseases,* 3**,** e499.

HUCK, J. H., STRUYS, E. A., VERHOEVEN, N. M., JAKOBS, C. & VAN DER KNAAP, M. S. 2003. Profiling of pentose phosphate pathway intermediates in blood spots by tandem mass spectrometry: application to transaldolase deficiency. *Clinical chemistry,* 49**,** 1375-1380.

HUSSON, S. J., MERTENS, I., JANSSEN, T., LINDEMANS, M. & SCHOOFS, L. 2007. Neuropeptidergic signaling in the nematode< i> Caenorhabditis elegans</i>. *Progress in neurobiology,* 82**,** 33-55.

HUTTER, H., WACKER, I., SCHMID, C. & HEDGECOCK, E. M. 2005. Novel genes controlling ventral cord asymmetry and navigation of pioneer axons in< i> C. elegans</i>. *Developmental biology,* 284**,** 260-272.

ISOJÄRVI, J. I., LAATIKAINEN, T. J., KNIP, M., PAKARINEN, A. J., JUNTUNEN, K. T. & MYLLYLA, V. V. 1996. Obesity and endocrine disorders in women taking valproate for epilepsy. *Annals of neurology,* 39**,** 579-584.

JARVILL-TAYLOR, K. J., ANDERSON, R. A. & GRAVES, D. J. 2001. A hydroxychalcone derived from cinnamon functions as a mimetic for insulin in 3T3-L1 adipocytes. *Journal of the American College of Nutrition,* 20**,** 327-336.

JEONG, M. R., HASHIMOTO, R., SENATOROV, V. V., FUJIMAKI, K., REN, M., LEE, M. S. & CHUANG, D.-M. 2003. Valproic acid, a mood stabilizer and anticonvulsant, protects rat cerebral cortical neurons from spontaneous cell death: a role of histone deacetylase inhibition. *FEBS letters,* 542**,** 74-78.

JIA, K., CHEN, D. & RIDDLE, D. L. 2004. The TOR pathway interacts with the insulin signaling pathway to regulate C. elegans larval development, metabolism and life span. *Development,* 131**,** 3897-3906.

JOHNSON, R. W. & CHAMBERLIN, H. M. 2008. Positive and negative regulatory inputs restrict< i> pax-6/vab-3</i> transcription to sensory organ precursors in< i> Caenorhabditis elegans</i>. *Mechanisms of development,* 125**,** 486-497.

JORGENSEN, E. M. 2005. Gaba.

JU, S. & GREENBERG, M. L. 2003. Valproate disrupts regulation of inositol responsive genes and alters regulation of phospholipid biosynthesis. *Molecular microbiology,* 49**,** 1595-1604.

KAGAWA, Y. 1978. Impact of Westernization on the nutrition of Japanese: changes in physique, cancer, longevity and centenarians. *Preventive medicine,* 7**,** 205-217.

KALANI, R., JUDGE, S., CARTER, C., PAHOR, M. & LEEUWENBURGH, C. 2006. Effects of caloric restriction and exercise on age-related, chronic inflammation assessed by C-reactive protein and interleukin-6. *The Journals of Gerontology Series A: Biological Sciences and Medical Sciences,* 61**,** 211-217.

KALETTA, T. & HENGARTNER, M. O. 2006. Finding function in novel targets: C. elegans as a model organism. *Nature Reviews Drug Discovery,* 5**,** 387-399.

KALMIJN, S., VAN BOXTEL, M., OCKE, M., VERSCHUREN, W., KROMHOUT, D. & LAUNER, L. 2004. Dietary intake of fatty acids and fish in relation to cognitive performance at middle age. *Neurology,* 62**,** 275-280.

KAMATH, R. S., FRASER, A. G., DONG, Y., POULIN, G., DURBIN, R., GOTTA, M., KANAPIN, A., LE BOT, N., MORENO, S. & SOHRMANN, M. 2003. Systematic functional analysis of the Caenorhabditis elegans genome using RNAi. *nature,* 421**,** 231-237.

KANTOR, P. F., LUCIEN, A., KOZAK, R. & LOPASCHUK, G. D. 2000. The antianginal drug trimetazidine shifts cardiac energy metabolism from fatty acid oxidation to glucose oxidation by inhibiting mitochondrial long-chain 3-ketoacyl coenzyme A thiolase. *Circulation Research,* 86**,** 580-588.

KAPAHI, P., CHEN, D., ROGERS, A. N., KATEWA, S. D., LI, P. W.-L., THOMAS, E. L. & KOCKEL, L. 2010. With TOR, less is more: a key role for the conserved nutrient-sensing TOR pathway in aging. *Cell metabolism,* 11**,** 453-465.

KENYON, C. 2005. The plasticity of aging: insights from long-lived mutants. *Cell,* 120**,** 449-460.

KENYON, C., CHANG, J., GENSCH, E., RUDNER, A. & TABTIANG, R. 1993. A C. elegans mutant that lives twice as long as wild type. *nature,* 366**,** 461-464.

KIM, K. H., GOHTANI, S., MATSUNO, R. & YAMANO, Y. 1999. Effects of oil droplet and agar concentration on gel strength and microstructure of o/w emulsion gel. *Journal of texture studies,* 30**,** 319-335.

KIS, B., SZUPERA, Z., MEZEI, Z., GECSE, Á., TELEGDY, G. & VÉCSEI, L. 1999. Valproate treatment and platelet function: the role of arachidonate metabolites. *Epilepsia,* 40**,** 307-310.

KURZ, C. L. & EWBANK, J. J. 2003. Caenorhabditis elegans: an emerging genetic model for the study of innate immunity. *Nature Reviews Genetics,* 4**,** 380-390.

LANJUIN, A., VANHOVEN, M. K., BARGMANN, C. I., THOMPSON, J. K. & SENGUPTA, P. 2003. < i> Otx/otd</i> Homeobox Genes Specify Distinct Sensory Neuron Identities in< i> C. elegans</i>. *Developmental cell,* 5**,** 621-633.

LEE, M.-H. & SCHEDL, T. 2001. Identification of in vivo mRNA targets of GLD-1, a maxi-KH motif containing protein required for C. elegans germ cell development. *Genes & development,* 15**,** 2408-2420.

LEE, R. Y., HENCH, J. & RUVKUN, G. 2001. Regulation of C. elegans DAF-16 and its human ortholog FKHRL1 by the daf-2 insulin-like signaling pathway. *Current Biology,* 11**,** 1950-1957.

LEON, A. S. & SANCHEZ, O. A. 2001. Response of blood lipids to exercise training alone or combined with dietary intervention. *Medicine and science in sports and exercise,* 33**,** S502-15; discussion S528-9.

LEVIN, B. E., DUNN-MEYNELL, A. A. & ROUTH, V. H. 1999. Brain glucose sensing and body energy homeostasis: role in obesity and diabetes. *American Journal of Physiology-Regulatory, Integrative and Comparative Physiology,* 276**,** R1223-R1231.

LI, S., ARMSTRONG, C. M., BERTIN, N., GE, H., MILSTEIN, S., BOXEM, M., VIDALAIN, P.-O., HAN, J.-D. J., CHESNEAU, A. & HAO, T. 2004. A map of the interactome network of the metazoan C. elegans. *Science,* 303**,** 540-543.

LIANG, B., MOUSSAIF, M., KUAN, C.-J., GARGUS, J. J. & SZE, J. Y. 2006. Serotonin targets the DAF-16/FOXO signaling pathway to modulate stress responses. *Cell metabolism,* 4**,** 429-440.

LIN, K., DORMAN, J. B., RODAN, A. & KENYON, C. 1997. daf-16: An HNF-3/forkhead family member that can function to double the life-span of Caenorhabditis elegans. *Science,* 278**,** 1319-1322.

LIU, L. X., SPOERKE, J. M., MULLIGAN, E. L., CHEN, J., REARDON, B., WESTLUND, B., SUN, L., ABEL, K., ARMSTRONG, B. & HARDIMAN, G. 1999. High-throughput isolation of Caenorhabditis elegans deletion mutants. *Genome research,* 9**,** 859-867.

LLOYD, K. A. 2013. A scientific review: mechanisms of valproate-mediated teratogenesis. *Bioscience Horizons,* 6.

LOKEY, E. & TRAN, Z. 1989. Effects of exercise training on serum lipid and lipoprotein concentrations in women: a meta-analysis. *International journal of sports medicine,* 10**,** 424-429.

LUCAS, K. A., PITARI, G. M., KAZEROUNIAN, S., RUIZ-STEWART, I., PARK, J., SCHULZ, S., CHEPENIK, K. P. & WALDMAN, S. A. 2000. Guanylyl cyclases and signaling by cyclic GMP. *Pharmacological reviews,* 52**,** 375-414.

LUND, J., TEDESCO, P., DUKE, K., WANG, J., KIM, S. K. & JOHNSON, T. E. 2002. Transcriptional Profile of Aging in< i> C. elegans</i>. *Current Biology,* 12**,** 1566-1573.

MAINS, P., KEMPHUES, K., SPRUNGER, S., SULSTON, I. & WOOD, W. 1990. Mutations affecting the meiotic and mitotic divisions of the early Caenorhabditis elegans embryo. *Genetics,* 126**,** 593-605.

MATTSON, M. P., CHAN, S. L. & DUAN, W. 2002. Modification of brain aging and neurodegenerative disorders by genes, diet, and behavior. *Physiological reviews,* 82**,** 637-672.

MATYASH, V., GEIER, C., HENSKE, A., MUKHERJEE, S., HIRSH, D., THIELE, C., GRANT, B., MAXFIELD, F. R. & KURZCHALIA, T. V. 2001. Distribution and Transport of Cholesterol inCaenorhabditis elegans. *Molecular Biology of the Cell,* 12**,** 1725-1736.

MAWHINNEY, E., CAMPBELL, J., CRAIG, J., RUSSELL, A., SMITHSON, W., PARSONS, L., ROBERTSON, I., IRWIN, B., MORRISON, P. & LIGGAN, B. 2012. Valproate and the risk for congenital malformations: Is formulation and dosage regime important? *Seizure,* 21**,** 215-218.

MCARDLE, K., ALLEN, T. S. & BUCHER, E. A. 1998. Ca2+-dependent muscle dysfunction caused by mutation of the Caenorhabditis elegans troponin T-1 gene. *The Journal of cell biology,* 143**,** 1201-1213.

MEHTA, R., STEINKRAUS, K. A., SUTPHIN, G. L., RAMOS, F. J., SHAMIEH, L. S., HUH, A., DAVIS, C., CHANDLER-BROWN, D. & KAEBERLEIN, M. 2009. Proteasomal regulation of the hypoxic response modulates aging in C. elegans. *Science,* 324**,** 1196-1198.

MELEGH, B. & TROMBITÁS, K. 1997. Valproate treatment induces lipid globule accumulation with ultrastructural abnormalities of mitochondria in skeletal muscle. *Neuropediatrics,* 28**,** 257-261.

MIETTINEN, T. A. 1971. Cholesterol production in obesity. *Circulation,* 44**,** 842-850.

MILLER, R. A., BUEHNER, G., CHANG, Y., HARPER, J. M., SIGLER, R. & SMITH-WHEELOCK, M. 2005. Methionine-deficient diet extends mouse lifespan, slows immune and lens aging, alters glucose, T4, IGF-I and insulin levels, and increases hepatocyte MIF levels and stress resistance. *Aging Cell,* 4**,** 119-125.

MISGELD, T., KUMMER, T. T., LICHTMAN, J. W. & SANES, J. R. 2005. Agrin promotes synaptic differentiation by counteracting an inhibitory effect of neurotransmitter. *Proceedings of the National Academy of Sciences of the United States of America,* 102**,** 11088-11093.

MITANI, S., DU, H., HALL, D. H., DRISCOLL, M. & CHALFIE, M. 1993. Combinatorial control of touch receptor neuron expression in Caenorhabditis elegans. *Development,* 119**,** 773-783.

MITTENDORF, V., ROBERTSON, E. J., LEECH, R. M., KRÜGER, N., STEINBÜCHEL, A. & POIRIER, Y. 1998. Synthesis of medium-chain-length polyhydroxyalkanoates in Arabidopsis thaliana using intermediates of peroxisomal fatty acid β-oxidation. *Proceedings of the National Academy of Sciences,* 95**,** 13397-13402.

MIYABAYASHI, T., PALFREYMAN, M. T., SLUDER, A. E., SLACK, F. & SENGUPTA, P. 1999. Expression and Function of Members of a Divergent Nuclear Receptor Family in< i> Caenorhabditis elegans</i>. *Developmental biology,* 215**,** 314-331.

MOON, T. W. & JOHNSTON, I. A. 1980. Starvation and the activities of glycolytic and gluconeogenic enzymes in skeletal muscles and liver of the plaice, Pleuronectes platessa. *Journal of comparative physiology,* 136**,** 31-38.

MORLAND, C., NORDENGEN, K. & GUNDERSEN, V. 2012. Valproate causes reduction of the excitatory amino acid aspartate in nerve terminals. *Neuroscience letters*.

MORONI, F. 1999. Tryptophan metabolism and brain function: focus on kynurenine and other indole metabolites. *European journal of pharmacology,* 375**,** 87-100.

MULLANEY, B. C. & ASHRAFI, K. 2009a. C. elegans fat storage and metabolic regulation. *Biochimica et Biophysica Acta (BBA)-Molecular and Cell Biology of Lipids,* 1791**,** 474-478.

MULLANEY, B. C. & ASHRAFI, K. 2009b. < i> C. elegans</i> fat storage and metabolic regulation. *Biochimica et Biophysica Acta (BBA)-Molecular and Cell Biology of Lipids,* 1791**,** 474-478.

MURIALDO, G., GALIMBERTI, C., GIANELLI, M., ROLLERO, A., POLLERI, A., COPELLO, F., MAGRI, F., FERRARI, E., SAMPAOLO, P. & MANNI, R. 1998. Effects of valproate, phenobarbital, and carbamazepine on sex steroid setup in women with epilepsy. *Clinical neuropharmacology,* 21**,** 52-58.

MURPHY, C. T., MCCARROLL, S. A., BARGMANN, C. I., FRASER, A., KAMATH, R. S., AHRINGER, J., LI, H. & KENYON, C. 2003. Genes that act downstream of DAF-16 to influence the lifespan of Caenorhabditis elegans. *nature,* 424**,** 277-283.

MYERS, C. D., GOH, P.-Y., ALLEN, T., BUCHER, E. A. & BOGAERT, T. 1996. Developmental genetic analysis of troponin T mutations in striated and nonstriated muscle cells of Caenorhabditis elegans. *The Journal of cell biology,* 132**,** 1061-1077.

NARBONNE, P. & ROY, R. 2008. Caenorhabditis elegans dauers need LKB1/AMPK to ration lipid reserves and ensure long-term survival. *nature,* 457**,** 210-214.

NERI, P., TAGLIAFERRI, P., DI MARTINO, M. T., CALIMERI, T., AMODIO, N., BULOTTA, A., VENTURA, M., ERAMO, P. O., VISCOMI, C. & ARBITRIO, M. 2008. In vivo anti-myeloma activity and modulation of gene expression profile induced by valproic acid, a histone deacetylase inhibitor. *British journal of haematology,* 143**,** 520-531.

NOVILLO, A., WON, S.-J., LI, C. & CALLARD, I. P. 2005. Changes in nuclear receptor and vitellogenin gene expression in response to steroids and heavy metal in Caenorhabditis elegans. *Integrative and Comparative Biology,* 45**,** 61-71.

O'ROURKE, E. J., SOUKAS, A. A., CARR, C. E. & RUVKUN, G. 2009. < i> C. elegans</i> Major Fats Are Stored in Vesicles Distinct from Lysosome-Related Organelles. *Cell metabolism,* 10**,** 430-435.

OGG, S., PARADIS, S., GOTTLIEB, S., PATTERSON, G. I., LEE, L., TISSENBAUM, H. A. & RUVKUN, G. 1997. The Fork head transcription factor DAF-16 transduces insulin-like metabolic and longevity signals in C. elegans. *nature,* 389**,** 994-999.

PANDOLFI, P. P., SONATI, F., RIVI, R., MASON, P., GROSVELD, F. & LUZZATTO, L. 1995. Targeted disruption of the housekeeping gene encoding glucose 6-phosphate dehydrogenase (G6PD): G6PD is dispensable for pentose synthesis but essential for defense against oxidative stress. *The EMBO journal,* 14**,** 5209.

PARADIS, S. & RUVKUN, G. 1998. Caenorhabditis elegans Akt/PKB transduces insulin receptor-like signals from AGE-1 PI3 kinase to the DAF-16 transcription factor. *Genes & development,* 12**,** 2488-2498.

PARK, E. C., GHOSE, P., SHAO, Z., YE, Q., KANG, L., XU, X. S., POWELL-COFFMAN, J. A. & RONGO, C. 2012. Hypoxia regulates glutamate receptor trafficking through an HIF-independent mechanism. *The EMBO journal,* 31**,** 1379-1393.

PEDEN, E., KIMBERLY, E., GENGYO-ANDO, K., MITANI, S. & XUE, D. 2007. Control of sex-specific apoptosis in C. elegans by the BarH homeodomain protein CEH-30 and the transcriptional repressor UNC-37/Groucho. *Genes & development,* 21**,** 3195-3207.

PIANO, F., MANGONE, M., STEIN, L. & KEMPHUES, K. J. 2000. RNAi analysis of genes expressed in the ovary of< i> Caenorhabditis elegans</i>. *Current Biology,* 10**,** 1619-1622.

PIERCE, S. B., COSTA, M., WISOTZKEY, R., DEVADHAR, S., HOMBURGER, S. A., BUCHMAN, A. R., FERGUSON, K. C., HELLER, J., PLATT, D. M. & PASQUINELLI, A. A. 2001. Regulation of DAF-2 receptor signaling by human insulin and ins-1, a member of the unusually large and diverse C. elegans insulin gene family. *Genes & development,* 15**,** 672-686.

POLINKO, E. S. & STROME, S. 2000. Depletion of a Cks homolog in< i> C. elegans</i> embryos uncovers a post-metaphase role in both meiosis and mitosis. *Current Biology,* 10**,** 1471-1474.

POON, T. & CAMERON, D. P. 1978. Measurement of oxygen consumption and locomotor activity in monosodium glutamate-induced obesity. *American Journal of Physiology-Endocrinology And Metabolism,* 234**,** E532.

PYLVÄNEN, V., KNIP, M., PAKARINEN, A., KOTILA, M., TURKKA, J. & ISOJÄRVI, J. I. 2002. Serum Insulin and Leptin Levels in Valproate-associated Obesity. *Epilepsia,* 43**,** 514-517.

PYLVÄNEN, V., PAKARINEN, A., KNIP, M. & ISOJÄRVI, J. 2006. Insulin-related metabolic changes during treatment with valproate in patients with epilepsy. *Epilepsy & Behavior,* 8**,** 643-648.

RADCLIFFE, P. A., VARDY, L. & TODA, T. 2000. A conserved small GTP-binding protein Alp41 is essential for the cofactor-dependent biogenesis of microtubules in fission yeast. *FEBS letters,* 468**,** 84-88.

RANGANATHAN, R., SAWIN, E. R., TRENT, C. & HORVITZ, H. R. 2001. Mutations in the Caenorhabditis elegans serotonin reuptake transporter MOD-5 reveal serotonin-dependent and-independent activities of fluoxetine. *The Journal of Neuroscience,* 21**,** 5871-5884.

RAO, J. S., BAZINET, R. P., RAPOPORT, S. I. & LEE, H. J. 2007. Chronic treatment of rats with sodium valproate downregulates frontal cortex NF-κB DNA binding activity and COX-2 mRNA1. *Bipolar disorders,* 9**,** 513-520.

RAPPLEYE, C. A., TAGAWA, A., LE BOT, N., AHRINGER, J. & AROIAN, R. V. 2003. Involvement of fatty acid pathways and cortical interaction of the pronuclear complex in Caenorhabditis elegans embryonic polarity. *BMC developmental biology,* 3**,** 8.

RÄTTYÄ, J., TURKKA, J., PAKARINEN, A. J., KNIP, M., KOTILA, M., LUKKARINEN, O., MYLLYLÄ, V. & ISOJÄRVI, J. 2001. Reproductive effects of valproate, carbamazepine, and oxcarbazepine in men with epilepsy. *Neurology,* 56**,** 31-36.

REED, L. J. 1969. Pyruvate dehydrogenase complex. *Current topics in cellular regulation.* Academic Press New York and London.

REIS, R. J. S., XU, L., LEE, H., CHAE, M., THADEN, J. J., BHARILL, P., TAZEARSLAN, C., SIEGEL, E., ALLA, R. & ZIMNIAK, P. 2011. Modulation of lipid biosynthesis contributes to stress resistance and longevity of C. elegans mutants. *Aging (Albany NY),* 3**,** 125.

REN, P., LIM, C.-S., JOHNSEN, R., ALBERT, P. S., PILGRIM, D. & RIDDLE, D. L. 1996. Control of C. elegans larval development by neuronal expression of a TGF-β homolog. *Science,* 274**,** 1389-1391.

RITTER, A. D., SHEN, Y., BASS, J. F., JEYARAJ, S., DEPLANCKE, B., MUKHOPADHYAY, A., XU, J., DRISCOLL, M., TISSENBAUM, H. A. & WALHOUT, A. J. 2013. Complex expression dynamics and robustness in C. elegans insulin networks. *Genome research,* 23**,** 954-965.

RIZKI, G., IWATA, T. N., LI, J., RIEDEL, C. G., PICARD, C. L., JAN, M., MURPHY, C. T. & LEE, S. S. 2011. The evolutionarily conserved longevity determinants HCF-1 and SIR-2.1/SIRT1 collaborate to regulate DAF-16/FOXO. *PLoS genetics,* 7**,** e1002235.

ROGINA, B. & HELFAND, S. L. 2004. Sir2 mediates longevity in the fly through a pathway related to calorie restriction. *Proceedings of the National Academy of Sciences of the United States of America,* 101**,** 15998-16003.

ROTTIERS, V., MOTOLA, D. L., GERISCH, B., CUMMINS, C. L., NISHIWAKI, K., MANGELSDORF, D. J. & ANTEBI, A. 2006. Hormonal Control of< i> C</i>.< i> elegans</i> Dauer Formation and Life Span by a Rieske-like Oxygenase. *Developmental cell,* 10**,** 473-482.

SAFRAN, M., DALAH, I., ALEXANDER, J., ROSEN, N., STEIN, T. I., SHMOISH, M., NATIV, N., BAHIR, I., DONIGER, T. & KRUG, H. 2010. GeneCards Version 3: the human gene integrator. *Database: the journal of biological databases and curation,* 2010.

SAGASTI, A., HOBERT, O., TROEMEL, E. R., RUVKUN, G. & BARGMANN, C. I. 1999. Alternative olfactory neuron fates are specified by the LIM homeobox gene lim-4. *Genes & development,* 13**,** 1794-1806.

SARAFI-REINACH, T. R. & SENGUPTA, P. 2000. The forkhead domain gene unc-130 generates chemosensory neuron diversity in C. elegans. *Genes & development,* 14**,** 2472-2485.

SAVAGE-DUNN, C. 2005. TGF-β signaling.

SAVAGE, C., DAS, P., FINELLI, A. L., TOWNSEND, S. R., SUN, C.-Y., BAIRD, S. E. & PADGETT, R. W. 1996. Caenorhabditis elegans genes sma-2, sma-3, and sma-4 define a conserved family of transforming growth factor beta pathway components. *Proceedings of the National Academy of Sciences,* 93**,** 790-794.

SCHACKWITZ, W. S., INOUE, T. & THOMAS, J. H. 1996. Chemosensory neurons function in parallel to mediate a pheromone response in C. elegans. *Neuron,* 17**,** 719-728.

SCHAFER, W. R. 2006. Genetics of egg-laying in worms. *Annu. Rev. Genet.,* 40**,** 487-509.

SCHMID, C., SCHWARZ, V. & HUTTER, H. 2006. AST-1, a novel ETS-box transcription factor, controls axon guidance and pharynx development in< i> C. elegans</i>. *Developmental biology,* 293**,** 403-413.

SEITAN, V. C., BANKS, P., LAVAL, S., MAJID, N. A., DORSETT, D., RANA, A., SMITH, J., BATEMAN, A., KRPIC, S. & HOSTERT, A. 2006. Metazoan Scc4 homologs link sister chromatid cohesion to cell and axon migration guidance. *PLoS biology,* 4**,** e242.

SHAHAM, S. & BARGMANN, C. I. 2002. Control of neuronal subtype identity by the C. elegans ARID protein CFI-1. *Genes & development,* 16**,** 972-983.

SHAW, W. M., LUO, S., LANDIS, J., ASHRAF, J. & MURPHY, C. T. 2007. The< i> C. elegans</i> TGF-β Dauer Pathway Regulates Longevity via Insulin Signaling. *Current Biology,* 17**,** 1635-1645.

SHERMAN, B. T. & LEMPICKI, R. A. 2009. Bioinformatics enrichment tools: paths toward the comprehensive functional analysis of large gene lists. *Nucleic acids research,* 37**,** 1-13.

SHTEINGAUZ, A., COHEN, E., BIALA, Y. & TREININ, M. 2009. The BTB-MATH protein BATH-42 interacts with RIC-3 to regulate maturation of nicotinic acetylcholine receptors. *Journal of cell science,* 122**,** 807-812.

SIMMER, F., MOORMAN, C., VAN DER LINDEN, A. M., KUIJK, E., VAN DEN BERGHE, P. V., KAMATH, R. S., FRASER, A. G., AHRINGER, J. & PLASTERK, R. H. 2003. Genome-wide RNAi of C. elegans using the hypersensitive rrf-3 strain reveals novel gene functions. *PLoS biology,* 1**,** e12.

SOLARI, F. & AHRINGER, J. 2000. NURD-complex genes antagonise Ras-induced vulval development in< i> Caenorhabditis elegans</i>. *Current Biology,* 10**,** 223-226.

SRIVASTAVA, A. & GUPTA, Y. 2001. Aspirin modulates the anticonvulsant effect of diazepam and sodium valproate in pentylenetetrazole and maximal electroshock induced seizures in mice. *Indian journal of physiology and pharmacology,* 45**,** 475-480.

STELZER, G., HAREL, A., DALAH, A., ROSEN, N., SHMOISH, M., INY-STEIN, T., SIROTA, A., MADI, A., SAFRAN, M. & LANCET, D. GeneCards: One stop site for human gene research. The 5th Congress of the Federation of the Israel Societies for Experimental Biology; Eliat, Israel, 2008.

STRYER, L. 1995. Biochemistry. *WH Freeman, New York*.

STURN, A., QUACKENBUSH, J. & TRAJANOSKI, Z. 2002. Genesis: cluster analysis of microarray data. *Bioinformatics,* 18**,** 207-208.

SULEIMAN, S. A., ALI, M. E., ZAKI, Z., EL-MALIK, E. & NASR, M. 1996. Lipid peroxidation and human sperm motility: protective role of vitamin E. *Journal of andrology,* 17**,** 530-537.

SZE, J. Y., VICTOR, M., LOER, C., SHI, Y. & RUVKUN, G. 2000. Food and metabolic signalling defects in a Caenorhabditis elegans serotonin-synthesis mutant. *nature,* 403**,** 560-564.

SZE, J. Y., ZHANG, S., LI, J. & RUVKUN, G. 2002. The C. elegans POU-domain transcription factor UNC-86 regulates the tph-1 tryptophan hydroxylase gene and neurite outgrowth in specific serotonergic neurons. *Development,* 129**,** 3901-3911.

TAKAGI, S., BÉNARD, C., PAK, J., LIVINGSTONE, D. & HEKIMI, S. 1997. Cellular and axonal migrations are misguided along both body axes in the maternal-effect mau-2 mutants of Caenorhabditis elegans. *Development,* 124**,** 5115-5126.

TAPIERO, H., TOWNSEND, D. & TEW, K. 2004. The role of carotenoids in the prevention of human pathologies. *Biomedicine & Pharmacotherapy,* 58**,** 100-110.

TATAR, M., BARTKE, A. & ANTEBI, A. 2003. The endocrine regulation of aging by insulin-like signals. *Science,* 299**,** 1346-1351.

TISSENBAUM, H. A. & GUARENTE, L. 2001. Increased dosage of a sir-2 gene extends lifespan in Caenorhabditis elegans. *nature,* 410**,** 227-230.

TOKUOKA, S. M., SAIARDI, A. & NURRISH, S. J. 2008. The mood stabilizer valproate inhibits both inositol-and diacylglycerol-signaling pathways in Caenorhabditis elegans. *Molecular Biology of the Cell,* 19**,** 2241-2250.

TOYODA, H., KINOSHITA-TOYODA, A. & SELLECK, S. B. 2000. Structural Analysis of Glycosaminoglycans inDrosophila and Caenorhabditis elegans and Demonstration That

tout-velu, a Drosophila Gene Related to EXT Tumor Suppressors, Affects Heparan Sulfate in Vivo. *Journal of Biological Chemistry,* 275**,** 2269-2275.

TSALIK, E. L., NIACARIS, T., WENICK, A. S., PAU, K., AVERY, L. & HOBERT, O. 2003. LIM homeobox gene-dependent expression of biogenic amine receptors in restricted regions of the< i> C. elegans</i> nervous system. *Developmental biology,* 263**,** 81-102.

TSOU, M.-F. B., HAYASHI, A., DEBELLA, L. R., MCGRATH, G. & ROSE, L. S. 2002. LET-99 determines spindle position and is asymmetrically enriched in response to PAR polarity cues in C. elegans embryos. *Development,* 129**,** 4469-4481.

TURYN, J., SCHLICHTHOLZ, B., DETTLAFF-POKORA, A., PRESLER, M., GOYKE, E., MATUSZEWSKI, M., KMIEĆ, Z., KRAJKA, K. A. & SWIERCZYNSKI, J. 2003. Increased activity of glycerol 3-phosphate dehydrogenase and other lipogenic enzymes in human bladder cancer. *Hormone and metabolic research,* 35**,** 565-569.

UBEDA, N., ALONSO-APERTE, E., PEREZ-MIGUELSANZ, J. & VARELA-MOREIRAS, G. 2013. Valproate induced effects on development in the rat are partially prevented by folinic acid and S-adenosylmethionine. *European Journal of Anatomy,* 4**,** 23-33.

VANDONGEN, A., VANERP, M. & VOSKUYL, R. 1986. Valproate reduces excitability by blockage of sodium and potassium conductance. *Epilepsia,* 27**,** 177-182.

VASHLISHAN, A. B., MADISON, J. M., DYBBS, M., BAI, J., SIEBURTH, D., CH'NG, Q., TAVAZOIE, M. & KAPLAN, J. M. 2008. An RNAi screen identifies genes that regulate GABA synapses. *Neuron,* 58**,** 346-361.

VISWANATHAN, G. A., SETO, J., PATIL, S., NUDELMAN, G. & SEALFON, S. C. 2008. Getting started in biological pathway construction and analysis. *PLoS computational biology,* 4**,** e16.

VISWANATHAN, M. & GUARENTE, L. 2011. Regulation of Caenorhabditis elegans lifespan by sir-2.1 transgenes. *nature,* 477**,** E1-E2.

WALLACE, B. G., NITKIN, R. M., REIST, N. E., FALLON, J. R., MOAYERI, N. N. & MCMAHAN, U. 1985. Aggregates of acetylcholinesterase induced by acetylcholine receptor-aggregating factor.

WANDERS, R., FERDINANDUSSE, S., JANSEN, G., VREKEN, P., WATERHAM, H., VAN ROERMUND, C. & VAN GRUNSVEN, E. 2001. Peroxisomal fatty acid alpha-and beta-oxidation in humans: enzymology, peroxisomal metabolite transporters and peroxisomal diseases. *Biochemical Society Transactions,* 29**,** 250-266.

WANDERS, R. J., JANSEN, G. A. & LLOYD, M. D. 2003. Phytanic acid alpha-oxidation, new insights into an old problem: a review. *Biochimica et Biophysica Acta (BBA)-Molecular and Cell Biology of Lipids,* 1631**,** 119-135.

WANG, M. C., MIN, W., FREUDIGER, C. W., RUVKUN, G. & XIE, X. S. 2011. RNAi screening for fat regulatory genes with SRS microscopy. *Nature methods,* 8**,** 135-138.

WANG, X., JIA, H. & CHAMBERLIN, H. M. 2006. The bZip proteins CES-2 and ATF-2 alter the timing of transcription for a cell-specific target gene in< i> C. elegans</i>. *Developmental biology,* 289**,** 456-465.

WARDEN, C. H. & FRIEDKIN, M. 1985. Regulation of choline kinase activity and phosphatidylcholine biosynthesis by mitogenic growth factors in 3T3 fibroblasts. *Journal of Biological Chemistry,* 260**,** 6006-6011.

WEN, C., LEVITAN, D., LI, X. & GREENWALD, I. 2000. spr-2, a suppressor of the egg-laying defect caused by loss of sel-12 presenilin in Caenorhabditiselegans, is a member of the SET protein subfamily. *Proceedings of the National Academy of Sciences,* 97**,** 14524-14529.

WESNES, K., WARD, T., MCGINTY, A. & PETRINI, O. 2000. The memory enhancing effects of a Ginkgo biloba/Panax ginseng combination in healthy middle-aged volunteers. *Psychopharmacology,* 152**,** 353-361.

WICKENS, M., BERNSTEIN, D. S., KIMBLE, J. & PARKER, R. 2002. A PUF family portrait: 3′ UTR regulation as a way of life. *TRENDS in Genetics,* 18**,** 150-157.

WIGHTMAN, B., BARAN, R. & GARRIGA, G. 1997. Genes that guide growth cones along the C. elegans ventral nerve cord. *Development,* 124**,** 2571-2580.

WILLIAMSON, J. R. & CORKEY, B. E. 1969. [65] Assays of intermediates of the citric acid cycle and related compounds by fluorometric enzyme methods. *Methods in enzymology,* 13**,** 434-513.

WOLKOW, C. A., KIMURA, K. D., LEE, M.-S. & RUVKUN, G. 2000. Regulation of C. elegans Life-Span by Insulinlike Signaling in the Nervous System. *Science,* 290**,** 147-150.

YAMADA, S., VAN DIE, I., VAN DEN EIJNDEN, D. H., YOKOTA, A., KITAGAWA, H. & SUGAHARA, K. 1999. Demonstration of glycosaminoglycans in< i> Caenorhabditis elegans</i>. *FEBS letters,* 459**,** 327-331.

YOUNG, V. R. Diet as a modulator of aging and longevity. Federation proceedings, 1979. 1994-2000.

YU, H.-L., LI, L., ZHANG, X.-H., XIANG, L., ZHANG, J., FENG, J.-F. & XIAO, R. 2009. Neuroprotective effects of genistein and folic acid on apoptosis of rat cultured cortical neurons induced by β-amyloid 31-35. *British journal of nutrition,* 102**,** 655-662.

YUE, J. T. & LAM, T. K. 2012. Lipid sensing and insulin resistance in the brain. *Cell metabolism,* 15**,** 646-655.

ZHANG, J., BAKHEET, R., PARHAR, R. S., HUANG, C.-H., HUSSAIN, M. M., PAN, X., SIDDIQUI, S. S. & HASHMI, S. 2011. Regulation of fat storage and reproduction by Krüppel-like transcription factor KLF3 and fat-associated genes in Caenorhabditis elegans. *Journal of molecular biology,* 411**,** 537-553.

ZHANG, Y., GUO, K., LEBLANC, R. E., LOH, D., SCHWARTZ, G. J. & YU, Y.-H. 2007. Increasing dietary leucine intake reduces diet-induced obesity and improves glucose and cholesterol metabolism in mice via multimechanisms. *Diabetes,* 56**,** 1647-1654.